
Development of 3D-printed therapeutic bandage contact lenses for the treatment of corneal injuries

Ghada Zidan

A thesis submitted to Auckland University of Technology in fulfilment of the
requirement for the degree of Doctor of Philosophy (PhD)

School of Science
Biomedical Sciences
Faculty of Health and Environmental Sciences
Auckland University of Technology
2020

Abstract

Corneal blindness is a leading cause of irreversible visual impairment worldwide and can occur due to improper healing of the corneal tissues after induced injury or corneal surgery. The corneal epithelium has a self-healing mechanism wherein the frequent movement and differentiation of limbal stem cells residing in the limbus continuously replenish the epithelial layer. However, a key factor in promoting this natural healing process is the control of the inflammatory response within the cornea via the use of anti-inflammatory medications. These medications are usually administered via eye drops, a delivery method that is associated with very poor drug bioavailability (< 5%). To overcome this, frequent administration of eye drops is required, and this can often be inconvenient for patients. Currently, bandage contact lenses (BCLs) are applied after surgeries to protect the injured cornea, reduce pain and promote healing. Often, topical medications are also prescribed in conjunction with BCLs and therefore require patients to adhere to the dosage regimen in order to promote healing and prevent complications.

The primary aim of this thesis is to develop a tailor-made novel 3D-printed medicated BCL for the treatment of mild, moderate and severe corneal injuries. The corneal bandage is designed to protect the injured cornea from the external environment and pathogens and act as a matrix to support the adhesion of the newly generated corneal cells, thereby promoting rapid corneal healing. Two types of therapeutics were loaded in the bandages: an anti-inflammatory corticosteroid drug, dexamethasone (DEX), used to reduce the inflammation of the injured cornea and promote self-regeneration post-surgeries or in cases of mild-moderate corneal injuries (presented in chapters 3 and 4); and the second being human corneal epithelial primary cells (HCEpC) which can be used to compensate for the loss of corneal stem cells in moderate-severe corneal injuries thereby minimising the need for corneal grafts (presented in chapters 5 and 6).

In chapter 3, an all-in-one drug-eluting silicone hydrogel BCL was developed to protect the injured eye while delivering dexamethasone (DEX) as an anti-inflammatory medication over a period of 2 weeks. p(HEMA-co-TRIS-co-PDMS) lenses were prepared and the molar ratios of the co-monomers were varied to determine their effect on the release profiles of DEX and the properties of BCLs. Extended release of DEX for up to 14

days was achieved from the prepared lenses with properties comparable to commercial silicone hydrogel contact lenses.

In chapter 4, Gelatine methacrylate (GelMA) BCLs were prepared by solvent casting and 3D-printing techniques. DEX was loaded within the hydrogel matrix in the presence of Polyethylene glycol diacrylate (PEGDA) as a crosslinker. It was found that the incorporation of PEGDA improved the lenses' resistance to handling and prolonged their degradation time, reduced the EWC values and extended the release of the incorporated drug.

In chapters 5 and 6, a BCL that can carry human corneal epithelial primary cells (HCEpC) for treatment of moderate-severe corneal injuries in patients with limbal stem cell deficiencies (LSCDs), GelMA hydrogel lenses were developed. In chapter 5, GelMA/PEGDA hydrogel meshes were 3D-printed, cured and dried, then the HCEpC were loaded within the meshes. The incorporation of PEGDA enhanced the mechanical properties of GelMA hydrogels, increased their degree of crosslinking and significantly reduced the *in vitro* degradation rates. Moreover, *in vitro* cell culture experiments using HCEpC showed high adhesion, proliferation and viability over a period of 1 week in all the 3D-printed meshes. In chapter 6, either hyaluronic acid (HA) or collagen were incorporated within the 8% GelMA hydrogel matrix. The effect of various hydrogel compositions on the properties of the 3D-printed meshes including shape, degree of crosslinking, ESR, biodegradability and cell viability of the printed meshes were evaluated. It was found that the incorporation of 0.5% HA within the hydrogel composition resulted in a continuous extruded filament and a good printed structure. Moreover, the incorporation of 1% collagen within the hydrogel composite obtained a smooth printed mesh and enhanced the adhesion and proliferation of the seeded cells resulting in the formation of cell sheets within the printed structure.

In conclusion, the feasibility of loading therapeutics within BCLs that can be 3D-printed was confirmed. Furthermore, the good viability of HCEpC within the hydrogel lenses demonstrates the promising potential for the use of cell-loaded BCLs in treatment of corneal injuries, and the viability of a convenient, non-invasive alternative to the currently available treatment protocols.

Table of Contents

Abstract	i
Attestation of Authorship	vii
Dedication	viii
Acknowledgement	ix
List of Figures	x
List of Tables.....	xv
List of Abbreviations	xvi
Chapter 1 Introduction and thesis overview	1
1.1 General introduction	2
1.1.1 Structure and function of the cornea	2
1.1.2 Causes of corneal injuries	4
1.1.3 Corneal healing	10
1.1.4 Current treatments for corneal injuries.....	11
1.1.5 Reason for utilisation of 3D-printing.....	13
1.2 Thesis aims	15
1.3 Thesis structure	16
1.4 Thesis overview	16
1.5 Research outputs arising from this thesis	18
1.5.1 Conference presentations.....	18
1.5.2 Journal publications	19
1.5.3 Book chapters.....	19
Chapter 2 Medicated ocular bandages and corneal health: potential excipients and active pharmaceutical ingredients	20
Abstract.....	21
2.1 Introduction.....	22
2.2 The current practice of bandages	22
2.2.1 Amniotic membrane bandages.....	22
2.2.2 Bandage contact lenses (BCL)	23
2.2.3 Collagen shields.....	23
2.3 Materials that can be used in medicated bandages	24
2.3.1 Collagen.....	24
2.3.2 Polymeric hydrogels.....	24
2.3.3 Silicone hydrogels	25
2.3.4 Hyaluronic acid.....	25
2.3.5 Chitosan.....	25
2.4 Medications for corneal wound healing	26
2.4.1 Anti-inflammatory medication.....	26
2.4.2 Growth factors	26

2.4.3	Stem cells	27
2.5	Strategies for drug entrapment	27
2.5.1	Soaking of corneal bandage	27
2.5.2	Surfactants and nanoparticles	28
2.5.3	Molecular imprinting	28
2.5.4	Multilayer contact lenses	28
2.6	Important considerations and potential applications.....	29
2.7	Conclusion	31
Chapter 3 An all-in-one drug-eluting silicone hydrogel bandage contact lens (BCL) for post-surgical recovery and corneal injuries.		32
Abstract		33
3.1	Introduction.....	34
3.2	Materials and methods	37
3.2.1	Materials	37
3.2.2	Preparation of silicone hydrogel lenses.....	37
3.3	Characterisation of hydrogel lenses.....	40
3.3.1	Fourier transform infrared (FTIR) analysis	40
3.3.2	Swelling studies.....	40
3.3.3	Drug content and release.....	40
3.3.4	Mechanical properties	41
3.3.5	Statistical analysis	42
3.4	Results and discussion.....	42
3.4.1	Preparation of silicone hydrogel lenses.....	42
3.4.2	Fourier transform infrared (FTIR) analysis.....	44
3.4.3	Swelling studies.....	46
3.4.4	Drug content and release.....	50
3.4.5	Mechanical properties	56
3.5	Conclusion	60
Chapter 4 3D-printed gelatine bandage contact lens (BCL) for ocular drug delivery of Dexamethasone.		62
Abstract		63
4.1	Introduction.....	64
4.2	Materials and methods	66
4.2.1	Materials	66
4.2.2	Preparation and characterisation of GelMA hydrogel.....	66
4.2.3	Preparation of BCLs using the solvent casting technique.....	68
4.2.4	Preparation of BCLs using the 3D-printing technique	69
4.3	Characterisation of the bandages	71
4.3.1	Microscopic examination	71
4.3.2	Swelling studies.....	71
4.3.3	<i>In vitro</i> degradation.....	71

4.3.4	<i>In vitro</i> drug release	71
4.3.5	Statistical analysis	72
4.4	Results and discussion	73
4.4.1	Characterisation of prepared GelMA.....	73
4.4.2	Preparation of GELMA film using the solvent casting technique	74
4.4.3	Preparation of GELMA films using the 3D-printing technique	75
4.4.4	Microscopic examination	76
4.4.5	Swelling studies	78
4.4.6	<i>In vitro</i> degradation.....	80
4.4.7	<i>In vitro</i> drug release	84
4.5	Conclusion	86
	Chapter 5 3D-printing of GelMA/PEGDA composite hydrogel meshes as potential cell-carrier for tissue regeneration.	87
	Abstract	88
5.1	Introduction.....	89
5.2	Materials and methods	93
5.2.1	Materials	93
5.2.2	Hydrogel preparation.....	94
5.2.3	Preparation of the 3D-printed meshes	95
5.2.4	Characterisation of the printed meshes	95
5.3	Results and Discussion	100
5.3.1	Preparation of the 3D-printed meshes	100
5.3.2	Characterisation of the printed meshes	103
5.4	Conclusion	123
	Chapter 6 3D-printed GelMA meshes as a cell-carrier for the treatment of moderate-severe corneal injuries	125
	Abstract	126
6.1	Introduction.....	127
6.2	Materials and methods	130
6.2.1	Materials	130
6.2.2	Hydrogel preparation.....	130
6.2.3	Preparation of the 3D-printed meshes	131
6.2.4	Characterisation of the printed meshes	132
6.3	Results and discussion	135
6.3.1	Hydrogel preparation.....	135
6.3.2	Preparation of the 3D-printed meshes	135
6.3.3	Characterisation of the printed meshes	137
6.4	Conclusion	147
	Chapter 7 General discussion	149
7.1	Thesis overview	150

7.2	Interpretation of main thesis findings.....	151
7.3	Thesis implications	153
7.4	Study limitations and future recommendations	158
7.5	Conclusion	161
	References.....	163

Attestation of Authorship

I hereby declare that this submission is my own work and that, to the best of my knowledge and belief, it contains no material previously published or written by another person (except where explicitly defined in the acknowledgement), nor material which to a substantial extent, has been submitted for the award of any other degree or diploma of a university or other institution of higher learning.

Signed:

Date: 23/01/2020

Dedication

I dedicate this thesis to my wonderful family with a special debt of gratitude, deep appreciation and sincere love to my beloved father, my mother's soul, my loving and supportive husband, my amazing son and my gorgeous daughter. I wouldn't have achieved this without you being by my side.

Love you all...

Acknowledgement

I would like to express my deepest gratitude to my supervisor and mentor Dr Ali Seyfoddin for his continual support and guidance, not only in science and the academic field but also in personal and life skills. I owe him so much for his supervision, instructive criticism, valuable assistance, and his encouraging words that made me more confident and motivated me to do better in my research and writing.

My sincere appreciation goes to Prof Ilva Rupenthal for her kind supervision, generous attitude, valuable guidance and insightful comments. She was always there for me when I needed her assistance anytime and anywhere regardless of her very busy schedule.

No words can express my deepest appreciation to Dr Carol Greene for her guidance during the cell-culture experiments, imaging using the confocal microscope, generous supervision, meticulous revision of all details of this thesis and guidance all the way. I am lucky to have her and all my supervisors during my PhD journey.

I would like to acknowledge AUT for receiving the Vice Chancellor's Doctoral Scholarship award and the NZ Leather and Shoe Research Association (LASRA) for the funding received to assist with the purchase of the bioprinter used in this research.

I would like to recognise AUT for all the facilities and workshops they provide for postgraduate students, especially the thesis formatting workshop by Sue Knox, which made my life so much easier. I appreciate the support I have received from school of science staff members, especially the school manager, Brid Lorigan, for accommodating all my PhD requests; and the very helpful and experienced technicians for assisting with some of the characterisation tests, especially Adrian Owens for the NMR analysis, Tony Chen for the LC-MS analysis and Yuan Tao for the SEM imaging. I would also like to thank Jennifer Jane McGhee and Mehek Dutta from the FMHS UoA for helping during the cell culture experiments.

A big thank you goes to my friends and colleagues at the Drug Delivery Research Group (DDRG) for generating a friendly atmosphere, assistance, constructive feedback, advice and encouragement all the way.

List of Figures

Figure 1.1. The structure of the human eye, showing the layers of the cornea (Adopted from.....	3
Figure 1.2. Corneal wound healing cascade after corneal surgery.....	5
Figure 3.1. SUNUV apparatus used for curing of films. Top view of the device (A) and an inverted view showing the small lamps working under 405 nm (B).....	38
Figure 3.2. The film support rig with 5 mm spherical probe placed on TA.XT <i>Plus C</i> Texture Analyser.....	41
Figure 3.3. The effect of the curing intensity on pHEMA hydrogel lenses, 1%EGDMA and 0.5% LAP. Curing under 24 W (A) and curing under 48 W (B).	42
Figure 3.4. The effect of the crosslinker concentration on silicone hydrogel films containing 0.75 mole% PDMS, 10 mole% TRIS and 0.5% LAP. Films shown had EGDMA concentrations of either 1% (A), 2% (B) and 3% (C).	43
Figure 3.5. Image of drug-loaded silicone hydrogel lenses prepared using 1, 2 or 3 mole% PDMS with either 5, 10 or 20 mole% TRIS.	43
Figure 3.6. The polymerisation reaction of HEMA monomers in the presence of EGDMA crosslinker.	44
Figure 3.7. Structure of Dexamethasone drug molecule.....	45
Figure 3.8. FTIR absorbance spectra of liquid (Liq) and crosslinked film (CF) of 0.5 mole% PDMS, 10 mole% TRIS silicone hydrogels with DEX (D) and no DEX (ND) incorporation.	46
Figure 3.9. EWC of p(HEMA-co-TRIS-co-PDMS) lenses prepared using various molar concentration of PDMS and TRIS after soaking for 24 h in PBS. *Statistically significant at $p < 0.05$; $n = 3$; mean \pm SD.....	47
Figure 3.10. The effect of TRIS monomer concentration (A) and PDMS monomer concentration (B) on the EWC of the prepared silicone hydrogel lenses.....	48
Figure 3.11. EWC of drug-loaded p(HEMA-co-TRIS-co-PDMS) lenses prepared using various molar ratios of PDMS with 10 mole% of TRIS after 24 h in PBS. *Statistically significant at $p < 0.05$; $n = 3$; mean \pm SD.	49
Figure 3.12. The effect of drug incorporation on the EWC of (HEMA-co-TRIS-co-PDMS) BCLs polymer compositions using various molar ratios of PDMS with 10 mole% of TRIS after 24 h in PBS. $p < 0.05$; $n = 3$; mean \pm SD.	50
Figure 3.13. Percentage increase in diameter of (HEMA-co-TRIS-co-PDMS) BCLs polymer compositions using various molar ratios of PDMS with 10 mole% of TRIS after 24 h in PBS. *Statistically significant at $p < 0.05$; $n = 3$; mean \pm SD.....	50
Figure 3.14. Percentage of DEX remaining in p(HEMA-co-TRIS-co-PDMS) lenses, containing either 1, 2 or 3 mole% PDMS with either 5, 10 or 20 mole% PDMS, after washing for 24 h in DI water. *Statistically significant at $p < 0.05$; $n = 3$; mean \pm SD.	51
Figure 3.15. Drug release profiles of DEX from the washed p(HEMA-co-TRIS-co-PDMS) lenses in PBS at 37 °C. $n = 3$; mean \pm SD.	52

Figure 3.16. Percentage of DEX released from p(HEMA-co-TRIS-co-PDMS) lenses in PBS at 37 °C during the first 7 days. n = 3; mean ± SD.....	53
Figure 3.17. Effect of TRIS monomer concentration (A) and PDMS monomer concentration (B) on the on the percentage drug released after 7 days for the prepared silicone hydrogel lenses.	54
Figure 3.18. Drug release profiles of DEX from the washed p(HEMA-co-TRIS-co-PDMS) lenses in PBS at 37 °C. n = 3; mean ± SD.	55
Figure 3.19. Percentage of DEX released from p(HEMA-co-TRIS-co-PDMS) lenses in PBS at 37 °C during the first 7 days. n = 3; mean ± SD.....	55
Figure 3.20. The effect of various concentrations of TRIS and PDMS on the stress-strain curves (A) and Young's modulus (B) of the hydrogel lenses. *Statistically significant at $p < 0.05$; n = 3; mean ± SD.....	57
Figure 3.21. The effect of DEX concentration on the stress-strain curves (A) and Young's modulus (B) of 5 mole% TRIS 95 mole% HEMA hydrogel lenses. *Statistically significant at $p < 0.05$; n = 3; mean ± SD.	58
Figure 3.22. The effect of TRIS concentration on the stress-strain curves (A) and the Young's modulus (B) of 3 mole% PDMS hydrogel lenses. *Statistically significant at $p < 0.05$; n = 3; mean ± SD.	59
Figure 3.23. The effect of PDMS concentration on the stress-strain curves (A) and Young's modulus (B) of 10 mole% TRIS silicone hydrogel lenses. *Statistically significant at $p < 0.05$; n = 3; mean ± SD.	60
Figure 4.1. The flask on the left shows the formation of GelMA after the 3 h reaction with MAA, the image on the right shows the dialysis of GelMA against DI under 50 °C for 1 week.	67
Figure 4.2. Crosslinked GelMA hydrogel film in between 2 acrylic sheets and spacer (A) and lenses cut from the film using a cork borer (B).....	69
Figure 4.3. The 3D printing process. Design of 1-layer using SolidWorks in stl format (A), Uploading the stl file in Slic3r software (B), Reuploading the same stl file and changing its orientation to orient the lines horizontally (C), merge and centre of both uploaded files (D), slicing of the stl file into 2-layer g-code (E) and 3D printing of the sliced file using Allevi printer software (F).	70
Figure 4.4. Methacrylation of gelatine to gelatine methacrylamide.....	73
Figure 4.5. 1H-NMR spectra of prepared GelMA (A) and porcine gelatine (B) samples in D ₂ O.	74
Figure 4.6. Images of vacuum-dried (A) and swollen (B) DEX-loaded GelMA lenses prepared using various concentrations of GelMA and PEGDA in the solvent casting. (Ruler is in mm increments).	74
Figure 4.7. Images of the printed meshes (top), vacuum dried meshes (middle) and swollen meshes (bottom) of formulations G5P0 (A), G5P10 (B), G8P0 (C) and G8P10 (D). (Ruler is in mm increments).	76
Figure 4.8. Microscopic images printed hydrogel meshes imaged immediately after printing (left) and microscopic image of vacuum-dried hydrogel meshes after vacuum	

drying (right) of #G5P0 (A), #G5P10 (B), #G8P0 (C) and #G8P10 (D). (White scale bar is 0.5 mm).	78
Figure 4.9. EWC of the prepared hydrogel BCLs after 24 h at 37 °C. *Statistically significant at $p < 0.05$; $n = 3$; mean \pm SD.	79
Figure 4.10. The effect of 3D-printing on the EWC of the prepared hydrogel BCLs after 24 h at 37 °C. *Statistically significant at $p < 0.05$; $n = 3$; mean \pm SD.	80
Figure 4.11. Degradation profiles of 5% GelMA (A) and 8% GelMA (B) hydrogel BCLs in PBS at 37 °C. $n = 3$; mean \pm SD.	81
Figure 4.12. Images of the vacuum-dried P0, P10 and P15 BCLs formulations of 5% GelMA (A), and 8% GelMA (B) after the degradation test in PBS at 37 °C on days 1, 2, 4 and 7.	82
Figure 4.13. The effect of 3D-printing on the degradation profiles of the BCLs in PBS at 37 °C. $n = 3$; mean \pm SD.	83
Figure 4.14. Images of vacuum-dried 3D-printed meshes for formulations #G5P0, #G5P10, #G8P0 and #G8P10 after the degradation test in PBS at 37 °C on days 1, 2, 4 and 7.	83
Figure 4.15. The effect of PEGDA incorporation on the drug release profiles of 5% GelMA (A) and 8% GelMA (B) BCLs in PBS at 37 °C. $n = 3$; mean \pm SD.	85
Figure 4.16. The effect of 3D-printing on the drug release profiles of G5P0, G5P10, G8P0, G8P10, #G5P0, #G5P10, #G8P0 and #G8P10 BCLs in PBS at 37 °C. $n = 3$; mean \pm SD.	86
Figure 5.1. Difference between physical and chemical crosslinking of gelatine showing the covalent bonds generated during the photopolymerisation reaction of GelMA.	91
Figure 5.2. SEM (A), vacuum-dried meshes after printing (B) and freeze dried meshes after swelling (C) ready to be imaged by the SEM.	96
Figure 5.3. 30 G, 27 G and 25 G needle sizes used in the printing of the hydrogel meshes.	101
Figure 5.4. Effect of printing speed on the printed mesh of 10% GelMA using 27 G needle and pressure of 12 PSI. The ruler is in mm increments.	102
Figure 5.5. Image of the cooled hydrogel in the syringe prior to printing (top), the extruded filament from the nozzle to determine the appropriate pressure (middle) and printed mesh (bottom). Images show the formulations P0 (A), P1 (B) and P10 (C). The ruler is in mm increments.	105
Figure 5.6. Effect of drying technique on 10% GelMA hydrogel meshes. Fragile freeze-dried meshes (A), and easy to handle vacuum-dried meshes (B).	106
Figure 5.7. Microscopic images of the printed hydrogel meshes imaged immediately after printing (left) and microscopic image of vacuum-dried hydrogel meshes (right) of P0 (A), P1 (B) and P10 (C), scale bar = 0.5 mm.	107
Figure 5.8. SEM images of printed 10% GelMA meshes. Images showing vacuum dried mesh (A), freeze-dried mesh (B), freeze-dried mesh after swelling of previously vacuum dried meshes (C) and freeze-dried mesh after swelling of previously freeze-dried meshes (D).	108

Figure 5.9. SEM images of 3D-printed 8% GelMA meshes after vacuum drying (left) and after freeze drying of the swollen meshes (right) of 8% GelMA (A), 8% GelMA+1% PEGDA (B) and 8% GelMA + 10% PEGDA (C). Smaller images on the top right represent their camera images.	109
Figure 5.10. The effect of crosslinking parameters on the sol fraction of 10% GelMA, 0.5% LAP hydrogel meshes after 24 h in PBS at 37 °C. *Statistically significant at $p < 0.05$; $n = 3$; mean \pm SD.	110
Figure 5.11. The effect of LAP concentration on the sol fraction of 10% GelMA hydrogels cured at 13 or 15 mW/cm ² for either 120, 150 or 180 sec. *Statistically significant at $p < 0.05$; $n = 3$; mean \pm SD.	111
Figure 5.12 The effect of GelMA concentration (9 and 10%) and 0.5% LAP on the sol fraction of the hydrogel meshes cured under various intensities for 120 s (A) and 150 s (B). *Statistically significant at $p < 0.05$; $n = 3$; mean \pm SD.	112
Figure 5.13. The effect of GelMA concentration (7, 8, 9 and 10%) and 0.5% LAP on the sol fraction of the hydrogel meshes cured under 13 mW/cm ² for 150 s. *Statistically significant at $p < 0.05$; $n = 3$; mean \pm SD.	113
Figure 5.14. The photo-polymerisation reaction of PEGDA.....	114
Figure 5.15. The effect of PEGDA concentration on the sol fraction of 8% GelMA hydrogel meshes cured under 13 mW/cm ² for 150 s. *Statistically significant at $p < 0.05$; $n = 3$; mean \pm SD.	114
Figure 5.16. Wet 10% GelMA hydrogel mesh at equilibrium swelling placed on the skin.	115
Figure 5.17. The swelling ratio of 10% GelMA dry hydrogel meshes within 24 h in PBS. $n = 3$; mean \pm SD.....	116
Figure 5.18. The effect of crosslinking intensities of 7, 8, 10, 12, 13, 14 and 14 mW/cm ² on the ESR of the 10% GelMA dry hydrogel meshes in PBS after 24 h. *Statistically significant at $p < 0.05$; $n = 3$; mean \pm SD.	117
Figure 5.19. The effect of PEGDA concentration on the ESR after 24 h of 8% GelMA dry hydrogel meshes. *Statistically significant at $p < 0.05$; $n = 3$; mean \pm SD.	118
Figure 5.20. Degradation profiles of 8 and 10% GelMA hydrogel meshes in PBS at 37 °C. $n = 3$; mean \pm SD.....	119
Figure 5.21. The effect of PEGDA concentration on the degradation profiles of 10% GelMA hydrogel meshes in PBS at 37 °C. $n = 3$; mean \pm SD.	120
Figure 5.22. The effect of photoinitiator concentration on cell viability. Z-stacked confocal microscopic image of 10% GelMA+0.3% LAP (A), 10% GelMA + 0.5% LAP (B) hydrogel meshes stained with live/dead assay after 1-week incubation with HCEpC. The green colour indicates the live cells, while the red colour presents the dead ones; scale bar = 100 μ m.	121
Figure 5.23. Z-stacked confocal microscopic images of 7% GelMA (A), 8% GelMA (B) and 10% GelMA (C) hydrogel meshes stained with live/dead assay after 1-week incubation with HCEpC. The green colour indicates the live cells, while the red colour presents the dead ones; scale bar = 100 μ m.	122

Figure 5.24. Z-stacked confocal microscopic image of 8%GelMA (A), 8% GelMA+1% PEGDA (B) and 8% GelMA+10% PEGDA (C) hydrogel meshes stained with live/dead assay after 1-week incubation with HCEpC. The green colour indicates the live cells, while the red colour are the dead ones.....	122
Figure 5.25. Phase-contrast image of 10% GelMA hydrogel carrying HCEpC after 1-week incubation.	123
Figure 6.1. GelMA synthesis from gelatine and MAA, showing the RGD motifs responsible for cell adhesion.	135
Figure 6.2. Images of the cooled hydrogel in the syringe prior to printing (top), the extruded filament from the nozzle to determine the appropriate pressure (middle) and printed mesh above a 1 cm ruler (bottom). Images show the formulations G (A), GH0.5 (B), GH1(C) and GC1 (D); ruler is in mm increments.....	138
Figure 6.3. Microscopic images printed hydrogel meshes imaged immediately after printing (left) and microscopic image (4X) of vacuum dried hydrogel meshes after vacuum drying (right) of G (A), GH0.5 (B), GH1 (C) and GC1 (D); scale bar = 0.5 mm..	139
Figure 6.4. SEM images of 3D-printed 8% GelMA meshes after vacuum drying (left) and after swelling test (right) of 8% GelMA (A), 8% GelMA + 0.5% HA (B), 8% GelMA + 1% HA (C) and 8% GelMA + 1% collagen (D).	141
Figure 6.5. The effect of hydrogel composition on the crosslinking properties of 8% GelMA hydrogel meshes cured under 13 mW/cm ² for 150 s. *Statistically significant at $p < 0.05$; n = 3; mean \pm SD.....	142
Figure 6.6. The effect of hydrogel composition on the ESR of 8% GelMA dry hydrogel meshes. *Statistically significant at $p < 0.05$; n = 3; mean \pm SD.	143
Figure 6.7. Degradation profiles of G, G0.5, GH1 and GC1 hydrogel meshes in PBS at 37 °C. n = 3; mean \pm SD.	144
Figure 6.8. Z-stacked confocal microscopic image of 8% GelMA (A), 8% GelMA + 0.5% HA (B), 8% GelMA + 1% HA (C), and 8% GelMA + 1% collagen (D) hydrogel meshes stained with live/dead assay after 1-week incubation with HCEpC. The green colour indicates the live cells, while the red colour shows the dead ones.	146

List of Tables

Table 3.1. Materials used and their role in the preparation of silicone hydrogel lenses.	36
Table 3.2. Silicone hydrogel formulations prepared using various molar ratios of PDMS and TRIS.....	39
Table 3.3. Silicone hydrogel formulations prepared using various molar ratios of PDMS with and without DEX loading.....	39
Table 4.1. GelMA hydrogel BCL formulations prepared using the solvent casting technique	68
Table 4.2. GelMA hydrogel BCL formulations prepared using the 3D-printing method.	69
Table 5.1. Composition of GelMA hydrogels for the crosslinking test.	94
Table 5.2. Composition of GelMA/PEGDA hydrogel composites.....	94
Table 5.3. Composition of GelMA hydrogel meshes tested for cell viability cured for 150 s under light intensity of 13 mW/cm ² using 405 nm lamp.	99
Table 5.4. Variation of printing parameters to obtain the best print for 10% GelMA .	101
Table 5.5. Printing parameters for 8% GelMA hydrogel meshes with/without PEGDA.	103
Table 6.1. Composition of the hydrogel composites.	131
Table 6.2. Printing parameters for 8%GelMA hydrogel meshes.	136

List of Abbreviations

3D	three-dimensional
μ	micro
°C	degree Celsius
AM	amniotic membrane
BCL	bandage contact lens
cm	centimetres
DEX	dexamethasone
DM	degree of methacrylation
DMSO	dimethyl sulfoxide
ECM	extracellular membrane
EGDMA	ethylene glycol dimethacrylate
ESR	equilibrium swelling ratio
FTIR	Fourier-transform infrared spectroscopy
G	gauge
g	gram(s)
GelMA	gelatine methacrylate
h	hour(s)
HA	hyaluronic acid
HCEC	human corneal endothelial cells
HCEpC	human corneal epithelial primary cells
HEMA	2-hydroxyethyl methacrylate
LAP	lithium phenyl-2,4,6-trimethylbenzoylphosphinate
LSD	limbal stem cell deficiency
M	molar concentration
mg	milligram
min	minute(s)
ml	millilitre(s)
mm	millimetre(s)
n	number
NMR	nuclear magnetic resonance
nm	nanometre
PBS	phosphate buffer saline
PDMS	polydimethylsiloxane
PED	persistent epithelial defects
PEGDA	poly(ethylene glycol) diacrylate
pHEMA	Poly(2-hydroxyethyl methacrylate)
rpm	revolutions per minute
s	second(s)
SEM	scanning electron microscope
SD	standard deviation
TMSP	trimethylsilylpropanoic acid
TRIS	tris(hydroxymethyl)aminomethane
W	watts
w/w	weight per weight

w/v	weight per volume
UV	ultraviolet

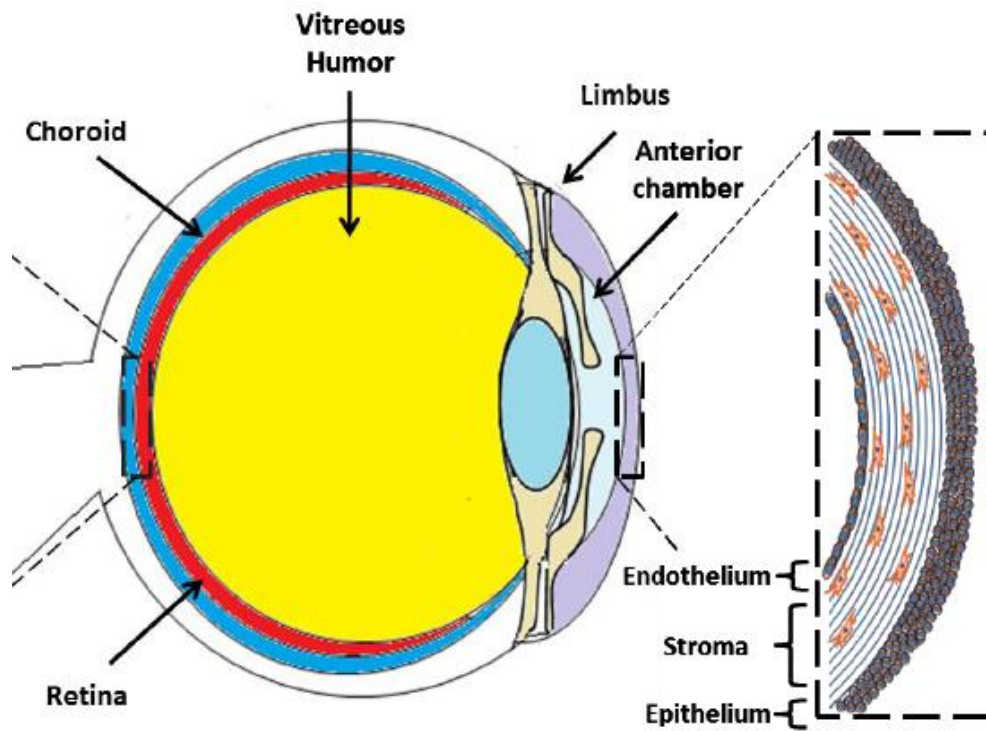
Chapter 1 Introduction and thesis overview

1.1 General introduction

1.1.1 Structure and function of the cornea

The anterior surface of the eye is composed of the cornea, conjunctiva and the limbus which is the zone between the two (Kurpakus-Wheater, Kernacki, & Hazlett, 2001). The cornea is a clear, avascular, dome shaped surface that covers the front of the eye (Dartt, 2010). It acts as a barrier, protecting the inner contents of the eye and it provides about two-thirds of the eye's refractive power. Therefore it has an important role in enabling clear vision (Meek & Knupp, 2015). The mechanical strength of the cornea is achieved through collagen fibrils, which have a small, uniform diameter and are positioned with a high degree of lateral order. This arrangement is what makes the cornea transparent and allows visible light into the eye. The cornea is kept smooth and healthy by the lubricant and antibacterial properties of the tear film that is secreted within the eye (Meek, 2008). The composition of the human cornea is illustrated in Figure 1.1. There are three main layers, the epithelium, stroma and endothelium, and two membranes known as the Bowman's and the Descemet's membranes.

The epithelium is about 53 μm thick and is the cornea's outermost layer (Reinstein, Archer, Gobbe, Coleman, & Silverman, 2008). Its primary function is to block the passage of foreign materials, such as dust, water, and bacteria from entering the eye, and to provide a smooth surface that can absorb oxygen and nutrients from the tears. The epithelium is filled with thousands of tiny nerve endings, which is why it can be extremely painful when a foreign body enters the eye. It is worth noting that the lipophilic nature of the epithelium is the main barrier to hydrophilic drugs (Barar, Asadi, Mortazavi-Tabatabaei, & Omid, 2009). The inner layer of the epithelium, where the epithelial cells anchor and organize themselves, is called the basement membrane (Yurchenco, 2011).



Cellular Corneal Layers

Figure 1.1. The structure of the human eye, showing the layers of the cornea (Adopted from (Rose et al., 2014)).

Following the basement membrane, there is a thin transparent film of collagen fibres called the Bowman's membrane; it is 8-14 μm thick and is not considered a drug barrier. Unfortunately, the Bowman's membrane cannot be regenerated if it gets damaged, and thus injuries can cause scar formation, which might lead to loss of vision if the injury covers a large area or is located near the centre of the cornea (Rawas-Qalaji & Williams, 2012).

The stroma is just below the Bowman's membrane and is the thickest layer of the cornea, constituting almost 90% of the corneal thickness (Meek & Knupp, 2015). It is hydrophilic in nature as it is composed primarily of water and collagen and thus it constitutes the main barrier to hydrophobic drugs crossing the cornea. Just below the stroma is the Descemet's membrane, a thin (6 μm) but a robust film of regenerative tissue that serves as a protective barrier against infection and injuries. It does, however, hinder drug absorption (Rawas-Qalaji & Williams, 2012). The Descemet's membrane is composed of collagen fibres that are different from those of the stroma, and are made by cells located in the endothelial layer of the cornea (Sridhar, 2018).

The endothelium is the thin, innermost layer of the cornea and its cells play a significant role in keeping the cornea clear. Normally, fluids slowly leak from the inside of the eye into the stroma, and the endothelium's primary task is to pump these fluids out of the stroma through the Na/K⁺ ATPase pumps. Without this pumping action, the stroma would swell with water and become thick and opaque (Rawas-Qalaji & Williams, 2012). Unlike the cells of the Descemet's membrane, endothelial cells that have been destroyed due to disease or trauma are not repaired by the body (Institute, 2019). In general, changes in one or more of the corneal layers can lead to increased light scattering and consequent loss of corneal transparency (Meek & Knupp, 2015).

1.1.2 Causes of corneal injuries

Accidents

Trauma and abrasion

Most ocular trauma injuries occur as a result of the impact from foreign bodies or abrasion of the corneal epithelium. After a corneal injury, the patient may suffer from severe pain and reduced vision. With symptoms usually improving as healing takes place. It was reported that patients can suffer from panic as a result of vision loss and a prolonged period of anxiety even after eye recovery (Ashby, Garrett, & Willcox, 2014).

Chemical burns

Chemical burns account for 5-22% of eye injuries and have a greater risk of affecting vision. (Ashby et al., 2014). They occur when corrosive substances are accidentally introduced to the eye such as building products or household cleaners that contain ammonia. Generally, alkaline burns are more serious than acidic burns since the hydroxyl ions cause saponification of the fatty acids in corneal cell membranes thereby causing cellular disruption. This leads to the deep penetration of the alkaline solutions into the underlying tissues causing severe damage to the cornea. On the other hand, acids denature corneal proteins causing coagulation necrosis, which forms a barrier that helps to prevent further penetration into corneal tissues. Chemical eye injuries require instant evaluation and emergency treatment (Eslani, Baradaran-Rafii, Movahedan, & Djalilian, 2014).

The main aim of treatment in the acute phase of corneal burns is to reduce inflammation, stimulate epithelialisation and prevent tissue necrosis. Successful

management of the acute phase can reduce scar formation and protect vision (A. Baradaran-Rafii, Aghayan, Arjmand, & Javadi, 2007; Fernandes, Sridhar, Sangwan, & Rao, 2005).

Corneal surgeries

Despite the safety of the procedures used in current corneal and refractive surgeries, LASIK surgery generates at least 2% complications with irregular wound healing patterns (Ljubimov & Saghizadeh, 2015). The cornea's response to injury after laser surgery differ from person to person. The immediate postoperative refractive results of LASIK or surface ablation are controlled by the programmed ablation zone geometry, the laser-tissue interaction and perioperative biomechanical responses which is not the same for all patients. Biological diversity in this response is the norm, even in genetically similar individuals or contralateral eyes of the same patient. Even in high precision refractive surgeries, the shape-subtraction model of photokeratectomy that forms the basis of the LASIK and PRK ablation routines assumes a biologically and mechanically inert cornea and does not take in consideration non-idealities in the laser-tissue interactions. Abnormal regulation of the healing mechanism can lead to serious complications such as keratectasia or loss of corneal transparency (Dupps Jr & Wilson, 2006).

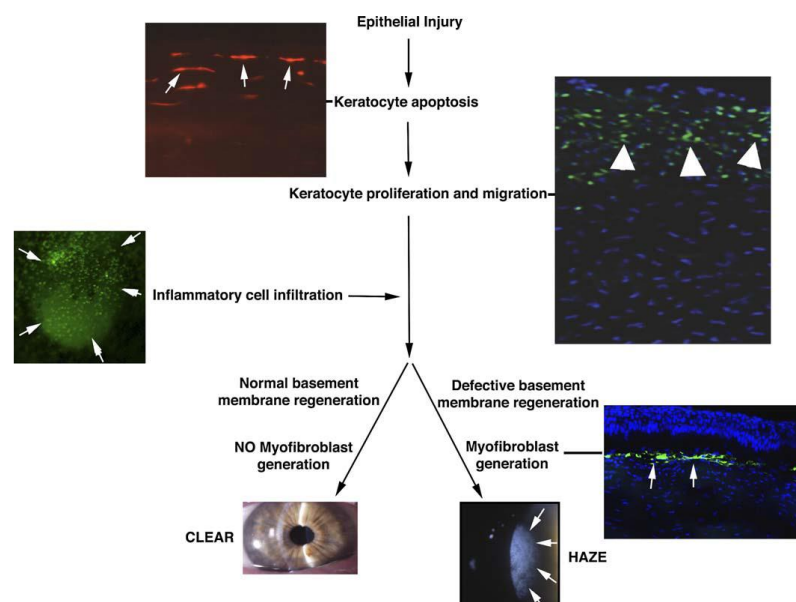


Figure 1.2. Corneal wound healing cascade after corneal surgery (Adapted from (Dupps Jr & Wilson, 2006)).

Corneal haze is one of the complications following photorefractive keratectomy. During the wound healing process, the transformation of stromal keratocytes into activated

fibroblasts that synthesize new collagen and extracellular matrix can lead to opacity (Klausner, Peer, Chapman, Multack, & Andurkar, 2007). Figure 1.2 shows the two wound healing reaction pathways that occur during laser surgeries. One results in proper healing that leads to the formation of a clear eye (on the left) and the other pathway due to uncontrolled healing results in corneal haze (on the right). Following epithelial injury, instantaneous programmed cell death (apoptosis) of underlying keratocytes occur and the dead cells are removed by the phagocytic action of the migrating bone marrow-derived cells. A few hours after apoptosis, residual stromal keratocytes undergo proliferation and migration to restore stromal cellularity. According to the type and extent of the injury, a high density of myofibroblasts can be generated in the cornea which leads to corneal haze (Dupps Jr & Wilson, 2006).

Corneal diseases/conditions

Corneal diseases are the reason more than 8 million people suffer from blindness worldwide (Zellander et al., 2014). Corneal diseases/conditions can be induced by extrinsic infectious pathogens or intrinsic autoimmune reactions (Tsai, Hsu, Hung, Chang, & Cheng, 2015). Epithelial cells can produce cytokines such as interleukin-1 (IL-1) in response to certain antigens such as microbes and toxic substances in the environment as a first-line defence mechanism for the eye. However, this defence mechanism can lead to migration of dendritic cells, neutrophils, T lymphocytes and other inflammatory cells into the cornea which might lead to swelling, dissolution of the stroma and opacity (Kurpakus-Wheater et al., 2001).

Generally, an immune response will cause an unacceptable level of tissue destruction. However, each tissue has a different degree of destruction tolerability; for example, a response to microbial infection that is protective in one tissue such as the lung may be pathological in another such as the eye. In the cornea, it is extremely important to control the inflammatory response in order to maintain vision and clarity (Kurpakus-Wheater et al., 2001). The following diseases/conditions can affect the cornea in a manner that requires effective treatments.

Infectious keratitis

Infectious or microbial keratitis occurs in the cornea as a result of a bacterial, viral or fungal infection. Infectious keratitis is common, but not limited, to contact lens wearers.

Corneal infections lead to severe complications such as corneal thinning and scarring, which might require surgical intervention if not properly treated (Tsai et al., 2015).

Bacterial keratitis usually results in corneal ulcers that can lead to perforations, which can seriously affect vision (Tabatabaei et al., 2017). Once the bacteria enter the corneal tissue, cytokines such as interleukin 1 and tumour necrosis factor (TNF) are released. Examples of bacterial species that affect the cornea are *Pseudomonas*, *Staphylococcus*, *Streptococcus*, *Moraxella* and *Salmonella* (Jhanji et al., 2011).

Fungal keratitis is one of the major causes of infectious keratitis, especially in developing countries. It is caused by fungi including *Fusarium solani*, *Aspergillus fumigatus*, *Penicillium citrinum*, *Candida albicans*, *Cephalosporium*, and *Curvularia* (Jhanji et al., 2011). It is usually challenging to treat fungal keratitis, and the infection can lead to corneal perforation in cases of treatment failure. Initial treatment is through antifungal topical medication such as Natamycin or Amphotericin B (H. C. Chen et al., 2006). Although the rate of progression of fungal keratitis is slow, the lack of ocular penetration of the antifungal topical therapy is a major limitation of the current therapies. Almost one-third of all fungal infections require surgical interventions for treating corneal perforations that occur as a result of pharmacological treatment failure (Jhanji et al., 2011).

The proliferation of micro-organisms and the associated inflammation within the corneal tissues causes corneal ulcers and perforations that can cause serious sight-threatening conditions that require intensive treatment. Amniotic membrane (AM) transplantation can be used to reduce inflammation, promote corneal wound healing and reduce scarring (Altay, Tamer, Burcu, & Balta, 2016).

Ulcers, perforations and epithelial defects

Corneal ulcers and perforations can occur due to infectious or non-infectious keratitis (Nejabat et al., 2009). Usually, epithelial defects caused by pathogens self-heal without complications, but in some cases where there is a malfunction of lids or tear film or nerve damage, chronic inflammation can lead to persistent epithelial defects (PED) and stromal melting (J. S. Kim, Kim, Hahn, & Park, 2001). Treatment for PED is achieved via correcting the underlying condition, suppressing of the inflammation and conservative

ocular surface management. Usually, surgical interventions including AM transplants are done only when medical treatment fails (A. Baradaran-Rafii et al., 2007).

Non-infectious corneal perforation usually occurs in ocular diseases affecting the precorneal tear film or other components of the ocular surface. One of the major causes of chronic epithelial defects is dry eye syndrome. Poor healing of chronic epithelial defects can lead to corneal ulceration or perforations that are sight-threatening (Jhanji et al., 2011). Autoimmune diseases such as rheumatoid arthritis, systemic lupus erythematosus, temporal arteritis, Wegener granulomatosis, sarcoidosis, and inflammatory bowel disease are another cause for chronic epithelial defects as they can cause corneal melting (Jhanji et al., 2011).

In the case of corneal perforations, it is vital to seal the aqueous leak, provide support to the perforated site and eliminate the causes of perforation while protecting the anterior segment from any further damage. This can be achieved through tissue adhesives, bandage contact lenses (BCL), patch grafts including AM, conjunctival flaps and penetrating or lamellar keratoplasty (Solomon et al., 2002).

Bullous keratopathy

Bullous keratopathy is a corneal disease caused by endothelial decompensation. The cell density of the endothelium is reduced, causing over hydration of the cornea leading to intraepithelial oedema that weakens the adhesion between the epithelium and stroma resulting in bullae formation. The main cause of bullous keratopathy is complicated cataract surgery (Vyas & Rathi, 2009). Secondary causes of bullous keratopathy can be failed corneal grafts, penetrating or blunt trauma, or refractory glaucoma. In cases of mild corneal decompensation, bullous keratopathy can be asymptomatic, however as the disease progresses, slight blurring of vision occurs due to increased corneal thickness and the folding of the Descemet membrane. Bulla formation occurs eventually causing discomfort or sometimes severe pain.

Partial or full-thickness corneal transplantation is the main treatment for bullous keratopathy. However, AM transplantation, anterior stromal micro puncture, collagen cross-linking, BCLs and conjunctival flap are some of the alternative treatments proposed, that can be used individually or in combination for treatment of bullous

keratopathy in cases of difficulties in processing a corneal transplant (Siu, Young, & Jhanji, 2014; Sonmez, Kim, & Aldave, 2007).

Band keratopathy (BK)

Patients with band keratopathy (BK) experience ocular pain and diminished vision due to the physical disruption and calcification of the peri-basement membrane area leading to breakdown of the corneal epithelium and instability of the ocular surface and in some cases keratocyte loss (Anderson, Prabhasawat, Alfonso, & Tseng, 2001; Fernandes et al., 2005). Ocular pain in band keratopathy is due to surface instability and epithelial irregularity (A. Baradaran-Rafii et al., 2007).

Band keratopathy is currently managed through the use of the chelating agent ethylenediaminetetraacetic acid (EDTA) with superficial keratectomy or excimer laser PTK to remove the calcific deposits (Im, Lee, & Yoon, 2010), however, there is a need for supporting treatments to reduce pain, promote healing and stability of the cornea and prevent opacity; this can be achieved through AM transplantation (Anderson et al., 2001). The AM protects the stroma from defects by replacing the removed basement membrane and stroma after surgery (Im et al., 2010).

Diabetic keratopathy

Diabetes has a significant influence on all the layers of the cornea. Moreover, it has a deleterious effect on the morphological, physiological, metabolic and clinical features of the cornea. Keratoepitheliopathy, a condition that occurs in almost one-quarter of diabetic patients, presents as superficial punctuate keratopathy, persistent epithelial defects or recurrent corneal erosion (Hiraoka, Amano, Oshika, Kato, & Hori, 2001; K. Inoue et al., 2001). Diabetes causes vascular changes in the tear gland and diabetic retinopathy which leads to dysfunction of the tear film and thus dry eye (Cousen, Cackett, Bennett, Swa, & Dhillon, 2007). Moreover, diabetic keratopathy can cause corneal oedema and persistent epithelial defects that can progress to scarring which might eventually lead to permanent loss of vision.

The cornea of a diabetic patient differs from the normal cornea in response to cataract surgery and is more susceptible to postoperative complications. It is common in diabetic patients to suffer from preoperative and/or postoperative dry eye disease due to aggressive treatments before and after surgery and worsening of the tear film function

as a result of the cataract surgery itself (X. Liu, Gu, & Xu, 2008). Moreover, diabetic patients suffer from delayed epithelial wound healing compared to non-diabetic patients, which might progress to intraocular infection and other postoperative complications (Wakuta et al., 2007). Controlling of blood sugar levels and eye lubrication is important in diabetic patients to prevent complications arising post corneal injuries. Other treatment protocols suggest using topical antibiotics and oral nicergoline to increase the arterial blood flow, BCLs, and covering the lid by a patch. Recent approaches implement growth factors to enhance corneal healing (Cousen et al., 2007; Saghizadeh, Kramerov, Yu, Castro, & Ljubimov, 2010) .

1.1.3 Corneal healing

Since the cornea is the major refractive surface of the eye, any mechanical or biological response following injury will affect the optical performance. The size and depth of the wound and the type of injury affect the healing mode and outcome. Corneal injury can be in the form of a scrape, incision, laser exposure, or other insults. Following the injury, there is usually a period of lag phase where the cells change their metabolic status and prepare for the wound healing process. Although the mechanism of wound healing is usually introduced as a linear cascade, it is more complex and involves simultaneous mechanisms that are influenced by numerous factors such as cytokines, growth factors, chemokines and their receptors. There are similarities in the healing processes between the epithelial, stromal and endothelial cells in relation to cell migration, dependence on growth factors and extracellular matrix (ECM) remodelling. However, there are significant differences in the healing mechanism of the different corneal cell populations (Dupps Jr & Wilson, 2006).

The corneal epithelium has a self-healing mechanism through frequent movement and differentiation of limbal stem cells residing in the limbus. Most epithelial injuries self-heal within 24 h, except for severe injuries from alkali burns, infections, or wound associated with diabetic retinopathy (Ashby et al., 2014). Corneal epithelial wound healing consists of continuous phases that start with cell death, followed by migration via sliding of the superficial cells to cover the denuded surface, followed by cell proliferation, differentiation and extracellular matrix (ECM) remodelling (Agrawal & Tsai, 2003; Ljubimov & Saghizadeh, 2015). This process involves growth factor/cytokine

and ECM signal-mediated interactions to re-establish epithelial integrity and restore corneal homeostasis (Ljubimov & Saghizadeh, 2015).

Stromal cells heal through a sequence of transformation of stromal keratocytes to fibroblasts and myofibroblasts (Ljubimov & Saghizadeh, 2015). Fibrin formation occurs at the early stage of wound healing to act as a provisional matrix to support migration and adhesion of corneal epithelial cells. Crosslinking of the expanding fibrin network is essential for corneal wound healing. Subsequently, fibronectin is deposited on the denuded corneal surface from tear film to facilitate cell adhesion and re-epithelisation during healing (Agrawal & Tsai, 2003).

Fibrotic scar formation in human skin cells will not affect tissue function, however, improper stromal wound healing can significantly reduce corneal transparency and affect vision. It is worth noting that stromal remodelling occurs upon direct damage to the stroma as in case of surgery, as well as upon the death of stromal cells after injury of the corneal epithelium through physical or chemical factors. Damage of the stroma triggers the release of inflammatory cytokines from epithelial cells and/or tear fluids. As for endothelial corneal healing, it usually occurs after corneal burns and surgeries for replacing dysfunctional endothelial cells only. Endothelial cells have extremely low proliferation rates, and healing occurs through transformation to mesenchymal cells, cell migration and spreading (Ljubimov & Saghizadeh, 2015).

1.1.4 Current treatments for corneal injuries

The treatment protocol set to promote effective corneal healing depends mainly on the cause and the severity of the injury. Some corneal injuries are caused by trauma or pathogens as explained above, and therefore elimination and treatment of the cause should be addressed in conjunction with the following treatment protocols.

Mild-moderate injuries

It is of paramount importance to control the inflammatory response within the cornea, following injuries, in order to preserve its clarity and vision (Kurpakus-Wheater et al., 2001). Although inflammation is a beneficial process that is required in the mechanism of wound healing, excessive levels of inflammation can lead to delayed corneal healing. Inflammation can be controlled via COX inhibitors or glucocorticosteroids. Early use of

steroids limits inflammation, protects the stroma from destruction and can prevent corneal opacity (Ashby et al., 2014; Gicquel, Bejjani, Ellies, Mercié, & Dighiero, 2007).

Anti-inflammatory medications are currently administered via eye drops. However, the major drawback when using eye drops is that most of the instilled drug is lost within the first 15-30 s due to high tear turn-over, rapid nasolacrimal drainage and conjunctival absorption. Moreover, only 5% of the drug successfully penetrates the cornea due to corneal barriers. As a result of this poor drug bioavailability, frequent administration of eye drops is required to achieve therapeutic outcomes. This is inconvenient for patients, especially if the eye is covered after surgery (Badawi, El-Laithy, El Qidra, El Mofty, & El Dally, 2008). Anti-inflammatory eye drops need to be administered every 2 h in the first 2 days, and then every 4 h (Kaczmarek, Tieppo, White, & Byrne, 2014).

BCLs are currently applied after eye surgeries, such as photorefractive keratectomy (PRK), to protect the eye after the removal of the corneal epithelium (Sánchez-González, López-Izquierdo, Gargallo-Martínez, De-Hita-Cantalejo, & Bautista-Llamas, 2019). Furthermore, they are used in cases of traumatic corneal abrasion to protect the injured cornea, reduce pain and promote healing. In both situations, topical medications containing either anti-inflammatory and/or antibiotic medication are prescribed. These patients would benefit from a drug-eluting BCL (Hui, Sheardown, & Jones, 2012).

Moderate-severe injuries

In some of the moderate and most of the severe corneal injuries, such as alkali burns, Steven-Johnson syndrome, post-radiation or after multiple surgeries, corneal limbal stem cells can be permanently damaged, therefore compromising the natural ability of the eye to regenerate new corneal epithelial cells (Pratoomsot et al., 2008).

The choice of treatment depends on the severity and the time since the primary injury. In cases of mild and partial limbal stem cell deficiency (LSCD), AM transplants can be effective. The presence of nutrients, anti-inflammatory regulators and growth factors in the AM, aid the re-epithelisation and reduction of inflammation, scarring, and vascularisation of the injured cornea, thereby promoting the expansion of the remaining limbal stem cells (Gheorghie, Pop, Mrini, Barac, & Vargau, 2016).

In severe cases, grafting small pieces of healthy limbal tissue from the **patient's other eye (limbal autografts)** or from the limbus of a **close relative (allograft)** is usually a successful treatment (Gheorghe et al., 2016). However, this is an invasive and expensive operation.

Another successful procedure used in various cases of LSCDs is stem cells transplants, which are usually fixed using AM sheets. Stem cells promote regeneration of the corneal epithelium and help restore epithelial clarity (Gheorghe et al., 2016), while the AM provides the required support, promoting cellular differentiation and proliferation throughout their formation into a new tissue (Y. Zhao & Ma, 2015).

1.1.5 Reason for utilisation of 3D-printing

After the approval of Spritam® (levetiracetam) as the first 3D-printed drug product in August 2015 (Fitzgerald, 2015), there has been a push to expand the 3D printing research for drug delivery and other medical applications. In the medical field, 3D printing technology can produce sophisticated and personalised products with viable market potential that can be made on-demand, increasing the safety margin, efficacy and accessibility of medicines (Norman, Madurawe, Moore, Khan, & Khairuzzaman, 2016). 3D-printing can allow the development of patient-specific, personalised BCLs for keratoconus patients or for BCLs with complex designs like lenses with hollow centre or mesh-like structure with a specific pore diameter. Moreover, cells can be incorporated in the bioink and printed into BCLs using 3D-bioprinting techniques. Therefore, this thesis aims to utilise the advantages that 3D-printing can bring to the field of medicated BCLs in the treatment of corneal injuries.

3D-printing in drug delivery

Drug delivery is the process of administering drugs or pharmaceutical compounds to their target site in the body for safely achieving their desired therapeutic effect (Jonathan & Karim, 2016; Tiwari et al., 2012). The conventional methods of fabrication of drug delivery systems might not be satisfactory for new therapies, which require advanced manufacturing techniques.

The capability of dispensing small volumes with accuracy, spatial control, and layer-by-layer assembly in 3D-printing allows for the preparation of devices and structures with

complex geometries, multiple active pharmaceutical ingredients and controlled release profiles. Also, the 3D-printed models can be easily modified before printing which reduces production costs and saves materials (J Long, Gholizadeh, Lu, Bunt, & Seyfoddin, 2016; Prasad & Smyth, 2016). Furthermore, geriatric and pediatric patients usually require personalized medication due to rapid modification of physiological and metabolic functions or due to dose adjustment (Buanz, Saunders, Basit, & Gaisford, 2011; Florence, 2010).

The microstructure and porosity of the drug delivery device (DDD) can be easily controlled by varying the parameters within the 3D-printing process. Traditional methods for producing matrix DDD with porous core structure include compression, moulding, solvent casting, the lost foam and vacuum forming methods. Conventional production methods can produce closed pores that are not permeable to liquids and entrap the drug hindering its release. Compared to conventional methods of fabrication, 3D-printing techniques have better control over pore sizes, connectivity, and distributions of internal pores (Cheah, Leong, Chua, Low, & Quek, 2002).

3D-printing in ocular medicine

The advances made in the use of 3D-printing in ophthalmology has led to the production of customised on-demand eyewear (W. B. Huang & Zhang, 2014). Currently, some metal or plastic devices and surgical instruments used by ophthalmologists are manufactured using 3D-printing (Canabrava et al., 2015; W. B. Huang & Zhang, 2014). Lupeanu et al. (2014) have developed an ophthalmic speculum and customised spatula using this technique (Lupeanu, Rennie, Rosu, & Moagar-Poladian, 2014). Moreover, 3D-printed sculptures and advanced models of a patient's eye are currently employed in some medical schools to introduce surgical techniques to students who can practice surgical procedures in a safe environment (Waran et al., 2014).

Moreover, 3D-printing technologies have been utilised in the fabrication of ocular prostheses (Ruiters, Sun, De Jong, Politis, & Mombaerts, 2016). Although ocular prosthesis has no function, it helps the patient psychologically and improves confidence (Ospina, Díaz, & Plaza, 2014). Initially, prostheses were fabricated by the impression-moulding method, which resulted in the poor fitting of the prosthesis (Ruiters et al., 2016). The 3D-printed impression-free mould omit the time-consuming steps of casting

and duplication of a conventional impression mould while ensuring a perfect fit for the patient (Abduo, Lyons, & Bennamoun, 2014).

1.2 Thesis aims

The primary aim of this thesis is to develop a novel 3D-printed medicated corneal bandage for the treatment of corneal injuries. Two types of therapeutics were loaded in the bandages prepared in this work: the first being an anti-inflammatory corticosteroid drug, Dexamethasone (DEX), used to reduce the inflammation of the injured cornea and promote self-regeneration post-surgeries or in cases of mild-moderate corneal injuries and the second being human corneal epithelial primary cells (HCEpC) used to compensate for the loss of corneal stem cells in moderate-severe corneal injuries and minimise the need for corneal grafts. In both types, the corneal bandage is designed to protect the injured cornea from the external environment and pathogens and act as a matrix to support the adhesion of the newly generated corneal cells thereby promoting rapid corneal healing.

The specific objectives of this thesis are:

- i. To develop a drug-loaded silicone hydrogel corneal bandage with suitable water content, mechanical properties and controlled release of DEX over the period of 1 week, which is the application time of the BCL.
- ii. To utilise the capabilities of 3D-printing technology of hydrogels in developing a drug-eluting gelatine bandage contact lens (BCL). The loaded DEX drug should have a controlled release profile over a period of 1 week.
- iii. To load HCEpC within a 3D-printed gelatine methacrylate (GelMA)/polyethylene glycol diacrylate (PEGDA) composite hydrogel meshes to be used as a potential cell carrier for tissue regeneration applications.
- iv. To develop a 3D-printed corneal bandage carrying HCEpC for the treatment of moderate-severe corneal injuries using various hydrogel compositions. The effect of hyaluronic acid (HA) and collagen incorporation within the GelMA hydrogel matrix on the properties of the 3D-printed bandages and the viability of the carried HCEpC will also be evaluated.

1.3 Thesis structure

This thesis consists of a general introduction (Chapter 1), a literature review (Chapter 2), four experimental chapters (Chapter 3-6), and a final general discussion (Chapter 7). The contents and rationales of the core chapters are described in the following section.

1.4 Thesis overview

Chapter 2: *Medicated ocular bandages and corneal health: potential excipients and active pharmaceutical ingredients.*

This chapter is a literature review discussing the current approaches for corneal regeneration treatments including amniotic membrane (AM) bandages, bandage contact lenses (BCL) and collagen shields in conjunction with frequent administration of therapeutic eye drops. The major drawback associated with eye drops is poor bioavailability and patient non-compliance that might lead to corneal wound healing complications and poor clinical outcomes. This review highlights the materials and therapeutics that can be used in medicated ocular bandages and various ways of incorporating drugs while discussing the limitations and challenges associated with developing medicated ocular bandages for clinical use. Hydrogel materials and therapeutics used in this thesis have been described in this literature review.

Chapter 3: *An all-in-one drug-eluting silicone hydrogel bandage contact lens (BCL) for post-surgical recovery and corneal injuries.*

Anti-inflammatories are prescribed after surgery and corneal injury to reduce inflammation and promote the natural mechanism of corneal healing. Due to the extremely low bioavailability of eye drops (<5%), frequent dosing of anti-inflammatories is required to achieve the desired clinical outcomes. Bandage contact lenses are currently applied prior to eye surgery and after traumatic corneal abrasion to protect the injured cornea, reduce pain and promote healing. However, topical medications containing either anti-inflammatories or antibiotics are prescribed. The delivery of therapeutics through contact lenses increase their resident time, control and extend their release and enhance their bioavailability to more than 50% when compared to the use of eye drops alone. Therefore, the aim of this chapter was to develop an all-in-one drug-eluting silicone hydrogel lenses to protect the injured eye while delivering

dexamethasone (DEX) as an anti-inflammatory medication over a period of 1 week. p(HEMA-co-TRIS-co-PDMS) lenses were prepared and the molar ratios of the comonomers were varied to investigate their effect on controlling the release of DEX and the mechanical properties of the BCLs.

Chapter 4: *3D-printed gelatine contact lens for ocular drug delivery of Dexamethasone.*

In this chapter, the use of hydrogels other than the traditional silicone hydrogels currently used for preparing contact lenses was explored. Gelatine hydrogels were chosen because they are clear, flexible and have high oxygen permeability. Moreover, their rheological properties allow their use as inks in extrusion-based 3D printers, which opens the door to a wide range of novel applications. Gelatine methacrylate (GelMA) hydrogel was used in this work to prepare the lenses via a photopolymerisation reaction. Different concentrations of Polyethylene glycol diacrylate (PEGDA) were tested to see their effect on DEX drug release profiles, water content and degradation of the prepared lenses.

Chapter 5: *3D-printing of GelMA/PEGDA composite hydrogel meshes as potential cell-carriers for tissue regeneration.*

In chapters 3 and 4, drug-eluting BCLs were loaded with DEX to reduce the inflammation and promote natural regeneration of the cornea in mild-moderate injuries. However, in cases of severe corneal injuries, limbal stem cell deficiency (LSCD) might occur, and thus the cornea loses its ability to regenerate, which results in scarring and loss of vision. Currently, corneal grafts or stem cell transplants are performed in severe cases of LSCD. However, these are invasive and expensive. Therefore, a novel non-invasive technique to deliver HCEpC to the injured cornea, via a 3D-printed hydrogel mesh carrier is proposed. The hydrogel mesh is placed on the ocular surface as a BCL to promote regeneration of the injured cornea, thereby eliminating the need for surgical intervention. Gelatine methacrylate (GelMA) is the most widely used hydrogel for creating 3D-printed scaffolds. However, it is difficult to print complex scaffolds entirely out of GelMA hydrogel due to its low stiffness and relatively low printing fidelity. Therefore, in this study, 3D-printed GelMA/Polyethylene glycol diacrylate (PEGDA) composite hydrogel meshes with high printing fidelity, adequate mechanical properties

and controllable degradation profiles will be developed and characterised as a cell carrier for BCL application and general tissue regeneration purposes.

Chapter 6: *3D-printed GelMA meshes as a cell-carrier for treatment of moderate-severe corneal injuries.*

In this chapter, other hydrogels were incorporated to GelMA hydrogel in the preparation of the BCL designed to carry HCEpC for the treatment of moderate-severe corneal injuries. Hyaluronic acid (HA) is a naturally occurring glycosaminoglycan of the extracellular matrix that has high water retention capabilities, adhesion properties and long ocular surface residence time. Moreover, HA becomes available, when an epithelial lesion is formed, to initiate the healing process in the injured cornea. Collagen (type I) is the most abundant stromal protein in the cornea and the main component of ECM and promotes proliferation and differentiation of epithelial cells. Therefore, HA and collagen were incorporated within the GelMA hydrogel mixtures to prepare the hydrogel meshes used as BCLs to analyse their effect on the mesh properties including shape, crosslinking, equilibrium swelling ratio, biodegradability and cell viability.

Chapter 7: *General discussion.*

The final chapter presents a quick thesis overview, interpretation of main thesis findings, thesis implications, study limitations and possible related future recommendations.

1.5 Research outputs arising from this thesis

1.5.1 Conference presentations

Zidan, G., Rupenthal, I.D., Greene, C., & Seyfoddin, A. (2019, July). 3D-printed hydrogel mesh as a human epithelial cell carrier for corneal regeneration. Poster presented at the 46th Annual Meeting & Exposition of the Controlled Release Society, Valencia, Spain.

Zidan, G., Rupenthal, I.D., Greene, C., & Seyfoddin, A. (2018, August). A 3D-printed contact lens for corneal healing. Presented at the 12th Annual Postgraduate Research Symposium, Auckland University of Technology, Auckland, NZ.

Zidan, G., Rupenthal, I. D., Greene, C., & Seyfoddin, A. (2017, June). A 3D-printed drug-eluting corneal bandage. *Translational Technologies between Benchtop and Bedside*. Presented in The MedTech Core Annual Conference, Auckland, NZ.

1.5.2 Journal publications

Zidan, G., Rupenthal, I. D., Greene, C., & Seyfoddin, A. (2018). Medicated ocular bandages and corneal health: potential excipients and active pharmaceutical ingredients. *Pharmaceutical development and technology*, 23(3), 255-260.

Al-Kinani, A. A., Zidan, G., Elsaid, N., Seyfoddin, A., Alani, A. W., & Alany, R. G. (2018). Ophthalmic gels: Past, present and future. *Advanced drug delivery reviews*, 126, 113-126.

Zidan, G., Rupenthal, I. D., Greene, C., & Seyfoddin, A. An all-in-one drug-eluting silicone hydrogel bandage contact lens (BCL) for post-surgical recovery and corneal injuries. *To be submitted*.

Zidan, G., Rupenthal, I. D., Greene, C., & Seyfoddin, A. 3D-printed gelatine contact lens for ocular drug delivery of Dexamethasone. *To be submitted*.

Zidan, G., Rupenthal, I. D., Greene, C., & Seyfoddin, A. 3D-printing of GelMA/PEGDA composite hydrogel meshes as potential cell-carriers for tissue regeneration. *To be submitted*.

Zidan, G., Rupenthal, I. D., Greene, C., & Seyfoddin, A. 3D-printed GelMA meshes as a cell-carrier for treatment of moderate-severe corneal injuries. *To be submitted*.

1.5.3 Book chapters

Zidan, G., Greene, C. and Seyfoddin, A. (2019). Formulation design in drug delivery. *Engineering Drug Delivery Systems*. Duxford, United Kingdom: Woodhead Publishing (An imprint of Elsevier).

Chapter 2 Medicated ocular bandages and corneal health: potential excipients and active pharmaceutical ingredients

Abstract

Corneal blindness can occur due to improper healing of the corneal tissues after induced injury or abrasion which can be accidental, pathogenic or after corneal surgery. Abnormal regulation of the healing mechanisms can lead to corneal opacity. Reducing inflammation and promoting epithelial wound healing is crucial for scar-free corneal recovery without eyesight complications. Current approaches for corneal wound healing involve amniotic membrane (AM) bandages, bandage contact lenses (BCL) and collagen shields in conjunction with frequent administration of therapeutic eye drops. The problem with eye drops is poor bioavailability and patient incompliance that might lead to corneal wound healing complications and poor clinical outcomes. Various methods have been proposed for loading drugs into medicated bandage lenses. There are advantages and limitations associated with each technique regarding the ease of manufacture, drug loading, release kinetics and suitability with various therapeutics and hydrogel types. There is still, however, no drug-eluting corneal bandage on the market despite the need for such a convenient and cost-efficient strategy for corneal wound healing. This review will highlight materials and therapeutics that can be used in medicated ocular bandages and various ways of incorporating drugs, while discussing the limitations and challenges associated with bringing medicated ocular bandages in the market.

2.1 Introduction

Corneal blindness can occur due to improper healing of the corneal tissues after induced injury or abrasion which can be accidental, pathogenic or after corneal surgery. Apart from acting as a protective shield from the external environment and pathogens, the cornea contributes to two-thirds of the eye's total focusing power. Abnormal regulation of the healing mechanisms can lead to corneal opacity (Klausner et al., 2007).

With cataract surgery being the most common procedure performed by ophthalmic surgeons worldwide (Lindstrom, 2015), and the constantly increasing numbers of refractive surgeries being performed, the need for new strategies for rapid scar-free corneal healing has gained even greater importance. Despite the safety of the procedures in current corneal and refractive surgeries, LASIK surgery generates at least 2% complications with irregular wound healing patterns (Ljubimov & Saghizadeh, 2015).

Moreover, corneal diseases are the second most common cause of blindness worldwide and can lead to serious corneal complications and loss of vision if not properly treated. If the abrasion involves more than half of the corneal surface, healing can take up to 5 days, and 28% of these patients will have recurrent symptoms for up to 3 months after injury (H. Dua & Forrester, 1987; Eke, Morrison, & Austin, 1999). Furthermore, recurrent corneal erosions (RCE), occurring due to the poor adhesion of the corneal epithelium to the underlying stroma, are quoted as being common due to the large number of associated conditions including trauma, epithelial dystrophies and systemic conditions such as diabetes (Das & Seitz, 2008; Ramamurthi, Rahman, Dutton, & Ramaesh, 2006).

Reducing inflammation and promoting epithelial wound healing is crucial for scar-free corneal recovery without eyesight complications. In this review, current approaches for corneal wound healing using ocular bandages will be discussed and current opportunities and limitations for their use highlighted.

2.2 The current practice of bandages

2.2.1 Amniotic membrane bandages

Amniotic membrane (AM) is an avascular fetal membrane harvested from placental tissue obtained from elective cesarean sections of pregnant women (Malhotra & Jain, 2014). Transplantation of AM has traditionally been utilised for ocular surface

reconstruction acting as a physical barrier that protects the cornea during the healing process and helps in reducing pain caused due to the friction of the eyelids with the injured corneal surface (Suri et al., 2013). Moreover, AM acts as a supporting matrix for the adhesion of epithelial cells and promotes wound healing due to its unique composition of hyaluronic acid, collagen and growth factors that have anti-angiogenic and anti-inflammatory functions (Hao, Ma, Hwang, Kim, & Zhang, 2000; Maharajan et al., 2007). However, AM is often associated with complicated processing such as extensive serological screening and critical handling and storage requirements. Moreover, AM can suffer from impaired transparency, poor mechanical strength and variable quality (Feng, Borrelli, Reichl, Schrader, & Geerling, 2014; Pratoomsoot et al., 2008; Wright, Mi, & Connon, 2013). Currently, there are relatively expensive in-clinic commercial products of AM bandages for the treatment of corneal diseases/conditions that require ocular surface reconstruction. Such marketed products include Prokera[®], AmbioDisc[™], BioDOptix[®], Aril[™] and Petil[™].

2.2.2 Bandage contact lenses (BCL)

Commercial silicone hydrogel bandage contact lenses (BCL) including Biofinity[®], ACUVUE[®], PureVision[®] and AIR OPTIX[®] are currently used after photorefractive keratectomy (PRK) to promote epithelial healing and control pain (Taylor et al., 2014). Clinical trials have shown a significant effect in pain relief after PRK surgery when applying topical eye drops in conjunction with BCL compared to topical medication alone (Cherry, 1996). Furthermore, extending the application of BCL from 4 to 7 days can enhance visual rehabilitation and reduce complications of post-surgical PRK patients (Mohammadpour et al., 2017).

2.2.3 Collagen shields

Collagen shields were first introduced in the late '80s as contact lens-shaped bandages fabricated from porcine scleral tissue that resembles the collagen of the human eye (C. H. Lee, Singla, & Lee, 2001; Poland & Kaufman, 1988), now there are currently marketed collagen shields by OASIS[®] Medical, Inc. (OASIS, n.d.). Collagen shields are used to promote corneal epithelial healing by protecting the injured cornea from the friction caused by blinking of the eyelids and from the external environment. They have also been used in the treatment of dry eye syndrome since they turn into lubricating gels

before they dissolve in 12, 24 or 72 h (Greenwald & Kleinmann, 2008). Moreover, corneal shields were found to prolong the contact time of topically applied medication after pre-soaking them in the drug solution (Agban, Lian, Prabakar, Seyfoddin, & Rupenthal, 2016; Colin, Malet, Chastel, & Richard, 1991; Willoughby, Batterbury, & Kaye, 2002).

2.3 Materials that can be used in medicated bandages

2.3.1 Collagen

Collagen is a biocompatible, biodegradable and very well tolerated biomaterial that is used in many medical applications including skin replacements, bone substitutes, artificial blood vessels and wound dressings (C. H. Lee et al., 2001). Being one of the major components of the extracellular matrix (ECM), it has a significant role in promoting cell adhesion, spreading and differentiation and therefore can promote corneal wound healing. Altering the strength and degradability of collagen bandages can be easily achieved through different degrees of cross-linking, which can also control the release rate of the entrapped drugs (Panduranga Rao, 1996; Weadock, Olson, & Silver, 1983).

2.3.2 Polymeric hydrogels

Hydrogels are the main components of ocular bandage lenses because of their hydrophilic nature and cross-linked polymeric networks that have high water absorbance capability (Peppas, Bures, Leobandung, & Ichikawa, 2000). Hydroxyethyl methacrylate (HEMA) and poly (hydroxyethylmethacrylate) (p-HEMA) are currently used in soft contact lens preparation and are the most common polymeric hydrogels utilised in drug-eluting contact lenses for controlled drug release up to 1 week. To increase the amount of the loaded drug and delay its diffusion, hydrophobic monomers such as 4-vinylpyridine (VP), or ionic monomers such as N-(3-aminopropyl)methacrylamide (APMA) can be incorporated into the hydrogel network to increase the interaction between the drug and the hydrogel molecules (Andrade-Vivero, Fernandez-Gabriel, Alvarez-Lorenzo, & Concheiro, 2007). Although those hydrogels lenses are soft and flexible, they have low gas permeability, and thus have to be removed daily (Filipe et al., 2016).

2.3.3 Silicone hydrogels

Silicone hydrogel contact lenses were introduced in the late '90s and gained high popularity since then due to their high oxygen permeability compared to polymeric hydrogels. This makes them suitable for use as extended wear contact lenses up to 30 days. Silicone hydrogel lenses are usually composed of siloxane macromer for enhanced oxygen permeability, that is copolymerised with a hydrogel phase consisting of a hydrophobic monomer such as tris[trimethylsiloxy] silylpropylmethacrylate (TRIS) and a hydrophilic monomer such as (N, N-dimethylacrylamide) (DMA), N-vinyl pyrrolidone (NVP) or HEMA. The hydrogel phase increases the lens wettability which is essential for comfort, adequate lens movement and sufficient ion transfer. Silicone hydrogel contact lenses can be used to deliver ophthalmic drugs to the eye with controlled release of medication from 20 days up to more than 3 months depending on the ratio between the hydrophobic and hydrophilic components (J. Kim, Conway, & Chauhan, 2008).

2.3.4 Hyaluronic acid

Hyaluronic acid is a naturally occurring anionic polysaccharide and an important component of the ECM that has shown the ability to control inflammation and promote corneal epithelial wound healing through stimulating corneal cell migration and proliferation (M. Inoue & Katakami, 1993; Nishida, Nakamura, Mishima, & Otori, 1991). The clinical applications of HA vary from cell culture and epithelial regeneration to cosmetic dermal fillers (Price, Berry, & Navsaria, 2007) and intra-articular injection improving joint motion and reducing pain in osteoarthritis patients (Moreland, 2003). In ophthalmology, HA is used in the treatment of dry eye syndrome due to its lubricating nature (Aragona, Papa, Micali, Santocono, & Milazzo, 2002) and to substitute the lost vitreous fluid during ocular surgeries (Kogan, Šoltés, Stern, & Gemeiner, 2007). Moreover, HA was able to prolong the release of topically applied ocular therapeutics (Cho et al., 2003).

2.3.5 Chitosan

Chitosan is a natural cationic polymer that is broadly used in topical dressings for wound healing in case of burns, due to its biocompatibility and antimicrobial activity, and in corneal tissue engineering (Jayakumar, Prabakaran, Kumar, Nair, & Tamura, 2011; Ozcelik et al., 2013; Rafat et al., 2008). The molecular weight, the degree of

deacetylation, ionic strength of chitosan and the pH of the medium are all factors that affect the anti-microbial capability of chitosan. Interestingly, the form of chitosan whether it is in solution, gel, film or combined with another material affects its anti-microbial effect as well (Dai, Tanaka, Huang, & Hamblin, 2011). It was found that chitosan can modulate the functions of inflammatory cells, accelerate wound healing through influencing the phases of the wound healing process (Cui, Lu, Teng, Li, & Li, 2017). Moreover, chitosan and chitosan derivatives can be used as drug and growth factors carrier while enhancing their permeability (Bernkop-Schnürch & Dünnhaupt, 2012).

2.4 Medications for corneal wound healing

2.4.1 Anti-inflammatory medication

Inflammation is triggered by corneal injury. Although inflammation is a beneficial process that is required in the mechanism of wound healing, excessive inflammation can lead to delayed corneal healing. Inflammation can be controlled via corticosteroids or non-steroidal anti-inflammatory medication. The early use of steroids limits inflammation protects the stroma from destruction and can prevent corneal opacity during the wound healing process; however, excessive use of corticosteroids can delay wound closure or induce glaucoma. Therefore, the use of steroids in corneal wound healing should be carefully managed (Ashby et al., 2014; Gicquel et al., 2007; Kadmiel, Janoshazi, Xu, & Cidlowski, 2016).

2.4.2 Growth factors

The effectiveness of growth factors in corneal wound healing has been clinically proven. Epidermal growth factor (EGF), hepatocyte growth factor (HGF) and transforming growth factor (TGF-1) are growth factors present in the human tears that can be used to stimulate epithelial growth. Exogenous EGF helps in corneal epithelial wound repair through promoting migration and proliferation of the epithelial cells. However, it is not always beneficial to use growth factors in corneal regeneration since they can inhibit corneal epithelial proliferation as in the case of TGF- α and TGF- β or overstimulate the healing process leading to scarring as in the case of fibroblast growth factor FGF (Agrawal & Tsai, 2003; Ashby et al., 2014).

2.4.3 Stem cells

Stem cell transplantation is the most significant clinical advance in the repair of damaged corneal epithelium in patients suffering from stem cell loss, mechanical trauma (including surgical) or burns due to their unique capabilities of stem cells, which allow them to differentiate into multiple lineage cells (C. C. Hsu et al., 2015; Ljubimov & Saghizadeh, 2015). Limbal epithelial stem cell (LESC) grafts are currently used for ocular surface reconstruction in the case of total limbal stem cell deficiency (C. C. Hsu et al., 2015). The most common sources of stem cells for clinical use are embryonic, adult and induced stem cells, with various advantages and limitations associated with each type (C. C. Hsu et al., 2015). Limbal stem cells can be grown ex-vivo onto AM or plastic tissue culture wells and then transferred to the surface of the eye through bandage lenses, fibrin gel or collagen shields (Rauz & Saw, 2010). Furthermore, autologous limbal grafts harvested from the patient's healthy eye can be delivered to the injured eye using amniotic membrane or contact lenses (Amescua, Atallah, Nikpoor, Galor, & Perez, 2014; Di Girolamo et al., 2009).

2.5 Strategies for drug entrapment

2.5.1 Soaking of corneal bandage

Several methods have been utilised to incorporate drugs into contact lenses; the simplest of which is soaking commercially available lenses or collagen shields in the drug solution to entrap the drug in the internal channels of the hydrogel (Xinming et al., 2008; J. Xu, Li, & Sun, 2011). The soaking method is straightforward and cost-effective and can be done with commercially available contact lenses (A. M. Ribeiro, Figueiras, & Veiga, 2015). The ability of commercially available soft contact lenses to act as a drug reservoir is related to the water content and the thickness of the lens, the concentration of the drug solution and the soaking time of the lens (Xinming et al., 2008). The soaking technique is limited only to small molecular weight and hydrophilic therapeutics and suffers from low entrapment, and fast diffusion of the drug from the lens and so frequent replacement of the lens is required making this less cost-effective and inconvenient for the patient (C.-C. Li & Chauhan, 2006; Xinming et al., 2008).

2.5.2 Surfactants and nanoparticles

Several techniques were employed for loading therapeutics in hydrogel contact lenses including surfactant aggregates and colloidal nanocarriers. Surfactant aggregates of Cyclosporine A have been successfully loaded into a hydrogel matrix resulting in the extension of the drug release profile with a linear release rate for more than 7 days and up to 29 days with a non-linear release profile (Kapoor & Chauhan, 2008). Others have used β -cyclodextrin as a complexing agent to enhance drug loading and prolong the release to more than 3 weeks, especially in the case of small molecular weight drugs (dos Santos et al., 2009; dos Santos, Couceiro, Concheiro, Torres-Labandeira, & Alvarez-Lorenzo, 2008). Colloidal nanocarriers including nanoparticles, nanoemulsions, nanosuspensions and liposomes can also be used to load drugs into contact lenses for more control over the release profile. The nanosize of the colloidal carriers allows the entrapment of lipophilic drugs within the hydrophilic hydrogel matrix without affecting the transparency of the lens. Furthermore, the encapsulation of therapeutics within the nanocarriers protect them from ocular enzyme degradation, thereby enhancing their bioavailability (Hu et al., 2011).

2.5.3 Molecular imprinting

Molecular imprinting is one of the techniques used to increase the drug loading capacity and control drug release through creating voids within the hydrogel macromolecular network that have a high affinity for the targeted drug. This technique increases the drug loading capacity and offers control over the release of therapeutics (Maulvi, Soni, & Shah, 2016). Those biomimetic hydrogels can extend the drug release for up to 1 week in the case of HEMA hydrogel lenses (Andrade-Vivero et al., 2007), or up to 2 months with silicone hydrogel lenses (Charles J White, McBride, Pate, Tieppo, & Byrne, 2011). However, it is difficult to produce a molecularly imprinted contact lens that controls the release of more than one drug. Moreover, molecular imprinting requires a high degree of crosslinking of the hydrogel, which might alter the lens elasticity, water content or oxygen permeability (K.-H. Hsu, S. Gause, & A. Chauhan, 2014).

2.5.4 Multilayer contact lenses

The use of multilayer contact lenses is another useful technique for entrapping drugs in bandage lenses. A thin ring-shaped layer of poly(lactic-co-glycolic) acid (PLGA) polymer

film holding the drug is sandwiched between two layers of p-HEMA hydrogel to control the release of the medication within the lens (Ciolino, Hoare, et al., 2009). The PLGA film has proven effective in controlling the release rate of various drugs in a zero-order manner for 1 month through adjusting the drug/polymer ratio and/or the molecular weight of the polymer (Ciolino, Dohlman, & Kohane, 2009; Ciolino et al., 2011). However, the effect of sterilisation and storage on the release of the drug into the hydrogel matrix should be considered to prevent loss of medication or a burst release effect (K. H. Hsu, S. Gause, & A. Chauhan, 2014).

2.6 Important considerations and potential applications

Drug delivery using bandage lenses were introduced in the late '60s by Wichterle et al. as a convenient non-invasive way to deliver ophthalmic drugs to the anterior eye segment (Wichterle & Lim, 1960). It is surprising that even five decades after the introduction of medicated ocular bandage lenses which have proven benefits, there are still no marketed products except for the naturally medicated AM bandages despite the obvious need. Apart from the technical challenges, there are high costs associated with clinical trials and the regulatory hurdles (K. H. Hsu et al., 2014). However, a well-designed medicated bandage lens will offer a safe, patient-friendly and efficient solution to many chronic patients that are having trouble adhering to the regular administration of ophthalmic medication via eye drops or in critical cases where frequent administration of therapeutics is required. It is worth mentioning that BCLs have to be handled with care and high hygiene, same as handling refractive contact lenses, to prevent the risk of infection.

For successful drug delivery using medicated bandage lenses, certain parameters have to be adjusted to overcome critical challenges during the design, manufacturing and storage processes. It is crucial to maximise the drug loading capacity for successful controlled delivery of the medication with no burst release to maintain the drug concentration between the minimum effective concentration (MEC) and the maximum safe concentration (MSC). Physical and surface properties such as shape, thickness, transparency, modulus, wettability, ion and oxygen permeability, protein and lipid binding must also be considered (L. W. Jones, Chauhan, Di Girolamo, Sheedy, & Smith III, 2016). Moreover, drug and content stability of medicated bandage lenses is of

paramount importance during preservation and storage (Xinming et al., 2008). Vitamin E is a biocompatible diffusion barrier that has proved to be effective in controlling the release of loaded drugs that can limit their diffusion during storage time (Dixon et al., 2015; Peng, Kim, & Chauhan, 2010). It can also enhance the stability of the loaded drugs, reduce water dehydration from the lens and act as a UV barrier (K.-H. Hsu, Fentzke, & Chauhan, 2013). Using a small volume of the packaging liquid and storing the BCL in refrigerated conditions might be useful to minimise the amount of drug diffusing out (Jung & Chauhan, 2012). Sterilisation of medicated BCL is another challenge since autoclaving can cause degradation of the loaded drugs so that the drugs can be added under sterile conditions after the autoclaving step or another way of sterilisation, such as radiation, may be adopted (Dixon et al., 2015).

The development of new materials, novel technologies and improved drug delivery devices must go hand in hand with the development of better pharmacotherapeutic agents for faster and more effective corneal healing. We now have a better understanding of the various pathways and mechanisms of wound healing, and this has led to the discovery of new therapeutic targets. Many of these newer therapies are still in the pipeline but have already shown great potential in pre-clinical and early clinical trials. The modulation of gap junctions, the channels of communication between cells, via the use of antisense peptides have shown much promise (Becker, Phillips, Duft, Kim, & Green, 2016; Ormonde et al., 2012). Nexagon[®] is one such peptide that transiently blocks the expression of Connexin43, a ubiquitous gap junction protein, thereby reducing the channels of communication between cells and stopping the spread of inflammation. It is currently being taken into a Phase III clinical trials for persistent epithelial defects by OcuNexus Therapeutics Inc (USA).

Topical mesenchymal stem cell treatment is another new area of research which has shown great potential. The topical application of autologous MSCs obtained from adipose tissue has been shown to bring about the closure of persistent epithelial defects (Agorogiannis, Alexaki, Castana, & Kymionis, 2012). However, research into the mechanisms of action and longevity of the treatment remains to be investigated and as such this treatment option has largely remained experimental.

Clearly, there are great strides being made in the development of new safe and effective ocular wound healing therapeutics. However, such advances also bring to the forefront the necessity of new and improved drug delivery techniques. Advancement in both these areas will ensure the success of future strategies.

2.7 Conclusion

Corneal blindness is a leading cause of visual impairment worldwide that can affect all age groups (World Health Organization, 2005). It can occur due to improper healing of the corneal tissue after induced injury or abrasion. With the high number of cataract and refractive surgeries being performed worldwide and corneal diseases being a common cause of blindness, rapid and scar-free healing of the cornea is crucial for improved wound healing and visual outcomes (Klausner et al., 2007). Various methods have been proposed for loading drugs into medicated bandage lenses. There are advantages and limitations associated with each technique regarding the ease of manufacture, drug loading, release kinetics and suitability with various therapeutics and hydrogel types. There is still, however, no drug-eluting corneal bandage on the market despite the need for such a convenient and cost-efficient strategy for corneal wound healing, especially in conditions where extensive topical treatment with eye drops is required such as corneal ulcers and infections.

**Chapter 3 An all-in-one drug-eluting
silicone hydrogel bandage contact
lens (BCL) for post-surgical
recovery and corneal injuries.**

Abstract

Anti-inflammatories are prescribed after surgeries and corneal injuries to reduce inflammation and promote the natural mechanism of corneal healing. Due to the extremely low bioavailability of eye drops (<5%), frequent dosing of anti-inflammatories is required to achieve the desired clinical outcomes. Bandage contact lenses (BCL) are currently applied following eye surgeries and traumatic corneal abrasion to protect the injured cornea, reduce pain and promote healing. However, topical medications containing either anti-inflammatories or antibiotics are prescribed. The delivery of therapeutics through contact lenses increase their resident time, control and extend their release and enhance their bioavailability to more than 50% compared to eye drops. The aim of this chapter is to develop an all-in-one drug-eluting silicone hydrogel lenses to protect the injured eye while delivering dexamethasone (DEX) as an anti-inflammatory medication over a period of 1 week. p(HEMA-co-TRIS-co-PDMS) lenses were prepared and the molar ratios of the co-monomers were varied to see their effect on controlling the release of DEX and the mechanical properties of BCLs. Extended release of DEX for up to 14 days was achieved in the prepared lenses with comparable mechanical properties to commercial silicone hydrogel contact lenses. It can be concluded that p(HEMA-co-TRIS-co-PDMS) can be used to prepare silicone hydrogel BCLs that are capable to deliver drugs to the injured cornea, which enhances patients-dose compliance and thus results in better clinical outcomes.

3.1 Introduction

The first step in developing a novel medicated corneal bandage for the treatment of corneal injuries was to look at the currently available BCLs that are used as a mechanical support and corneal cover in certain corneal injuries. Then try to develop a novel therapeutic BCL and load it with the anti-inflammatory drug DEX to be used in cases of mild/moderate corneal injuries and post corneal surgeries instead of currently used eye drop treatment that has very low bioavailability.

Apart from acting as a protective shield from the external environment and pathogens, the cornea contributes to 65-75% of the eye's total focusing power. A clear, transparent and scar-free cornea is, therefore, necessary for proper vision. Unfortunately, corneal blindness is a leading cause of irreversible visual impairment worldwide and can affect all age groups (World Health Organization, 2005). This occurs due to improper healing of the corneal tissues after induced injury or abrasion that can be accidental (chemical or burns), pathogenic (bacterial, viral or fungal infection) or after corneal surgery (cataract or refractive). With the increase in corneal surgeries such as cataract and refractive surgeries, the need for treatments that support rapid and scar-free corneal healing has become essential (Ljubimov & Saghizadeh, 2015; Riley, Grupcheva, Malik, Craig, & McGhee, 2001).

Anti-inflammatories are prescribed post-surgeries and following corneal injuries to reduce inflammation, oedema and promote the natural mechanism of corneal healing (El-Harazi & Feldman, 2001; Kaczmarek et al., 2014). Due to the extremely low bioavailability of eye drops (<5%), frequent dosing of anti-inflammatories is required to achieve the desired clinical outcomes. The eye drops need to be administered every 2 h in the first 2 days, and then every 4 h (Kaczmarek et al., 2014). This requires the patient to open the eye bandage following the surgery several times a day to apply the eye drops and is inconvenient. This can also lead to patient non-compliance that might cause post-operative complications including pain, interstitial keratitis and endophthalmitis, which are related to poor sealing of the wound site (Jabs, Mudun, Dunn, & Marsh, 2000).

The delivery of therapeutics through contact lenses increases their residence time, controls and extends their release and enhances their bioavailability to more than 50% when compared to eye drops (Jung, Abou-Jaoude, Carbia, Plummer, & Chauhan, 2013).

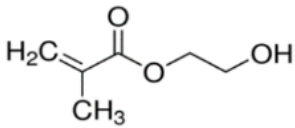
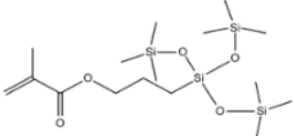
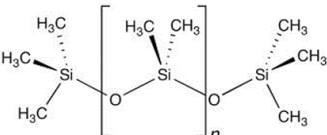
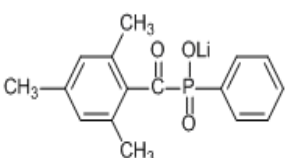
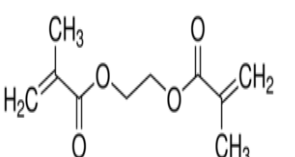
Moreover, since the release rate of therapeutics from a contact lens is close to the rate of corneal drug adsorption, less drug is lost during tear drainage (C. J. White & Byrne, 2010). This enables administration of lower drug doses, and therefore less local and systemic toxicity (Kaczmarek et al., 2014). BCLs are currently applied post-surgeries such as photorefractive keratectomy (PRK) to protect the eye after the removal of the corneal epithelium. Furthermore, they are used after traumatic corneal abrasion to protect the injured cornea, reduce pain and promote healing (Sánchez-González et al., 2019; Taylor et al., 2014). In both cases, topical medications containing either anti-inflammatories and/or antibiotics are prescribed, such patients would benefit from a drug-eluting BCL (Hui et al., 2012).

Contact lenses made of optically clear hydrogels are designed to fit on the eye in a stable and tolerated manner. Polymerised hydroxyethyl methacrylate (pHEMA) is the main hydrophilic monomer used in the preparation of soft contact lenses. It can be used alone in conventional hydrogel contact lenses for daily use or with siloxane monomers in silicone hydrogel-based contact lenses for extended use (Nicolson & Vogt, 2001). The incorporation of the hydrophobic siloxane monomers within the hydrogel matrix in silicone hydrogel lenses enhances oxygen and ion permeability, and thus prevent corneal hypoxia and neovascularisation, which cause oedema, blurred vision and increased risk of infection (Ang & Efron, 1990; Ćuruvija-Opačić, 2007; Paterson, Liu, Brook, & Sheardown, 2015; Weeks, Luensmann, Boone, Jones, & Sheardown, 2012).

In silicone hydrogel lenses, usually consists of chains of siloxane derivatives, one hydrophobic monomer and one or more hydrophilic monomer. Examples of hydrophobic monomers include polydimethylsiloxane (PDMS); 3-methacryloxy-2-hydroxypropyloxy propylbis (trimethylsiloxy) methylsilane (TRIS), tris-(trimethylsiloxypropyl) propylvinyl carbamate (TPVC), poly(dimethylsiloxy) di(silylbutanol) bis(vinyl carbamate) (PBVC); Exemplars of hydrophilic monomers include 2-hydroxyethyl methacrylate (HEMA); N,N-dimethyl acrylamide (DMA), N-Vinyl-2-Pyrrolidone (NVP), and N-vinylacetamide (NVA) and polyvinylpyrrolidone (PVP) (Gonzalez-Mejome et al., 2014; L. Jones & Powell, 2013). Surprisingly, there hasn't been enough research on tailoring the drug release rate from drug-loaded silicone hydrogel contact lenses by altering the monomer lens composition and the network structure, while maintaining sufficient mechanical properties for clinical use.

In this chapter, drug-loaded p(HEMA-co-TRIS-co-PDMS) silicone hydrogel lenses were prepared and the molar ratios of the co-monomers were varied in the tested hydrogel formulations to control the release of the hydrophobic steroid, dexamethasone (DEX). DEX acts as an anti-inflammatory drug that helps to control pain, swelling and redness of the injured eye (Kaczmarek et al., 2014). The silicone hydrogel lenses were prepared using Ethylene glycol dimethacrylate (EGDMA) as a crosslinker (Lasowski & Sheardown, 2016) and Lithium Phenyl(2,4,6-trimethylbenzoyl)phosphinate (LAP) as a photoinitiator. Table 3.1 shows the structure and function of the materials, used in this work, to prepare the different formulations of p(HEMA-co-TRIS-co-PDMS) silicone hydrogels.

Table 3.1. Materials used and their role in the preparation of silicone hydrogel lenses.

Name	Function	Structure
HEMA 2-hydroxyethyl methacrylate	Hydrophilic polymer	
TRIS Methacryloxy-propyltris (trimethylsiloxy) silane	Hydrophobic monomer	
PDMS Poly (dimethylsiloxane)	Hydrophobic macromer	
LAP Lithium Phenyl(2,4,6-trimethyl benzoyl) phosphinate	Photoinitiator	
EGDMA Ethylene glycol dimethacrylate	Crosslinker	

HEMA and PDMS were selected in this study because they are popular monomers that are used together in commercial contact lenses such as ACUVUE® OASYS®, ACUVUE® Advance®, and ACUVUE® TruEye® by Johnson and Johnson (Soluri, Hui, & Jones, 2012). PDMS is incorporated as an oxygen permeability enhancing monomer, while it has been reported that the use of HEMA prolonged the drug release profile from a drug-loaded

silicone hydrogel lens compared to the use of DMA as the hydrophilic monomer, which was contributed to the lower resistance to diffusion of DMA monomers compared to pHEMA (Guidi, Hughes, Whinton, Brook, & Sheardown, 2014). TRIS was chosen as another hydrophobic co-monomer to test its effect on controlling the drug release of DEX from the prepared silicone hydrogel BCLs. Previous studies showed the prolonged release of the incorporated drugs for more than 3 months using TRIS as a comonomer (J. Kim et al., 2008). Moreover, TRIS has been previously incorporated with the siloxane macromer lotrafilcone in the preparation Air OPTIX™ and Air OPTIX™ NIGHT&DAY contact lenses by CIBA VISION (M. Yang et al., 2016).

3.2 Materials and methods

3.2.1 Materials

Dexamethasone (DEX) was purchased from Flem Pharma, Shanghai, China. Methacryloxypropyltris(trimethylsiloxy)silane, SIM6487.6 (TRIS) with Mwt. of **422.82** g/mol and Methacryloxypropyl terminated polydimethylsiloxane, DMS-R18 (PDMS) with Mwt. of 4500-5500 g/mol from Gelest Inc., Pennsylvania, USA. Lithium phenyl-2,4,6-trimethylbenzoylphosphinate (LAP) from Allevi, Philadelphia, USA. Ethylene glycol dimethacrylate (EGDMA), 2-hydroxyethyl methacrylate (HEMA) and Phosphate buffered saline (PBS) tablets 1.0 M, pH 7.4 (25 °C) from Sigma-Aldrich, New Zealand. All other chemicals were of analytical grade.

3.2.2 Preparation of silicone hydrogel lenses

In order to determine the light intensity suitable for curing the hydrogels, 2 similar hydrogel formulations made from a mixture of HEMA, 1% EGDMA and 0.5% LAP were cured under either 24 or 48 W, and the resulting crosslinked pHEMA hydrogel films were visually evaluated. The pHEMA hydrogel lenses were prepared by mixing HEMA, EGDMA and LAP in a dark vial, on a magnetic stirrer, for 2 h until the LAP dissolves. The mixture was then sonicated in ice for 15 min to remove oxygen and enhance the photopolymerisation reaction. The sonicated hydrogel mixture was injected between two acrylic plates, that have a U-shaped spacer, of a 0.35 mm thickness, in between. The sheets holding the hydrogel were put under LED light at 405 nm, using an intensity of either 24 or 48 W, for 120 s. Figure 3.1 shows the SUNUV apparatus used to cure the

hydrogel films. The cured films were left overnight, soaked in distilled water to wash the unreacted monomers, then cut into circles with a cork borer 13 mm in diameter.

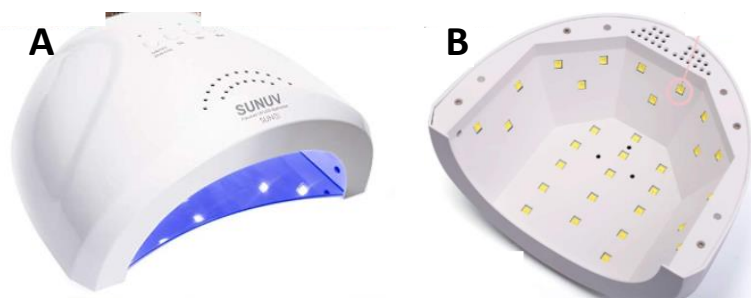


Figure 3.1. SUNUV apparatus used for curing of films. Top view of the device (A) and an inverted view showing the small lamps working under 405 nm (B).

In order to determine the best concentration of EGDMA required to polymerise the silicone hydrogel formulations. Three silicone hydrogel formulations containing 0.75 mole% PDMS, 10 mole% TRIS and 89.25 mole% HEMA were prepared with either 1, 2 or 3% w/w EGDMA and the produced films were visually compared.

Nine formulations of various molar ratios of the hydrophobic monomers (TRIS and PDMS) were copolymerised with the hydrophilic monomer (HEMA) to produce the drug-loaded $p(\text{HEMA-co-TRIS-co-PDMS})$ films. Table 3.2 shows the composition of each hydrogel formulation. Two grams of each formulation was prepared by dissolving LAP in the EGDMA/HEMA mixture, as previously mentioned. DEX was dissolved in 1 g of isopropanol, then the PDMS and TRIS were added. The aqueous solution was added to the alcoholic solution and vortexed, then nitrogen gas was bubbled for 15 min to deoxygenate the mixture. The volume of isopropanol evaporated during bubbling the N_2 gas was compensated and the mixture was degassed in ice using a sonicator for 10 min. The sonicated mixture was injected in between two acrylic plates, with a U-shaped spacer of a thickness of 0.35 mm to produce a film with uniform thickness, then cured for 8 min under 24W 405 nm LED light. The film was carefully removed from the sheets and dried in a vacuum oven at room temperature for 4 days to remove the alcohol. Each dried film was washed in 100 ml of DI water for 24 h to get rid of the unreacted monomers, which was confirmed by spectrophotometric analysis of the washing water. The washed films were cut into circular lenses using a cork borer of 13 mm in diameter, dried in a vacuum oven at room temperature, and kept dry until further characterised.

Table 3.2. Silicone hydrogel formulations prepared using various molar ratios of PDMS and TRIS.

Formula code	PDMS (mole%)	TRIS (mole%)	HEMA (mole%)	EGDMA (% w/w)	LAP (% w/w)	DEX (% w/w)
1P 5T	1	5	94	3	0.5	1
1P 10T	1	10	89	3	0.5	1
1P 20T	1	20	79	3	0.5	1
2P 5T	2	5	93	3	0.5	1
2P 10T	2	10	88	3	0.5	1
2P 20T	2	20	78	3	0.5	1
3P 5T	3	5	92	3	0.5	1
3P 10T	3	10	87	3	0.5	1
3P 20T	3	20	77	3	0.5	1

Furthermore, 8 hydrogel formulations were prepared with 10 mole% TRIS and various molar ratios of PDMS to see the effect of incorporating DEX within the hydrogel formulation. Thus, 4 of those formulations contained 1% DEX and 4 had no drug incorporated. EGDMA (3%) and LAP (0.5%) were added as a crosslinker and photoinitiator, respectively. All the variations within the prepared hydrogel formulations are listed in Table 3.3 below.

Table 3.3. Silicone hydrogel formulations prepared using various molar ratios of PDMS with and without DEX loading.

PDMS (mole%)	TRIS (mole%)	HEMA (mole%)	EGDMA (% w/w)	LAP (% w/w)	DEX (% w/w)
0.5	10	89.5	3	0.5	-
0.5	10	89.5	3	0.5	1
0.75	10	89.25	3	0.5	-
0.75	10	89.25	3	0.5	1
1	10	89	3	0.5	-
1	10	89	3	0.5	1
1.5	10	88.5	3	0.5	-
1.5	10	88.5	3	0.5	1

3.3 Characterisation of hydrogel lenses

3.3.1 Fourier transform infrared (FTIR) analysis

Liquid mixtures and crosslinked films of each formulation were analysed using a Nicolet iS10 FTIR spectrophotometer (Thermo Scientific, USA). The samples were tested at attenuated total reflectance (ATR) mode using a diamond ATR crystal. The spectra of the samples were recorded in the range of 4000-400 cm^{-1} with an average of 32 scans at a resolution of 4 cm^{-1} .

3.3.2 Swelling studies

The amount of water that each lens can hold was determined gravimetrically using a sensitive balance. Three vacuum dried lenses from each hydrogel formulation were weighed (DW), then they were immersed in 3 ml PBS for 24 h, blotted gently with tissue papers and then reweighed to record the swollen weight (SW). The equilibrium water content (EWC) of all hydrogel formulations were calculated using the following equation **Error! Reference source not found.**(Guidi et al., 2014).

$$EWC (\%) = \frac{(SW - DW)}{DW} \times 100$$

3.3.3 Drug content and release

To determine the effect of hydrophobic monomers on retaining the drug within the hydrogel films during the washing period, the theoretical drug content (per gram) of each polymerised hydrogel film was calculated and compared to the practical drug content remaining after the washing phase. Moreover, the washing water of each film was measured using UV spectrophotometry (Ultrospec 7000, BIOCHROM, UK) at an absorption wavelength of 242 nm to determine the percentage of drug lost during the washing period.

The *in vitro* drug release profiles of DEX from the hydrogel cut lenses were studied in 5 ml PBS buffer (pH=7.4) in a 15 ml conical tubes with caps on at 50 rpm on a benchtop shaker (SK-300, Lab Companion, Korea), placed in an incubator room that was maintained at 35 ± 2 °C. for a period of 14 days. At predetermined time intervals (1, 2, 3, 4, 5, 6, 7, 8, 9, 10 and 13 days), the whole 5 ml of the incubation media from each sample was collected and replaced by fresh media to maintain sink conditions. The

concentrations of DEX in the release media were determined by UV spectrophotometry (Ultrospec 7000, BIOCHROM, UK) against a calibration curve at an absorption wavelength of 242 nm.

The cumulative concentration of DEX released as ($\mu\text{g}/\text{lens}$) and the cumulative concentration released as (%) of the total remaining DEX in the lenses after the washing phase were plotted against time for each sample. Three lenses of each hydrogel formulation were tested, and the results were presented as a mean value \pm SD.

3.3.4 Mechanical properties

The Young's modulus and the tensile strength of the printed bandage were determined by TA.TX *Plus C* Texture Analyser (Stable Micro Systems, Ltd, England, UK). The washed hydrogel film was cut into square pieces of 20 x 20 mm and the fully swollen hydrogel pieces were placed in-between a film support rig and punctured by a 5mm spherical probe at a rate of 0.5 mm/s as shown in Figure 3.2.



Figure 3.2. The film support rig with 5 mm spherical probe placed on TA.TX *Plus C* Texture Analyser (Adopted from (Smewing, 2015)).

The stress versus strain values for the polymer films were plotted using the texture analyser software, and Young's modulus was determined by calculating the slope of the stress versus strain curve in the linear region (Kaczmarek et al., 2014). The tensile

strength of the films was recorded by using the maximum force applied until the breakpoint is reached (ElShaer et al., 2016; Gilhotra & Mishra, 2008).

3.3.5 Statistical analysis

Data were subjected to one-way analysis of variance (ANOVA) using Microsoft 365 Excel. Post hoc multiple comparisons were determined by the Tukey's test with the levels of significance set at $P < 0.05$. All data were presented as means \pm SD.

3.4 Results and discussion

3.4.1 Preparation of silicone hydrogel lenses

HEMA liquid hydrogel monomers undergo a polymerisation reaction to prepare the commercially known soft hydrogel lenses. Light initiates a free radical chemical reaction in the presence of a photoinitiator, which crosslinks the hydrogel monomers to form a stable polymer with reasonable mechanical properties (Gonzalez-Meijome et al., 2014). Each photoinitiator works under a specific wavelength to initiate this free radical reaction. LAP photoinitiator, which is used in this study, works under a wavelength of 405 nm.

The pHEMA hydrogel lenses cured under 405 nm light with an intensity of 24 W for 120 s were clear and showed good mechanical properties, however, the ones that were cured under the intensity of 48 W were opaque and very weak as shown in Figure 3.3. This indicates that the intensity of 48 W was too high and had a negative effect on the polymerised hydrogel.

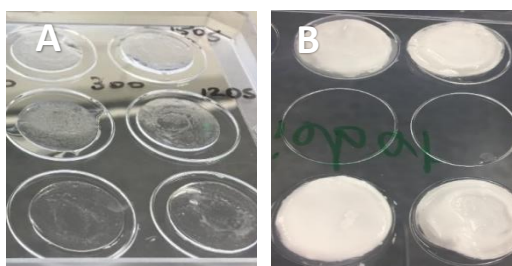


Figure 3.3. The effect of the curing intensity on pHEMA hydrogel lenses, 1%EGDMA and 0.5% LAP. Curing under 24 W (A) and curing under 48 W (B).

Moreover, the cured films prepared using 1 and 2% EGDMA were very weak and couldn't withstand removing from the sheets and cutting. On the other hand, the 3% EGDMA

was the minimum crosslinker concentration that produced well-cured films, that are flexible, yet easy to handle as seen in Figure 3.4.



Figure 3.4. The effect of the crosslinker concentration on silicone hydrogel films containing 0.75 mole% PDMS, 10 mole% TRIS and 0.5% LAP. Films shown had EGDMA concentrations of either 1% (A), 2% (B) and 3% (C).

All lenses of the drug-loaded silicone hydrogel formulations with various monomer ratios had smooth surfaces and had sufficient mechanical properties to handle all the characterisation tests performed. Figure 3.5 shows sample lenses prepared from the nine formulations stated in Table 3.2 above with various molar ratios of PDMS and TRIS. From visual examination of the BCLs shown in Figure 3.5, the lenses with the lowest TRIS conc (5 mol%) were more transparent than the higher concentrations (10 and 20%).

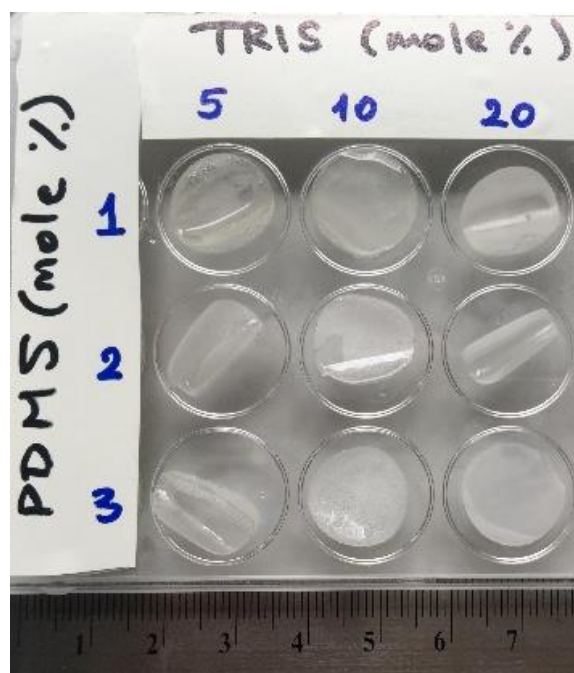


Figure 3.5. Image of drug-loaded silicone hydrogel lenses prepared using 1, 2 or 3 mole% PDMS with either 5, 10 or 20 mole% TRIS.

3.4.2 Fourier transform infrared (FTIR) analysis

The polymerisation reaction of HEMA hydrogel using the crosslinker EGDMA is presented in Figure 3.6. The FTIR spectrum of the hydrogel liquid (Liq) and crosslinked films (CF) with the drug (D) or with no drug (ND) are presented in Figure 3.8. The peaks showing in the range of 3150–3600 cm^{-1} are attributed to the stretching of the hydroxyl (O-H) groups; 2800–3050 cm^{-1} are related to the CH stretching of methyl groups ($-\text{CH}_3$) and methylenes ($-\text{CH}_2-$). The peak 1718 cm^{-1} within the 1680-1780 cm^{-1} region relates to the stretching vibration of the free (C=O), and the band at 1646 cm^{-1} within the 1610-1660 region is attributed to the bending vibration of the -OH groups (Su, Zhou, Zhang, Liu, & Zhang, 2016). The complete crosslinking of the pHEMA hydrogel was confirmed by the disappearance of the C=C stretching peak at **1638 cm^{-1}** in all the crosslinked films (CF) (Kusuma, Gunawan, Smith, & Freeman, 2010; D. Zhao et al., 2015).

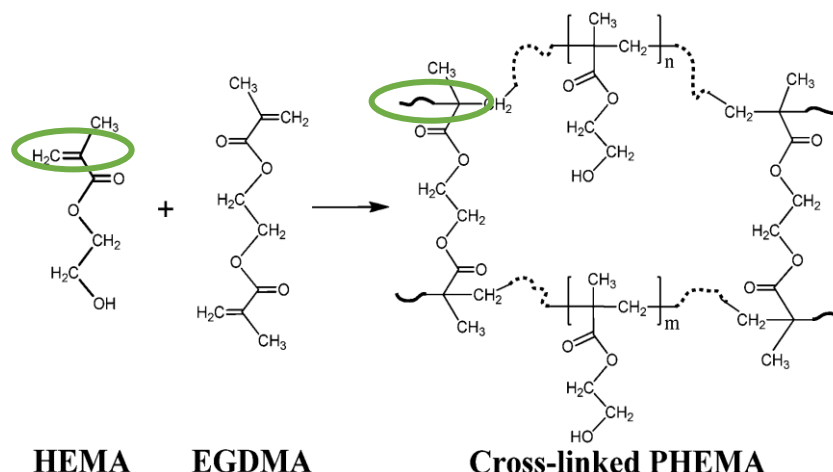


Figure 3.6. The polymerisation reaction of HEMA monomers in the presence of EGDMA crosslinker (adapted from (Su et al., 2016)).

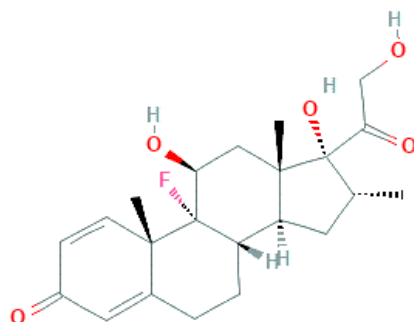


Figure 3.7. Structure of Dexamethasone drug molecule (Adopted from (*Dexamethasone*, CID=5743)).

With the incorporation of DEX (structure is shown in Figure 3.7 above), the spectrum of the DEX-loaded silicone hydrogel cured films (CF D) were very similar to those with no drug loaded (CF ND), which indicates there were no significant chemical changes within the polymer backbone with DEX incorporation within the hydrogel matrix, which confirms that there was no interaction between the polymer and DEX and thus the incorporation of DEX did not alter the polymer structure of the hydrogel.

Although the bands related to the drug overlapped with the bands of some of the other components of the formulation, the characteristic absorbance bands of DEX at 1718 and 1646 cm^{-1} were observed in the spectra of the crosslinked film (CF) with the drug (D). Those peaks are assigned to the stretching vibration of -C=O and the bending vibration of the O-H groups, respectively (Jingjunjiao Long, Nand, Bunt, & Seyfoddin, 2019). Moreover, there was an obvious increase in the wavelength of the peaks within the regions of 3600-3150 and 3050-2800 cm^{-1} compared to the spectra of the crosslinked film with no drug (CF ND). These peaks are assigned to the O-H stretching vibration of the hydroxyl groups and the stretching vibrations of the -CH_3 groups, respectively, which is present within the dexamethasone molecular structure (Chiang, Yu, Chao, & Dong, 2012).

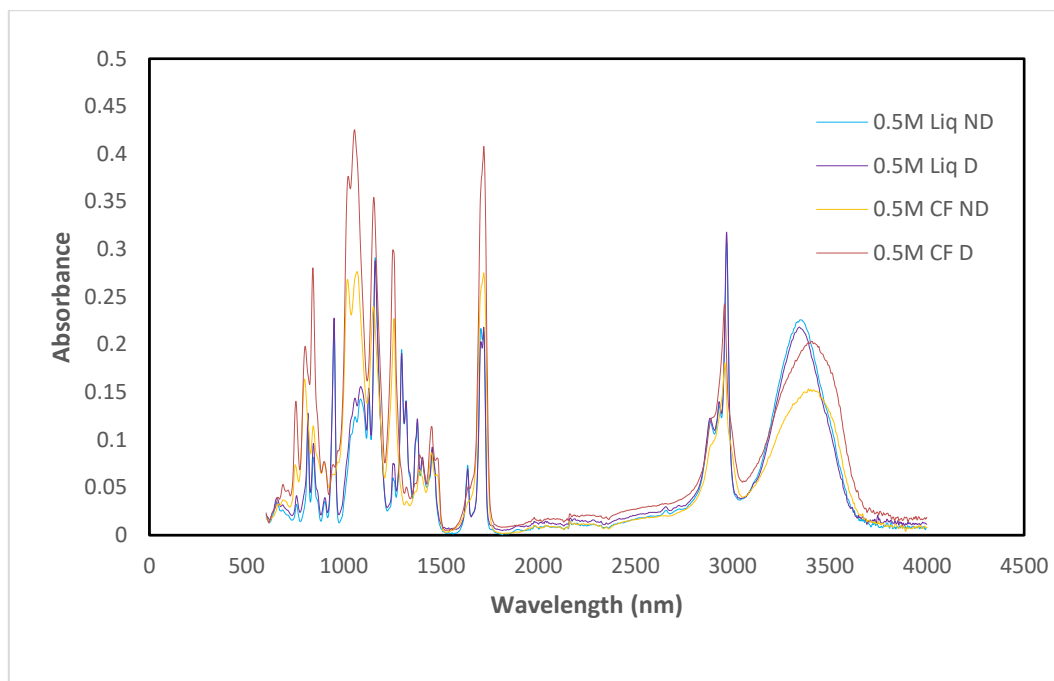


Figure 3.8. FTIR absorbance spectra of liquid (Liq) and crosslinked film (CF) of 0.5 mole% PDMS, 10 mole% TRIS silicone hydrogels with DEX (D) and no DEX (ND) incorporation.

3.4.3 Swelling studies

The ability of the polymerised hydrogel to absorb large amounts of water increases the hydrophilicity of the lenses, which in turn enhances the lens permeability and allows for an extended application period without disturbing the eye (Musgrave & Fang, 2019). However, it is expected that the high-water content will increase the diffusion of the incorporated drug and thus affects its release profile (Guidi et al., 2014). Therefore, a balance between the water content is important to achieve lens comfort without compromising the controlled release of the incorporated drug. The water content of marketed silicone hydrogel contact lenses containing PDMS and TRIS as the hydrophobic monomers ranged between 24 and 47%, with lenses incorporating TRIS (Air Optix™ Night & Day) having the minimum water content, while lenses having PDMS (Acuvue® Advance®) having the maximum (Gonzalez-Meijome et al., 2014).

Studies verified that all the tested *p*(HEMA-*co*-TRIS-*co*-PDMS) lenses reached the EWC within the first 3 h. From the values obtained in Figure 3.9, the water content of the silicone hydrogel lenses decreased with the increase in the concentration of the hydrophobic monomers PDMS and TRIS. The highest EWC of $54 \pm 0.92\%$ was obtained from 1P 5T lenses, while the lowest EWC of $14 \pm 1.44\%$ was obtained from the 3P 20T. In general, all the hydrogel compositions, except for the ones that contain the highest

concentration of TRIS (20 mole%), showed water content between 24 and 54%, which is within the acceptable water content values of commercial silicone hydrogel contact lenses (L. Cheng, Muller, & Radke, 2004).

By illustrating the effect of hydrophobic monomers on the water content as in Figure 3.10, it is clear that the concentration of TRIS had the most significant effect on the EWC, with the reduction EWC values of 54, 44.3 and 14% for formulations of 1 mole % PDMS with 5, 10 and 20 mole% TRIS, respectively. Moreover, in formulations containing 20 mole% TRIS, the increase in the concentration of PDMS from 1 to 3 mole% didn't have a significant decrease in the EWC values in these lenses, which confirmed that TRIS concentration had the main effect on the water content of the tested silicone hydrogel lens compositions.

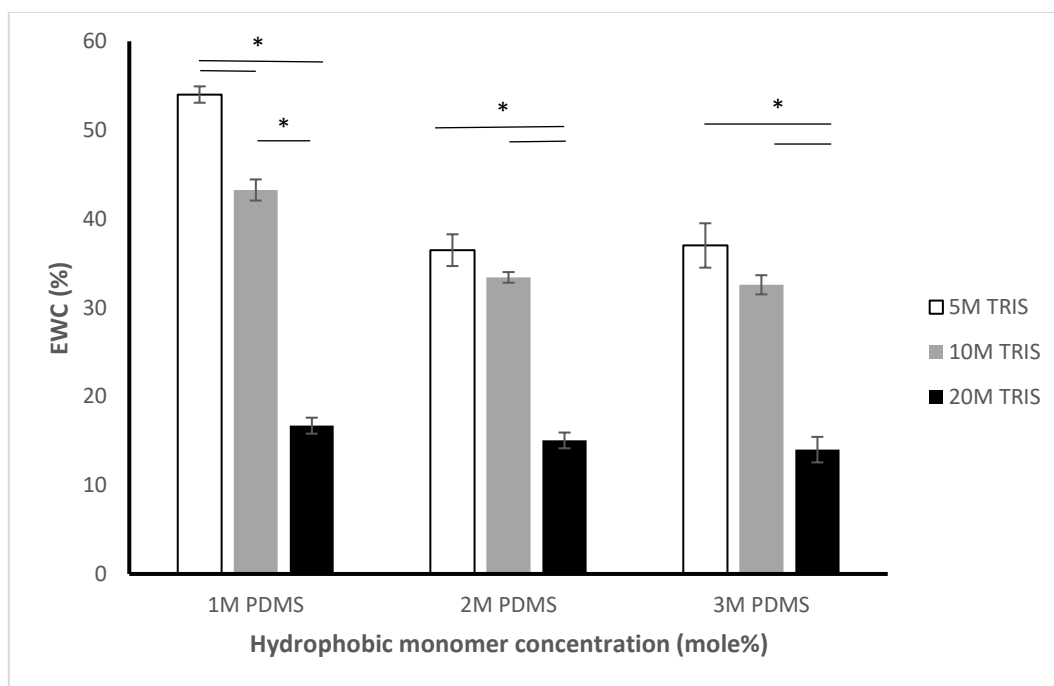


Figure 3.9. EWC of p(HEMA-co-TRIS-co-PDMS) lenses prepared using various molar concentration of PDMS and TRIS after soaking for 24 h in PBS. *Statistically significant at $p < 0.05$; $n = 3$; mean \pm SD.

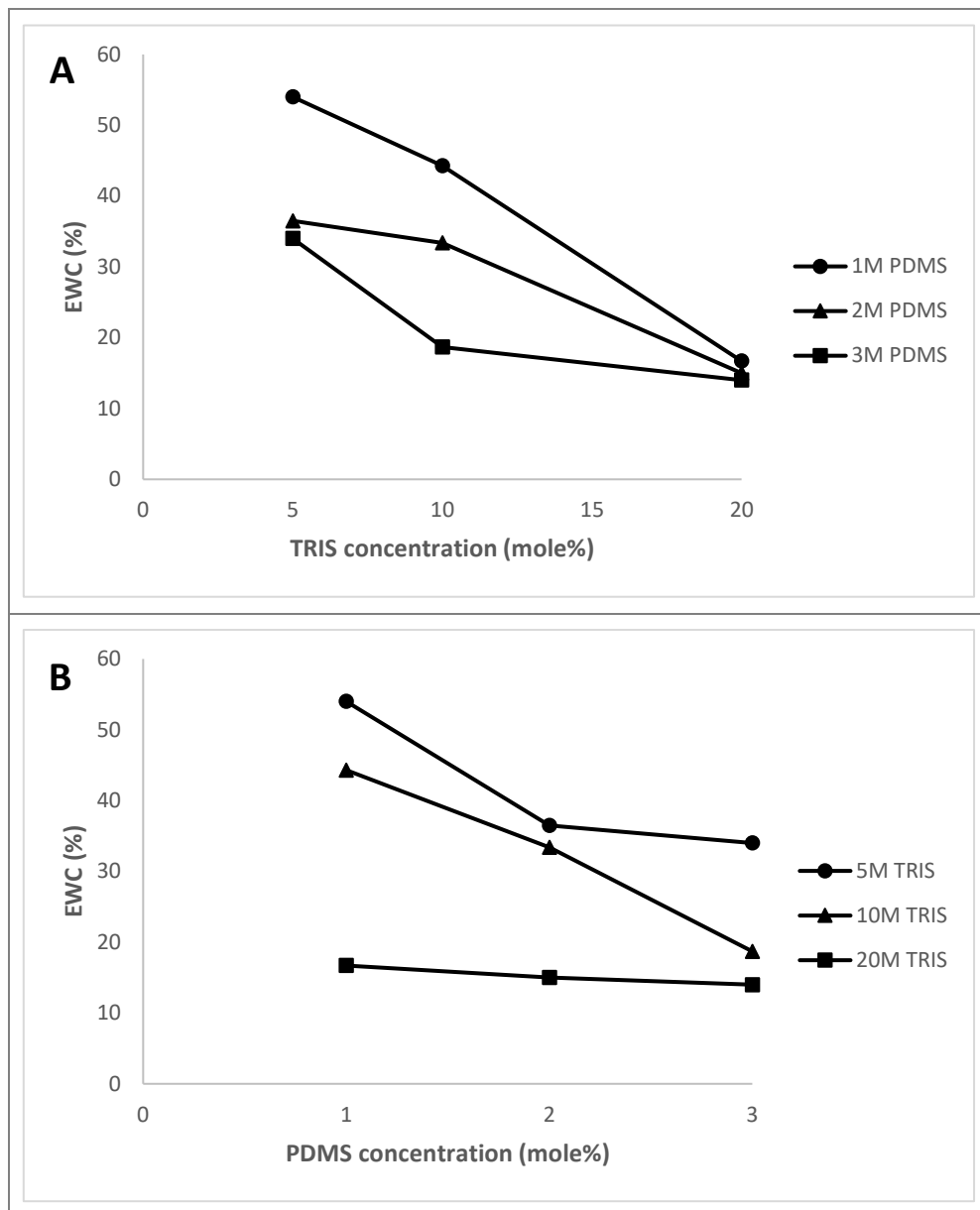


Figure 3.10. The effect of TRIS monomer concentration (A) and PDMS monomer concentration (B) on the EWC of the prepared silicone hydrogel lenses.

Comparing the effect on EWC of various molar concentrations of PDMS in formulations containing 10 mole% TRIS is shown in Figure 3.11 below. The EWC of the lenses with 0.5, 0.75, 1, 1.5, 2 and 3 mole% PDMS were 44 ± 0.9 , 44 ± 0.9 , 43 ± 1.2 , 35 ± 0.6 and $32 \pm 1.1\%$, respectively. There was no significant difference between 0.5, 0.75 and 1 mol % PDMS, neither between 1.5, 2 and 3 mol% PDMS. These results confirmed that the concentration of PDMS within the hydrogel formulation had minimal effect on the water content of the 10 mole% TRIS silicone hydrogel lenses, and they were all within the acceptable limit of commercial silicone hydrogel contact lenses.

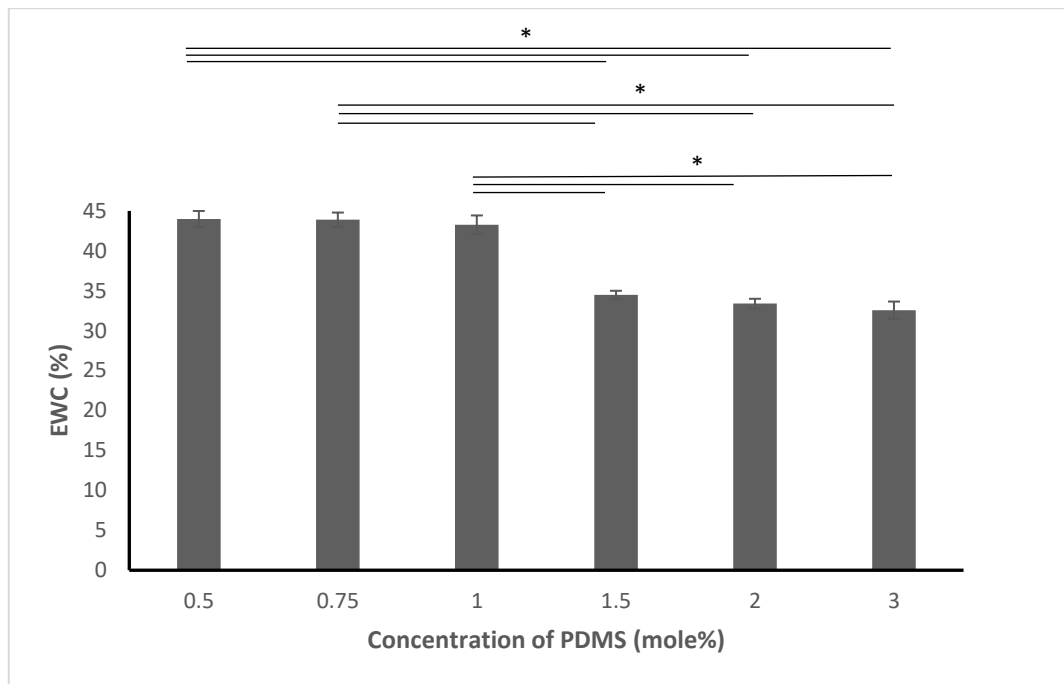


Figure 3.11. EWC of drug-loaded p(HEMA-co-TRIS-co-PDMS) lenses prepared using various molar ratios of PDMS with 10 mole% of TRIS after 24 h in PBS. *Statistically significant at $p < 0.05$; $n = 3$; mean \pm SD.

The effect of drug incorporation on the EWC of 10 mole % TRIS with either 0.5, 0.75, 1 or 1.5 mol % PDMS hydrogel lenses was tested and the results are illustrated in Figure 3.12. The incorporation of the drug resulted in a slight increase in the EWC of some of the silicon hydrogel formulations, however this increase was not significant. This increase in the EWC values effect on the EWC values might be contributed to the created channels created after the diffusion of the drug from the lenses during the 24 h of the soaking period. More water was able to enter the lenses through those empty channels increasing the EWC of those lenses compared to the lenses that had no previously loaded drug.

Furthermore, the effect of drug incorporation on the diameter of the swollen BCLs containing 10 mole% TRIS with either 0.5, 0.75, 1 or 1.5 mole% PDMS hydrogel lenses was tested and the results are illustrated in Figure 3.13. The presence of drug within the lens had the same effect reported in the EWC above, where lenses with the drug had a higher increase in diameter compared to lenses with no drug. However, it was noted that the minimum increase in diameter of the prepared BCLs of various PDMS concentrations was found in lenses containing 1 mole% PDMS, while the maximum increase was found in drug-loaded lenses of 0.5 mole% PDMS.

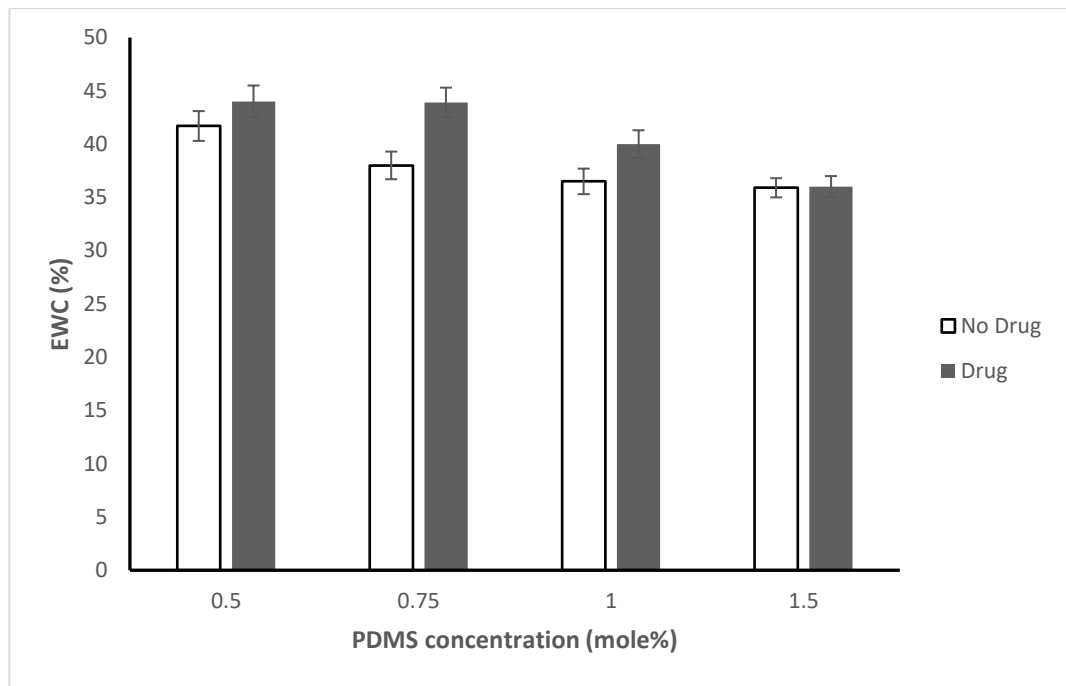


Figure 3.12. The effect of drug incorporation on the EWC of (HEMA-co-TRIS-co-PDMS) BCLs polymer compositions using various molar ratios of PDMS with 10 mole% of TRIS after 24 h in PBS. $p < 0.05$; $n = 3$; mean \pm SD.

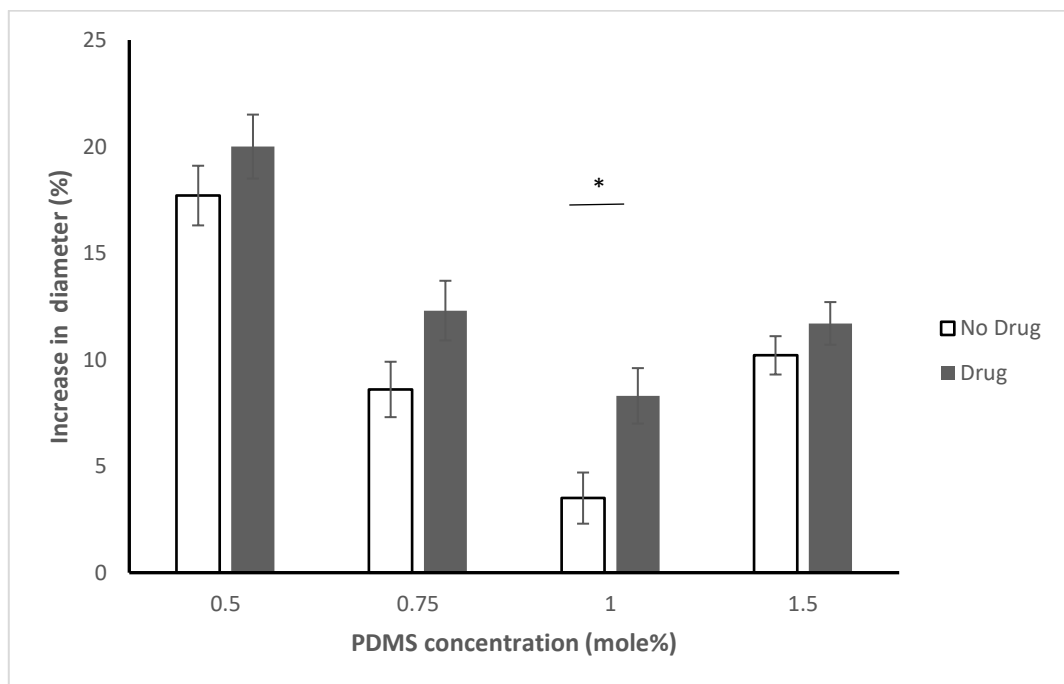


Figure 3.13. Percentage increase in diameter of (HEMA-co-TRIS-co-PDMS) BCLs polymer compositions using various molar ratios of PDMS with 10 mole% of TRIS after 24 h in PBS. *Statistically significant at $p < 0.05$; $n = 3$; mean \pm SD.

3.4.4 Drug content and release

Diffusion is the main drug release mechanism from the polymeric matrix of contact lenses to the release media (Carvalho et al., 2015). Hydrophobic drugs, such as DEX,

partition into the hydrophobic silicone rich phases (Costa et al., 2003). This increased hydrophobic interactions between the drug and the polymer network are expected to slow its release (Kaczmarek et al., 2014). Moreover, the crosslinking density within the gel matrix affects the hydrogel porosity and thus the drug diffusion from the lens to the release media (Hoare & Kohane, 2008).

During washing of the lenses in DI water, part of the loaded drug diffused in the washing water. The washing water was analysed using a UV spectrophotometer at $\lambda=242$ to determine the concentration of the drug that escaped from the cured film during the washing period. Figure 3.14 shows the percentage of DEX remaining in each hydrogel film after being washed. The hydrophobic monomers concentrations had a significant effect on retaining the drug within the hydrogel polymer films. Increasing the concentrations of PDMS and TRIS within the hydrogel formulations, reduced the amount of drug lost from the polymer films. Moreover, it was clear that the TRIS concentration had the greatest effect on inhibiting the diffusion of the drug, with more than 82% DEX remaining in the films of 3P 20T hydrogel formulation compared to 61 % from the 3P 5T ones.

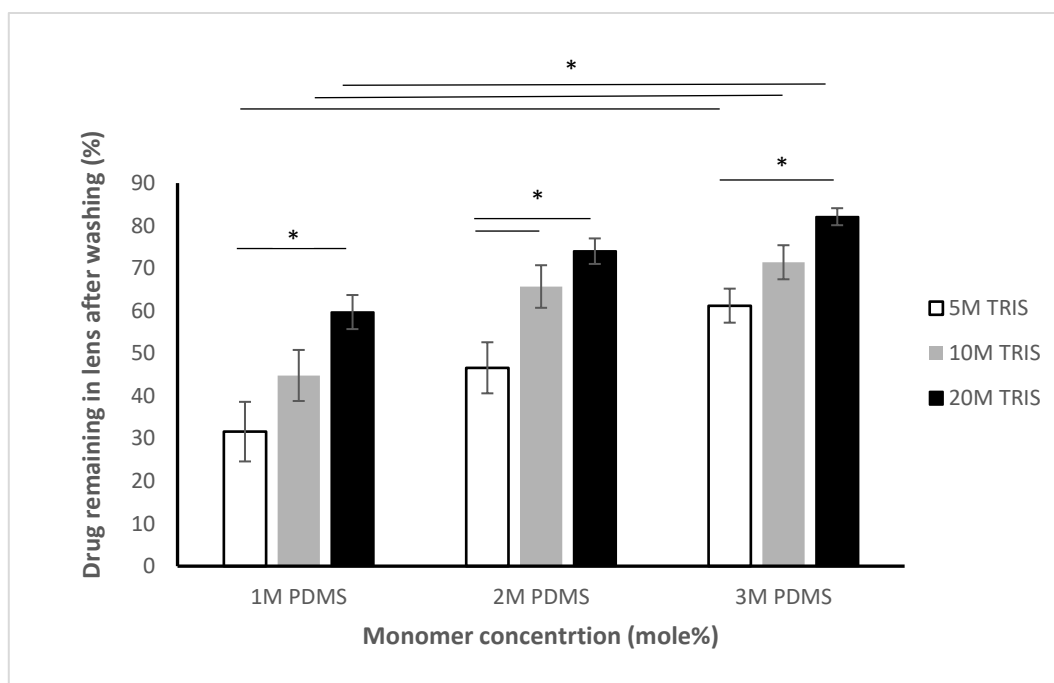


Figure 3.14. Percentage of DEX remaining in p(HEMA-co-TRIS-co-PDMS) lenses, containing either 1, 2 or 3 mole% PDMS with either 5, 10 or 20 mole% PDMS, after washing for 24 h in DI water. *Statistically significant at $p < 0.05$; $n = 3$; mean \pm SD.

A drug release experiment was performed for all the formulations mentioned in Table 3.2 above. The concentrations of DEX released from each lens at selected time intervals were illustrated in Figure 3.15. In general, increasing the concentrations of the hydrophobic monomers prolonged the release rate of DEX. This might be attributed to the high crosslinking density of the silicone hydrogel polymer due to the complex structure of the crosslinked polymer network and the high molecular weight of the incorporated siloxane monomers, which in turn rendered it difficult for the drug to diffuse from the hydrogel matrix (Andrade-Vivero et al., 2007; Hu et al., 2011).

The patterns of the drug release profiles were related to the concentrations of the incorporated hydrophobic monomers PDMS and TRIS. As expected, formulation 1P 5T showed the most rapid drug release profile because it had the lowest concentrations of PDMS and TRIS. Moreover, it reached a plateau after 4 days with only $211.9 \pm 6.8 \mu\text{g}$ released from each lens, compared to more than $472 \mu\text{g}$ released from lenses of formulation 3P 20T that did not reach a plateau in 14 days.

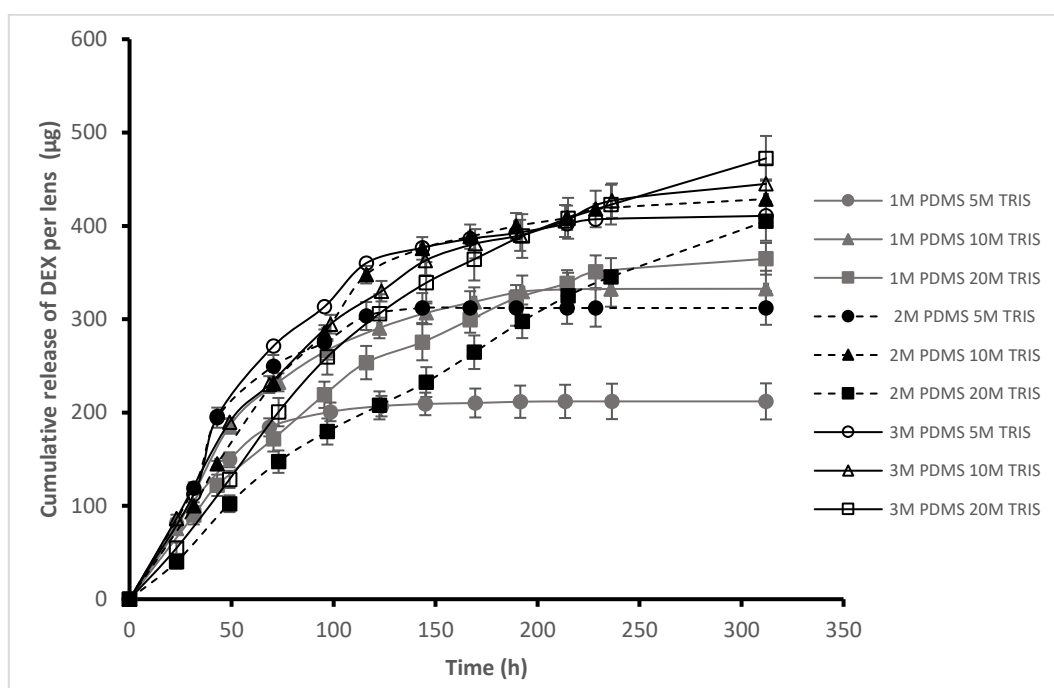


Figure 3.15. Drug release profiles of DEX from the washed p(HEMA-co-TRIS-co-PDMS) lenses in PBS at 37 °C. n = 3; mean \pm SD.

It is worth noting that all the tested formulations had different drug content due to the amount of drug lost during the washing stage. A diagram comparing the drug released from the lenses of each formulation compared to the total drug content at the start of

the release experiment is shown in Figure 3.16. All the silicone hydrogel formulations had an extended-release profile for DEX, except for formulations 1P 5T and 2P 5T, which confirmed the significant effect of TRIS concentration on the drug release of DEX as previously illustrated in the analysis of the washing water. The slowest drug release rates of DEX were obtained from the lenses of formulation 2P 20T with only 54% of the drug released within the first 7 days.

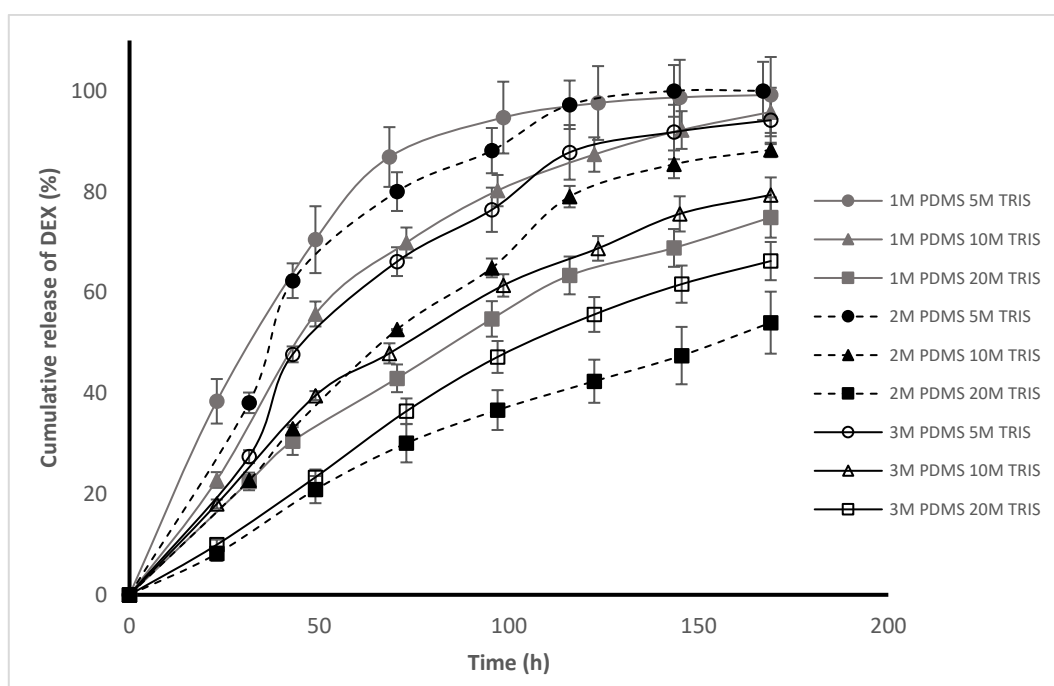


Figure 3.16. Percentage of DEX released from p(HEMA-co-TRIS-co-PDMS) lenses in PBS at 37 °C during the first 7 days. n = 3; mean \pm SD.

A comparative diagram showing the effect of the concentration of each hydrophobic monomer on the drug release profile of the prepared silicone hydrogel lenses is presented in Figure 3.17. It shows that both PDMS and TRIS had the same effect on the drug release profiles, where the release of drug is extended by increasing the concentrations of the hydrophobic monomers, except for the formulation of 3P 20T which released 66.2% of the drug at day 7 compared to 54% for 2P 20T hydrogel composition. This might be attributed to an interaction between TRIS and PDMS at this high concentration of TRIS or a slight phase separation that resulted in the rapid escape of the drug (Guidi et al., 2014). Moreover, it was shown that rapid release rate of DEX was observed in all formulations containing 5M TRIS, so those formulations are not suitable for the purpose of the study. These drug release findings were correlated with the EWC results previously illustrated in Figure 3.9 above, where formulations

containing 5 mole% TRIS had the highest water content and the ones with 20 mole% TRIS had the lowest. This correlation between the increased material swelling and drug release rate confirms that the water content of the lenses is an important factor in the release of incorporated drugs (Guidi et al., 2014). Drug release at day 7 was chosen in this comparison since the BCL is intended to be applied on the eye for 7 days. Moreover, some formulations reached 100% release on day 7, I wanted to show that other formulations were still releasing the drug after 7 days and the

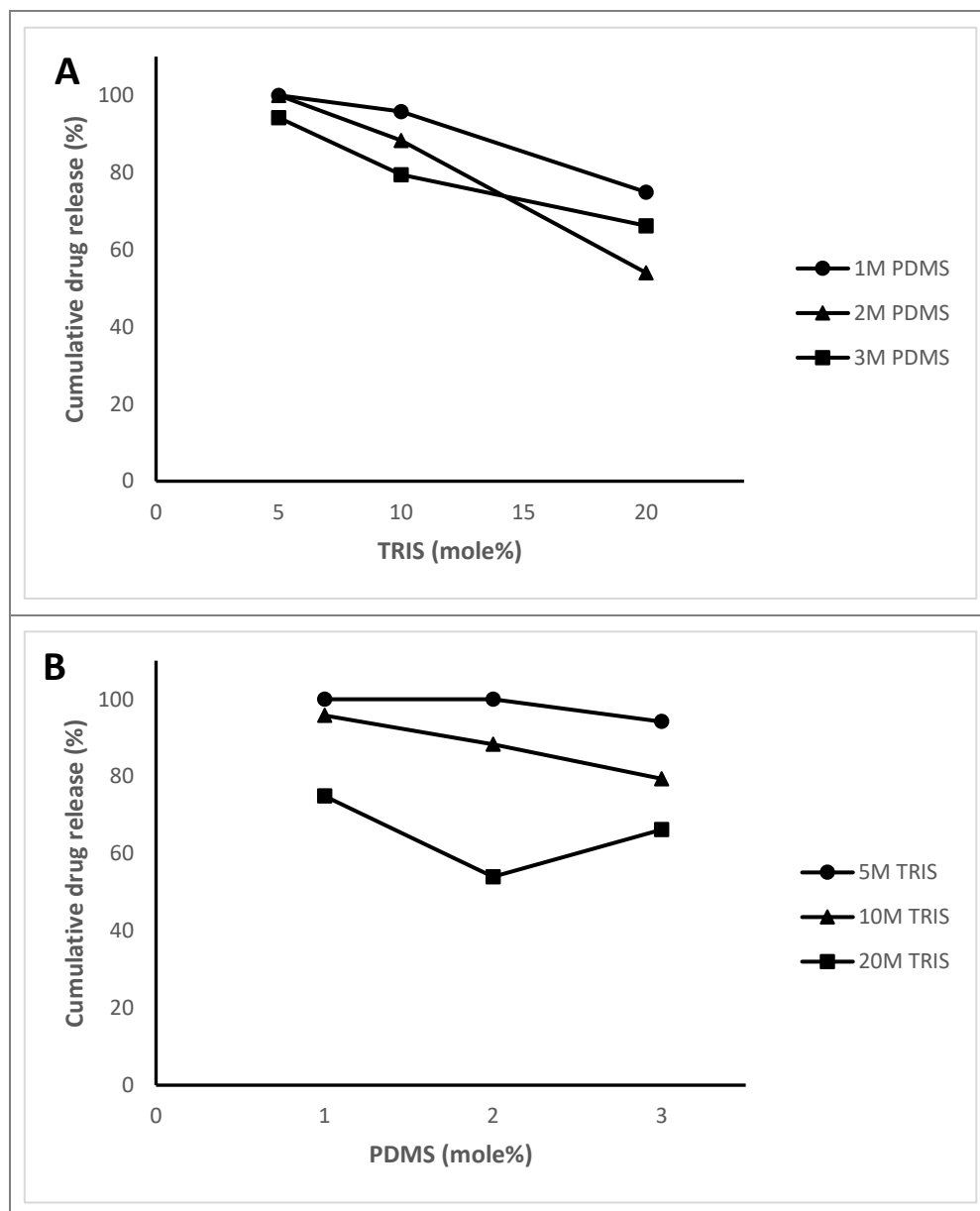


Figure 3.17. Effect of TRIS monomer concentration (A) and PDMS monomer concentration (B) on the on the percentage drug released after 7 days for the prepared silicone hydrogel lenses.

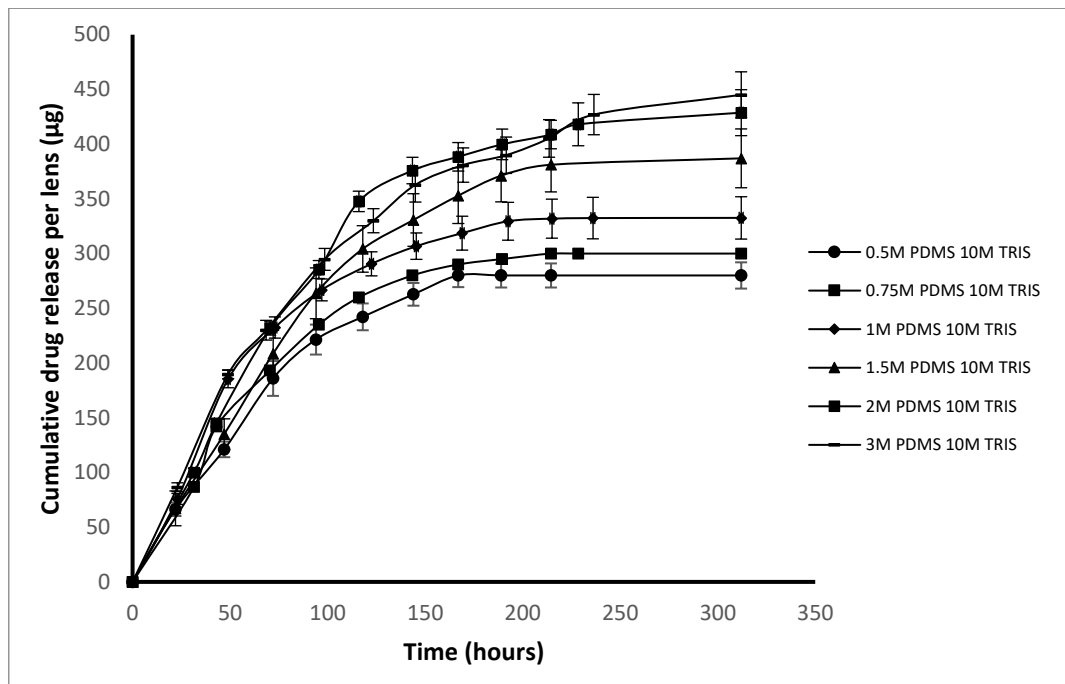


Figure 3.18. Drug release profiles of DEX from the washed p(HEMA-co-TRIS-co-PDMS) lenses in PBS at 37 °C. n = 3; mean \pm SD.

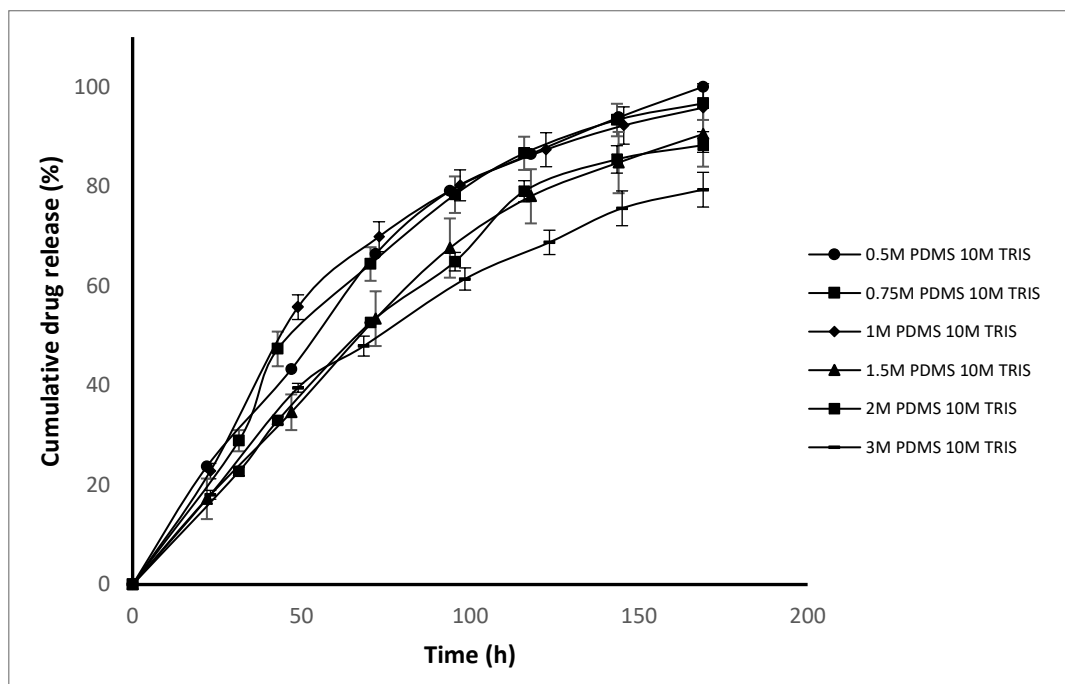


Figure 3.19. Percentage of DEX released from p(HEMA-co-TRIS-co-PDMS) lenses in PBS at 37 °C during the first 7 days. n = 3; mean \pm SD.

Comparing the effect of PDMS concentrations on the drug release profiles of the hydrogel formulations revealed that increasing the concentration of PDMS prolonged the release of DEX from the hydrogel lenses and prevented more drug from escaping

during the washing phase. The drug release profiles of the hydrogel lens formulations composed of 10 mole% TRIS with either 1.5, 2 or 3 mole% PDMS showed extended-release profiles of DEX for 7 days, which render those formulations suitable for making drug-loaded BCLs.

3.4.5 Mechanical properties

Elastic modulus, or Young's modulus, is stress (force per unit area) required to produce a unit of recoverable strain (elastic deformation) in a material. Therefore, Young's modulus, which is measured in Mega Pascal (MPa) is a measure of how well a material resists reversible deformation, i.e. how elastic is the material (Franklin, 2004; Gonzalez-Meijome et al., 2014). In silicone hydrogel contact lenses, flexible lenses fits better to the surface of the eye and adds to the patient's comfort. However, the lens requires to be adequately stiff to maintain the shape during use. Therefore, the modulus of commercial contact lenses is commonly found within the range from 0.3 to 1.5 MPa (Childs et al., 2016; Horst, Brodland, Jones, & Brodland, 2012).

Comparing the effect of hydrophobic monomers on the mechanical properties of the drug-loaded hydrogel lenses are illustrated in Figure 3.20. All the tested hydrogel compositions had accepted Young's modulus compared to the commercial lenses. The pHEMA hydrogel lens with no incorporated hydrophobic monomers had the lowest Young's modulus and tensile strength values of 0.5 ± 0.05 and 0.5 ± 0.03 MPa, respectively, compared to the formulations that had no incorporated hydrophobic monomers within the hydrogel matrix, which indicates that those lenses were more flexible. The incorporation of 5 mole% TRIS resulted in increasing the stiffness and the strength of the lenses as indicated by the increase in Young's modulus and tensile strength values to 1.5 ± 0.1 and 0.9 ± 0.04 MPa, respectively. This is in agreement with other studies showing that that silicone hydrogel lenses had higher tensile strength compared to pHEMA hydrogel ones, which might be contributed to the effective transfer of stress between the hydrophilic and hydrophobic polymer networks within the silicone hydrogel lenses (J. J. Wang, Liu, & Wei, 2012). However, it was found that by incorporating PDMS with TRIS in the formulation, Young's modulus values were reduced to 0.7 ± 0.04 and 0.6 ± 0.04 MPa by the incorporation of 1 and 3 mole% PDMS,

respectively. This might be contributed to the elastic properties of PDMS, which improved the flexibility of the lenses (Musgrave & Fang, 2019).

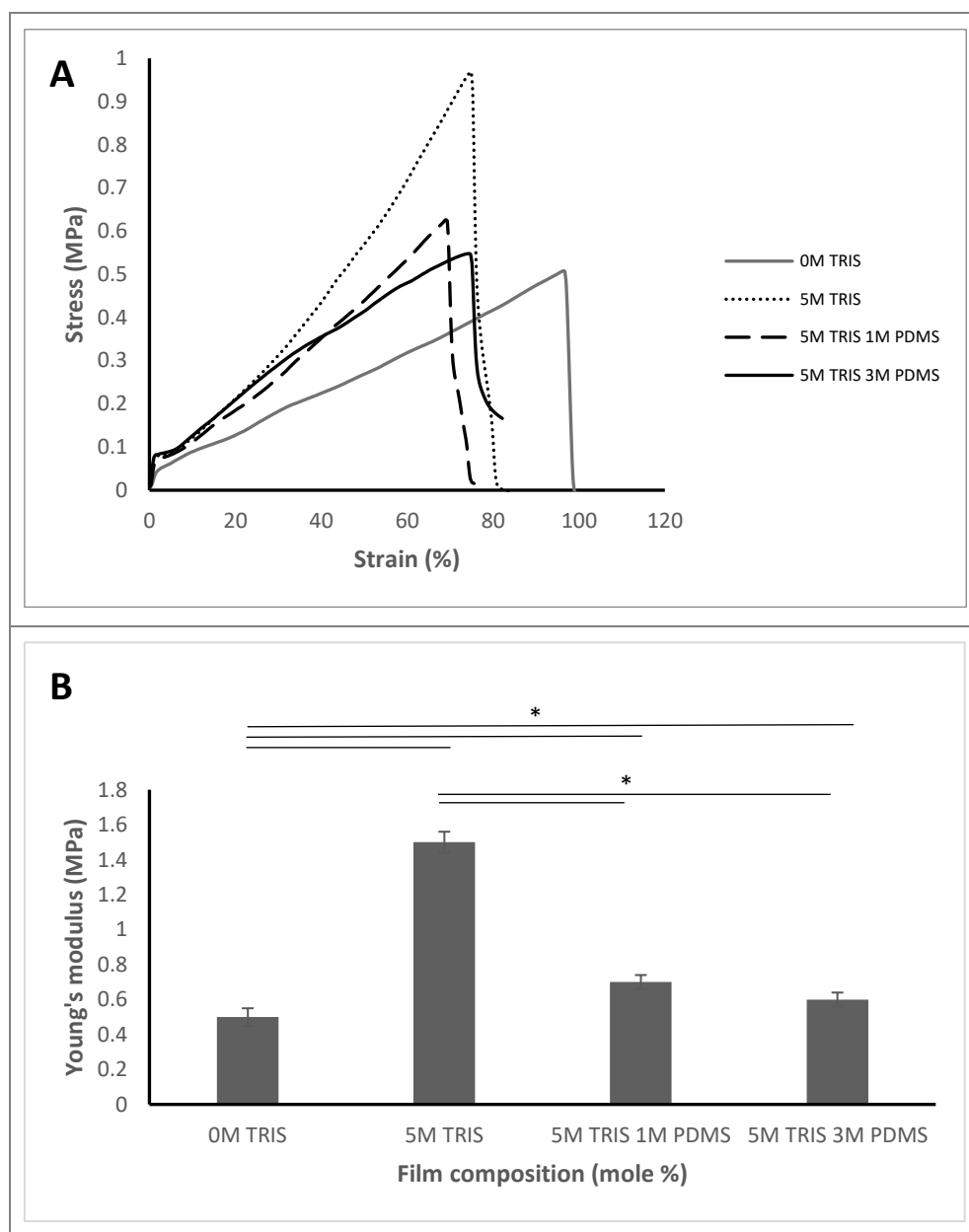


Figure 3.20. The effect of various concentrations of TRIS and PDMS on the stress-strain curves (A) and Young's modulus (B) of the hydrogel lenses. *Statistically significant at $p < 0.05$; $n = 3$; mean \pm SD.

The effect of incorporating the drug into the silicone hydrogel lenses was analysed by preparing 3 formulations of 5 mole% TRIS, 95 mole% HEMA with either 0, 0.5 or 1% DEX, and the stress-strain data generated from the texture analyser were plotted in Figure 3.21. The incorporation of the drug increased Young's modulus and resulted in stiffer lenses. On the other hand, it produced tougher and stronger lenses that had higher elongation at break and strength values. It was noted that there was no significant

difference between the incorporation of 0.5 and 1% DEX within the hydrogel formulations.

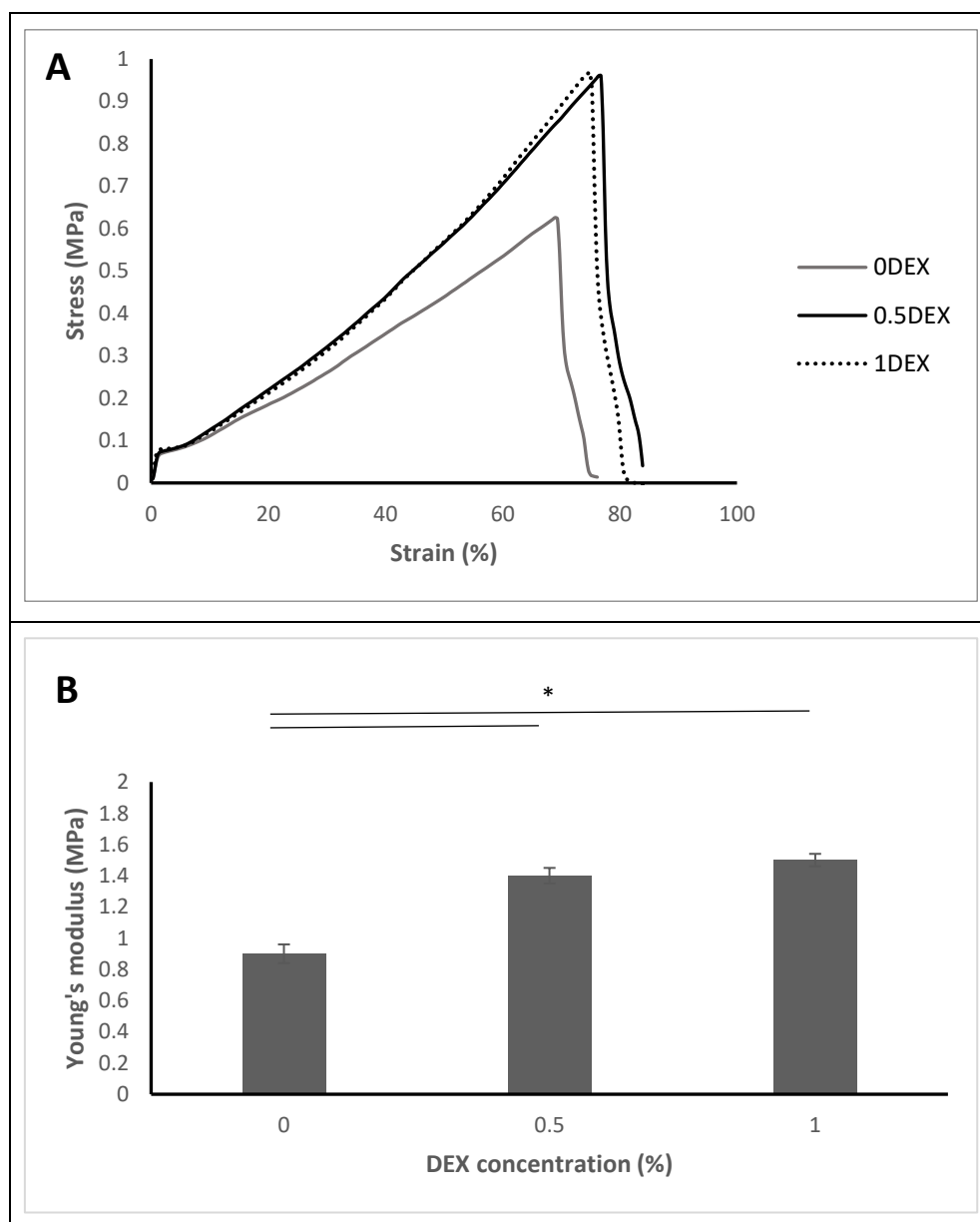


Figure 3.21. The effect of DEX concentration on the stress-strain curves (A) and Young's modulus (B) of 5 mole% TRIS 95 mole% HEMA hydrogel lenses. *Statistically significant at $p < 0.05$; $n = 3$; mean \pm SD.

To determine the effect of concentration of TRIS monomer on the mechanical properties of the drug-loaded silicone hydrogel lenses, 3 formulations of 3 mole% PDMS were prepared using either 5, 10 or 20 mole% TRIS and the results of the stress-strain analysis were presented in Figure 3.22. In general, increasing the concentration of TRIS resulted in decreasing the elongation at break values and reduced the toughness of the hydrogel lenses. The Young's modulus of the lenses containing the highest concentration of TRIS

(20 mole%) had the highest Young modulus values and thus the stiffest lenses. On the other hand, there was no significant difference between Young's modulus of hydrogel formulations with 5 and 10 mole% TRIS. These findings excluded the formulations containing 20 mole% TRIS from the desired application because they are stiff and brittle.

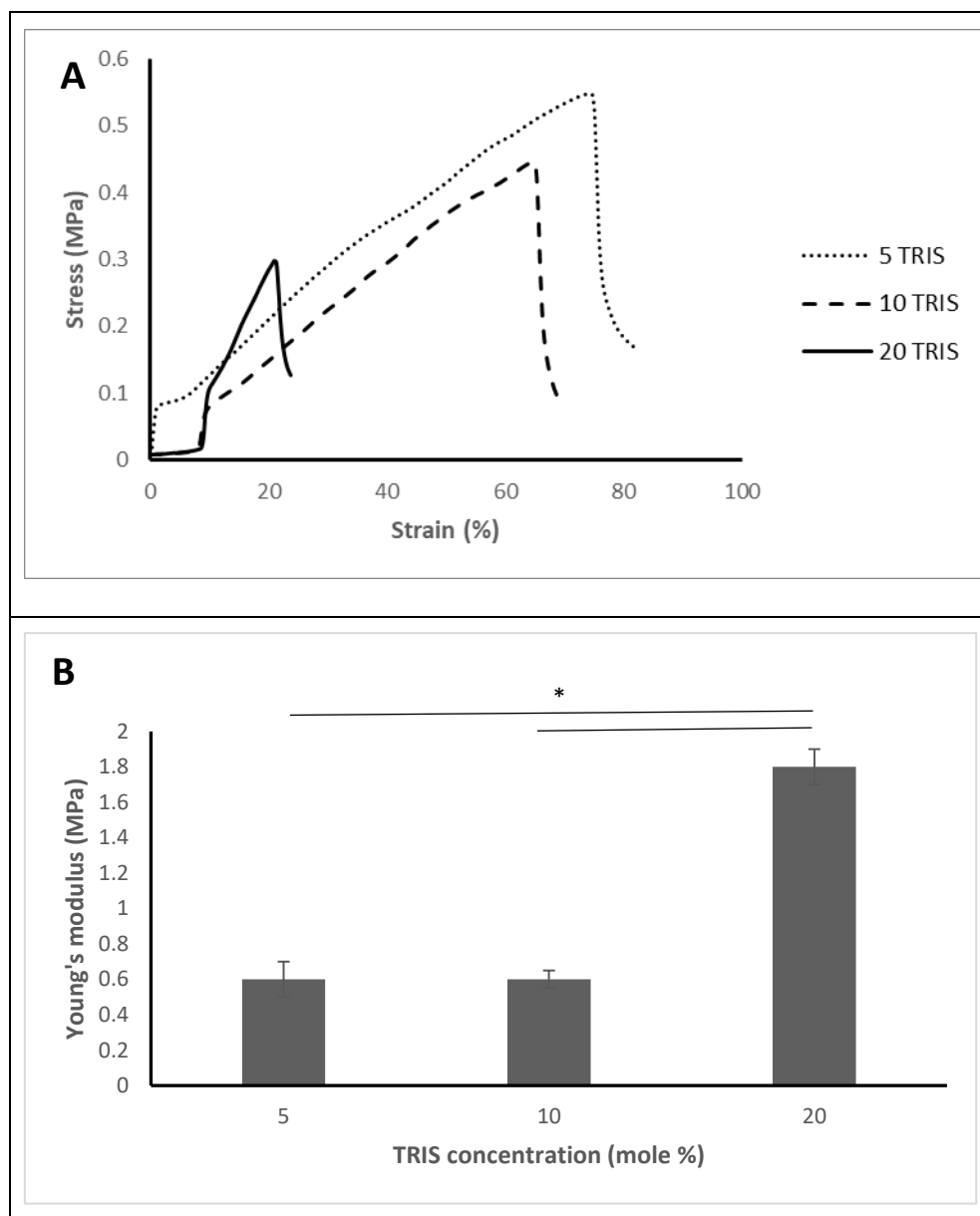


Figure 3.22. The effect of TRIS concentration on the stress-strain curves (A) and the Young's modulus (B) of 3 mole% PDMS hydrogel lenses. *Statistically significant at $p < 0.05$; $n = 3$; mean \pm SD.

To determine the effect of PDMS monomer concentration on the mechanical properties of the drug-loaded silicone hydrogel lenses, 3 formulations of 10 mole% TRIS were prepared using either 0.5, 1, 2 or 3 mole% PDMS and the results of the stress-strain analysis are presented in Figure 3.23. Generally, the higher the concentration of PDMS

in the formulation, the lower Young's modulus, which resulted in more flexible and thus softer lenses. However, there was no significant difference in Young's modulus values between the hydrogel formulations containing 0.5 and 1 mole% PDMS and the ones containing 2 and 3 mole% PDMS. However, it was noted that the lenses containing 0.5% PDMS showed the highest elongation at break values, which indicates that they are tough, and the lenses produced can be more durable during use.

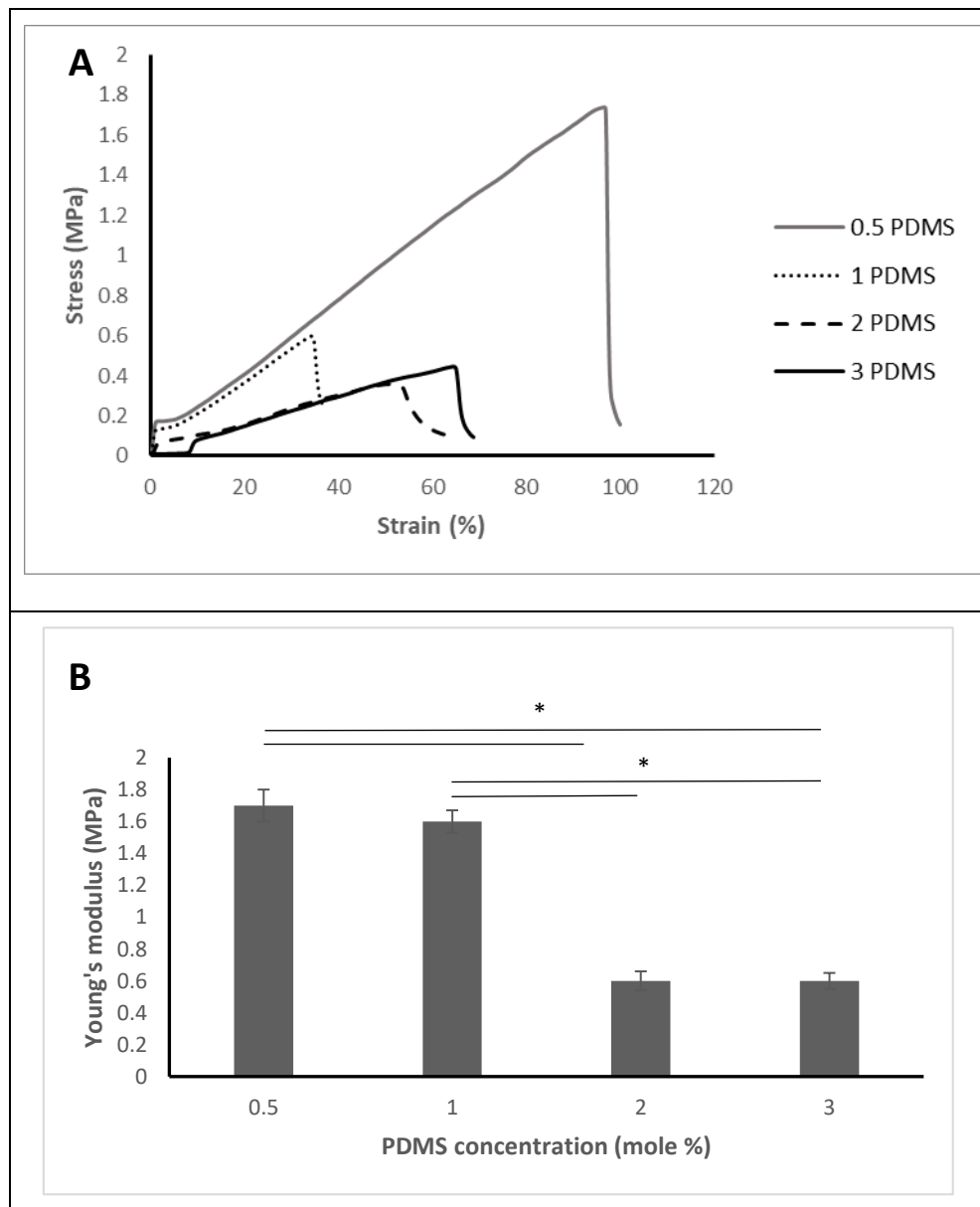


Figure 3.23. The effect of PDMS concentration on the stress-strain curves (A) and Young's modulus (B) of 10 mole% TRIS silicone hydrogel lenses. *Statistically significant at $p < 0.05$; $n = 3$; mean \pm SD.

3.5 Conclusion

In this chapter, the possibility of controlling dexamethasone release from silicone hydrogel BCL was assessed by adjusting the concentrations of the incorporated

monomers. By changing the hydrophobic to hydrophilic monomer ratio and the mole% of the hydrophobic monomers TRIS and PDMS in the prepared p(HEMA-*co*-TRIS-*co*-PDMS) BCLs, extended-release of DEX for up to 14 days was achieved in lenses with comparable mechanical properties to commercial silicone hydrogel contact lenses.

Ideal drug-loaded contact lenses should be biocompatible, oxygen permeable and provide controlled release of accurate dose within the time they are in use. In terms of oxygen permeability, the high oxygen permeability of commercially available silicone hydrogel contact lenses is due to the presence of siloxane groups. All the tested silicone hydrogel compositions in this work are similar to that of commercial silicone hydrogels, which indicates their high oxygen permeability. Moreover, they should be comfortable and easy to handle and have minimum interference with the patient's vision (A. M. Ribeiro et al., 2015).

**Chapter 4 3D-printed gelatine
bandage contact lens (BCL) for
ocular drug delivery of
Dexamethasone.**

Abstract

Drug-eluting contact lenses have been widely studied as an alternative to eye drops due to their ability to prolong the drug resident time, enhance bioavailability and improve patient compliance. Silicone hydrogel polymers are commonly used in drug-eluting contact lenses, due to their transparency, suitable mechanical properties and high oxygen permeability. Gelatine hydrogels are clear, flexible and have high oxygen permeability, therefore, they are also a suitable contact lens material. Moreover, their rheological properties allow their use as inks in extrusion-based 3D printers, therefore opening the door to a wide range of newer applications. However, the solubility of gelatine hydrogels at body temperature limits their pharmaceutical use. Adding methacrylate groups to gelatine produces gelatine methacrylate (GelMA), which undergoes a photoinitiated polymerisation reaction to produce covalently crosslinked insoluble hydrogels. This chapter aims to develop 3D-printed drug-loaded GelMA hydrogel lenses to deliver dexamethasone (DEX) to the eye over a period of 1 week. Drug-loaded GelMA/PEGDA hydrogel lenses were prepared using the solvent casting and the 3D-printing techniques. Two concentrations of GelMA (5 and 8%) were tested with 4 concentrations of PEGDA (0, 5, 10, and 15%). The prepared lenses were characterised to determine the equilibrium water content (EWC), in vitro degradation, and drug release profile of DEX. The results showed that the incorporation of PEGDA improved the lenses' resistance to handling and protected them during the degradation test, reduced the EWC values and prolonged the release of the incorporated drug. It was noted that the lenses prepared using the 3D-printing technique showed a higher EWC and thus resulted in rapid drug release profiles compared to the lenses prepared using the solvent casting technique. However, the 3D-printed lenses showed controlled release drug profiles of DEX until they degraded.

4.1 Introduction

In the previous chapter, I have loaded DEX within silicone hydrogel BCLs, which is the currently used material in BCLs available in the market. In this chapter, I would like to explore a new material that can be used to prepare therapeutic BCLs, yet can be 3D-printed to benefit from the advantages that the 3D-printing technology can bring to the manufacturing of drug delivery systems. Therefore GelMA hydrogel was chosen as the hydrogel base.

Drug-eluting contact lenses have been widely studied as an alternative to eye drops due to their ability to increase the drug resident time, bioavailability and improve patient compliance (J. Xu et al., 2018). Due to the high drug bioavailability (up to 50%) reported from drug-eluting contact lenses, fewer drug doses are administered resulting in lower side effects and complications and better clinical outcomes. It is common to use silicone hydrogel polymers in drug-eluting contact lenses, due to their transparency, mechanical properties and high oxygen permeability (Maulvi et al., 2016). However, far less research has been done on modifying other hydrogel polymers to suit this application.

Gelatine is a protein hydrogel obtained from the partial hydrolysis of collagen obtained from a natural origin (X. Wang et al., 2017). Due to its high biocompatibility, unique chemical, physical nature and being a Generally Regarded As Safe (GRAS) material by the FDA, it has been extensively used as a drug carrier and component in many drug delivery systems (Hathout & Omran, 2016). In particular, gelatine has been used in ocular drug delivery systems including eye drops (Y.-H. Cheng et al., 2016), nanoparticles (Mahor et al., 2016), in situ gels (Y. Song et al., 2018) and films (Rathore, Nema, & Sisodia, 2010).

Gelatine polymers are not widely used in the preparation of drug-eluting corneal bandages because of their **high solubility and poor mechanical properties**. To overcome these drawbacks, some have formulated gelatine/chitosan composites (Xin-Yuan & Tian-Wei, 2004), incorporated a synthetic polymer such as PVA (Jain, Carvalho, Banthia, & Banerjee, 2011) or added a crosslinker within the hydrogel formulation (El-Feky, Zayed, Elshaiar, & Alsharif, 2018). However, gelatine hydrogels are clear, flexible and have high oxygen permeability, therefore, they are suitable candidates in preparing corneal bandages (Z. Zhang, Ortiz, Goyal, & Kohn, 2014).

Following the use of 3D-printing technology in pharmaceutical research, further investigation into printable materials, that can be used to formulate current and future drug delivery systems should be considered. The rheological properties of gelatine hydrogels allow their printability using extrusion-based 3D printers, which opens the door to a wide range of newer applications using this polymer (Kalkandelen et al., 2017). Incorporation of 3D-printing techniques in the production of medicated contact lenses facilitates patient-specific requirements, including special designs and sizes. Moreover, the lens can be printed with pores to promote oxygen permeability and prevent corneal hypoxia.

Gelatine hydrogels are soluble at body temperature. Therefore, to formulate contact lenses out of gelatine, the hydrogel should be crosslinked into a non-water-soluble polymer. Adding methacrylate groups to the amine-containing side groups of gelatine by reaction with methacrylic anhydride (MA) produces a compound named gelatine methacrylate (GelMA). GelMA undergoes a photoinitiated free-radical polymerisation in the presence of a photoinitiator and light to produce covalently crosslinked hydrogels (Y. Wang et al., 2018). Although GelMA hydrogels are insoluble, they are highly degradable, and therefore rapid drug release profiles from those hydrogels are expected without incorporation of a crosslinking agent (Yue et al., 2015).

Polyethylene glycol diacrylate (PEGDA) is a long-chain, hydrophilic, crosslinking monomer which contains double-bond acrylate groups at each end of the PEG chain. It has the ability to undergo fewer photopolymerisation reactions to give a stable polymer that has shown the ability to provide drug release for extended periods of time (McAvoy, Jones, & Thakur, 2018). PEGDA polymers have been used in numerous drug delivery applications including implants (Mau, Nazir, John, & Seitz, 2019), microneedles (Gao et al., 2019) and dressings (Mostafalu et al., 2017) due to their biocompatibility and tissue-like properties.

Dexamethasone (DEX) was chosen in this study as the model drug due to its lipophilic nature and high corneal penetration. It is used to reduce inflammation, swelling, redness and irritation due to infections or following eye surgeries (Gaudio, 2004; Guidi et al., 2014).

In this chapter, drug-loaded GelMA/PEGDA hydrogel lenses were prepared using photopolymerisation reaction in the presence of Lithium Phenyl(2,4,6-trimethylbenzoyl)phosphinate (LAP) as a photoinitiator and cured under LED light of 405 nm. Two concentrations of GelMA (5 and 8%) were tested with 4 concentrations of PEGDA (0, 5, 10, and 15%). Some of those formulations were prepared using both the solvent casting and 3D-printing techniques to produce the lenses. The 3D-printing technique allowed for the presence of pores within the lens, which might increase oxygen permeability to the cornea. The prepared lenses were characterised to determine the equilibrium water content, *in vitro* degradation, and drug release of DEX.

4.2 Materials and methods

4.2.1 Materials

Lithium phenyl-2,4,6-trimethylbenzoylphosphinate (LAP) and printing needles from Allevi, Philadelphia, USA. Dimethyl sulfoxide (DMSO), EssentQ[®], Scharlab S.L., Barcelona, Spain. Porcine gelatine type A with 300 Bloom value, Deuterium oxide (D₂O) 99.9 atom % D, methacrylic anhydride, polyethylene glycol diacrylate (PEGDA, M_n700) and Phosphate buffered saline (PBS) tablets 1.0M, pH 7.4 (25 °C) from Sigma-Aldrich, New Zealand. All other chemicals were of analytical grade.

4.2.2 Preparation and characterisation of GelMA hydrogel

In this work, GelMA was synthesised according to the previously reported method (Kuo et al., 2018). Briefly, 10% (w/v) of gelatine from porcine skin was dissolved in PBS at 50 °C. Then, 0.6 g of methacrylic anhydride per g of gelatine was added to the gelatine solution dropwise at a rate of 0.5 ml/min under vigorous stirring, the mixture was left to react under 50 °C and stirring for 3 h. At the end of the reaction, the mixture was transferred to falcon tubes and centrifuged at 100g for 2 min to remove the excess MAA as shown in Figure 4.1. After filtration, all the supernatants were transferred to a beaker and diluted 1:1 with PBS to stop the reaction and then dialysed against DI water at 50 °C for 1 week using a cellulose dialysis tubing of 14000 MWCO (Thermofisher, New Zealand). The deionised water was changed twice daily in the first 3 days, then once a day to remove salts and excess methacrylic acid. The pH of the GelMA solution was adjusted to 7.4 then transferred to 50ml falcon tubes for freeze-drying. The produced sponge-like solid (GelMA) was stored at -80 °C until further use.

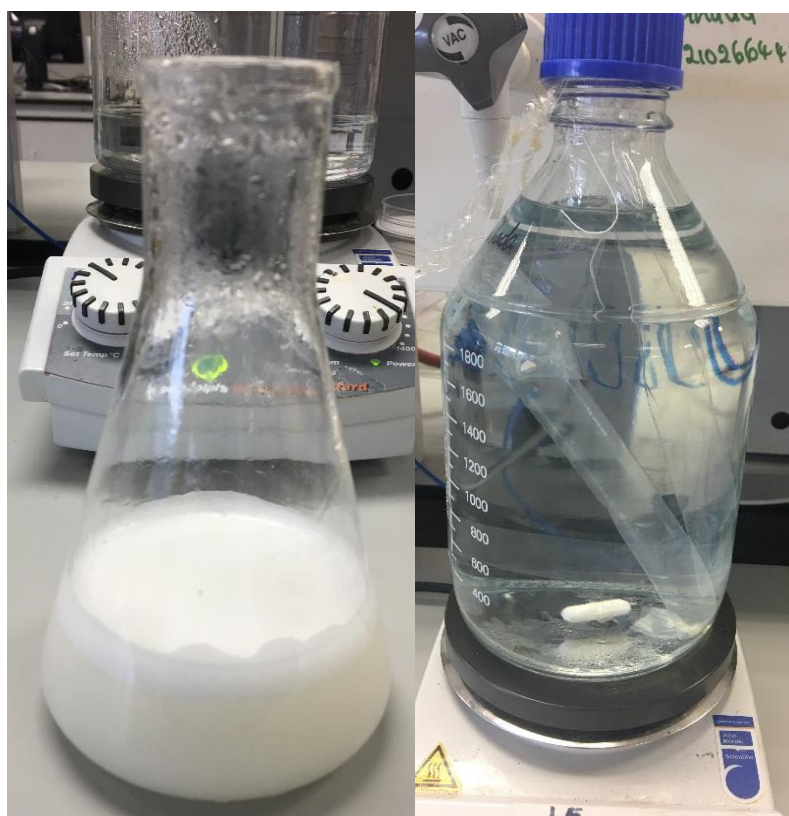


Figure 4.1. The flask on the left shows the formation of GelMA after the 3 h reaction with MAA, the image on the right shows the dialysis of GelMA against DI under 50 °C for 1 week.

The degree of methacryloyl functionalisation of the GelMA was quantified using ^1H NMR according to a previously described methods using an NMR spectrometer (Bruker Ascend 400, Germany) NMR spectrometer operating at 400.13 MHz equipped with the TopSpin 3.5b.91.pl.7 software. The spectrometer was fitted with a 5 mm probe type: PA BBO 400S1 BBF-H-D-05 Z and all experiments were performed at a constant temperature of 40 °C. Each experiment excited the nuclei with a single 30° pulse and obtained 64 transients with a spectral width of 8012.8 Hz and FID size of 65,536 data points. The ^1H -NMR spectra were calibrated against the internal standard 3-(trimethylsilyl) propanoic acid D4 sodium salt TMSP to give the zero point in the δ (ppm) scale.

To prepare the NMR samples, 20 mg of GelMA was completely dissolved in 1 ml deuterium oxide containing 0.05% w/v TMSP for calibration. Porcine gelatine was also

examined for calculating the degree of methacryloyl substitution using the following equation (X. Li et al., 2016).

$$DM = 1 - \left(\frac{\text{lysine methylene proton of GelMA}}{\text{lysine methylene proton of gelatine}} \right) \times 100\%$$

4.2.3 Preparation of BCLs using the solvent casting technique

A total of 3 g of each hydrogel formulation was prepared, containing 1% w/w DEX and 0.5% w/w LAP, while the concentrations of GelMA and PEGDA were varied as stated in Table 4.1. The DEX was dissolved in 1 ml of DMSO before adding the PBS. The LAP and GelMA were added to the drug mixture and dissolved using a magnetic stirrer at 60 °C. Finally, the PEGDA was added and mixed well before pouring into a 10 ml syringe and injected between two acrylic plates, that have a U-shaped spacer, of a 0.35 mm thickness, in between. The sheets holding the hydrogel were put under LED light at 405 nm, using an intensity of 24 W, for 180 seconds and then cut into lenses with a cork borer 13 mm in diameter as shown in Figure 4.2.

Table 4.1. GelMA hydrogel BCL formulations prepared using the solvent casting technique

Formulation symbol	DEX (% w/w)	LAP (% w/w)	GelMA (% w/w)	PEGDA (% w/w)
G5P0	1	0.5	5	0
G5P5	1	0.5	5	5
G5P10	1	0.5	5	10
G5P15	1	0.5	5	15
G8P0	1	0.5	8	0
G8P5	1	0.5	8	5
G8P10	1	0.5	8	10
G8P15	1	0.5	8	15

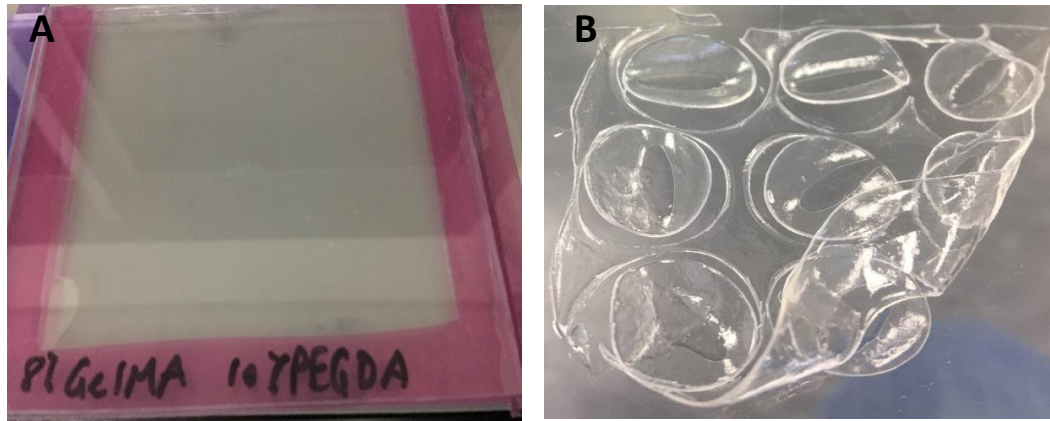


Figure 4.2. Crosslinked GelMA hydrogel film in between 2 acrylic sheets and spacer (A) and lenses cut from the film using a cork borer (B).

4.2.4 Preparation of BCLs using the 3D-printing technique

The hydrogels were prepared as previously mentioned, and the hydrogel mixture was then transferred to a 10ml Luer lock syringe, the black plunger was removed from the white piston and put on top of the syringe, then the syringe was inverted and the contents were pushed to get rid of the excess air. The whole syringe was wrapped with aluminium foil and inserted in a beaker full of ice for 8 minutes to enhance the physical gelation of GelMA, then left at room temperature overnight until the printing time. Four of the previously prepared formulations were chosen to be prepared using the 3D-printing of the solvent casting technique.

Table 4.2. GelMA hydrogel BCL formulations prepared using the 3D-printing method.

Formulation symbol	DEX (% w/w)	LAP (% w/w)	GelMA (% w/w)	PEGDA (% w/w)
#G5P0	1	0.5	5	0
#G5P10	1	0.5	5	10
#G8P0	1	0.5	8	0
#G8P10	1	0.5	8	10

The bandages were designed as a mesh structure using SolidWorks CAD software as shown in Figure 4.3 (A). The design was set to be 10 ± 0.5 mm in length, 10 ± 0.5 mm in width, with a 0.5 mm gap between the lines. The thickness of the lines were designed to be 0.2 mm, which is equal to the internal diameter (ID) of the needle used for printing. The STL file of the design generated by SolidWorks was uploaded into Repetier-Host

software twice to generate two layers. Each layer was rotated so that the lines of the first layer were vertically facing and the lines of the second layer were horizontally facing as shown in Figure 4.3 (B & C). Then the 2 layers were centred and merged to form a mesh structure with crossing vertical and horizontal lines and internal pores of 0.5mm in diameter as shown in Figure 4.3 (D). After adjusting the printing parameters using Slic3r software, the design was sliced into 2 layers, using the same software, to enable its printing in a layer-by-layer format. Figure 4.3 (E) shows the sliced g-code file generated by slice3r software and the path of the printing nozzle.

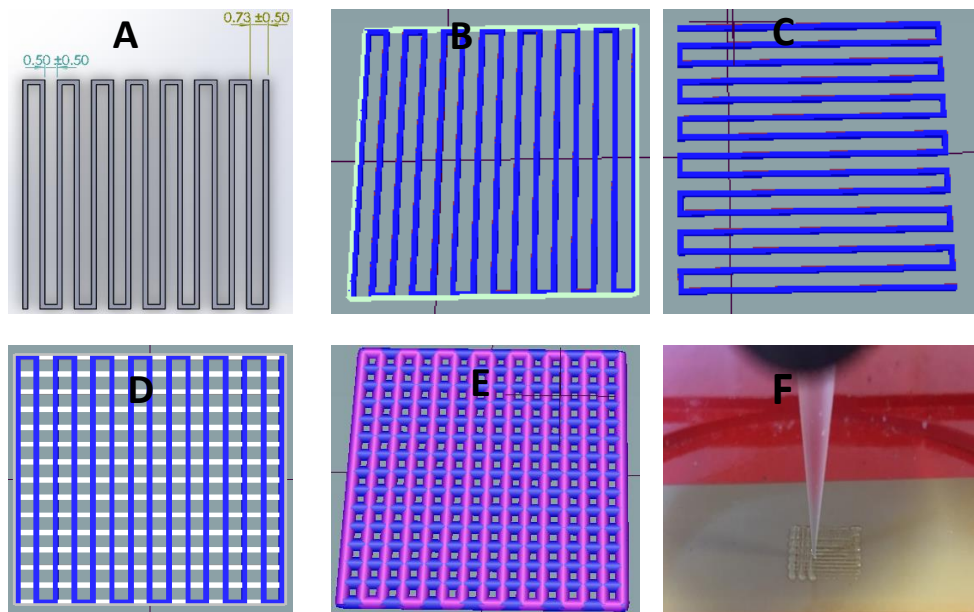


Figure 4.3. The 3D printing process. Design of 1-layer using SolidWorks in stl format (A), Uploading the stl file in Slic3r software (B), Reuploading the same stl file and changing its orientation to orient the lines horizontally (C), merge and centre of both uploaded files (D), slicing of the stl file into 2-layer g-code (E) and 3D printing of the sliced file using Allevi printer software (F).

The g-code was uploaded into the Allevi 3D-printer software, to allow the extrusion the hydrogel through the nozzle and print the bandage layer-by-layer using the Allevi 2 3D-printer (Allevi, Philadelphia, USA). Figure 4.3 (F) shows how the second layer of the bandage was printed on top of the first layer. The printed bandages were cured under an LED light of 405 nm for 3 min, then they were kept at room temperature in a vacuum oven for 24 h. The meshes were printed on glass slides covered by plastic tape to prevent the adhesion of the printed structure and to facilitate its removal.

4.3 Characterisation of the bandages

4.3.1 Microscopic examination

Optical images of the 3D-printed bandages were taken just after printing and after vacuum drying. The optical images were captured using a digital microscope (Leica ICC50HD-DM750, New Zealand) to show the diameter of the printed lines and the pore size of the meshes. Measurements were taken from 3 different sites on each mesh for 3 printed meshes.

4.3.2 Swelling studies

The equilibrium water content (EWC) was determined gravimetrically using a sensitive balance. Three vacuum dried meshes from each hydrogel formulation weighed (DW), then they were immersed in 3 ml PBS for 24 h, blotted gently with tissue papers and then reweighed to record the swollen weight (SW). The EWC of all hydrogel formulations were calculated using the following equation (Hoch, Schuh, Hirth, Tovar, & Borchers, 2012; Noshadi et al., 2017; Yin, Yan, Wang, Fu, & Suo, 2018).

$$EWC (\%) = \frac{(SW - DW)}{DW} \times 100$$

4.3.3 *In vitro* degradation

To test the *in-vitro* degradation profile of the cured printed meshes, 12 meshes of each formulation were dried in a vacuum oven at room temperature for 48 h and their weights were recorded (W_1). Then the meshes were immersed in 3 ml of PBS in plastic well plate dishes and kept in an incubation room at temperature 36 ± 1 °C. At various time intervals at days 1, 2, 4, and 7, three meshes of each formulation were carefully removed from the PBS solution and dried in a vacuum oven at room temperature for 48 h then reweighed (W_2). The percentage weight remaining after degradation at each time point is referred to as the gel fraction (%) and was calculated using the following equation (Bukhari, Khan, Rehanullah, & Ranjha, 2015; Y. Wang et al., 2018).

$$Gel\ fraction (\%) = \frac{w_2}{w_1} \times 100$$

4.3.4 *In vitro* drug release

The *in vitro* drug release profiles of DEX from the hydrogel cut lenses were studied by inserting each lens into dialysis membrane tubes (cut off 3500 MWCO) with a 1 ml of

PBS (pH=7.4) and then the wrapped tubes were placed in capped glass containers containing 39 ml of a PBS solution caps on a benchtop shaker (SK-300, Lab Companion, Korea) at 50 rpm. The shaker was placed in an incubator room that was maintained at 35 ± 2 °C for a period of 14 days. At predetermined time intervals, 3 ml of the media from each sample was collected and replaced by fresh media to maintain sink conditions. The concentrations of DEX in the release media were determined by comparing the areas of the drug peaks generated by an LC-MS Agilent 1260 Infinity Quaternary LC system (Santa Clara, CA 95051 USA) against a DEX calibration curve.

The system consisted of the following components: 1260 quaternary pump (model number: G1311B), 1260 infinity ALS sampler (model number: G1329B), 1200 series autosampler thermostat FC/ALS/Therm (model number: G1330B), 1260 infinity TCC column component (model number: G1316A), 1260 infinity diode array detector (DAD) (model number: G4212B), connected to a 6420 triple quadrupole LC/MS system with multimode ionisation source (model number: G1948B) operating in positive electrospray ionisation mode.

Waters XSelect CSH C18 (2.1 x 100 mm, 3 μ m) HPLC column was used for this analysis. The first mobile phase was composed of water containing 0.1% (v/v) formic acid while the second mobile phase was acetonitrile containing 0.1% (v/v) formic acid. The initial gradient condition was 97:3 (A:B). From 0 to 12 min the B was increased to 25%, from 12 to 13.5 min the B was increased to 90% and from 13.5 to 15.5 min, B was decreased to 3%. The total run time of each sample was 23 min.

The MS ionisation source conditions were as follows: capillary voltage of 1.8 kV, drying gas temperature of 325 °C, drying gas flow 6 L/min, vaporiser temperature of 200 °C. The positive ion mode was performed with MRM for quantitative analysis. The precursor-to-product ion transition used for DEX was $[M+H]^+$ m/z 393.2- \rightarrow 373.2 with a fragmentor voltage of 87 V and collision energy of 4 eV.

4.3.5 Statistical analysis

Data were subjected to one-way analysis of variance (ANOVA) using Microsoft 365 Excel. Post hoc multiple comparisons were determined by the Tukey's test with the levels of significance set at $P < 0.05$. All data were presented as means \pm SD.

4.4 Results and discussion

4.4.1 Characterisation of prepared GelMA

Introducing methacryloyl substitution groups to gelatine via a chemical reaction with methacrylic anhydride (MAA) results in the formation of gelatine methacrylamide (GelMA) as shown in Figure 4.4. ¹H-NMR spectra were used to determine the amount of methacrylate and methacrylamide groups in the prepared GelMA. There was an apparent decrease in the free lysine signal (NH₂CH₂CH₂CH₂CH₂-) of the unmodified gelatine at 3.0 ppm, and the DM of the prepared GelMA was calculated as 67.4 ± 2.14%.

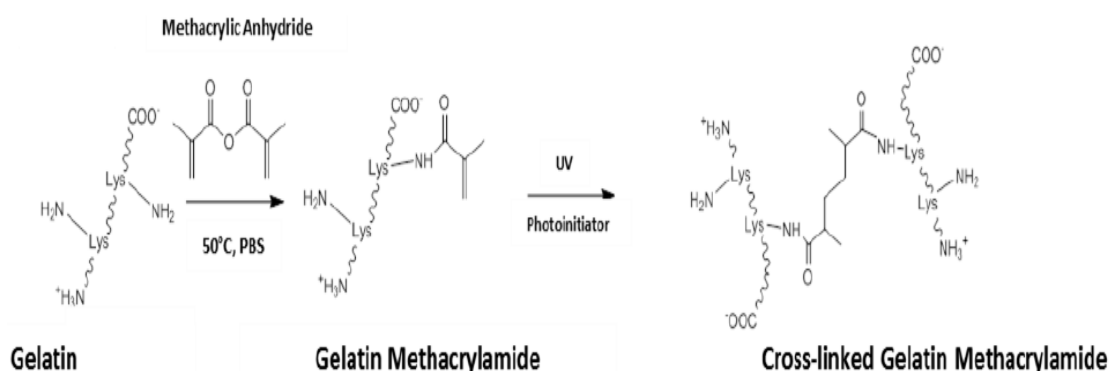


Figure 4.4. Methacrylation of gelatine to gelatine methacrylamide (Adopted from ((Rose et al., 2014)).

In comparison with the ¹H-NMR spectra of gelatine shown in Figure 4.5 (B), new proton peaks belonging to methacryloyl groups of GelMA appeared between 6.0–5.4 ppm and at 1.9 ppm as shown in Figure 4.5 (A). The chemical shifts between 5.7–5.6 and 5.5–5.4 ppm are for the acrylic protons (CH₂=C(CH₃)CONH-) of methacrylamide groups (lysine and hydroxylysine residues), while the peak at 1.9 ppm is for the methyl protons (CH₂=C(CH₃)CO-) of methacryloyl groups, as well as additional small peaks 5.7 ppm for the acrylic protons (CH₂=C(CH₃)COO-) of methacrylate groups (M. Zhu et al., 2019).

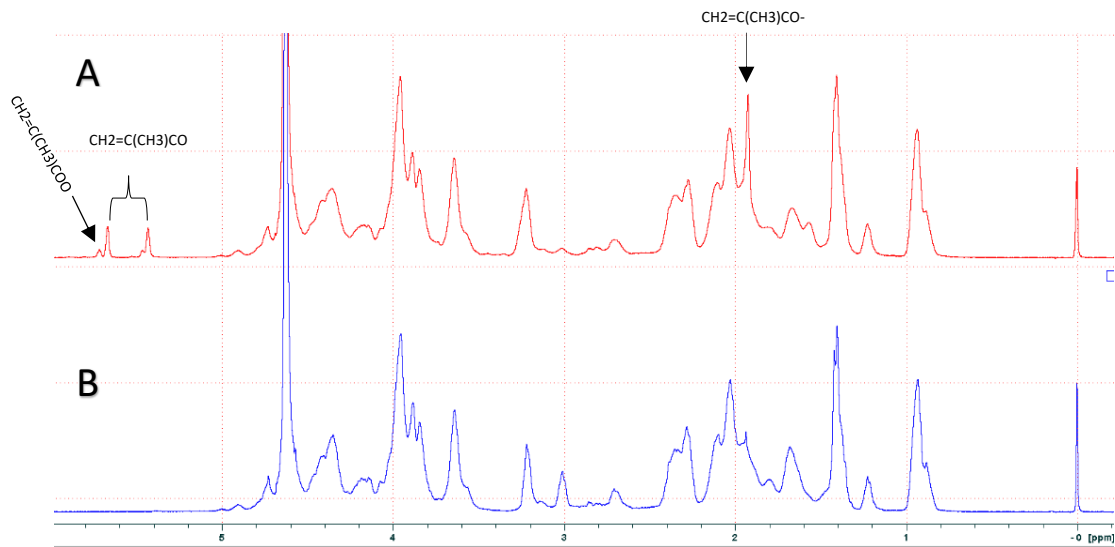


Figure 4.5. $^1\text{H-NMR}$ spectra of prepared GelMA (A) and porcine gelatine (B) samples in D_2O .

4.4.2 Preparation of GELMA film using the solvent casting technique

A photopolymerisation crosslinking reaction was performed to develop the GelMA BCLs, where light is used to initiate a free radical reaction using LAP photoinitiator. This free radical leads to a series of polymerisation reactions within the hydrogel monomers (propagation step), which end after all the monomers are polymerised. In this work, GelMA hydrogel formulations were cured under 405 nm LED light with an intensity of 24 W for 180 s. This was sufficient to polymerise the liquid hydrogel to a film, which was cut into circular lenses of 13 mm in diameter.

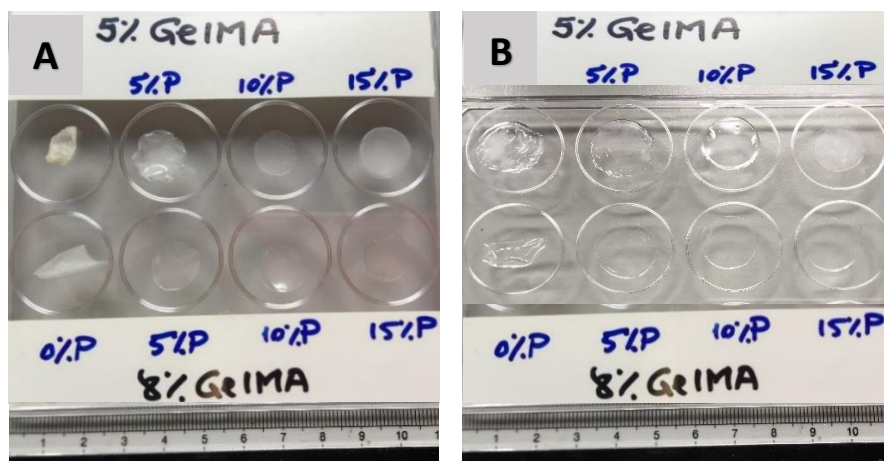


Figure 4.6. Images of vacuum-dried (A) and swollen (B) DEX-loaded GelMA lenses prepared using various concentrations of GelMA and PEGDA in the solvent casting. (Ruler is in mm increments).

The effect of the concentrations of GelMA and PEGDA on the developed lenses can be seen in Figure 4.6. Both 5% and 8% GelMA hydrogel formulations with no incorporated

PEGDA created sticky and fragile lenses that were easily deformed and couldn't retain their circular shapes, although the lenses obtained from 8% GelMA were stronger than the ones obtained from 5% GelMA. This goes in line with the results of another study that illustrated the effect of the increase in GelMA concentration from 5 to 15% that resulted in enhancement of the compressive modulus of the prepared hydrogels (Hutson et al., 2011).

The incorporation of PEGDA resulted in clear circular lenses that withstood handling during the characterisation tests. This was in compliance with the studies that incorporated PEGDA with GelMA to increase the degree of crosslinking and inhibit the biodegradation rates in bone regeneration materials, which revealed that GelMA/PEGDA hydrogels showed much stronger mechanical properties compared to pure GelMA hydrogels (Y. Wang et al., 2018).

4.4.3 Preparation of GELMA films using the 3D-printing technique

All hydrogel compositions were extruded using a 25 G nozzle with an inner diameter (ID) of 0.26 mm. Images of the printed meshes of the hydrogel formulations are presented in Figure 4.7. It is obvious that although all formulations were printed using the same nozzle size, the printed lines of #G5P0 meshes were thicker and the pores were not visible compared to #G8P10 meshes. This might be contributed to the lower density of the hydrogel that resulted in filament spreading of 5%GelMA hydrogels during printing.

The printing speed of #G5P0, #G5P10, #G8P0 and #G8P10 hydrogel formulations were 4, 4, 3 and 3 mm/s respectively. The printing speed of the 5% GelMA formulations was increased to compensate for rapid flow from the printing nozzle that led to the formation of thicker printed lines. Moreover, it was difficult for the printed lines of the 5% GelMA hydrogel formulations to retain their structure compared to the printed lines of the higher density 8% GelMA formulations, this might be contributed to the low density of the hydrogel that might have an effect on its rheological properties.

It is worth noting that the drying of the #G5P10 meshes resulted in the rupture of the structure. This might be contributed to the higher concentration of PEGDA compared to the concentration of GelMA, which resulted in huge shrinkage of the structure while it was attached to the plastic tape and thus the mesh was ruptured. On the other hand,

the higher concentration of GelMA maintained the structure and there was no visual shrinkage after the drying process.

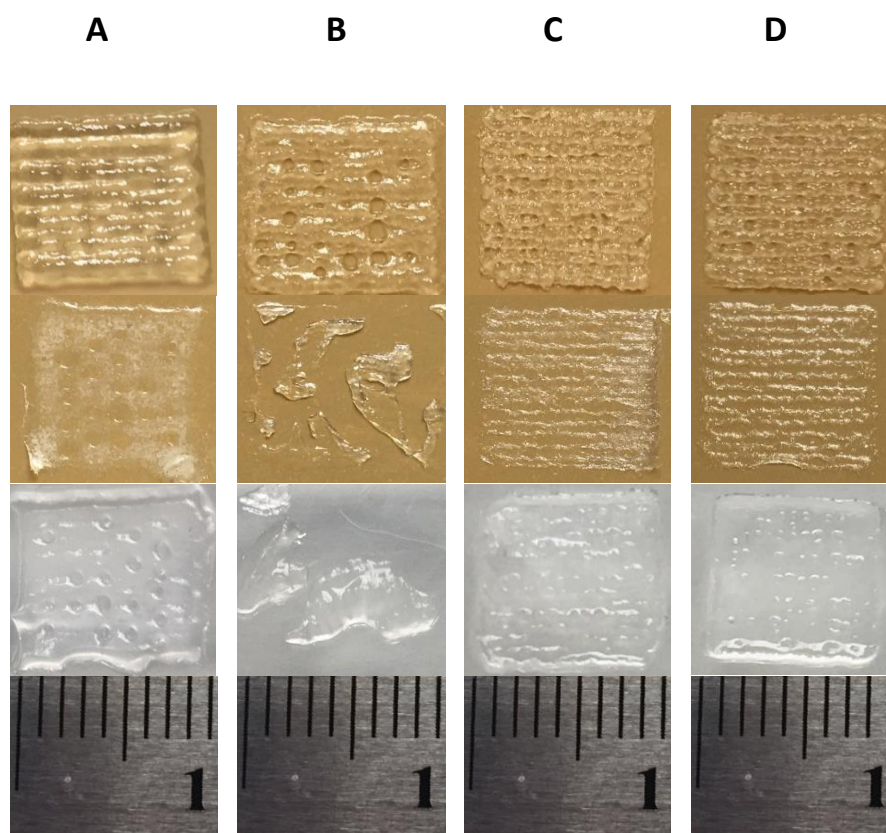


Figure 4.7. Images of the printed meshes (top), vacuum dried meshes (middle) and swollen meshes (bottom) of formulations G5P0 (A), G5P10 (B), G8P0 (C) and G8P10 (D). (Ruler is in mm increments).

4.4.4 Microscopic examination

The printed hydrogel meshes were imaged under the microscope to determine the effect of hydrogel composition on the diameter of the printed lines, just after printing and following vacuum drying of the meshes.

It was obvious that although all the hydrogels were extruded from nozzles with the same ID, the printed lines of the 5% GelMA hydrogels with and without the incorporation of PEGDA were almost double the diameter of the printed lines of 8% GelMA with or without PEGDA incorporation. This might be explained by the fact that **low-density** hydrogel solutions were extruded quicker from the 3D-printer nozzle, which resulted in thicker printed lines.

There was no change in the line measurements of #G5P0 hydrogel (0.7 ± 0.71 mm) before and after drying, however, the pore diameter increased from 0.3 ± 0.2 to 0.5 ± 0.2 mm after drying. Moreover, there was a significant shrinkage of the hydrogel meshes of #G5P10 after drying that resulted in rupture of the whole structure.

On the other hand, the hydrogel meshes of 8% GelMA maintained their shape in both compositions with and without PEGDA. The printed lines of #G8P0 and #G8P10 decreased in diameter from 0.32 ± 0.05 to 0.15 ± 0.07 mm after drying, while the pore size maintained the same diameter of 0.74 ± 0.13 mm.

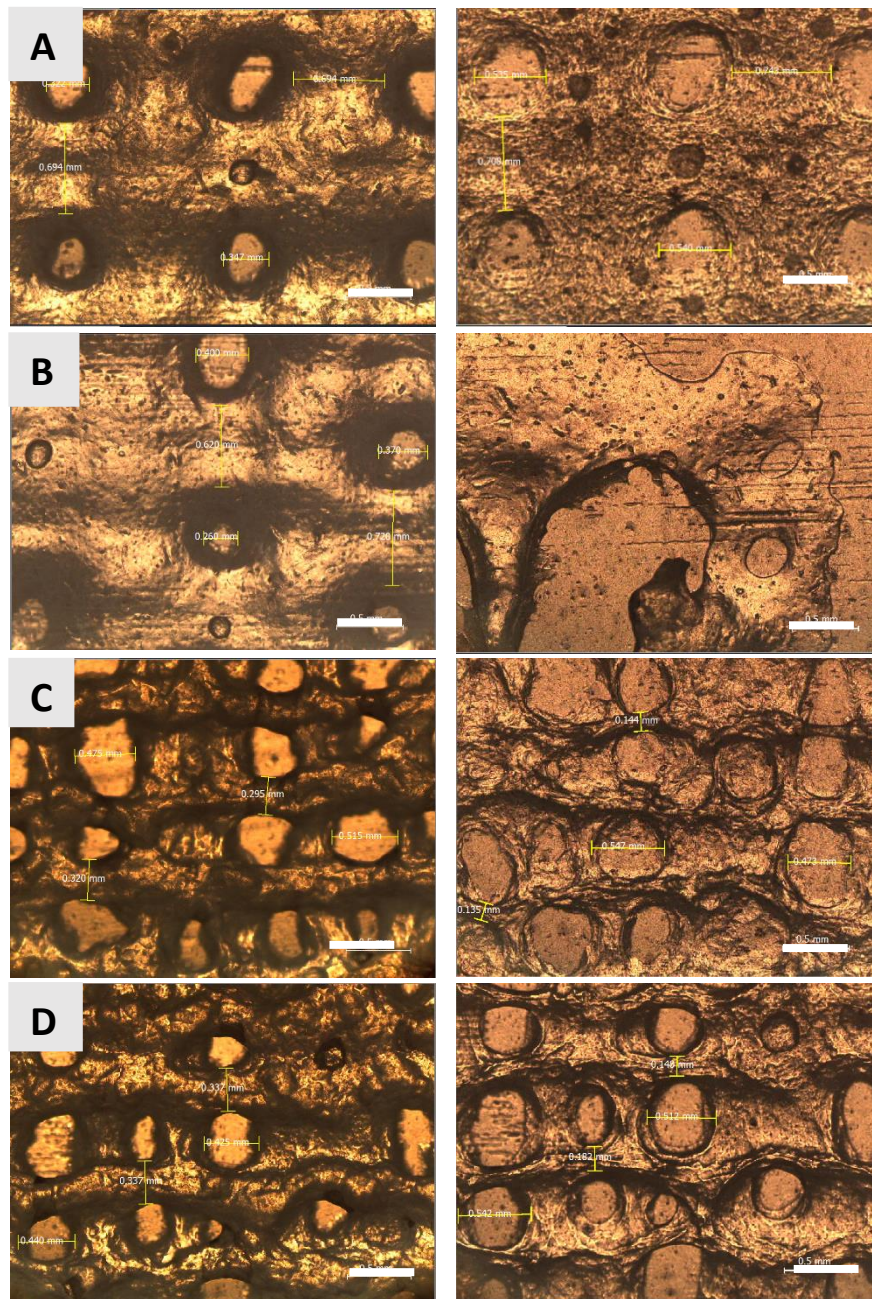


Figure 4.8. Microscopic images printed hydrogel meshes imaged immediately after printing (left) and microscopic image of vacuum-dried hydrogel meshes after vacuum drying (right) of #G5P0 (A), #G5P10 (B), #G8P0 (C) and #G8P10 (D). (White scale bar is 0.5 mm).

4.4.5 Swelling studies

In case of varying the concentrations of PEGDA within the 5 and 8% GelMA hydrogel formulations prepared using the solvent casting technique, the EWC decreased significantly with the amount of PEGDA added in both the 5 and 8% hydrogel formulations, as shown in Figure 4.9. This is explained by the increased degree of crosslinking as the concentration of PEGDA increases.

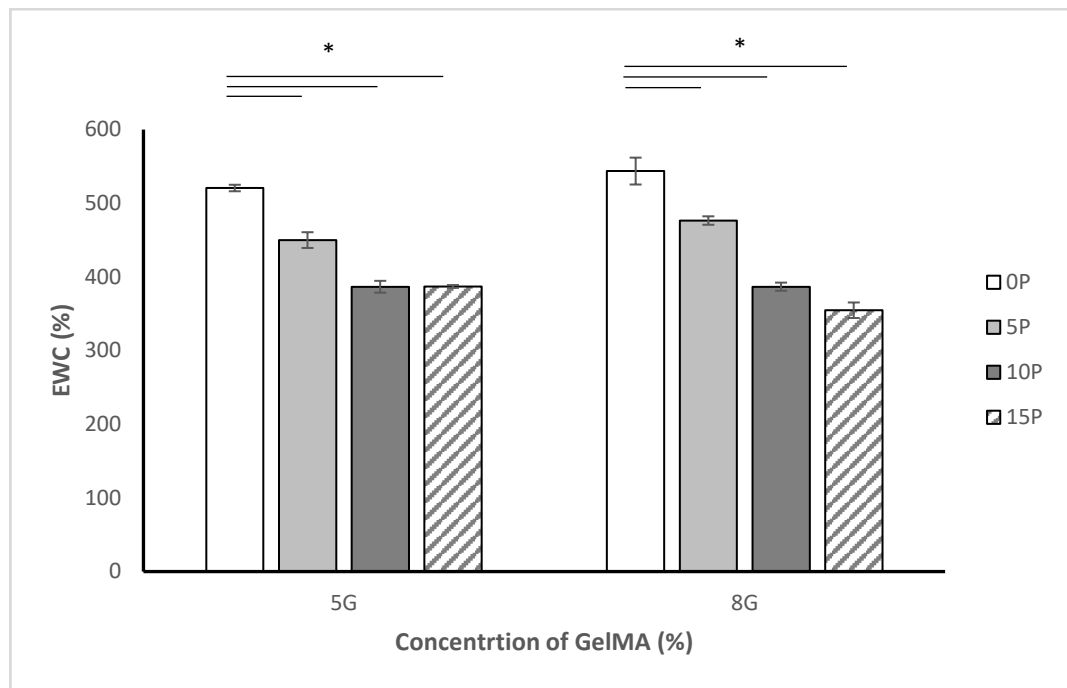


Figure 4.9. EWC of the prepared hydrogel BCLs after 24 h at 37 °C. *Statistically significant at $p < 0.05$; $n = 3$; mean \pm SD.

The high crosslinking degree improved the stiffness of the hydrogel meshes and resulted in low hydrogel swelling and thus lower water content (Y. Wang et al., 2018). However, the 5% and 8% GelMA hydrogel lenses reached their minimum EWC with the incorporation of 10% PEGDA at $368.6 \pm 8.06\%$ and $386.7 \pm 5.54\%$ and thus incorporating a higher percentage of PEGDA didn't show a significant decrease in the EWC values.

It is worth noting that the PEGDA concentration had a larger effect on the EWC when compared to the effect of GelMA concentrations. There was no significant difference between the EWC of G5P5 and G8P5, the EWC of G5P10 and G8P10 and the ECW of G5P15 and G8P15 as illustrated in Figure 4.9 above.

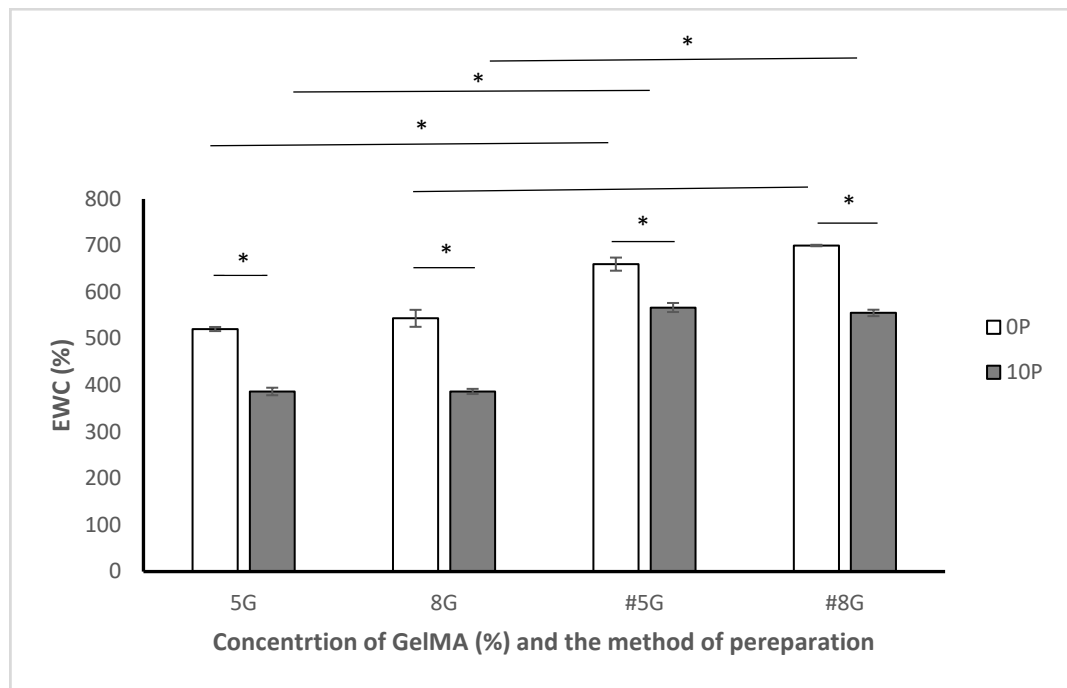


Figure 4.10. The effect of 3D-printing on the EWC of the prepared hydrogel BCLs after 24 h at 37 °C. *Statistically significant at $p < 0.05$; $n = 3$; mean \pm SD.

Testing the effect of method of preparation on some of the prepared hydrogel meshes indicated that there was a significant increase in the EWC values of the 3D printed hydrogel meshes compared to the ones prepared using the solvent casting techniques of the same hydrogel formulation. This might be because of the presence of pores within the 3D-printed hydrogel matrix, which increased the surface area of the hydrogel exposed to the PBS solution and thus more water is absorbed.

4.4.6 *In vitro* degradation

The degradation profiles of BCL of the hydrogel formulations mentioned in Table 4.1 above, prepared using the solvent casting technique, in PBS at 37 °C is illustrated in Figure 4.11. Both 5 and 8% GelMA hydrogel meshes showed a similar degradation trend. The BCLs that had no incorporated PEGDA degraded in 4 days. The incorporation of 5% PEGDA extended the degradation profile to 7 days, while the incorporation of 10 and 15% PEGDA significantly delayed the degradation of the lenses for more than 14 days. Those degradation profiles can be attributed to the increase in the crosslinking degree within the lenses with a higher concentration of PEGDA (Y. Wang et al., 2018). There was no significant difference in the degradation profiles with the increase in the concentration of PEGDA from 10 to 15% in both concentrations of GelMA hydrogel lenses. This is in agreement with the results of the EWC and can be explained that the

hydrogels reached their maximum crosslinking density at 10% concentration of PEGDA (Krumova, Lopez, Benavente, Mijangos, & Perena, 2000).

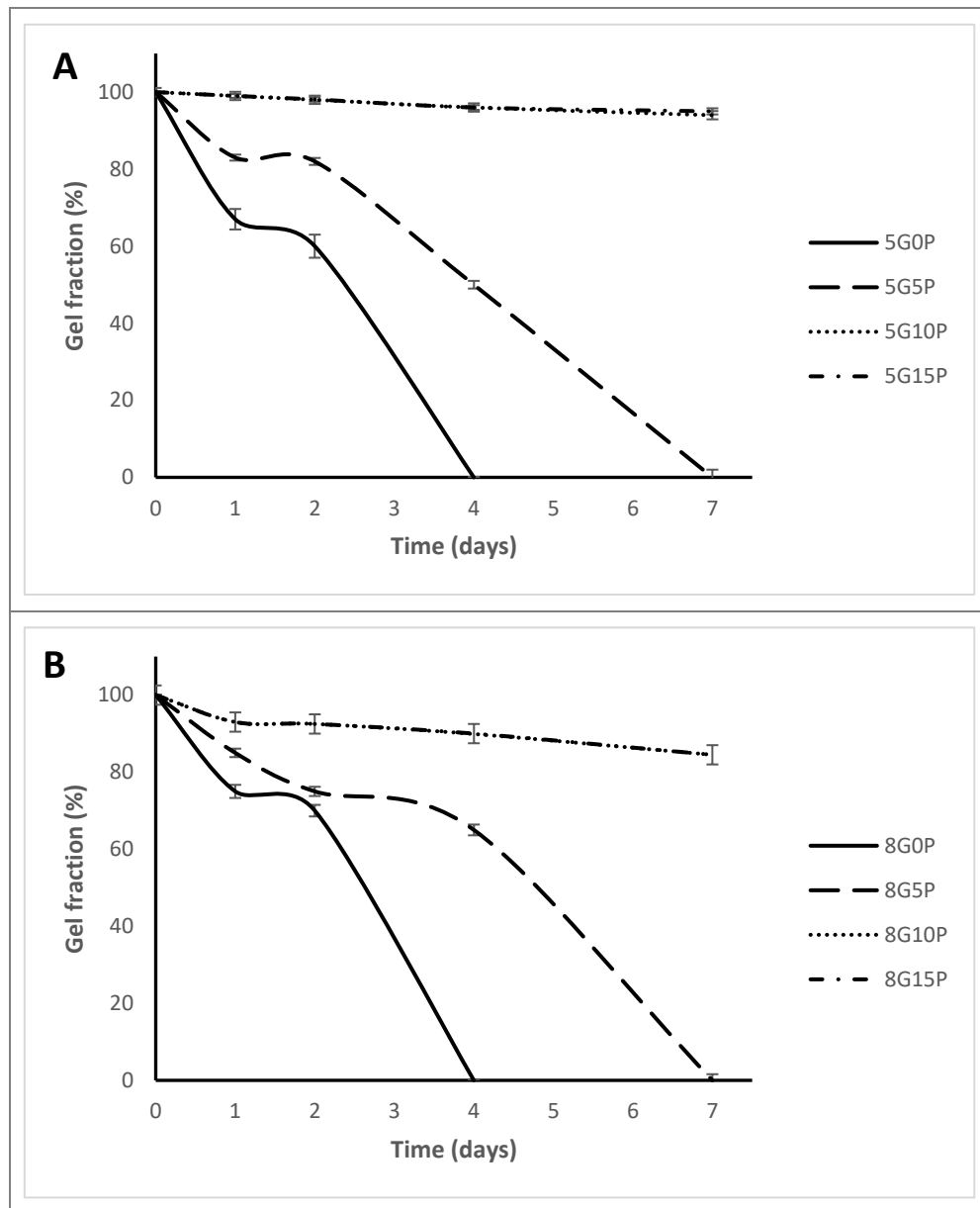


Figure 4.11. Degradation profiles of 5% GelMA (A) and 8% GelMA (B) hydrogel BCLs in PBS at 37 °C. n = 3; mean ± SD.

Although the lenses that had 5% GelMA finally degraded at the same time as the 8% GelMA BCL, the degradation rates of 8%GelMA lenses were slower compared to the 5%GelMA. This might be due to the high crosslinking density generated from the photo crosslinking reaction of the higher 8% GelMA concentrations within the hydrogel (Rizwan et al., 2017).

To visualise the effect of the degradation test on the shape of the BCL, the lenses that were removed from days 1, 2, 4 and 7 were vacuum dried and imaged. From the images of the lenses shown in Figure 4.12, it was clear that the optimum tested PEGDA concentration was 10% in both the lower and the higher GelMA concentrations. Surprisingly, G5P15 lenses retained their structure compared to the G8P15 ones following the *in vitro* degradation test. This might be attributed to the higher swelling ratio values of the 8%GelMA lenses, which might have resulted in rupture of the lenses (Kawaguchi & Oishi, 2004).

Degradation tests of the 3D-printed BCLs in PBS at 37 °C were performed and the generated degradation profiles were compared to the same hydrogel formulations that were prepared using the solvent casting technique as illustrated in Figure 4.13 below. 3D-printing 5 and 8% GelMA hydrogel formulations that had no incorporated PEGDA seemed to have slowed the degradation profiles of the BCL compared the solvent casting technique. This might be contributed to the printed mesh structure with vertical and horizontal lines, which might have had a role in maintaining the structure during degradation. However, there were no significant difference between the BCLs prepared by the 3D-printing and the solvent casting techniques when 10% of the PEGDA were incorporated within the GelMA hydrogel formulations. This shows that the crosslinking effect of PEGDA was more predominant and the degradation profiles of the BCLs were not affected by the preparation method.

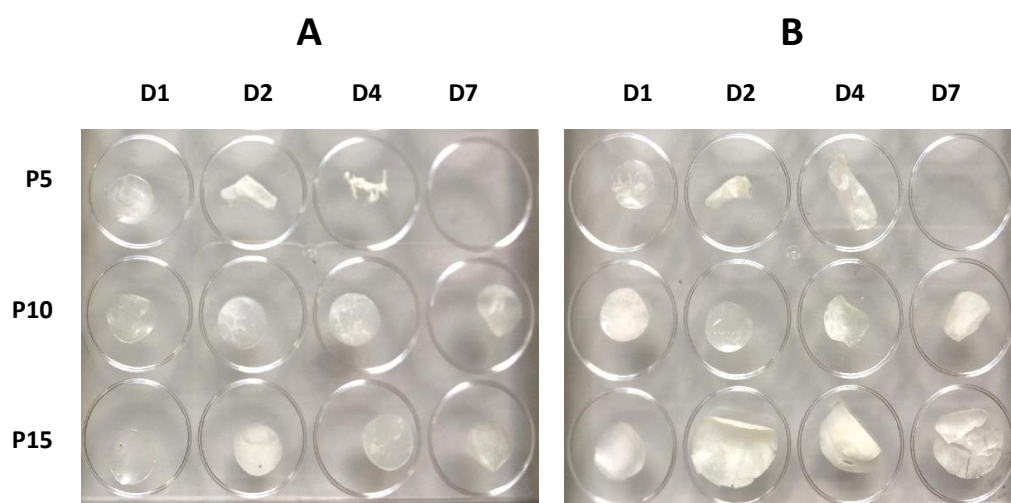


Figure 4.12. Images of the vacuum-dried P0, P10 and P15 BCLs formulations of 5% GelMA (A), and 8% GelMA (B) after the degradation test in PBS at 37 °C on days 1, 2, 4 and 7.

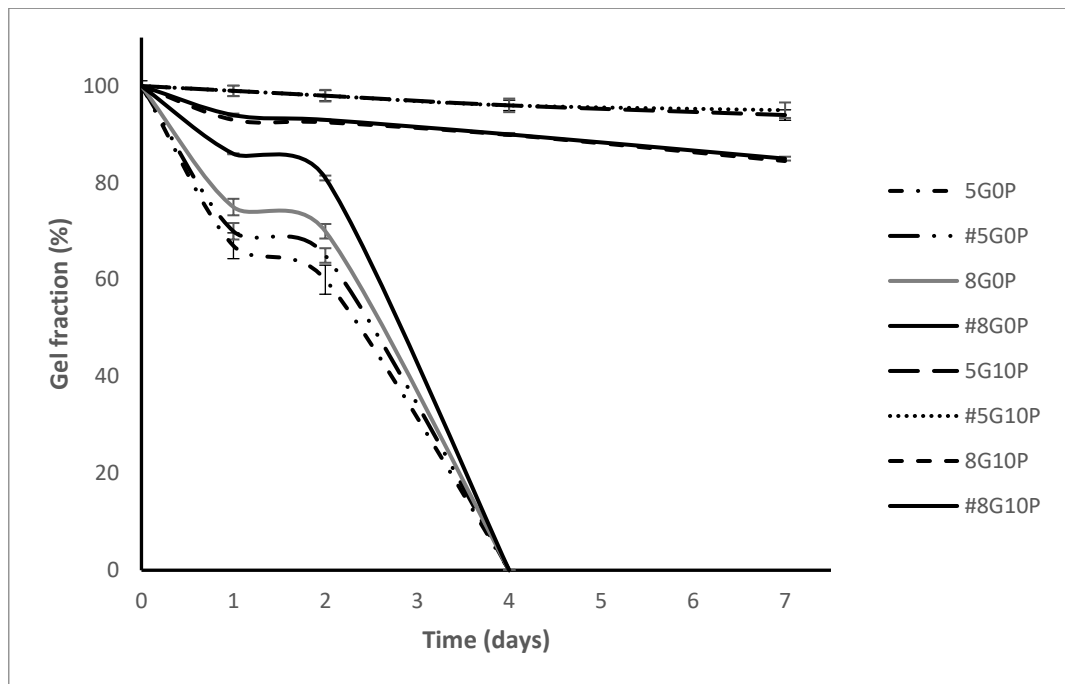


Figure 4.13. The effect of 3D-printing on the degradation profiles of the BCLs in PBS at 37 °C. n = 3; mean ± SD.

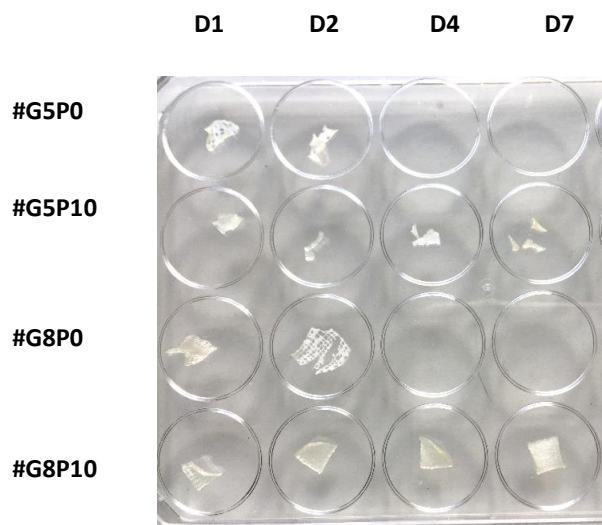


Figure 4.14. Images of vacuum-dried 3D-printed meshes for formulations #G5P0, #G5P10, #G8P0 and #G8P10 after the degradation test in PBS at 37 °C on days 1, 2, 4 and 7.

The images of the 3D-printed BCLs after the degradation test presented in Figure 4.14 shows how the structure of the tested printed BCL survived the degradation test. All the printed meshes maintained their shape until they fully degraded on D4 for #G5P0 and #G8P0 BCLs or for the ones that didn't degrade after 7 days (#G5P10 and #G8P10). Due to the rupture of the #G5P10 meshes after drying, the degradation test of those meshes was done using the resulting fragments, which didn't degrade during the test. It is worth

noting that although the printed meshes of #G8P10 did not shrink after drying, the meshes that were dried after the degradation test, significantly shrunk. This might be as a result of the high concentration of PEGDA within the hydrogel formulation.

4.4.7 *In vitro* drug release

Three BCLs from each of the tested hydrogel formulations prepared by the solvent casting technique were used in the *in vitro* drug release study. The % cumulative drug released per lens of each formulation was plotted against the corresponding time interval as illustrated in Figure 4.15 for 5% and 8% GelMA hydrogel formulations, respectively.

All the tested formulations showed a sustained release pattern of DEX from the BCLs for the whole duration of the test, even in the hydrogel formulations with no incorporated PEGDA. This shows that DEX was successfully entrapped within the hydrogel network of the polymerised GelMA during the photocrosslinking reaction (Schacht, 2004). However, BCLs of G5P0 and G8P0 formulations degraded at D4 and thus the maximum concentration of DEX released was 82.7 ± 7.9 and $65.6 \pm 0.7\%$ from the tested BCLs, respectively.

As expected, the incorporation of PEGDA resulted in slower drug release rates, where the % of DEX released from the BCLs of G5P5, G5P10 and G5P15 after 7 days were 78.0 ± 6.8 , 61.7 ± 0.14 and $60.3 \pm 0.3\%$, respectively. It was noted that although the incorporation of 5 and 10% PEGDA within the hydrogel formulations resulted in a significantly prolonged drug release rate, there was no significant difference between the release profiles of the BCLs that had 10 and 15% PEGDA within their hydrogel composition. This might be due to GelMA hydrogels reaching maximum crosslinking density using 10% PEGDA and therefore there was no further delay in the drug release of DEX with the increase in the concentration of PEGDA from 10 to 15%. This is in line with the previous degradation results of the BCLs presented in Figure 4.11 above.

On the other hand, there was no significant difference between the drug release profiles of the formulations of G8P5 and G8P10 BCLs, releasing 64.0 ± 2.8 and $63.7 \pm 4.0\%$ of their original drug content after 7 days. The increase in the concentration of PEGDA to

15% resulted in a prolonged release of DEX from the tested BCLs reaching $50.1 \pm 1.3\%$ after 7 days.

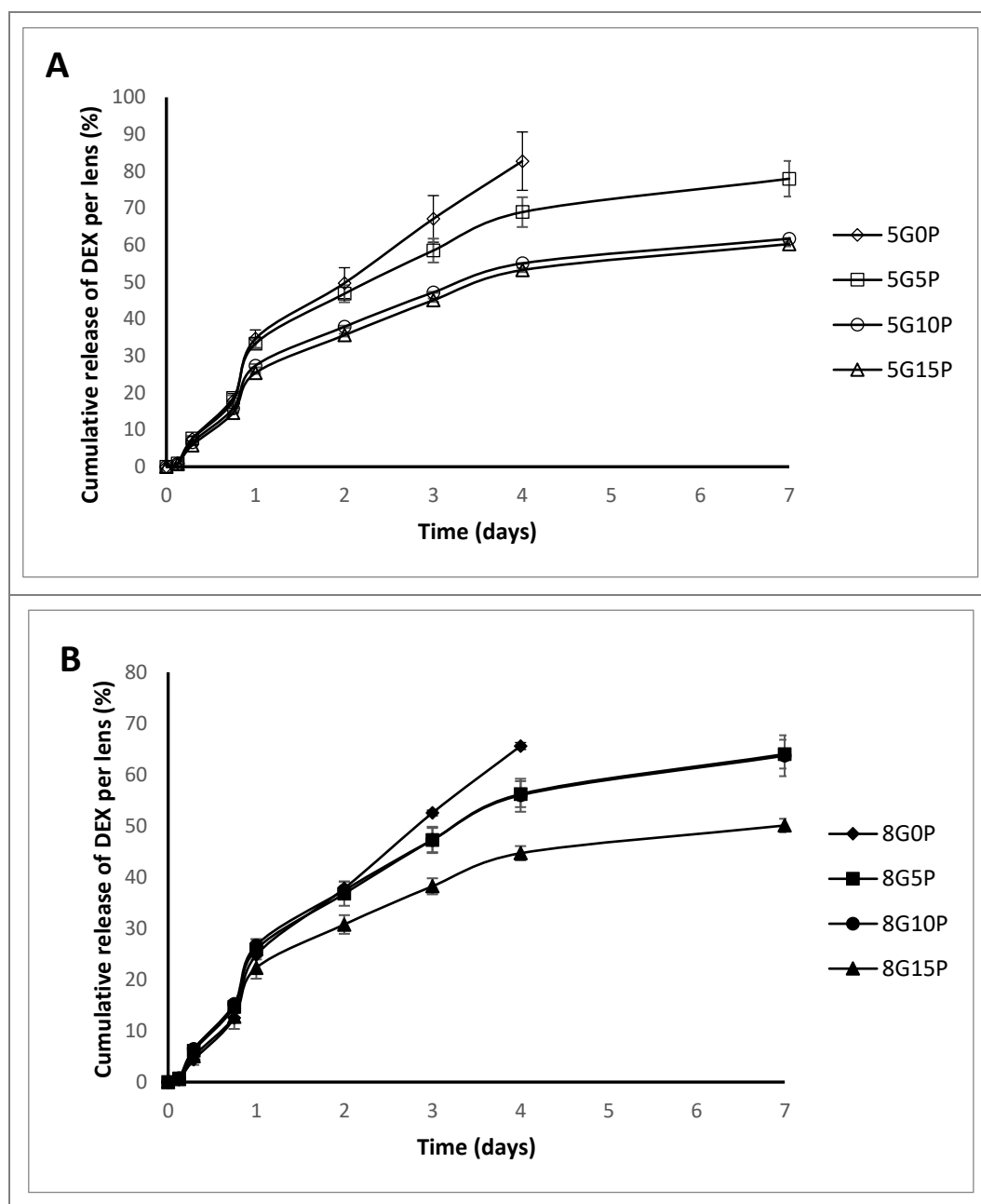


Figure 4.15. The effect of PEGDA incorporation on the drug release profiles of 5% GelMA (A) and 8% GelMA (B) BCLs in PBS at 37 °C. n = 3; mean \pm SD.

The effect of preparation method on the drug release profiles of the tested BCLs is illustrated in Figure 4.16. There was no significant difference between the two methods of preparation in the drug release profiles from BCLs prepared with 5% GelMA and 0% PEGDA, however, the 3D-printed lenses of the 8% GelMA and 0% PEGDA showed rapid release from the BCLs compared to the ones prepared using the solvent casting

technique. This might be explained by the higher swelling ratio of the 3D-printed lenses as previously illustrated in Figure 4.10 above. The higher the water content is expected to increase the pore size within the hydrogel matrix, and eventually promote the quick escape of the loaded drug (Hori et al., 2007). The same patterns of drug release profiles were noticed in the BCLs of the formulations containing 8% GelMA and 10% PEGDA, where the 3D-printed lenses showed rapid DEX release profile patterns compared to the solvent casted ones.

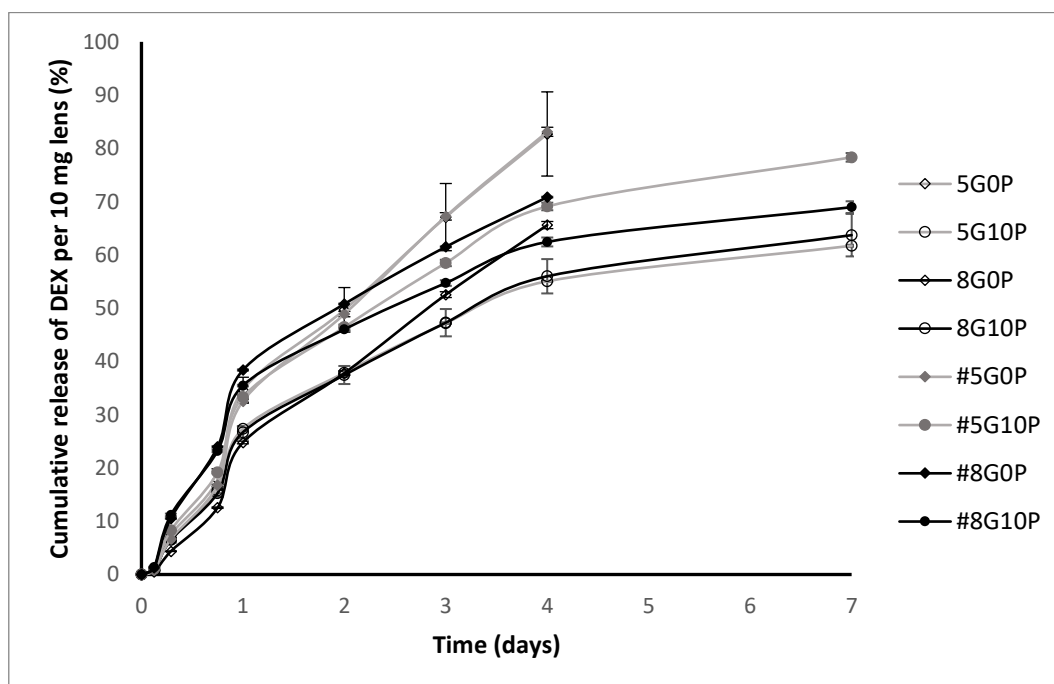


Figure 4.16. The effect of 3D-printing on the drug release profiles of G5P0, G5P10, G8P0, G8P10, #G5P0, #G5P10, #G8P0 and #G8P10 BCLs in PBS at 37 °C. n = 3; mean \pm SD.

4.5 Conclusion

In this chapter, 5 and 8% GelMA BCLs were prepared using various concentrations of PEGDA using the solvent casting and the 3D-printing techniques. The prepared lenses were evaluated for swelling, degradation and drug release properties. It was found that the incorporation of PEGDA improved the lenses' resistance to handling and protected them during the degradation test, reduced the EWC values and prolonged the release of the incorporated drug. It was found that the 3D-printing technique increased the EWC and thus resulted in a rapid drug release profiles compared to the lenses prepared using the solvent casting technique. However, there was still a sustained release of DEX from the 3D-printed lenses until they were fully degraded.

**Chapter 5 3D-printing of
GelMA/PEGDA composite hydrogel
meshes as potential cell-carrier for
tissue regeneration.**

Abstract

Tissue engineering can be used for the regeneration and repair of damaged tissues or replacing non-functional organs in order to avoid the limitations associated with organ transplantation. The most common technique currently used in tissue engineering is seeding cells and trophic factors into premanufactured scaffolds made from hydrogels. Gelatine methacrylate (GelMA) is the most widely used hydrogel bioink for creating 3D-printed scaffolds. After printing, GelMA is permanently crosslinked upon exposure to light and the presence of a photoinitiator within the hydrogel matrix. However, it is difficult to print complex scaffolds entirely out of GelMA hydrogel due to its low Young's modulus values and relatively low printing fidelity. The aim of this chapter is to incorporate polyethylene glycol diacrylate (PEGDA) within the GelMA hydrogel meshes to enhance their mechanical properties and control their degradation profiles for tissue regeneration purposes. Hydrogel meshes were 3D-printed and crosslinked using free radical photo-polymerisation reaction by incorporating LAP as a photoinitiator and curing under LED light (405 nm). The effect of PEGDA (0, 1 and 10%) on hydrogel mesh properties including shape, crosslinking, equilibrium swelling ratio (ESR), biodegradability and cell viability were evaluated. The incorporation of PEGDA enhanced the mechanical properties of GelMA hydrogels, increased their degree of crosslinking and significantly reduced the *in vitro* degradation rates. Moreover, *in vitro* cell culture experiments using human corneal epithelial primary cells (HCEpC) showed high adhesion, proliferation and viability over a period of 1 week in all the 3D-printed meshes. This proved that PEGDA can be incorporated with GelMA or other hydrogel polymers as a polymeric crosslinker without a negative effect on the viability of the seeded cells.

5.1 Introduction

After confirming the feasibility of printing drug-eluting BCLs loaded with DEX, to reduce the inflammation and promote natural regeneration of the cornea in mild-moderate injuries, in the previous chapter. It is important to check the feasibility of seeding cells on the printed hydrogel matrix and test the cell viability. The cell-loaded 3D-printed hydrogel meshes can be as novel non-invasive technique to deliver HCEpC to the injured cornea or in any tissue regeneration application.

Tissue degradation can occur in a wide range of diseases and injuries, which results in organ dysfunction and thus failure. When this happens, organ transplantation can be one of the treatment options; however, this is not always an option due to the high costs and scarcity of the donated organs. Tissue engineering can solve this problem by helping in the regeneration and repair of the damaged tissues or replacing the entire organ (Hutson et al., 2011; Khademhosseini, Langer, Borenstein, & Vacanti, 2006). The most common technique currently used in tissue engineering is seeding cells and trophic factors into premanufactured scaffolds that are made from hydrogels (Hutson et al., 2011; Slaughter, Khurshid, Fisher, Khademhosseini, & Peppas, 2009).

Hydrogels are networks of natural or synthetic polymers dispersed in water, and therefore are hydrophilic in nature. Hydrogels are favourable due to their high-water absorption capability, making them similar in nature and composition to the body's extracellular matrix (Sullad, Manjeshwar, & Aminabhavi, 2010). A wide range of natural and synthetic polymeric hydrogels and their composites have been developed for tissue regeneration purposes (Gerecht et al., 2007).

Hydrogels from protein origin have been widely used in tissue regeneration due to their physical properties and high biocompatibility (Yue et al., 2015). Gelatine is a protein produced by partial hydrolysis of collagen, which is the major protein component in skin, bone, cartilage and connective tissues. Since gelatine is a denatured protein, it is known for its high biocompatibility and low immunogenicity (B. Lee, Lum, Seow, Lim, & Tan, 2016). Moreover, gelatine contains numerous arginine-glycine-aspartic acid (RGD) sequences that enable cell attachment; and a matrix metalloproteinase (MMP) target sequence that enables cell remodelling (Yunxiao Liu & Chan-Park, 2010; Vandooren, Van den Steen, & Opdenakker, 2013).

At a temperature of ~45 °C, gelatine dissolves in aqueous solutions and is in a liquid state (sol). However, it undergoes a physical crosslinking process upon cooling, causing hydrogel gelation (gel). During the gelation process, the chains undergo a conformational disorder-order transition to recover the triple-helix structure of collagen (Bigi, Cojazzi, Panzavolta, Rubini, & Roveri, 2001). The process from sol to gel and back to sol again (sol-gel-sol) is reversible and temperature dependant. However, at body temperature (37 °C), gelatine is in the sol state, which limits its use for in-vivo applications (Y. Wang et al., 2018).

Various crosslinking techniques, including physical or chemical reactions, have been utilised to polymerise hydrogels for different biomedical applications (Y. Wang et al., 2018). Usually, hydrogels that are used as cell carriers for tissue regeneration are chemically crosslinked to help maintain their structure in biological fluids (Drury & Mooney, 2003). To enhance the mechanical properties of gelatine hydrogels in aqueous media, researchers have used chemical crosslinkers including glutaraldehyde (Bigi et al., 2001), dialdehyde starch (DAS) (Mu et al., 2010), dialdehyde carboxymethylcellulose (DCMC) (Mu, Guo, Li, Lin, & Li, 2012), genipin (Muzzarelli, 2009), and phenolic compounds such as caffeic and tannic acids (X. Zhang et al., 2010). However, chemical crosslinking agents are usually toxic and thus cannot be used in tissue engineering applications as shown in Figure 5.1, which provides a non-toxic alternative for gelatine crosslinking that is safe to use with cells (Y. Wang et al., 2018).

Since only less than 5% of the amino acid residues of gelatine are methacrylated in GelMA, the resulting hydrogel still has most of the functional gelatine motifs useful for cell attachment and remodelling (Van Den Bulcke et al., 2000). The stiffness of GelMA hydrogels can be manipulated by controlling the concentration of GelMA, the amount of photoinitiator and the crosslinking reaction time, which all contribute to the degree of crosslinking of the hydrogel (Wei et al., 2015). Thus, GelMA is widely used as a bioink in bioprinting applications, where it covalently crosslinks after printing upon exposure to light and presence of a photoinitiator within the hydrogel matrix. A schematic figure that shows the difference between physical gelation of gelatine and chemical gelation of GelMA is presented in Figure 5.1.

The use of PEGDA is common in tissue engineering applications since it is a biocompatible, nonimmunogenic and photocrosslinkable polymer with robust mechanical properties that can be easily modified (Guo & Chu, 2005); however, PEGDA polymer has a slow hydrolytic degradation (Browning & Cosgriff-Hernandez, 2012; Hockaday et al., 2012). Moreover, cells cannot directly attach to PEGDA since it is a synthetic hydrogel with no bioactivity (Hutson et al., 2011). This problem can be solved with the incorporation of bioactive polymers and peptides including gelatine, hyaluronic acid and laminin (Ali, Saik, Gould, Dickinson, & West, 2013; Fu et al., 2012; Ouasti et al., 2011; F. Yang et al., 2005).

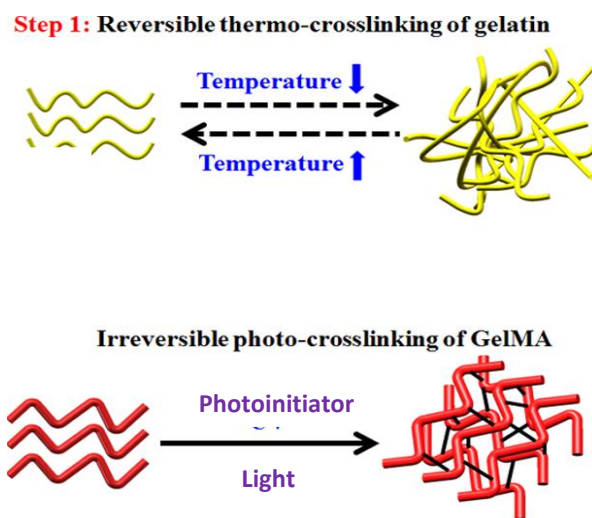


Figure 5.1. Difference between physical and chemical crosslinking of gelatine showing the covalent bonds generated during the photopolymerisation reaction of GelMA. (Adapted from (Yin et al., 2018)).

Various photoinitiators have been used in free radical hydrogel polymerisation reactions, where each photoinitiator works best under a certain light wavelength. The most commonly used photoinitiator for tissue engineering applications that works under the UV range (365 nm) is 2-hydroxy-4'-(2-hydroxyethoxy)-2-methylpropiophenone, which is known as Irgacure 2959. However, Irgacure 2595 has low water solubility and requires prolonged exposure to UV light, which may cause DNA damage and impair cellular functions of the cells present within the hydrogel polymer (Monteiro et al., 2018; Williams, Malik, Kim, Manson, & Elisseeff, 2005). Therefore, a photoinitiator that works in the visible light range is preferable when downstream applications involve living cells. Lithium phenyl-2,4,6-trimethylbenzoylphosphinate (LAP) is a water-soluble photoinitiator that works in the visible range (405 nm) and is used due to its

cytocompatibility and effectiveness at low concentrations (Fairbanks, Schwartz, Bowman, & Anseth, 2009).

The use of 3D-printing technology to generate 3D hydrogel scaffolds has been proven to be more successful in cell culture. It has been demonstrated that cells behave differently in a 3D environment compared to cells cultured in monolayers (2D), showing responses more comparable to those in native tissues (Pampaloni, Reynaud, & Stelzer, 2007). Therefore, 3D-bioprinting technology has been widely utilised in tissue engineering applications (Murphy & Atala, 2014). Hydrogels are often employed as bioinks in the bioprinting processes that are printed into complex scaffolds using 3D-printing technology. Cells can either be incorporated within the hydrogel and thus the ink is referred to as “bioink” or seeded onto the hydrogel scaffold after printing.

Currently, the most common method utilised in tissue engineering is expanding the patients’ cells in culture media, which are then transferred to a pre-printed 3D hydrogel scaffold. It is important that 3D-printed scaffolds achieve the functionality of the tissues they are replacing, therefore they must be biocompatible, biodegradable and with mechanical properties similar to the original tissues. It is worth mentioning that porous engineered scaffolds have the ability to guide cell differentiation and assembly within the 3D structure (Yin et al., 2018). Precise control of the internal structure of the scaffolds can be **achieved by 3D-printing techniques** to represent the complexity of the natural extracellular matrix and pores to accommodate cell attachment and growth of the seeded cells (Colosi, Costantini, Barbetta, & Dentini, 2017; Pati et al., 2014).

Inkjet printing, laser-assisted printing, stereolithography and extrusion-based printing are common bioprinting strategies used in tissue engineering. However, extrusion-based printing has become the most widely used technique due to its simplicity, low cost and compatibility with a wide range of bioinks (Sheth et al., 2016; Y. S. Zhang et al., 2017). In extrusion-based 3D printing, which is the technique used in this work, the polymer hydrogel is precisely extruded from a syringe via a nozzle of known internal diameter and deposited in a layer-by-layer manner to print the desired structure. This structure is pre-designed by computer software and thus this model is referred to as computer-aided design (CAD). The cells are added to the 3D printed meshes after the printing, curing and drying processes.

Although hydrogels used in tissue engineering are required to have low polymer concentrations, low stiffness and low crosslinking densities to allow for cell diffusion, migration and proliferation (Seliktar, 2012), 3D-printing requires hydrogels to have high viscosity and stiffness to allow for accurate extrusion, high shape fidelity during printing and sufficient mechanical stability to maintain the complex shape of the crosslinked hydrogel structure after printing (A. Ribeiro et al., 2017). Therefore, a promising approach to overcome this challenge is to use hydrogel composites, where the functions of cell encapsulation and mechanical support come from two different materials (Melchels et al., 2016).

The aim of this chapter is to develop 3D-printed GelMA/PEGDA composite hydrogel meshes as a cell carrier for tissue regeneration purposes, with high printing fidelity, adequate mechanical properties and controllable degradation profile. Hydrogel meshes were prepared by free radical photo-polymerisation using blue visible light (405 nm) and LAP as a photoinitiator. The effect of 3 PEGDA concentrations (0, 1 and 10%) on hydrogel mesh properties including shape, crosslinking, equilibrium swelling ratio, biodegradability and cell viability were evaluated. It is hypothesised that the supplementation of GelMA hydrogels with PEGDA will create a photocrosslinkable hydrogel composite with better mechanical and degradation properties suitable for several tissue engineering applications.

5.2 Materials and methods

5.2.1 Materials

An Allevi2 double extruder 3D-bioprinter, printing needles, and lithium phenyl-2,4,6-trimethylbenzoylphosphinate (LAP) were obtained from Allevi, Philadelphia, USA. Polyethylene glycol diacrylate (PEGDA, M_n 700) and Phosphate Buffered Saline (PBS) tablets 1.0M, pH 7.4 (25 °C) were from Sigma-Aldrich, New Zealand. Human corneal epithelial primary cells (HCEpC) were provided by the New Zealand National Eye Bank, Department of Ophthalmology, University of Auckland, New Zealand. All components of culture media were from Gibco™, Thermofisher Scientific, New Zealand. All other chemicals were of analytical grade.

5.2.2 Hydrogel preparation

GelMA was prepared as stated in the Preparation and characterisation of GelMA hydrogel section in chapter 4 (p. 66). To choose the best printable GelMA concentration to be used in this study, 7, 8, 9 and 10% w/v GelMA hydrogels were prepared, printed and characterised. Two concentrations of LAP, 0.3 and 0.5% w/v were used with 10% GelMA to test the effect of the photoinitiator concentration on the crosslinking reaction. Furthermore the curing intensity and time were varied for those hydrogel formulations to determine the optimum curing conditions of the hydrogel meshes. Table 5.1 lists the various hydrogel compositions prepared and the crosslinking parameters applied to choose the optimum amount of photoinitiator and curing conditions for the 3D-printed hydrogel meshes.

Table 5.1. Composition of GelMA hydrogels for the crosslinking test.

GelMA (% w/v)	LAP (% w/v)	Curing intensity (mW/cm²)	Curing time (s)
10	0.3	13 & 15	120, 150 & 180
10	0.5	7, 8, 10, 12, 13, 14 & 15	120, 150 & 180
9	0.5	7, 8, 10, 12 & 13	120 & 150
8	0.5	13	150
7	0.5	13	150

After determining the optimum crosslinking parameters, PEGDA was incorporated with 8% GelMA and 0.5% LAP in a concentration of either 0, 1 or 10% w/v as shown in Table 5.2 and the printed hydrogels were characterised and viability studies were performed as outlined below.

Table 5.2. Composition of GelMA/PEGDA hydrogel composites.

Formulation symbol	GelMA (% w/v)	LAP (% w/v)	PEGDA (% w/v)
P0	8	0.5	0
P1	8	0.5	1
P10	8	0.5	10

To prepare the hydrogels, LAP was first dissolved in PBS using a magnetic stirrer at 60 °C. Then GelMA was added to the solution and mixed at the same temperature for around 20 min until fully dissolved. In the case of P1 and P10 formulations, PEGDA was added to the warm GelMA solution and mixed well. The hydrogel mixture was then transferred to a 10 ml Luer lock syringe, the black plunger was inserted, then the contents of the syringe were inverted and pushed to get rid of the excess air. The whole syringe was wrapped with aluminium foil and inserted in a beaker full of ice for 8 min to enhance the physical gelation of GelMA, then left at room temperature overnight until the printing process.

5.2.3 Preparation of the 3D-printed meshes

A square mesh design with crossing vertical and horizontal lines was created using SolidWorks CAD. The dimensions of the square were set to be 10 ± 0.5 mm in diameter, with a 0.5 mm gap between the lines. A detailed description of the printing process is found under "Preparation using the 3D-printing method" section in chapter 4 (p. 69).

Various crosslinking parameters were used to cure the printed hydrogel meshes in this work using the blue light (405 nm) lamp present in the Allevi2 bioprinter from a height distance of 10 mm. The intensity of the lamp varied between 7 and 15 mW/cm² and the curing time tested was either 120, 150 or 180 s.

The 3D printed meshes of 10% GelMA, 0.5% LAP cured for 150 s at 13 mW/cm² were either freeze-dried or vacuum dried while still on the slide. In the freeze-drying technique, the printed cured meshes were kept in the freezer under -18 °C overnight then put in a freeze dryer for 24 h. In the vacuum-drying technique, the printed cured meshes were kept at room temperature in a vacuum oven for 24 h.

5.2.4 Characterisation of the printed meshes

Visual and microscopic examination

Visual examination and camera images of the syringe carrying the prepared hydrogel (ink) prior to the printing process were performed. Images of the extruded ink filament at the used printing pressure were taken to show the consistency of the filament. Images of the hydrogel mesh printed on a glass slide were taken just after printing against a

ruler to show the printed mesh size. The glass slide was covered with plastic tape to prevent adhesion of the hydrogel to the slide and aid the removal after drying.

After vacuum drying of the printed meshes, they were imaged using a camera, an optical microscope and a scanning electron microscope (SEM). The optical images were captured using a digital microscope (Leica ICC50HD-DM750, New Zealand) to show the diameter of the printed lines and the pore size of the meshes. Measurements were taken from three different places for each mesh for three printed meshes.

After drying, meshes were soaked for 24 h in 3 ml PBS, then removed and kept at $-4\text{ }^{\circ}\text{C}$ for 24 h then placed in a freeze drier (Martin Christ, Alpha2-4 LDplus, John Morris Group, New Zealand) for 48 h before SEM imaging to view the internal structure of the wetted meshes.

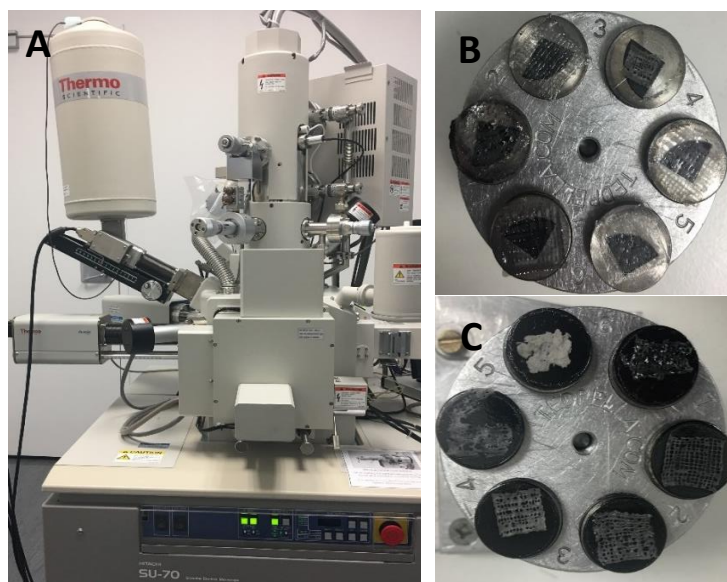


Figure 5.2. SEM (A), vacuum-dried meshes after printing (B) and freeze dried meshes after swelling (C) ready to be imaged by the SEM.

Prior to SEM imaging, all meshes were placed on metallic stubs and coated with platinum under vacuum for 20 s using an ion sputter coater (Hitachi E-1045, UK) for visualisation. The images were scanned using a Schottky field emission SEM (Hitachi SU-70, UK) under a working voltage of 5 kV. Three meshes were imaged for each hydrogel composition. Figure 5.2 shows the SEM imaging microscope used to view the dried meshes and the mounted meshes after sputtering ready to be imaged.

Degree of crosslinking

The printed, cured meshes were dried in a vacuum oven for 48 h, and the dry weight of each sample (w_1) was recorded using a 5 decimal place balance. The meshes were then immersed in 3 ml PBS solution at 37 °C. After 24 h, the meshes were removed from the PBS solution and dried in a vacuum oven for 48 h. The weight of the dry meshes (w_2) was recorded. The sol fraction is the amount of hydrogel that was not crosslinked and thus dissolved in PBS. It can be calculated using the following equation (Bukhari et al., 2015; Ranjha & Qureshi, 2014).

$$\text{Sol fraction (\%)} = \frac{(w_1 - w_2)}{w_1} \times 100$$

In this work, data from crosslinking test of 10% GelMA hydrogels that were cured using various crosslinking intensities of 7, 8, 10, 12, 13, 14 or 15 mW/cm² and different curing times of 120, 150 or 180 s were used to determine the optimum crosslinking parameters. Table 5.1 above shows the hydrogel formulations prepared and the curing parameters used for each composition. At least three meshes were tested under each crosslinking parameter. To determine the optimum photoinitiator concentration for crosslinking of GelMA hydrogels, the sol fraction of 10% GelMA hydrogels was compared with either 0.3 or 0.5% LAP cured at 13 or 15 mW/cm² for either 120, 150 or 180 s as illustrated in Table 5.1. above. This test was done in triplicates.

To determine the effect of GelMA concentration and curing parameters (intensity and time) on the crosslinking of the hydrogel meshes, 9 and 10% GelMA hydrogels were printed and cured under 13 or 15 mW/cm² for either 120, 150 or 180 s. Then, four concentrations of GelMA (7, 8, 9 and 10%) were cured at 13 mW/cm² for 150 s and their sol fractions were compared to choose the most suitable GelMA concentration for printing, this test was done on triplicates. Table 5.1 above shows the hydrogel formulations prepared and the curing parameters used for each composition.

Furthermore, to compare the effect of PEGDA on 8%GelMA hydrogels, the sol fraction of all hydrogel compositions prepared in Table 5.2 above were compared. Three meshes were used from each composition.

Swelling studies

The swelling ratio was determined gravimetrically using a sensitive balance, where the weights of three meshes (DW) were obtained after drying in a vacuum oven for at least 48 h. Those meshes were placed in 3 ml of PBS at room temperature and removed after 1, 2, 3, 4 and 24 h, blotted gently with tissue papers and then weighed to record the swollen weight (SW) and the swelling ratio was calculated using the following equation. A graph of the swelling ratio against time was plotted for 10% GelMA meshes to determine the equilibrium swelling ratio (ESR). For all other formulations, the ESR at 24 h were calculated and compared (Hoch et al., 2012; Noshadi et al., 2017; Yin et al., 2018).

$$\text{Swelling ratio (\%)} = \frac{(SW - DW)}{DW} \times 100$$

***In vitro* degradation**

To test the *in-vitro* degradation profile of the cured meshes, 12 meshes of each formulation were dried in a vacuum oven at room temperature for 48 h and their weights were recorded (W1). Then the meshes were immersed in 3 ml of PBS in plastic well plate dishes and kept in an incubation room at temperature 36 ± 1 °C. At days 1, 2, 3, 4, 5, 6, 7 and 14, three meshes of each formulation were carefully removed from the PBS solution and dried in a vacuum oven at room temperature for 48 h and then reweighed (W2). The percentage weight remaining at each time point is referred to as the gel fraction (%) and was calculated using the following equation (Bukhari et al., 2015; Y. Wang et al., 2018).

$$\text{Gel fraction (\%)} = \frac{W2}{W1} \times 100$$

Cell viability

In all cell viability experiments, the printed and cured meshes were dried in a vacuum oven for 48 h at room temperature. Before seeding the cells, the dried meshes were individually placed in the wells of a 12-well plate and put under UV light in a fume hood for 30 min to be sterilised. Table 5.3 shows the composition of GelMA hydrogel meshes tested for cell viability.

Table 5.3. Composition of GelMA hydrogel meshes tested for cell viability cured for 150 s under light intensity of 13 mW/cm² using 405 nm lamp.

GelMA% (w/w)	LAP% (w/w)	PEGDA % (w/w)
10	0.3	0
10	0.5	0
7	0.5	0
8	0.5	0
8	0.5	1
8	0.5	10

HCEpC extracted from human donor tissue, were used in this experiment. A cell suspension of 1x10⁶ cells per millilitre of cell culture was prepared. The meshes were sterilised under UV light for 30 min prior to use, then 100 µl of the previously mentioned cell suspension was pipetted onto the mesh and left for 15 min to settle before adding 500 µl of culture media and incubated for 1 week.

The culture media was prepared as a 1:9 ratio of 10% Foetal Calf Serum (FCS): MEM, GlutaMAX™ Supplement, then 1% of Antibiotic-Antimycotic (100) was added. Fresh culture medium was added on day 1 and the medium was replaced every other day. On day 2, the meshes were removed and placed in a clean plate with fresh culture media. After 7 days, the cells were stained using Invitrogen LIVE/DEAD® Viability/Cytotoxicity solution for mammalian cells (Thermo Fisher Scientific) that was prepared from the purchased kit according to the manufacturer's instructions.

Meshes were removed from the culture media and washed with PBS before staining. A volume equal to 100 µl of the LIVE/DEAD prepared solution was added to the hydrogel meshes and left for 20 to 40 min at room temperature. Meshes were then washed with PBS for 15 min, then removed and mounted on glass slides for imaging under a fluorescence microscope using an excitation/emission wavelength of $r \sim 495$ nm/ ~ 515 nm for calcein AM and $ex/em \sim 495$ nm/ ~ 635 nm for EthD-1. The resultant images were used to visualise the proportion of live to dead cells after 7 days of incubation.

Statistical analysis

Data were subjected to one-way analysis of variance (ANOVA) using Microsoft 365 Excel. Post hoc multiple comparisons were determined by the Tukey's test with the levels of significance set at $P < 0.05$. All data were presented as means \pm SD.

5.3 Results and Discussion

5.3.1 Preparation of the 3D-printed meshes

During the printing process, the printing parameters were set using Slice3r software to adjust the layer height, printing speed and the nozzle diameter. The layer height is the distance travelled upwards by the nozzle at the end of each printed layer, for it to be in the correct position ready to print the following layer on top of the previous printed one. The layer height depends mainly on the internal diameter of the needle used since this will in-turn control the thickness of the extruded filament and thus the height of the printed layer.

The speed is the distance travelled by the nozzle in mm/s while the hydrogel is extruded during the printing process of each layer. Setting the appropriate printing speed is critical to obtain a high-resolution print. Lower speed will cause thicker lines and smaller pore sizes, while higher speed will cause incomplete printed lines since the contact time between the extruded filament and the slide or the previously printed layer is not sufficient for adhesion to occur.

Various printing trials were performed using the Allevi bioprinter to optimise the printing parameters and obtain a high-resolution print. Table 5.4 is an example of some of the printing trials performed for 10% GelMA hydrogel meshes. In those printing trials, various needle sizes, extrusion pressures and printing speeds were tested until a good printed structure was reproducible.

The gauge number indicates the inner diameter of the printing needle, where higher gauge numbers represent needles with a smaller inner diameter (ID). Example of printing needles with various sizes are shown in

. Choosing a suitable needle for each print depends on the resolution required and the viscosity of the hydrogel. Needles with smaller ID are usually required in high resolution printed objects. However, the diameter is restricted to the viscosity of the hydrogel extruded through that needle.

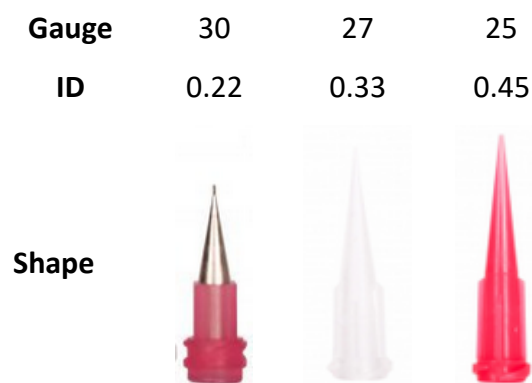


Figure 5.3. 30 G, 27 G and 25 G needle sizes used in the printing of the hydrogel meshes.

The 30 G pink-coloured base needle with a metal tapered nozzle of ID=0.16 gave the highest resolution print, however, it was not used for further printing because of frequent blockage of the needle during the printing in case of all tested hydrogel compositions. Therefore, the next available size up, which was the transparent plastic tapered needle with size 27 G and an inner diameter of 0.21 mm, was used.

Table 5.4. Variation of printing parameters to obtain the best print for 10% GelMA

Print No.	Needle size (G)	Pressure (PSI)	Speed (mm/s)	Comments
1	30	25	2	Thick lines, very small distance between lines and no visible pores
2	30	25	3	Good print, defined lines and pores, but needle blocks often
3	30	25	4	Quick speed, printed lines are not continuous
4	30	21	2	The pressure is not sufficient for continuous flow, 1 st part not printed
5	30	32	6	Very high pressure, thick printed structure with no pores
6	27	25	3	High pressure since the nozzle is wider than 30 G
7	27	16	3	Good pressure, but the slow speed formed thick printed lines and thus low resolution
8	27	15	4	Best print

Various printing speeds were tested to determine the required speed that would produce a high-resolution print. The optimum speed depends on the rheological properties of the hydrogel and whether the extruded filament is continuous or not. Hydrogels with high shear-thinning properties and continuous extruded filaments usually require higher printing speeds. However, very high speed might cause gaps in the printed structure and incomplete printed lines as shown in Figure 5.4.

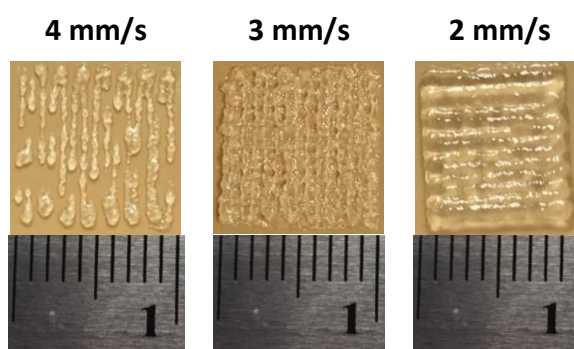


Figure 5.4. Effect of printing speed on the printed mesh of 10% GelMA using 27 G needle and pressure of 12 PSI. The ruler is in mm increments.

Since all the GelMA hydrogel compositions in this work were printed using 27 G needles, the nozzle diameter was adjusted to 0.21 mm in Slic3r software settings before slicing the stl uploaded file. The pressure applied on the hydrogel to extrude the filament should be adjusted before printing. For setting the pressure, it is customary to start with low pressure and gradually increase the pressure until a continuous filament is produced. The pressure required to obtain a continuous filament depends on the viscosity of the material and the diameter of the nozzle. For the same material, higher pressure is required to extrude the filament from nozzles with a smaller inner diameter (ID) compared to the bigger ID ones.

Printing trials of various GelMA concentrations (7, 8, 9 and 10%) were performed to determine the most appropriate printing concentration. The sample with 7% GelMA had a printable viscosity at room temperature, however, the printed filament did not retain its shape after printing due to the low density of the GelMA solution. Moreover, the physical gelation rates of low concentrated 7% GelMA hydrogels are known to be too slow to maintain high structural integrity (Yin et al., 2018), which resulted in the spreading of the printed lines and thus low precision of the printed structure.

In the case of 9 and 10% GelMA, maintaining a continuous extruded filament was hard due to the high density of the inks. This led to some unprinted parts within the lines as shown in the middle image of Figure 5.4 that was printed using a 30 G needle, at a pressure of 25 PSI and 3 mm/s. The best continuous filament that gave high-resolution print was obtained using 8% GelMA hydrogel, therefore this concentration was used for comparing the effect of the incorporation of PEGDA to the GelMA within the hydrogel composition.

Due to the high molecular weight of PEGDA, it had a positive effect on the rheological properties of the hydrogel. As the concentration of PEGDA increased, the pressure required to extrude the filament from the same nozzle (27 G) increased. Moreover, the filaments of 8% GelMA with 1 and 10% PEGDA (P1 and P10) were not as continuous as the one with no PEGDA (P0), so a lower printing speed of 2 mm/s was required to achieve continuous printing lines, compared to a printing speed of 3 mm/s in case of 8%GelMA (P0) where there was no PEGDA present. The variation in the printing parameters due to the incorporation of 1 and 10% PEGDA into the 8% GelMA hydrogel is shown in Table 5.5.

Table 5.5. Printing parameters for 8% GelMA hydrogel meshes with/without PEGDA.

	8%GelMA (P0)	8%GelMA +1%PEGDA (P1)	8%GelMA +10%PEGDA (P10)
Needle (G)	27	27	27
Pressure (PSI)	12	12.4	13.1
Speed (mm/s)	3	2	2

5.3.2 Characterisation of the printed meshes

Visual and microscopic examination

The colour of the cooled hydrogels (P0, P1 and P10, Table 2) was compared as shown in Figure 5.5. The incorporation of PEGDA to 8% GelMA in P1 and P10, led to the formation of a clear hydrogel upon cooling, compared to the slight yellowish colour of the 8% GelMA (P0), this might be contributed to the transparent colour of PEGDA.

Upon extrusion of the three hydrogel formulations (P0, P1 and P10) from the 27 G needle, there was a consistent flow of filament at pressures of 12, 12.4 and 13.1 PSI for

hydrogel formulations P0, P1 and P10, respectively as shown in Figure 5.5. Therefore, those pressure values were chosen to extrude the filament of each hydrogel composition during printing.

The printed meshes of all the three hydrogel formulations had a high-resolution print at speeds of 3, 2 and 2 mm/s for hydrogel formulations P0, P1 and P10, respectively. The printed meshes are shown at the lower images of Figure 5.5. It was noted that the incorporation of PEGDA in hydrogels P1 and P10 required a lower speed of 2 mm/s compared to the speed of 3 mm/s used in printing P0. Due to the high viscosity of PEGDA, the filaments of P1 and P10 were not extruded as quick as the P0 filament, which required slowing down the movement of the printing nozzle to obtain a uniform print. The effect of the printing speed on the printed structure is illustrated in Figure 5.4 above.

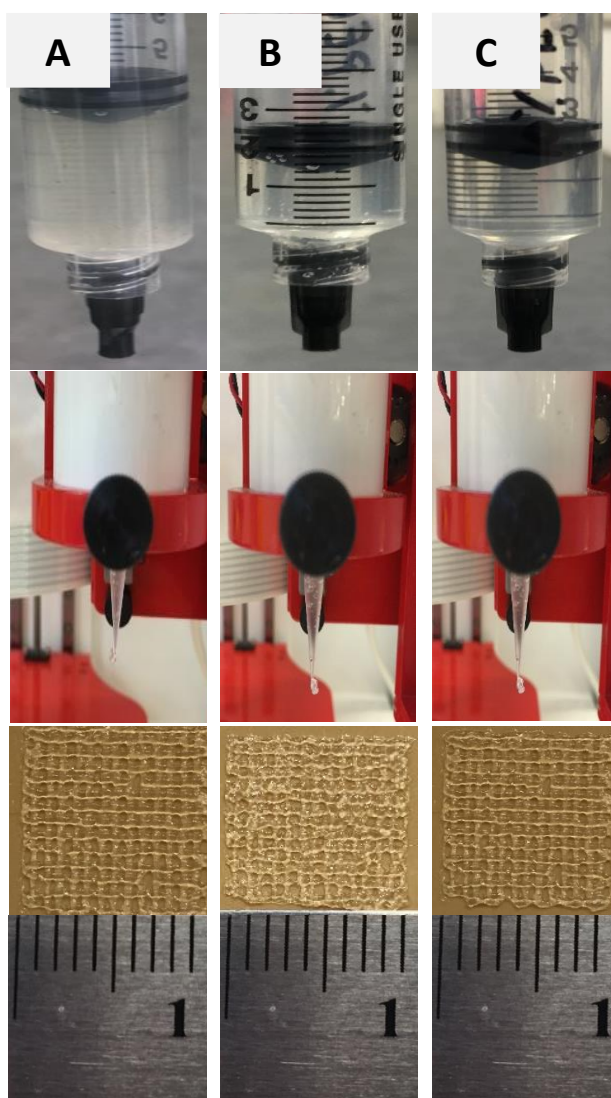


Figure 5.5. Image of the cooled hydrogel in the syringe prior to printing (top), the extruded filament from the nozzle to determine the appropriate pressure (middle) and printed mesh (bottom). Images show the formulations P0 (A), P1 (B) and P10 (C). The ruler is in mm increments.

Visual and physical inspection of the printed and cured 10% GelMA hydrogel meshes after freeze-drying and vacuum drying showed that the freeze-dried meshes were too fragile and hard to handle, while the vacuum dried meshes were able to withstand handling and semi-folding as shown in Figure 5.6.



Figure 5.6. Effect of drying technique on 10% GelMA hydrogel meshes. Fragile freeze-dried meshes (A), and easy to handle vacuum-dried meshes (B).

The microscopic images of the printed meshes of hydrogel formulations P0, P1 and P10 illustrated the effect of PEGDA incorporation in the hydrogel composition. In Figure 5.7(A), the image of the printed formulation P0 shows smooth printed lines of 0.16 ± 0.05 mm in diameter and consistent pore sizes of 0.5 ± 0.1 mm in diameter, which indicated that the 8% GelMA hydrogel composition had high printing resolution under the used pressure and speed.

The incorporation of 1% PEGDA in formulation P1 led to less smooth printed lines of 0.23 ± 0.11 mm in diameter and smaller pores, of 0.4 ± 0.09 mm in diameter, compared to P0 as shown in Figure 5.7(B). This might be contributed to the slower speed of 2 mm/s used during printing. Moreover, the incorporation of 10% PEGDA in the GelMA hydrogel composition led to thicker lines of a diameter of 0.33 ± 0.15 mm and smaller pores of 0.33 ± 0.14 mm in diameter. This might be contributed to the higher viscosity of PEGDA and the lower printing speed, which resulted in printed thicker lines.

After vacuum drying, the meshes of P0 and P1 looked almost the same as before drying as shown in Figure 5.7(A) and (B), however, meshes of P10 had a considerable shrinkage due to the high content of PEGDA, which behaved like a high concentration crosslinker in the hydrogel formulation. This shrinkage was further confirmed by the dimensions of the vacuum-dried P10 meshes under the microscope, where the line diameter was 0.15 ± 0.08 mm and the pore diameter was 0.29 ± 0.12 mm. On the other hand, the dimensions of the printed lines and the pore size of P0 and P1 hydrogel meshes after drying were almost the same as before drying.

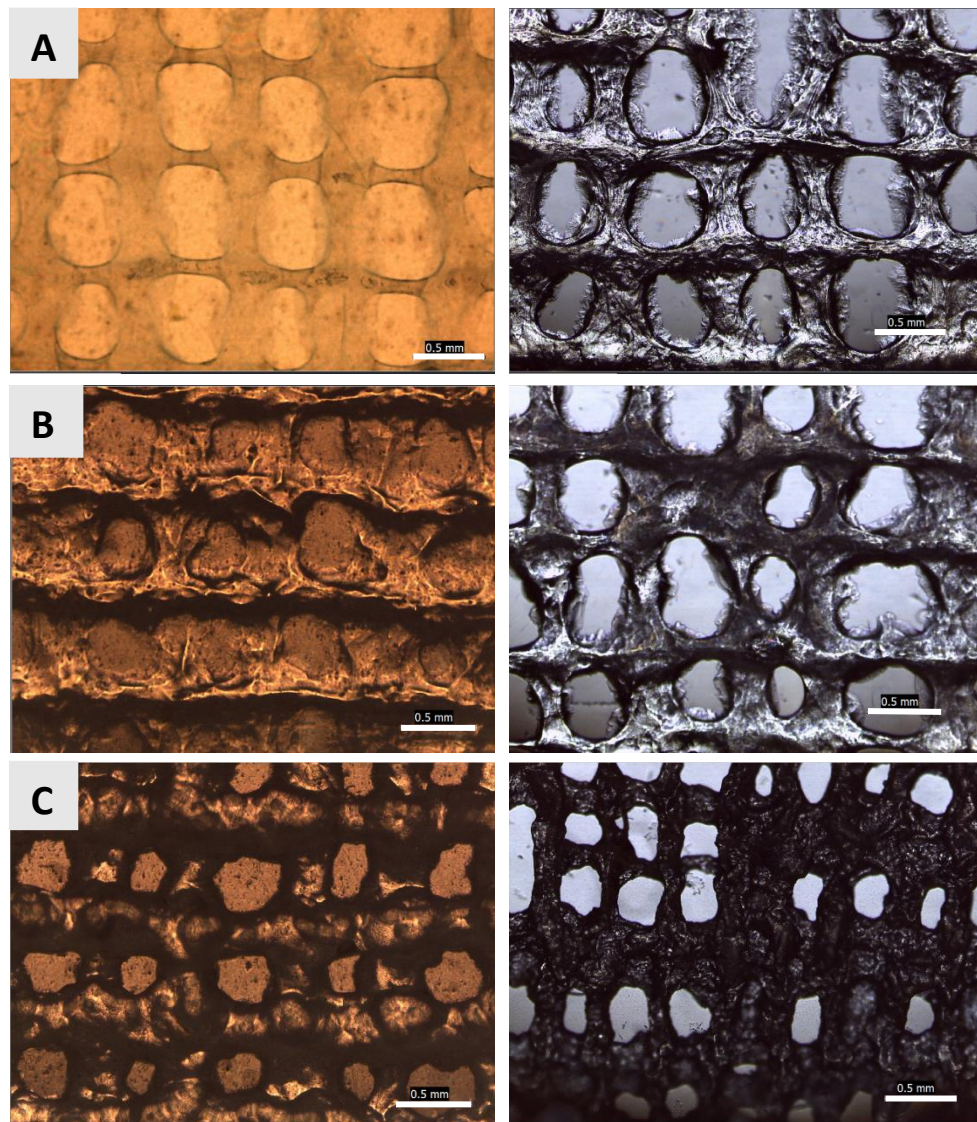


Figure 5.7. Microscopic images of the printed hydrogel meshes imaged immediately after printing (left) and microscopic image of vacuum-dried hydrogel meshes (right) of P0 (A), P1 (B) and P10 (C), scale bar = 0.5 mm.

The 10% GelMA, 0.5% LAP hydrogel meshes were viewed under the SEM to show the effect of the drying technique on the mesh structure. Figure 5.8(A) shows the line diameter of vacuum-dried printed 10% GelMA hydrogel meshes to be 0.34 ± 0.12 mm and pore size of 0.37 ± 0.19 mm, while the line diameter of the freeze-dried meshes that retained their printed structure was 0.25 ± 0.11 mm as shown in Figure 5.8(B). Moreover, the pore sizes of the freeze-dried meshes were considerably smaller compared to the vacuum dried meshes with a pore size of 0.14 ± 0.05 mm.

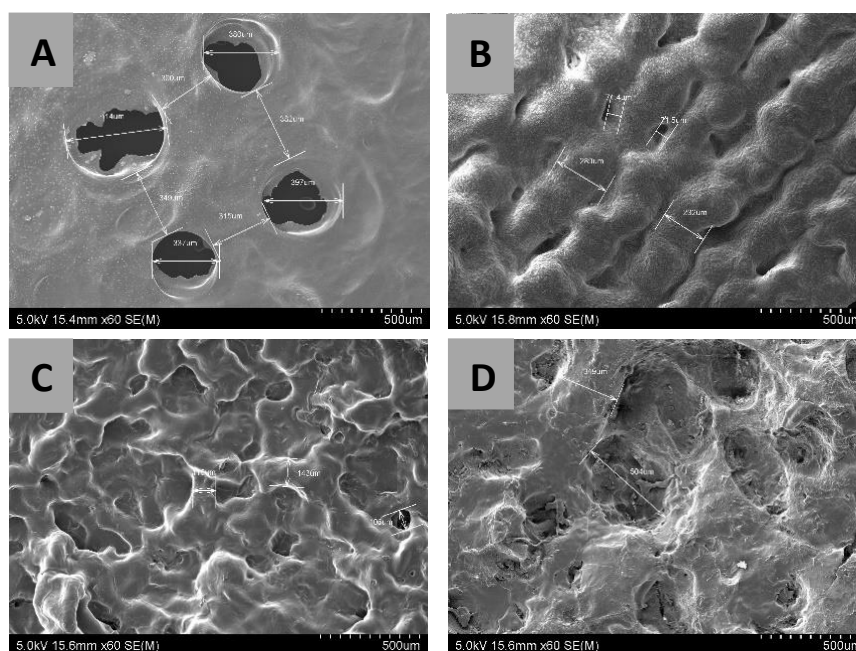


Figure 5.8. SEM images of printed 10% GelMA meshes. Images showing vacuum dried mesh (A), freeze-dried mesh (B), freeze-dried mesh after swelling of previously vacuum dried meshes (C) and freeze-dried mesh after swelling of previously freeze-dried meshes (D).

Both vacuum-dried and freeze-dried meshes were immersed in PBS for 24 h until equilibrium swelling, then they were carefully removed and freeze-dried to maintain the swollen structure of the meshes before imaging by SEM. Figure 5.8(C) and (D) show that the pores generated after swelling of the vacuum-dried swollen meshes were smaller but the structure is more intact than the previously freeze-dried ones. Since freeze-drying produced fragile hard to handle meshes, vacuum drying technique was used in this work to produce a mesh that can stay intact during handling.

Furthermore, SEM was used to characterise the structure of vacuum-dried P0, P1 and P10 8% GelMA hydrogel meshes before swelling and the freeze dried structure after swelling in PBS to determine the effect of hydration on the mesh structure as shown in Figure 5.9. There were no obvious pores in the hydrated P0 meshes, while a porous structure was shown in P1 and P10 hydrated meshes were PEGDA was incorporated. There was no significant difference in the shape or dimensions between P0 and P1 meshes before and after swelling. On the other hand, the SEM images confirmed the shrunk mesh structure of the vacuum-dried P10 hydrogel meshes that was previously observed in the microscopic images.

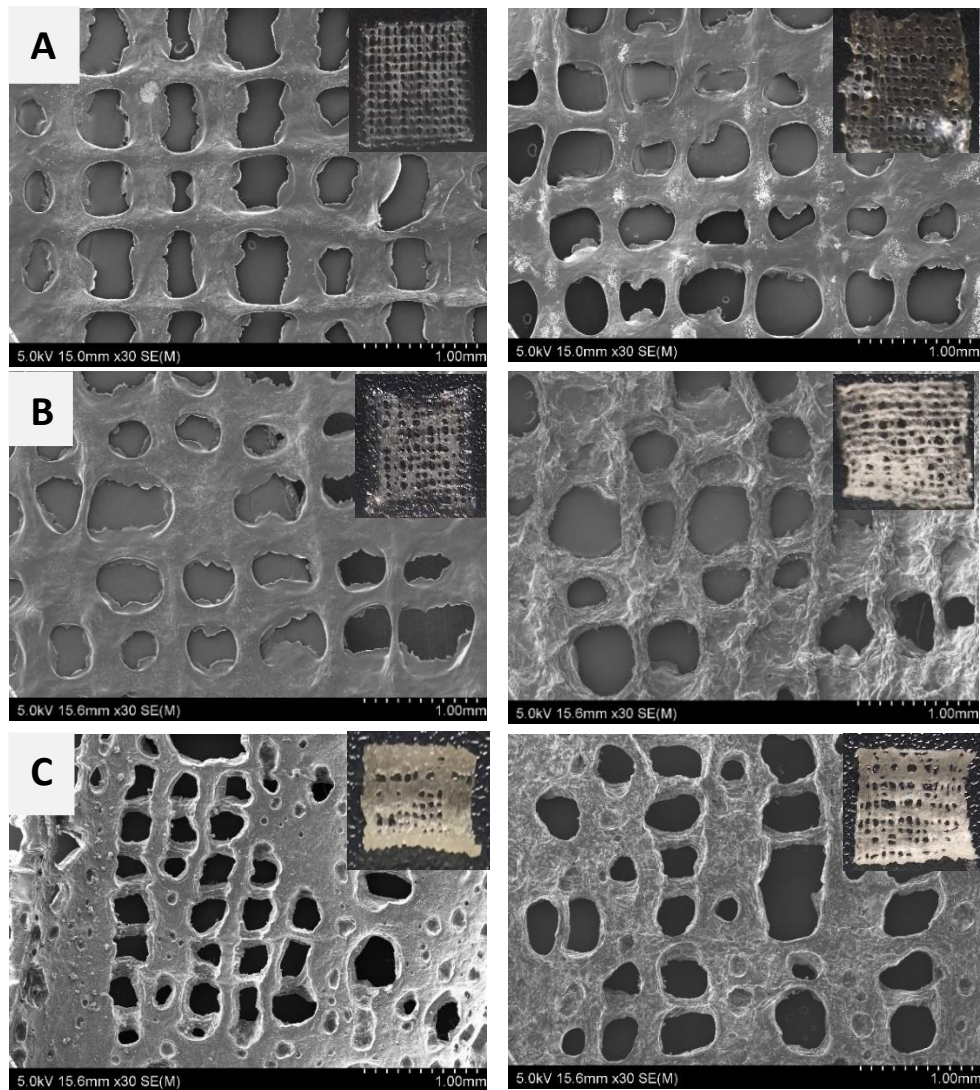


Figure 5.9. SEM images of 3D-printed 8% GelMA meshes after vacuum drying (left) and after freeze drying of the swollen meshes (right) of 8% GelMA (A), 8% GelMA+1% PEGDA (B) and 8% GelMA + 10% PEGDA (C). Smaller images on the top right represent their camera images.

Degree of crosslinking

Despite the ability of the gelatine hydrogel meshes to retain their structure after printing due to temporary physical gelation, this structure can be easily be smudged or dissolved in water. Therefore, a permanent crosslinking process is essential to polymerise the printed hydrogel. In this work, a photopolymerisation crosslinking reaction is performed where light is used to initiate a free radical reaction using LAP photoinitiator. This free radical leads to a series of polymerisation reactions within the hydrogel monomers (propagation step) that end after all the monomers are polymerized. Furthermore, the degree of crosslinking affects the physical state, elasticity and swelling properties of the hydrogel (Bukhari et al., 2015; Çaykara & Turan, 2006). Therefore, a crosslinking test is

performed to determine the necessary crosslinking time and, if necessary, the photoinitiator concentration.

Photopolymerisation of GelMA hydrogels produces an irreversible covalently bonded network structure with higher thermal and mechanical stability than physically crosslinked gelatine (Hoch et al., 2012; Yin et al., 2018). The degree of crosslinking of photopolymerised hydrogels depends on the amount of the photoinitiator, the concentration of the hydrogel and the crosslinking parameters, such as curing time and intensity. To determine the crosslinking parameters required to crosslink GelMA hydrogels, we used 10% GelMA, since this is the maximum concentration of hydrogel that is used in all the printed hydrogel formulations, and 0.5% LAP as a photoinitiator.

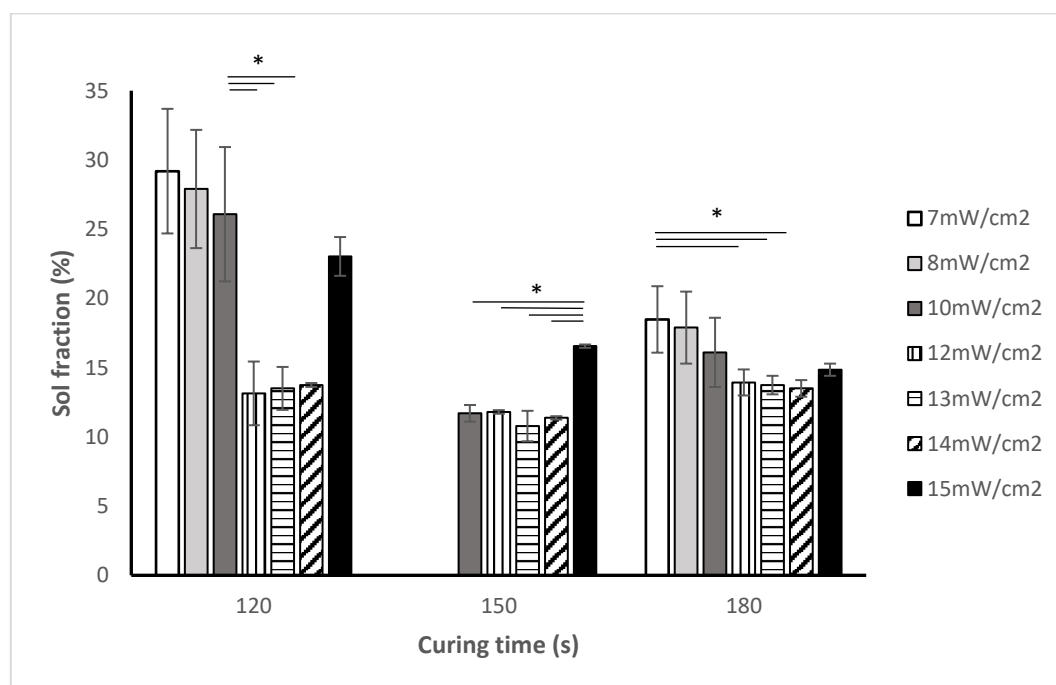


Figure 5.10. The effect of crosslinking parameters on the sol fraction of 10% GelMA, 0.5% LAP hydrogel meshes after 24 h in PBS at 37 °C. *Statistically significant at $p < 0.05$; $n = 3$; mean \pm SD.

The lower the sol fraction, the more the sample has crosslinked. A sol fraction of 100% correlates to a sample that has not crosslinked at all, while a sol fraction of 0% correlates to a sample that has completely crosslinked. The sol fraction remaining from the crosslinked hydrogels after soaking in PBS for 24 h is presented in Figure 5.10. At each time point of either 120, 150 or 180 s, the sol fraction decreased with increasing the light intensity, which indicates better crosslinking, however, the highest intensity of 15mW/cm² had a negative effect on the crosslinking of hydrogels. This might be because

this intensity was too strong and affected the internal structure of the crosslinked hydrogel. This might be explained by the type of reactions that can happen in a polymer as an effect of light application. Higher light intensities and/or prolonged exposure can result in bond breaking reaction instead of bond forming reaction, which might have happened in case of $15\text{mW}/\text{cm}^2$ intensity resulting in a higher sol fraction (Chatani et al., 2014).

In regard to the curing time, hydrogels that were cured for 150 s had the highest degree of crosslinking, followed by 180 s and then 120 s. This might be because the extra exposure time of 180 s to the light causes degradation of part of the polymer chains, and thus reduces the crosslinking density. It was also noted that curing the hydrogels for 150 s gave almost the same degree of crosslinking over a wider range of light intensities, which indicated that this was the most suitable time for curing of the hydrogels.

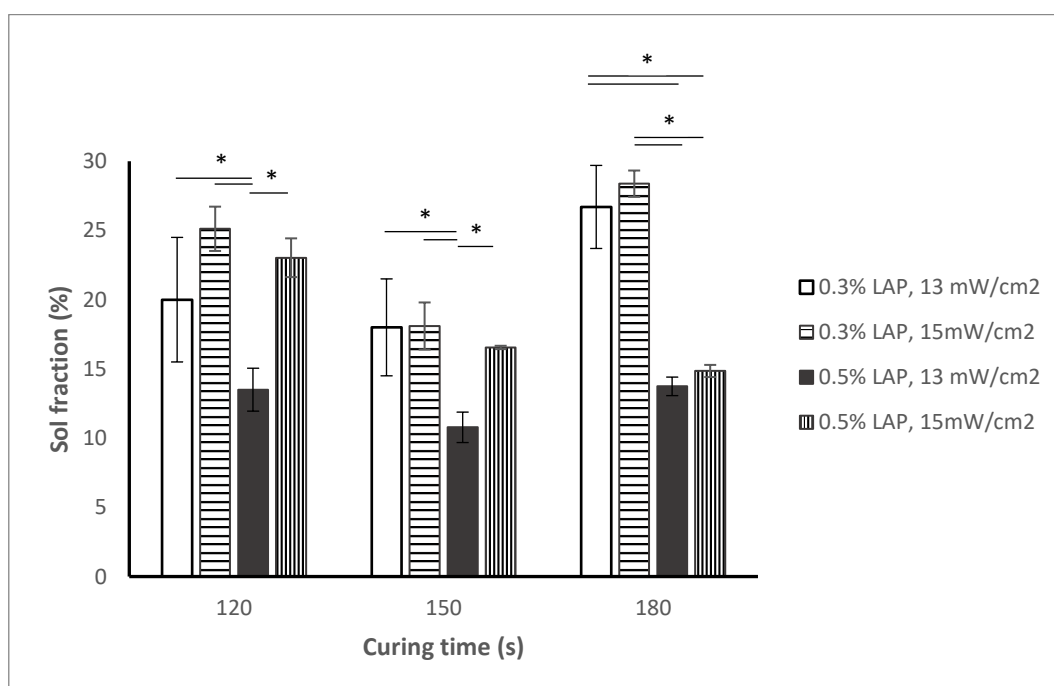


Figure 5.11. The effect of LAP concentration on the sol fraction of 10% GelMA hydrogels cured at 13 or 15 mW/cm^2 for either 120, 150 or 180 sec. *Statistically significant at $p < 0.05$; $n = 3$; mean \pm SD.

In regards to the crosslinking test that was performed to compare the 0.3 and 0.5% photoinitiator (LAP) concentration in the hydrogel showed that at light intensity of $13\text{mW}/\text{cm}^2$, there was a significant difference between the degree of crosslinking of 0.3 and 0.5% hydrogels at all time intervals, with better crosslinking at the 0.5% LAP concentration as shown in Figure 5.11.

In general, the highest degree of crosslinking of 10% GelMA hydrogels was achieved with 0.5% LAP concentration under a light intensity of 13 mW/cm² with no significant difference between the three tested time intervals. This shows that 0.3% LAP concentration is insufficient to fully crosslink the 10% concentration of GelMA hydrogels.

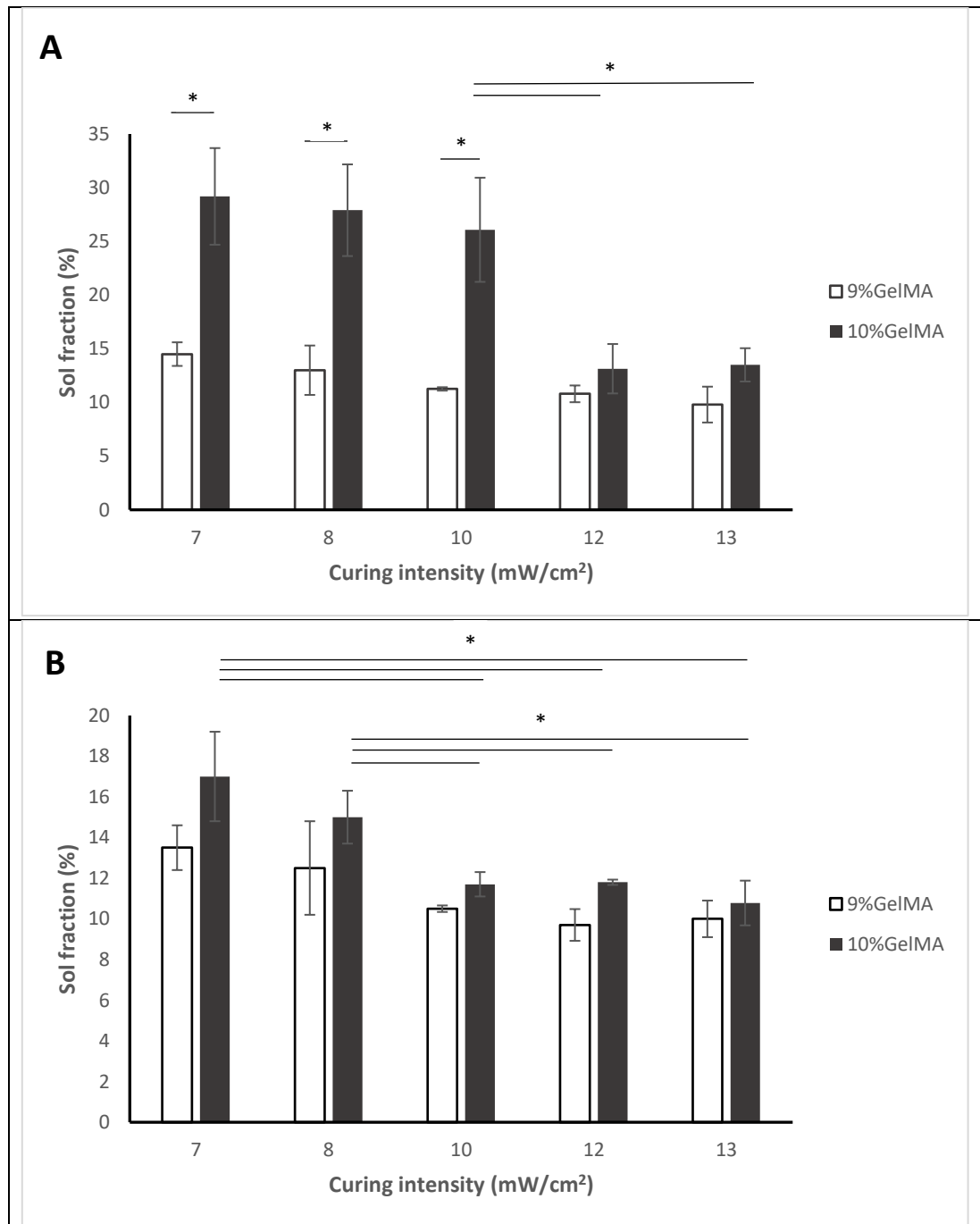


Figure 5.12 The effect of GelMA concentration (9 and 10%) and 0.5% LAP on the sol fraction of the hydrogel meshes cured under various intensities for 120 s (A) and 150 s (B). *Statistically significant at $p < 0.05$; $n = 3$; mean \pm SD.

To show the effect of the same crosslinking parameters and photoinitiator concentration on different concentrations of GelMA; 9 and 10% GelMA hydrogels were compared with the results of the crosslinking test as illustrated in Figure 5.12. The 9% GelMA hydrogels had a better degree of crosslinking compared to 10% GelMA under all the crosslinking parameters tested. Moreover, there was no significant difference between the sol fractions of 9% GelMA hydrogel at all the tested light intensities and times. This indicates that the 9% GelMA was fully crosslinked after exposing for 120 s under 7 mW/cm², and any further increase in intensity or time did not add to the degree of crosslinking.

However, the 10% GelMA hydrogels required higher curing intensities of more than 10 mW/cm² and a minimum of 150 s to fully reach the same degree of crosslinking of the 9% GelMA hydrogels. This was further confirmed when 8 and 9% GelMA hydrogels were crosslinked under 13 mW/cm² for 150 s, with a better degree of crosslinking for 8%GelMA hydrogels as shown in Figure 5.13.

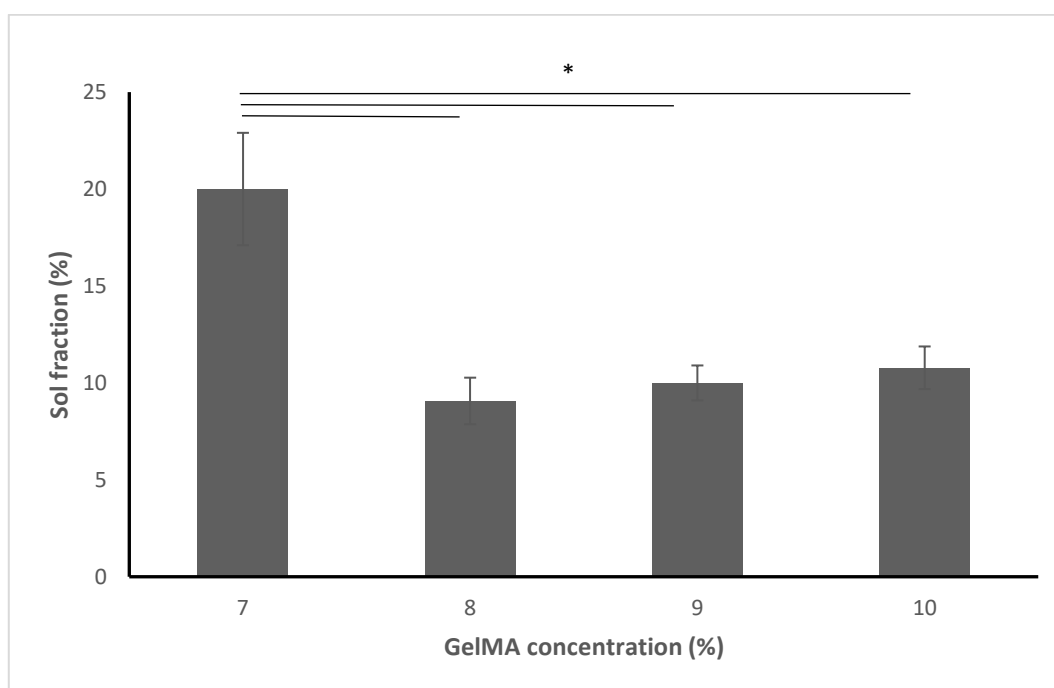


Figure 5.13. The effect of GelMA concentration (7, 8, 9 and 10%) and 0.5% LAP on the sol fraction of the hydrogel meshes cured under 13 mW/cm² for 150 s. *Statistically significant at $p < 0.05$; $n = 3$; mean \pm SD.

On the other hand, 7% GelMA had a higher sol fraction (%) than 8% GelMA, which might be due to the very low concentration of GelMA and thus there are less methacrylated groups available in the crosslinking reaction. With those results in mind, the 8% GelMA,

0.5% LAP hydrogel composition was chosen to be used in further hydrogel comparisons involving incorporation of PEGDA.

PEGDA is a hydrophilic hydrogel that gels rapidly at room temperature in the presence of a photoinitiator and UV or visible light due to the formation of a crosslinked polymer network as shown in Figure 5.14. Therefore, it is expected that their incorporation with 8% GelMA will lead to the formation of a composite hydrogel that has a more crosslinked polymer network compared to pure GelMA hydrogels (P0).

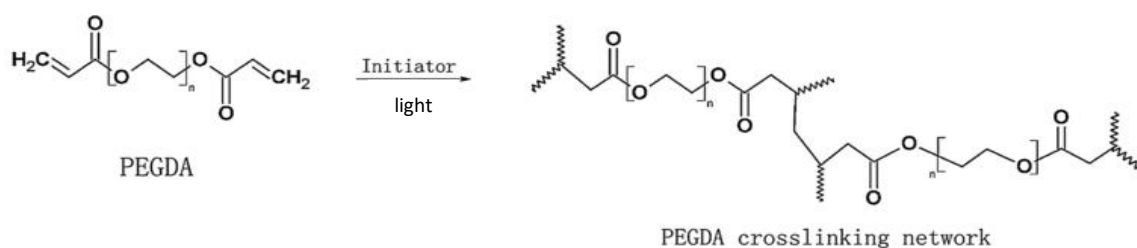


Figure 5.14. The photo-polymerisation reaction of PEGDA (Adapted from (Tan et al., 2012)).

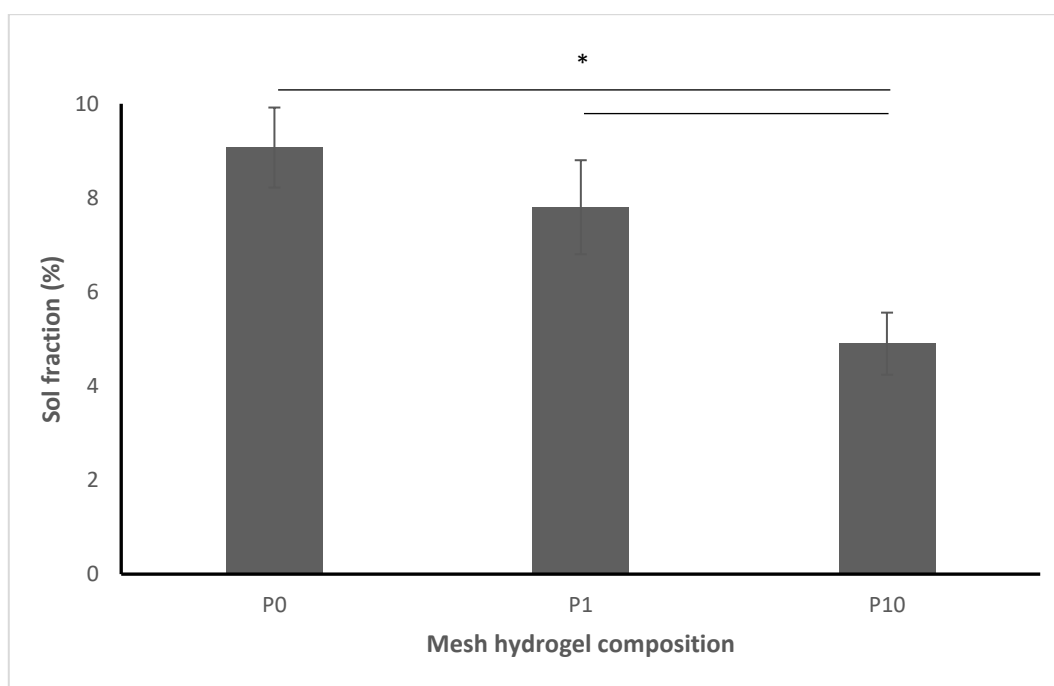


Figure 5.15. The effect of PEGDA concentration on the sol fraction of 8% GelMA hydrogel meshes cured under 13 mW/cm² for 150 s. *Statistically significant at $p < 0.05$; $n = 3$; mean \pm SD.

The incorporation of 1% PEGDA to 8% GelMA hydrogel led to a reduction in the sol fraction from 9.07 \pm 0.9 to 7.8 \pm 1.0%, while the incorporation of 10% PEGDA had a sol fraction of only 4.9 \pm 0.7% as shown in Figure 5.15. This was as a result of the high degree of crosslinking due to the incorporation of PEGDA in the polymer network.

Swelling studies

The swelling ratio is the amount of water absorbed by a hydrogel compared to its dry weight. It is dependent on the mesh size of the polymer network, the degree of crosslinking in the network and the polymer-solvent interaction (Hoch et al., 2012). The ESR is the maximum water uptake taken by the hydrogel. It was found that 10% GelMA hydrogels reached ESR between 3-4 h and maintained this ratio for more than 24 h as illustrated in Figure 5.17. Therefore, the ESR of the hydrogel compositions was calculated at 24 h in PBS. The wetted swollen hydrogel meshes were transparent and had good adhesion to the skin as shown in Figure 5.16.



Figure 5.16. Wet 10% GelMA hydrogel mesh at equilibrium swelling placed on the skin.

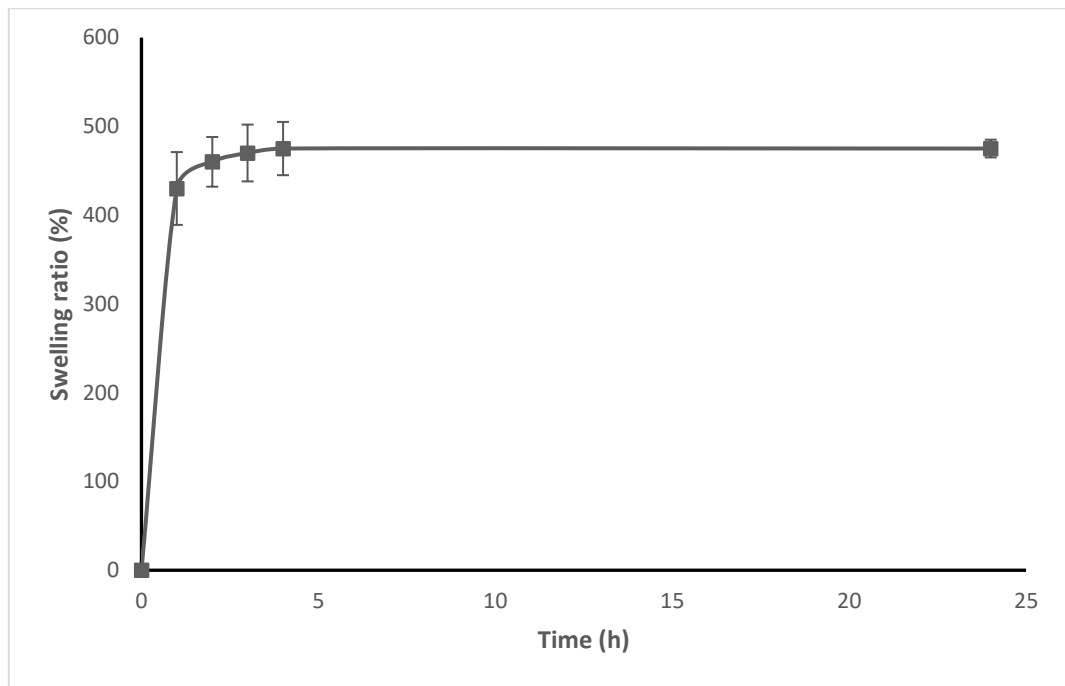


Figure 5.17. The swelling ratio of 10% GelMA dry hydrogel meshes within 24 h in PBS. n = 3; mean \pm SD.

Curing the 10% GelMA hydrogel printed meshes under various light intensities and for different time intervals resulted in different crosslinking degrees of the GelMA, higher degrees of crosslinking means more of the gelatine is crosslinked and thus not degraded in the first 24 h. The higher the gelatine content in the hydrogel, the higher the ESR since the swelling ratio generally reflects the high capability of gelatine to take up and hold water (Hoch et al., 2012). Therefore, it was found that the hydrogels that had the lowest sol fraction in Figure 5.10, had the highest ESR% in Figure 5.18.

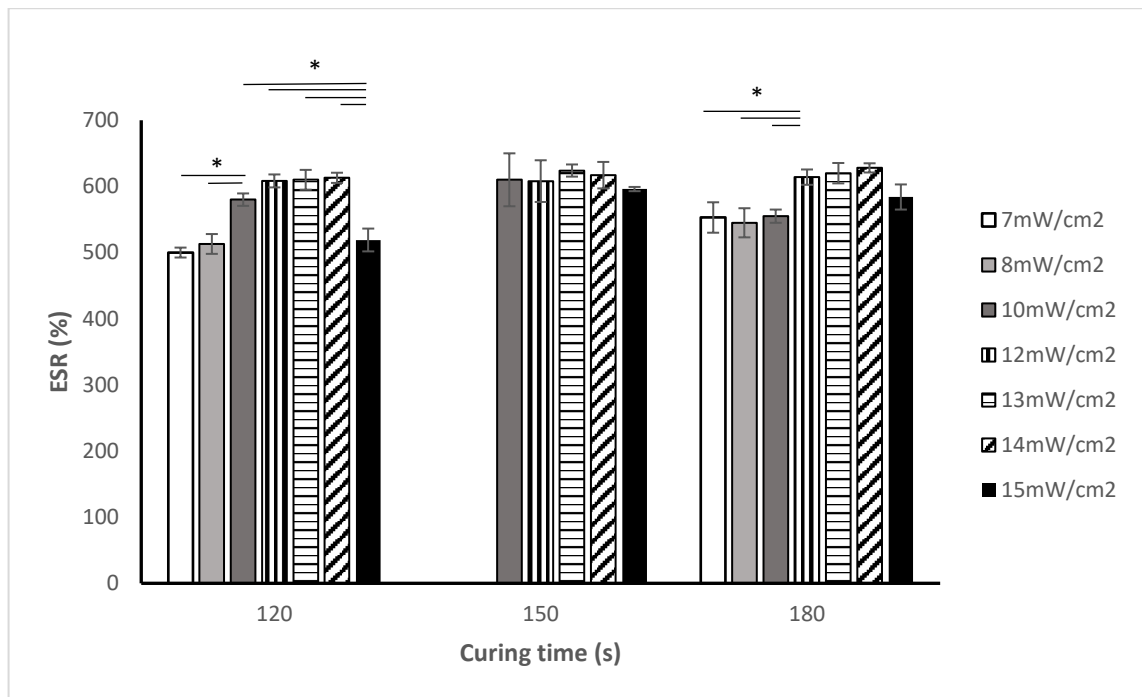


Figure 5.18. The effect of crosslinking intensities of 7, 8, 10, 12, 13, 14 and 14 mW/cm² on the ESR of the 10% GelMA dry hydrogel meshes in PBS after 24 h. *Statistically significant at $p < 0.05$; $n = 3$; mean \pm SD.

All hydrogels have a certain degree of swelling that affects their mechanical and functional properties. Therefore, the ESR is an essential factor to be considered in all hydrogels used for tissue engineering applications (Y. Wang et al., 2018). At lower degrees of swelling, the hydrogel polymer chains are closer to each other and the density of the entire hydrogel network is high. This enhances the interaction between the polymer chains, which forms a hydrogel with high mechanical properties. On the other hand, the high degree of swelling dilutes the hydrogel network and weakens the Van der Waals forces, which reduces of the tensile strength of hydrogels (Jing Jing Wang & Liu, 2012).

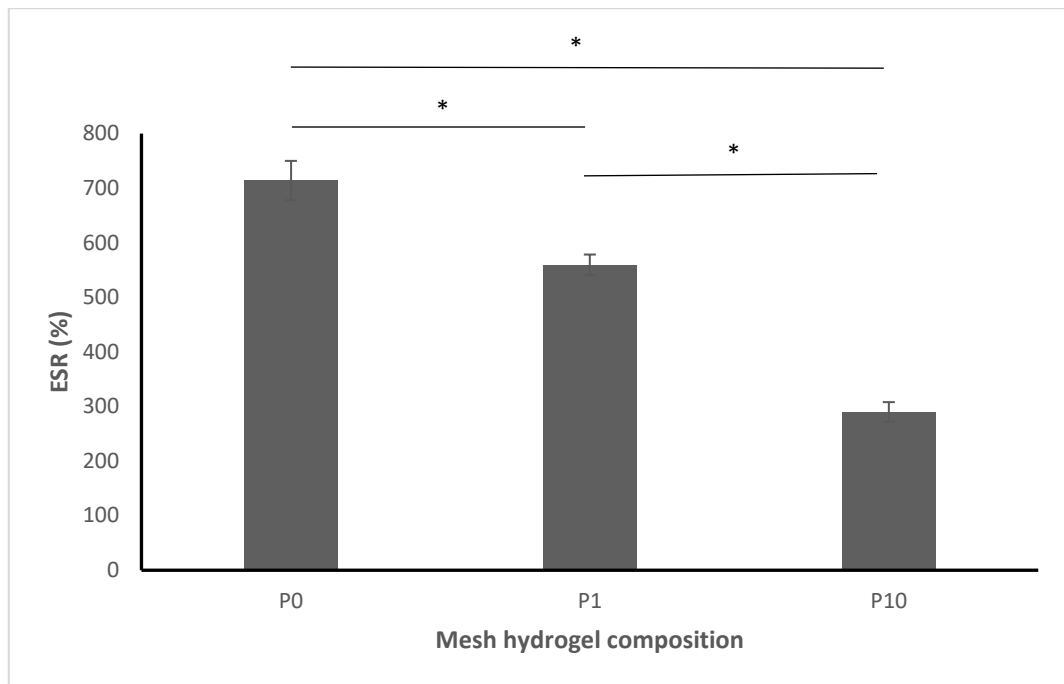


Figure 5.19. The effect of PEGDA concentration on the ESR after 24 h of 8% GelMA dry hydrogel meshes. *Statistically significant at $p < 0.05$; $n = 3$; mean \pm SD.

In this study, the ESR of P0, P1 and P10 hydrogel meshes were 714.2 ± 36 , 559.4 ± 19 and 290.9 ± 18 , respectively. The swelling ratio of the hydrogel decreased significantly with the increase in the amount of PEGDA incorporated. The presence of PEGDA increased the degree of crosslinking, which led to a lower swelling ratio and improved the stiffness of the hydrogel meshes which was clearly obvious with the easy handling of the meshes without being broken compared to the PEGDA free hydrogel meshes (Y. Wang et al., 2018). This was in accordance with another study that showed that crosslinker concentration increases the crosslinking density and thus reduces the swelling ratio (Noshadi et al., 2017).

***In vitro* degradation**

Hydrogels used in tissue engineering should meet specific requirements to promote the generation of new tissues. They should mimic the extracellular matrix, promote proliferation and differentiation of the desired cells and should be biodegradable to allow cell remodelling. Therefore, it is crucial to develop hydrogels with tuneable mechanical and biological properties to meet those requirements (Hutson et al., 2011).

GelMA hydrogel meshes have a degradation profile *in vitro* and *in vivo* depending on the concentration of GelMA and the photoinitiator and the crosslinking parameters applied

on the printed structure. On the other hand, PEGDA is not biodegradable therefore the incorporation of PEGDA to GelMA is suspected to affect the degradation profile of the printed meshes. The effect of the change in GelMA concentration on the degradation profile of the printed meshes were studied. The degradation profiles of 8 and 10% GelMA hydrogels with 0.5%LAP and cured at 13 mW/cm² for 150 s were compared. Moreover, the effect of incorporation of 1 (P1) and 10% (P10) PEGDA to 8% GelMA hydrogel using 0.5%LAP and cured at 13 mW/cm² for 150 s were evaluated.

GelMA hydrogels had an initial slow degradation rate where 50% of the matrix degraded within the first 4 days, followed by quick degradation of the rest of the matrix in the last day. There was no significant difference between the degradation profile of 8 and 10% GelMA as shown in Figure 5.20.

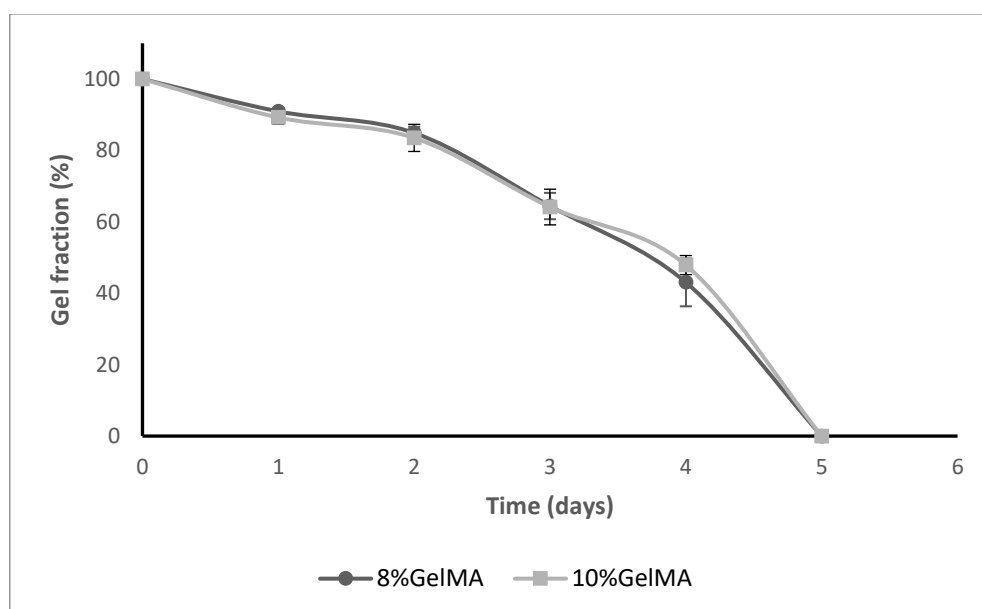


Figure 5.20. Degradation profiles of 8 and 10% GelMA hydrogel meshes in PBS at 37 °C. n = 3; mean ± SD.

When PEGDA was incorporated within the hydrogel network of GelMA, they influenced the degradation profile of pure 10% GelMA (P0) as shown in Figure 5.21. The hydrogel (P1) degraded in 6 days instead of 5 days in the case of (P0) hydrogel, with no significant difference in the gel fraction of the first 4 days where 50% of the hydrogel was degraded. However, the remaining 50% degraded in the last 2 days in case of P1 instead of 1 day in case of P0. On the other hand, the presence of a higher concentration of PEGDA in the hydrogel matrix in case of (P10) hydrogels, enhanced the crosslinking of the polymer

network resulting in a more compact structure and significantly prolonged the degradation rate of the hydrogel mesh to more than 2 weeks.

Thus, the incorporation of PEGDA led to a higher degree of crosslinking and thus longer degradation time *in vitro*, which overcame the short comes of pure GelMA hydrogels. This was in coherence with another study, where the degradation rate decreased in formulations with a higher degree of methacrylation in GelMA hydrogels due to the formation of a higher crosslinked polymer network (Nguyen, McKinney, Miller, Bongiorno, & McDevitt, 2015).

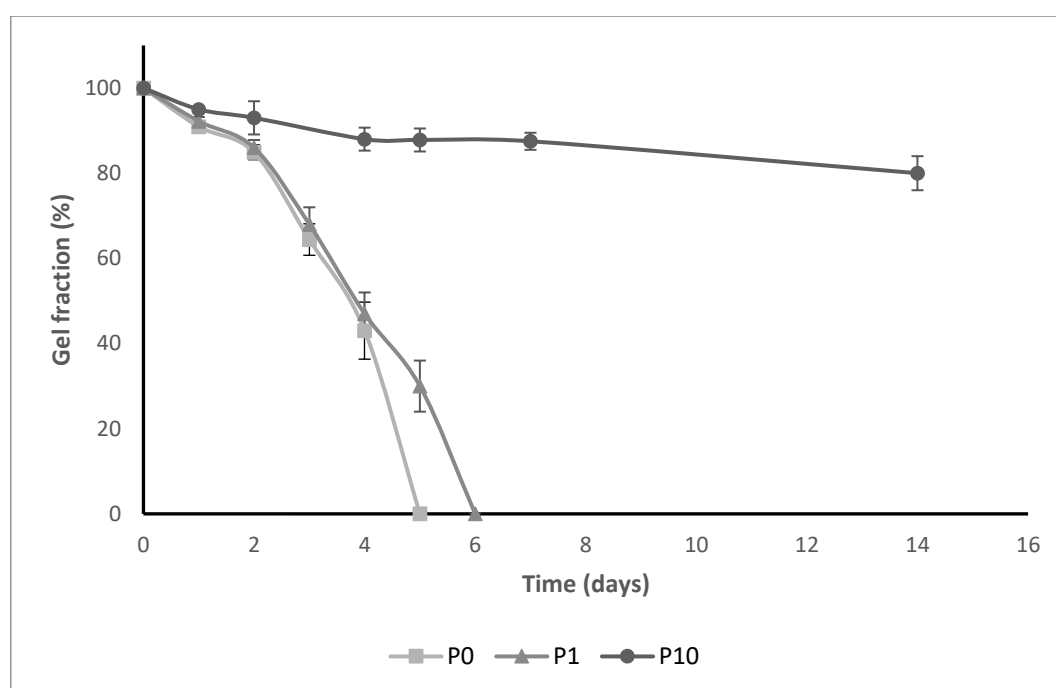


Figure 5.21. The effect of PEGDA concentration on the degradation profiles of 10% GelMA hydrogel meshes in PBS at 37 °C. n = 3; mean \pm SD.

Cell viability

The effect of the hydrogel mesh composition on the viability and growth of the encapsulated cells was examined to determine the feasibility of using these composite hydrogels in tissue engineering applications. The distribution of viable cells within the printed hydrogel meshes was also investigated since this is an essential factor for 3D-printed scaffolds (J. Park et al., 2017).

Live cells are distinguished from dead cells by the presence of abundant intracellular esterase activity, determined by the enzymatic conversion of the virtually nonfluorescent **cell-permeant** calcein AM (present in the dye used) to the intensely

fluorescent calcein, which is well retained within live cells, producing an intense uniform green fluorescence (ex/em \sim 495 nm/ \sim 515 nm). On the other hand, the used EthD-1 dye penetrates cells with damaged membranes and undergoes a 40-fold enhancement of fluorescence upon binding to nucleic acids, thereby producing a bright red fluorescence in dead cells (ex/em \sim 495 nm/ \sim 635 nm).

At first, the effect of the photoinitiator concentration was investigated where hydrogel meshes of 10% GelMA using either 0.3 and 0.5% LAP concentrations and cured at 13mW/cm² for 150 s were used to test cell viability. Cell viability results can be seen in Figure 5.22, both hydrogel compositions had very high cell viability and well distributed within the whole hydrogel mesh. However, the cells appeared denser in the hydrogel mesh crosslinked with higher LAP concentration (0.5%). This might be attributed to the higher gel fraction within the 0.5% LAP hydrogel meshes resulting in more crosslinked GelMA, which is able to accommodate a greater number of cells.

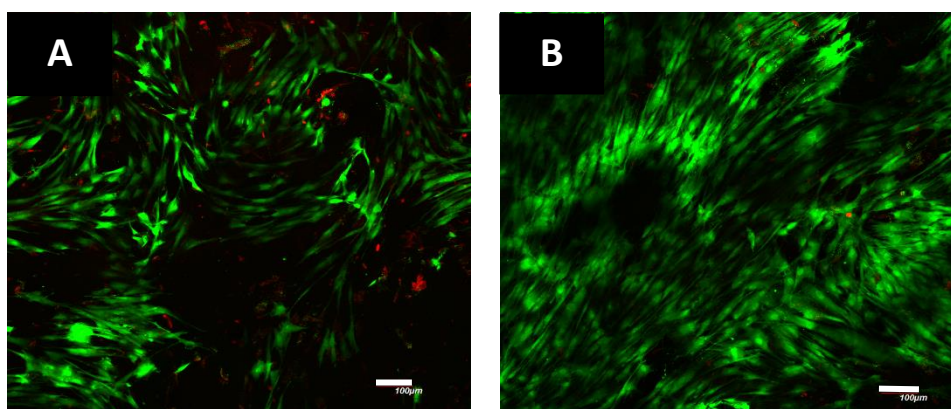


Figure 5.22. The effect of photoinitiator concentration on cell viability. Z-stacked confocal microscopic image of 10% GelMA+0.3% LAP (A), 10% GelMA + 0.5% LAP (B) hydrogel meshes stained with live/dead assay after 1-week incubation with HCEpC. The green colour indicates the live cells, while the red colour presents the dead ones; scale bar = 100 μ m.

When the cell viability was compared in various concentrations of GelMA as illustrated in Figure 5.23, the highest number of cells was observed in the 7% GelMA hydrogel matrix. This might be due to the cells being more free within the lower density hydrogel matrix of the 7% GelMA hydrogel matrix, which had an impact on the rate of cell growth, migration, distribution and proliferation (J. Park et al., 2017).

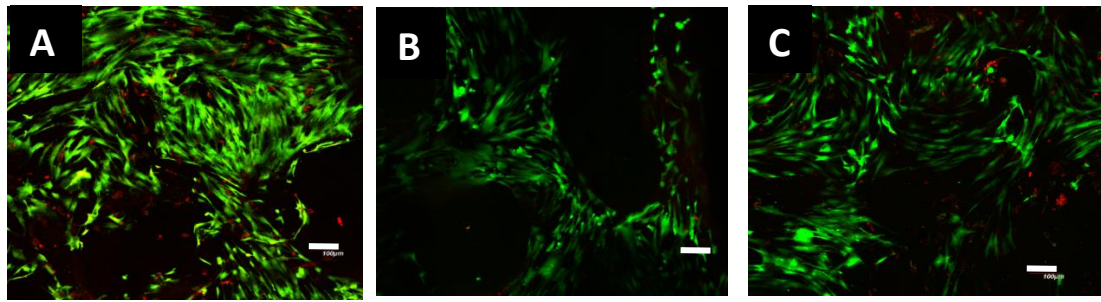


Figure 5.23. Z-stacked confocal microscopic images of 7% GelMA (A), 8% GelMA (B) and 10% GelMA (C) hydrogel meshes stained with live/dead assay after 1-week incubation with HCEpC. The green colour indicates the live cells, while the red colour presents the dead ones; scale bar = 100 μ m.

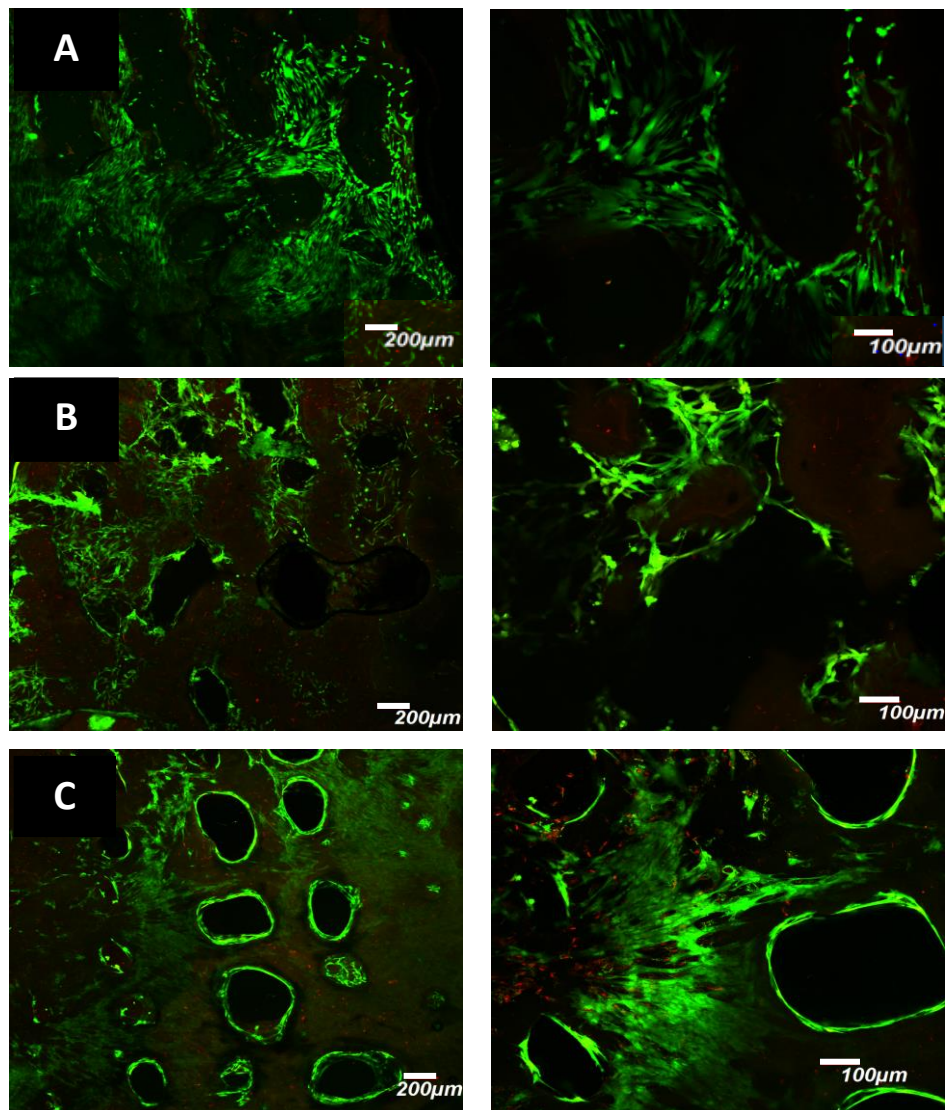


Figure 5.24. Z-stacked confocal microscopic image of 8%GelMA (A), 8% GelMA+1% PEGDA (B) and 8% GelMA+10% PEGDA (C) hydrogel meshes stained with live/dead assay after 1-week incubation with HCEpC. The green colour indicates the live cells, while the red colour are the dead ones.

Furthermore, the live/dead cell staining assay was used to investigate the cell viability of HCEpC cultured on the surface of the GelMA and the GelMA/PEGDA hydrogel meshes for 7 days (Figure 5.24). Almost all cells were alive with a good distribution within the hydrogel matrix after culturing for 7 days for all the tested meshes. This showed that the incorporation of PEGDA had no negative effect on cell viability and thus can be used for seeding cells in tissue engineering applications.

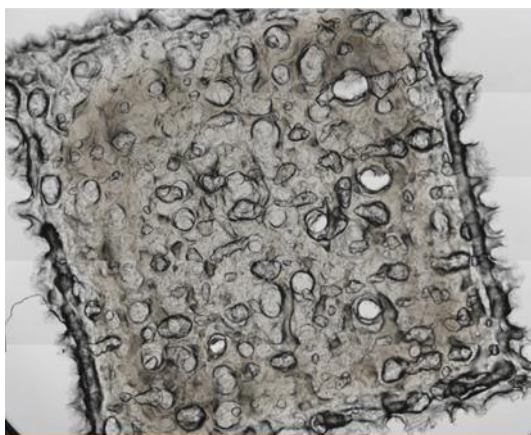


Figure 5.25. Phase-contrast image of 10% GelMA hydrogel carrying HCEpC after 1-week incubation.

Interestingly, although all the tested GelMA hydrogel meshes that had no PEGDA incorporated fully degraded within 5 days when they were inserted in PBS at 37 °C, the hydrogel meshes in the cell culture experiment retained their mesh structure for more than 14 days. This shows that the cells were fully integrated within the mesh structure, which helped maintain its original shape despite the degradation of the hydrogel matrix as shown in Figure 5.25.

5.4 Conclusion

In this work, the effect of different crosslinking parameters on 10% GelMA hydrogels was studied, which revealed that the best curing intensities were between 10-14 mW/cm² and the most suitable curing time was 150 s. The lower concentration of 0.3% LAP was insufficient to crosslink 10% GelMA hydrogels; therefore, a concentration of 0.5% LAP was used in all other tests. The most appropriate printable concentration of the tested GelMA hydrogels was 8% GelMA since it gave the highest crosslinking degree with reasonable crosslinking density that did not obstruct the cell proliferation within

the hydrogel matrix. Therefore, this concentration of GelMA (P0) was used to compare the effect of PEGDA incorporation within the hydrogel mesh structure.

The crosslinking degree, swelling ratio, in-vitro degradation and cell viability were studied in the three hydrogel formulations, P0, P1 and P10. The incorporation of PEGDA enhanced the mechanical properties of GelMA hydrogels, increased their degree of crosslinking and significantly reduced the *in vitro* degradation rates. *In vitro* cell culture experiments using HCEpC showed high adhesion, proliferation and viability over a period of 1 week. This proved that PEGDA can be incorporated with GelMA or other hydrogel polymers as a polymeric crosslinker to prolong the biodegradation of tissue-engineered hydrogels without a negative effect on the viability of the seeded cells.

**Chapter 6 3D-printed GelMA meshes
as a cell-carrier for the treatment of
moderate-severe corneal injuries**

Abstract

Corneal stem cells migrate from the limbus to the cornea to substitute the natural daily loss of corneal epithelial cells or in case of corneal injuries. However, limbal stem cell deficiency (LSCD) might occur if these corneal limbal stem cells are permanently damaged in severe conditions or injuries. Failure in migration of limbal stem cells to the corneal epithelium due to LSCD leads to the migration of adjacent cells from the conjunctiva resulting in scarring and blindness. Currently, corneal grafts or stem cell transplants are performed in severe cases of LSCD. However, these are invasive and expensive. In this work, a novel non-invasive technique is proposed to deliver HCEpC to the injured cornea, via a hydrogel mesh carrier. The hydrogel mesh is proposed to be placed on the ocular surface as a bandage contact lens (BCL) to promote regeneration of the injured cornea without the need for surgical intervention. It was found that hyaluronic acid (HA) has a stimulatory effect on the migration and proliferation of epithelial corneal cells and thus promotes corneal epithelial tissue healing. Moreover, collagen hydrogels promote proliferation and differentiation of epithelial cells; however, they have low mechanical properties. Therefore, the aim of this chapter is to incorporate HA and collagen within GelMA hydrogel matrix as a carrier for HCEpC for treatment moderate-severe corneal injuries. The effect of various hydrogel compositions on the mesh properties including shape, degree of crosslinking, equilibrium swelling ratio (ESR), biodegradability and cell viability of the printed meshes were evaluated. It was found that 8% GelMA is a good hydrogel base for the 3D-printed scaffolds. The incorporation of a small concentration of HA within the hydrogel composition is beneficial during the printing process. The presence of collagen within the hydrogel composite obtained a smooth printed mesh and enhanced the adhesion and proliferation of the seeded cells resulting in the formation of cell sheets within the printed structure.

6.1 Introduction

In the previous chapter, PEGDA was incorporated to extend the degradation time of the BCLs and the concentrations and molecular weights of PEGDA used did not affect cell viability, which proved to be non-toxic and suitable for tissue regeneration applications including repairs of corneal injuries. In this chapter, I would like to investigate the incorporation of materials that promote cell growth, not only the ones that prove to be non-cytotoxic. Therefore, I have incorporated HA for its lubricating and corneal healing properties, and collagen since it is proved from literature that it enhances cell adhesion and proliferation.

The cornea is essential for the maintenance of clear vision. Thus, it is of paramount importance that the corneal epithelium is rapidly regenerated after corneal injury or surgery. Corneal epithelial healing involves the migration of epithelial cell sheets from the remaining intact epithelium and proliferation of the basal epithelial cells surrounding the injured part to restore the normal multi-layered architecture of the epithelium and promote adhesion of the newly regenerated epithelium to the underlying connective tissue (H. S. Dua, Gomes, & Singh, 1994; Gomes, Amankwah, Powell-Richards, & Dua, 2004).

The factory that produces epithelial corneal stem cells that later differentiate into epithelial cells is located in the limbus, which is a narrow circular tissue located between the cornea (transparent) and the sclera (opaque) (Cotsarelis, Cheng, Dong, Sun, & Lavker, 1989; Schermer, Galvin, & Sun, 1986). Corneal stem cells migrate from the limbus to the cornea to substitute the natural daily loss of corneal epithelial cells. However, these corneal limbal stem cells can be permanently damaged in certain cases such as alkali burns, in Steven Johnson syndrome, after radiation or multiple surgeries especially when ischaemia occurs in more than half of the limbal region, which results in limbal stem cell deficiency (LSCD) (Pratoomsot et al., 2008). Moreover, in certain cases, including dry eye syndrome and diabetic keratopathy, it is difficult for the epithelial cells to regenerate since the source of stem cells is already compromised. This is referred to as a persistent epithelial defect (PED), which is characterised by a non-healing epithelial lesion after the failure of treatment with standard therapies after 2 weeks (McCulley, Horowitz, Hussein, & Horowitz, 1993; Ziaei, Greene, & Green, 2018).

Failure in migration of limbal stem cells to the corneal epithelium leads to the infiltration of adjacent cells from the conjunctiva resulting in neovascularisation, chronic inflammation, ingrowth of fibrous tissue and scarring, all of which lead to reduced vision and eventually blindness (A. Huang & Tseng, 1991; T. Nakamura, Inatomi, Sotozono, Koizumi, & Kinoshita, 2016). Depending on the severity and the time passed from the primary injury, the choice of treatment is made. In **mild and partial LSCD**, amniotic membrane (AM) transplants can be effective. The presence of nutrients, anti-inflammatory regulators and growth factors in the AM, aid the re-epithelisation and reduction of inflammation, scarring, and vascularisation of the injured cornea, thereby promoting the expansion of the remaining limbal stem cells (Gheorghe et al., 2016). In **severe cases**, grafting small pieces of healthy limbal tissue from the patient's other eye (limbal autografts) or from the limbus of a close relative (allograft) is usually a successful treatment (Gheorghe et al., 2016). However, this is an invasive and expensive operation.

Stem cell therapy and tissue engineering are promising novel approaches in the treatment of injured corneas where LSCD occurs, where the transplanted stem cells promote regeneration of the corneal epithelium and help restore epithelial clarity (Gheorghe et al., 2016). Stem cell transplant is a recently successful procedure used in various cases of LSCDs. In this process, stem cells are cultured in the presence of growth factors on a scaffold sheet of a biological (AM) or biosynthetic (fibrin, collagen) origin. The scaffold provides the required support, promoting cellular differentiation and proliferation throughout their formation into new tissue. Hydrogels can be designed to mimic the mechanical and biological properties of soft tissues and are therefore the perfect candidate for tissue engineering scaffolds. Modifying the hydrogel polymer precursors can affect the mechanical and biodegradable properties of the hydrogels and may provide signals that help in specific cell attachment (Chandler et al., 2011; Hutson et al., 2011).

Gelatine is a protein-based material derived by hydrolysis of collagen. Due to its high solubility, biodegradability, biocompatibility and low cost it has been extensively used in many pharmaceutical and food applications (R. T. Jones, 2004; WM, JY, & GH, 2013). Moreover, gelatine can be chemically crosslinked or modified to have advanced mechanical and biochemical properties. Crosslinked gelatine-based materials have been used owing to their high water content and transparency, in ocular therapeutics as

bioadhesives (H. C. Park, Champakalakshmi, Panengad, Raghunath, & Mehta, 2011; Yamamoto et al., 2013), scaffolds (Alireza Baradaran-Rafii, Biazar, & Heidari-Keshel, 2015; Lai, 2013a; Lai, Li, Cho, & Yu, 2012) and cell-sheet carriers (Lai, 2013b; Lai & Li, 2010a; Lai et al., 2013). Mammalian gelatine such as porcine and bovine gelatines have high cell adhesion properties since they have a high number of specific domains that bind to cell-surface receptors and other extracellular matrices (ECM) proteins such as fibronectin (Katagiri, Brew, & Ingham, 2003; Rose et al., 2014).

Hyaluronic acid (HA) is a naturally occurring glycosaminoglycan of the extracellular matrix. Due to its viscoelastic properties, high water retention capabilities, adhesion properties and long ocular surface residence time, it is used in intraocular surgeries (M. Inoue & Katakami, 1993; Völker-Dieben, Regensburg, & Kruit, 1994) and as wetting agent in the treatment of dry eye syndrome (M. Korogiannaki, Guidi, Jones, & Sheardown, 2015; Maulvi, Soni, & Shah, 2015; Troiano & Monaco, 2008). Although there is no HA in the normal corneal basement membrane, HA becomes available when an epithelial lesion is formed to initiate the healing process of an injured cornea (M. Nakamura, Mishima, Nishida, & Otori, 1994). Moreover, it was found that levels of HA increase during the epithelial wound healing process in animal models, with a stimulatory effect on the migration and proliferation of epithelial corneal cells (Asari et al., 1996; MIYAUCHI et al., 1990). Furthermore, it was reported that HA promotes corneal epithelial tissue healing after various ocular surgical procedures due to its role in facilitating the adhesion, migration and proliferation of the cells (Gomes et al., 2004; Lai et al., 2010; Lu, Lai, Ma, & Hsiue, 2008).

Collagen (type I) is the most abundant protein present in the corneal stroma and a major component of the ECM. It is biocompatible, biodegradable and possesses low immunogenicity, therefore it is a suitable material for use as a corneal scaffold (Ye et al., 2014). Collagen hydrogels promote proliferation and differentiation of epithelial cells; however, they have low mechanical properties. This can be improved with cross-linking and with the incorporation of other hydrogels (Tsai et al., 2015). Chemically cross-linked recombinant human collagen (RHC) hydrogels have been successfully used to treat patients suffering from corneal thinning (Merrett et al., 2008; Rose et al., 2014). In the case of 3D-printing, it is hard to use collagen hydrogels solely as inks due to their slow thermal gelation, which makes it very difficult for a structure to retain its shape while

printing. Incorporation of other rigid hydrogels such as alginate can prevent diffusion of collagen through the surface of the printed structure (Latinovic, Hough, & Ou-Yang, 2010; Pataky et al., 2012).

This chapter aims to deliver human corneal epithelial primary cells (HCEpC) to the injured cornea, via a hydrogel mesh carrier placed on the ocular surface as a corneal bandage, to promote regeneration of the injured cornea with no need for surgical intervention. Gelatine methacrylate (GelMA) or its composites with either hyaluronic acid or collagen were used to prepare the hydrogel matrix. The hydrogel was printed in the form of a mesh structure and the HCEpC were seeded on the mesh and incubated for 1 week to promote cell proliferation and differentiation. The effect of various hydrogel compositions on the mesh properties including shape, crosslinking, equilibrium swelling ratio, biodegradability and cell viability was evaluated.

6.2 Materials and methods

6.2.1 Materials

An Allevi2 double extruder 3D-bioprinter, printing needles and lithium phenyl-2,4,6-trimethylbenzoylphosphinate (LAP) from Allevi, Philadelphia, USA. Porcine gelatine type A with 300 Bloom value, Deuterium oxide (D₂O) 99.9 atom % D, methacrylic anhydride and Phosphate buffered saline (PBS) tablets 1.0M, pH 7.4 (25 °C) were obtained from Sigma-Aldrich, New Zealand. Sodium hyaluronate (HA1.5 MDa) was from Lifecore Biomedical, Chaska, Minnesota, USA. The collagen used in this study was provided by the New Zealand Leather and Shoe Research Association (LASRA).

6.2.2 Hydrogel preparation

GelMA was prepared as stated in the Preparation and characterisation of GelMA hydrogel section in chapter 4 (p. 66). To prepare the hydrogels, LAP was first dissolved in PBS using a magnetic stirrer at 50 °C. Then the GelMA was added to the solution and mixed at the same temperature for around 20 min until fully dissolved. The hydrogel mixture was then transferred to a 10 ml Luer lock syringe, the black plunger was inserted, then the contents of the syringe were pushed to remove the excess air. The whole syringe was wrapped with aluminium foil and inserted in a beaker full of ice for 8

min to enhance the physical gelation of GelMA, then left at room temperature overnight until the printing time.

To prepare GH0.5 and GH1 hydrogels, the required volume of PBS was divided into two halves, one was kept at 4 °C to dissolve the HA, and the other was heated to 50 °C to dissolve LAP and GelMA. Then, both solutions were mixed at 37 °C to prepare GH0.5 and GH1, where GH0.5 and GH1 had 0.5% and 1% of HA of the total hydrogel volume, respectively. The hydrogels were transferred to a 10 ml syringe, inserted in ice for 8 min and left at room temperature overnight until the printing time.

Collagen is insoluble in cold and hot PBS, therefore, to prepare 1 ml of GC1 hydrogel, 0.01 g of collagen was dissolved in 0.25 ml cold 0.5 N acetic acid overnight, while LAP and GelMA were dissolved in 0.75 ml PBS at 50 °C. Both mixtures were mixed at 37 °C before being transferred to a 10 ml syringe, inserted in ice for 8 min and left at room temperature overnight until the printing time.

Table 6.1. Composition of the hydrogel composites.

Formulation symbol	Abbreviation	GelMA (% w/v)	LAP (% w/v)	HA (% w/v)	Collagen (% w/v)
F1	G	8	0.5	-	-
F2	GH0.5	8	0.5	0.5	-
F3	GH1	8	0.5	1	-
F4	GC1	8	0.5	-	1

6.2.3 Preparation of the 3D-printed meshes

A square mesh design with crossing vertical and horizontal lines was created using SolidWorks CAD. The dimensions of the square were set to be 10 ± 0.5 mm in diameter, with a 0.5 mm gap between the lines. A detailed description of the printing process is found under “Preparation using the 3D-printing method” section in chapter 4 (p. 69).

All printed hydrogel meshes in this work were cured under the previously set and tested parameters in chapter 5 under the Allevi bioprinter 405 nm lamp set at an intensity of 13 mW/cm² for 150 s to crosslink the printed meshes.

The printed and cured hydrogel meshes were vacuum dried while still on the slide. In the vacuum-drying technique, the printed cured meshes were kept under vacuum at room temperature in a vacuum oven for 24 h.

6.2.4 Characterisation of the printed meshes

Visual and microscopic examination

Visual examination and camera images of the syringe carrying the prepared hydrogel (ink) after the printing process. Images of the extruded ink filament at the used printing pressure were taken to show the consistency of the filament and to give an idea on the viscosity of the ink. Images of the hydrogel mesh printed on a glass slide were taken just after printing against a ruler to show the printed mesh size. The glass slide was covered with plastic tape to prevent adhesion of the hydrogel to the slide and aid with easy removal after drying.

After vacuum drying of the printed meshes, they were imaged using a camera, an optical microscope and a scanning electron microscope. The optical images were captured using a digital microscope (Leica ICC50HD-DM750, New Zealand) to show the diameter of the printed lines and the pore size of the meshes. Measurements were taken from three different places for each mesh for three printed meshes.

After drying, meshes were soaked for 24 h in 3 ml PBS, then removed and kept at -4 °C for 24 h then placed in a freeze drier (Martin Christ, Alpha2-4 LDplus, John Morris Group, New Zealand) for 48 h before SEM imaging to view the inside structure of the wetted meshes.

Prior to SEM imaging, all meshes were placed on metallic stubs and coated with platinum under vacuum for 20 s using an ion sputter coater (Hitachi E-1045, UK) for visualisation. The images were scanned using Schottky field emission SEM (Hitachi SU-70, UK) under a working voltage of 5 kV. Three meshes were imaged for each hydrogel composition.

Degree of crosslinking

The printed, cured meshes were dried in a vacuum oven for 48 h, and the dry weight of each sample (w_1) was recorded. The meshes were then immersed in 3 ml PBS solution at 37 °C. After 24 h, the meshes were removed from the PBS solution and dried in a vacuum oven for 48 h. The weight of the dry meshes (w_2) was recorded. The sol fraction is the amount of hydrogel that was not crosslinked and thus dissolved in PBS. It can be calculated using the following equation (Bukhari et al., 2015; Ranjha & Qureshi, 2014).

$$\text{Sol fraction (\%)} = \frac{(w_1 - w_2)}{w_1} \times 100$$

To compare the effect of incorporation of HA and collagen on the 8% GelMA hydrogels, the sol fraction of all hydrogel compositions prepared in Table 5.2 were compared. At least, three meshes were used from each composition.

Swelling studies

The swelling ratio was determined gravimetrically using a sensitive balance. Three vacuum dried meshes from each hydrogel formulation weighed (DW), then they were immersed in 3 ml PBS for 24 h, blotted gently with tissue papers and then reweighed to record the swollen weight (SW). The equilibrium swelling ratio (ESR) of all hydrogel formulations was calculated using the following equation (Hoch et al., 2012; Noshadi et al., 2017; Yin et al., 2018).

$$ESR (\%) = \frac{(SW - DW)}{DW} \times 100$$

***In vitro* degradation**

To test the in-vitro degradation profile of the cured printed meshes, 12 meshes of each formulation were dried in a vacuum oven at room temperature for 48 h and the weight was recorded (W_1). Then the meshes were immersed in 3 ml of PBS in plastic well plate dishes and kept in an incubation room at temperature 36 ± 1 °C. At various time intervals at days 1, 2, 4 and 7, three meshes of each formulation were carefully removed from the PBS solution and dried in a vacuum oven at room temperature for 48 h then reweighed (W_2). The percentage weight remaining after degradation at each time point

was referred to as the gel fraction (%) and was calculated using the following equation (Bukhari et al., 2015; Y. Wang et al., 2018).

$$\text{Gel fraction (\%)} = \frac{W_2}{W_1} \times 100$$

The degradation profiles of the tested hydrogel formulations with 0.5% LAP cured at 13 mW/cm² for 150 s were compared.

Cell viability

To determine the effect of HA and collagen concentration on cell viability, 8% GelMA, 0.5% LAP hydrogel printed meshes containing either 0.5% HA, 1% HA or 1% collagen were cured at 13 mW/cm² by a 405 nm lamp for 150 s.

In all cell viability experiments, the printed and cured meshes were put in a vacuum oven for 48 h at room temperature to dry. Before seeding the cells, the dried meshes were individually placed in wells of a 12-well plate and put in a fume hood under UV light for 30 min to be sterilised. Table 5.2 above shows the composition of GelMA hydrogel meshes tested for cell viability.

HCEpC extracted from donor tissues were used in this experiment. A cell suspension of 1x10⁶ cells per millilitre of cell culture medium was prepared. Prior sterilisation of the meshes, 100 µl of the previously mentioned cell suspension was pipetted into the mesh and left 15 min to settle before adding 500 µl of the culture medium and incubated for 1 week.

The culture medium was prepared as a 1:9 ratio of 10% Foetal Calf Serum (FCS): MEM, GlutaMAX™ Supplement, then 1% of Antibiotic-Antimycotic (100) was added. Fresh culture medium was added on day 1 and the medium was replaced every other day during the week. At day 2, the meshes were removed and placed in a clean plate with fresh culture media.

After 7 days, Invitrogen LIVE/DEAD® Viability/Cytotoxicity Kit for mammalian cells (Thermo Fisher Scientific) was prepared according to the manufacturer's instructions. A volume of 100 µl of the prepared solution were added to the hydrogel meshes and left for 20 to 40 min at room temperature to stain the cells. Meshes were then washed with PBS for 15 min, then removed and mounted on glass slides for imaging under a

fluorescence microscope. The resultant images were used to visualise the proportion of live to dead cells over a period of 7 days.

Statistical analysis

Data were subjected to one-way analysis of variance (ANOVA) using Microsoft 365 Excel. Post hoc multiple comparisons were determined by the Tukey's test with the levels of significance set at $P < 0.05$. All data were presented as means \pm SD.

6.3 Results and discussion

6.3.1 Hydrogel preparation

Introducing methacryloyl substitution groups to gelatine via a chemical reaction with methacrylic anhydride (MAA) results in the formation of gelatine methacrylate (GelMA) as shown in Figure 6.1. Unlike gelatine, GelMA undergoes permanent fast chemical gelation upon exposure to light irradiation in the presence of photoinitiators. The produced GelMA retains the excellent biocompatibility and bioactivity of gelatine, such as cell adhesion, spreading, and proliferation due to the presence of cell-adhesive RGD motifs and MMP-degradable amino acid sequences within its structure (Yue et al., 2015).

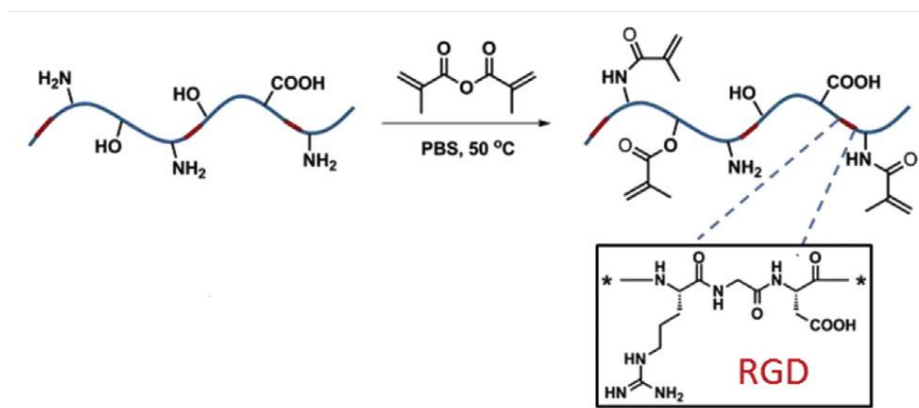


Figure 6.1. GelMA synthesis from gelatine and MAA, showing the RGD motifs responsible for cell adhesion (Adapted from (Yue et al., 2015)).

6.3.2 Preparation of the 3D-printed meshes

Table 5.5 shows the printing parameters used with each hydrogel composition to obtain the best print. Clear plastic tapered needle of inner diameter (ID) 0.21 mm (27 G) was used in printing all hydrogel formulations since this small diameter was sufficient to extrude a continuous flow of the hydrogel filament and print a high-resolution line at the set pressure and speed. However, the (GH1) hydrogel formulation was too viscous

to be extruded via the 27 G needles, therefore the 25 G needles with an inner diameter of 0.26 mm were used.

Table 6.2. Printing parameters for 8%GelMA hydrogel meshes.

	8%GelMA (G)	8% GelMA +0.5 %HA (GH0.5)	8% GelMA +1% HA (GH1)	8% GelMA +1% collagen (GC1)
Needle (G)	27	27	25	27
Pressure (PSI)	12	7.7	8.1	6.9
Speed (mm/s)	3	3	3	4

It was noted that the incorporation of HA to 8% GelMA hydrogel reduced the required pressure to extrude the hydrogel filament during printing. This might be due to the shear-thinning properties of HA hydrogels (L. Ouyang, C. B. Highley, C. B. Rodell, W. Sun, & J. A. Burdick, 2016; Stratesteffen et al., 2017; S. Wang, Lee, & Yeong, 2015). Shear-thinning materials undergo disassembly (shear-thinning) when injected through a syringe and then reassemble within seconds (self-healing) once they are extruded out of the needle and shear forces are removed (Loebel, Rodell, Chen, & Burdick, 2017). Hydrogels with shear-thinning properties are perfect candidates in bioprinting applications since minimum pressure is required to extrude those inks out of the nozzles during printing, which is very helpful if cells are incorporated within the hydrogel since this will reduce the load on the carried cells and thus produce a printed structure with high cell viability. In this work, the incorporation of 0.5% HA within the hydrogel matrix reduced the printing pressure from 12 to 7.7 PSI in printing hydrogels G and GH0.5, respectively, using the same printing needle of 27 G.

Moreover, all hydrogels were printed at a speed of 3 mm/s, while hydrogel formulation (GC1), containing 1% collagen was printed at a higher speed of 4 mm/s. This might be due to the presence of 0.5 N acetic acid within the hydrogel, which might have lowered its viscosity. The low viscosity of GC1 hydrogel resulted in lowering the pressure used for printing from 12 PSI in case of the G hydrogel to 6.9 PSI in the GC1 hydrogel as shown in Table 5.5 above.

6.3.3 Characterisation of the printed meshes

Visual and microscopic examination

The colour of the cooled hydrogels is shown in Figure 5.5. The incorporation of HA to 8% GelMA in GH0.5 and GH1, led to the formation of a turbid hydrogel upon cooling, compared to the colour of the 8%GelMA (G), this might be contributed to the immiscibility of HA in GelMA hydrogel. Moreover, the presence of 1% collagen in GC1 hydrogel formulation resulted in a white hydrogel colour since the collagen hydrogel was white in colour.

The incorporation of 0.5% HA within the 8%GelMA in GH0.5 hydrogel composition resulted in a continuous flow filament extruded from the 27 G needle as shown in Figure 5.5(B), this might be related to the shear-thinning properties of HA as explained by Loebel et al. (Loebel et al., 2017) and as indicated by the low extrusion pressure of 7.7 PSI. On the other hand, the higher concentration of 1% HA resulted in a hydrogel with high density that was difficult to extrude from 25 G needles and failed to obtain a continuous filament when extruded using 25 G needles as shown in Figure 5.5(C). In the case of GC1 hydrogel, the incorporation of acetic acid required to dissolve the collagen resulted in a hydrogel with low density and thus a continuous flow.

Although the printed meshes of the G hydrogel had high-resolution print as shown in Figure 5.5(A), the incorporation of 0.5 and 1% HA in GH0.5 and GH1 hydrogels, respectively, resulted in a print with inconsistent lines. This can be explained by the difficulty in proper mixing of the high viscosity HA hydrogel with 8%GelMA at 37 °C, which caused inconsistent extrusion of the filament. It is worth noting that due to the instability of HA at high temperatures, it was not possible to mix the viscous HA hydrogel with the GelMA at 50 °C or to use any sonication. In this work, the molecular weight of HA used was very high (1500 kDa); using lower molecular weight or lower concentrations of HA is expected to mix properly with the GelMA due to the formation of lower viscosity HA solutions.

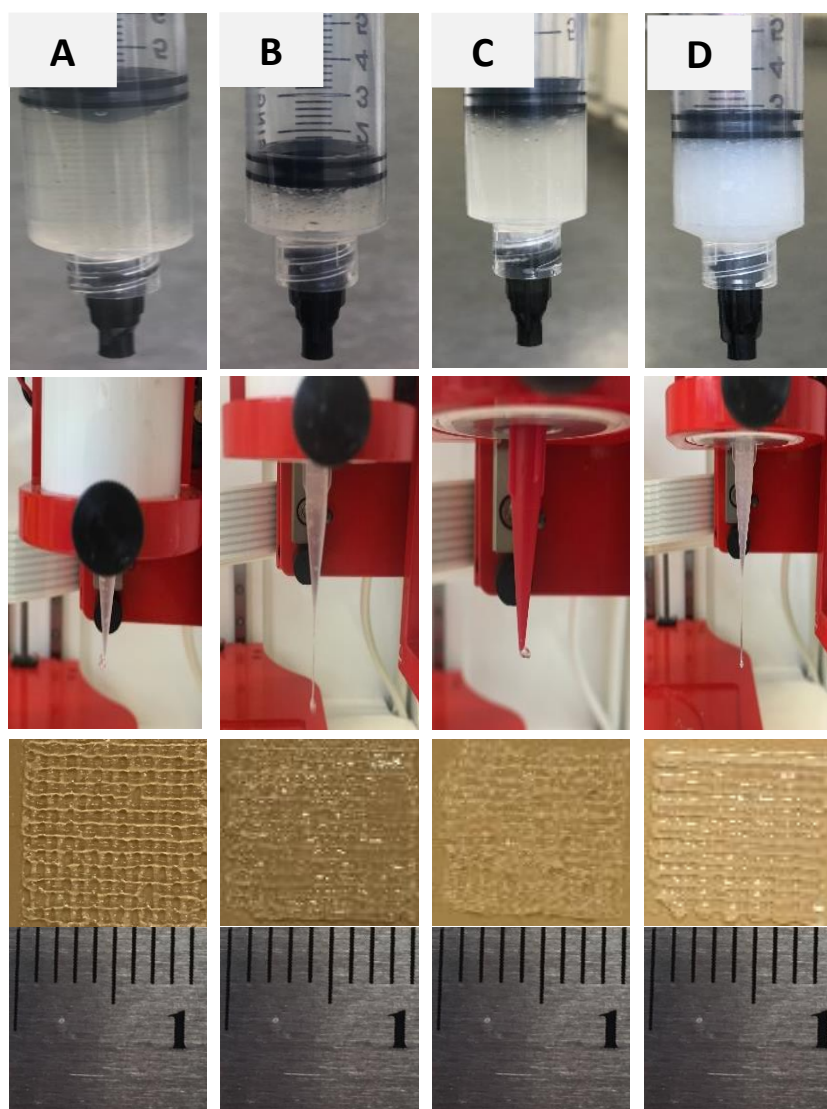


Figure 6.2. Images of the cooled hydrogel in the syringe prior to printing (top), the extruded filament from the nozzle to determine the appropriate pressure (middle) and printed mesh above a 1 cm ruler (bottom). Images show the formulations G (A), GH0.5 (B), GH1(C) and GC1 (D); ruler is in mm increments.

In the case of collagen incorporation in GC1 hydrogel, the structure had a high resolution and the printed lines retained their shape after printing. Moreover, the continuous filament and the low viscosity of the ink allowed for increasing the printing speed to 4 mm/s compared to G hydrogels. All of which resulted in smoother and thinner lines in the printed structure as shown in Figure 5.5.

The microscopic images of the printed meshes of hydrogel formulations G, GH0.5, GH1 and GC1 illustrated the effect of HA and collagen incorporation in the hydrogel composition. In Figure 5.7(A), the image of the printed formulation G shows smooth

printed lines which indicates that 8%GelMA hydrogel composition had high printing resolution under pressure of 12 PSI and speed of 3 mm/s.

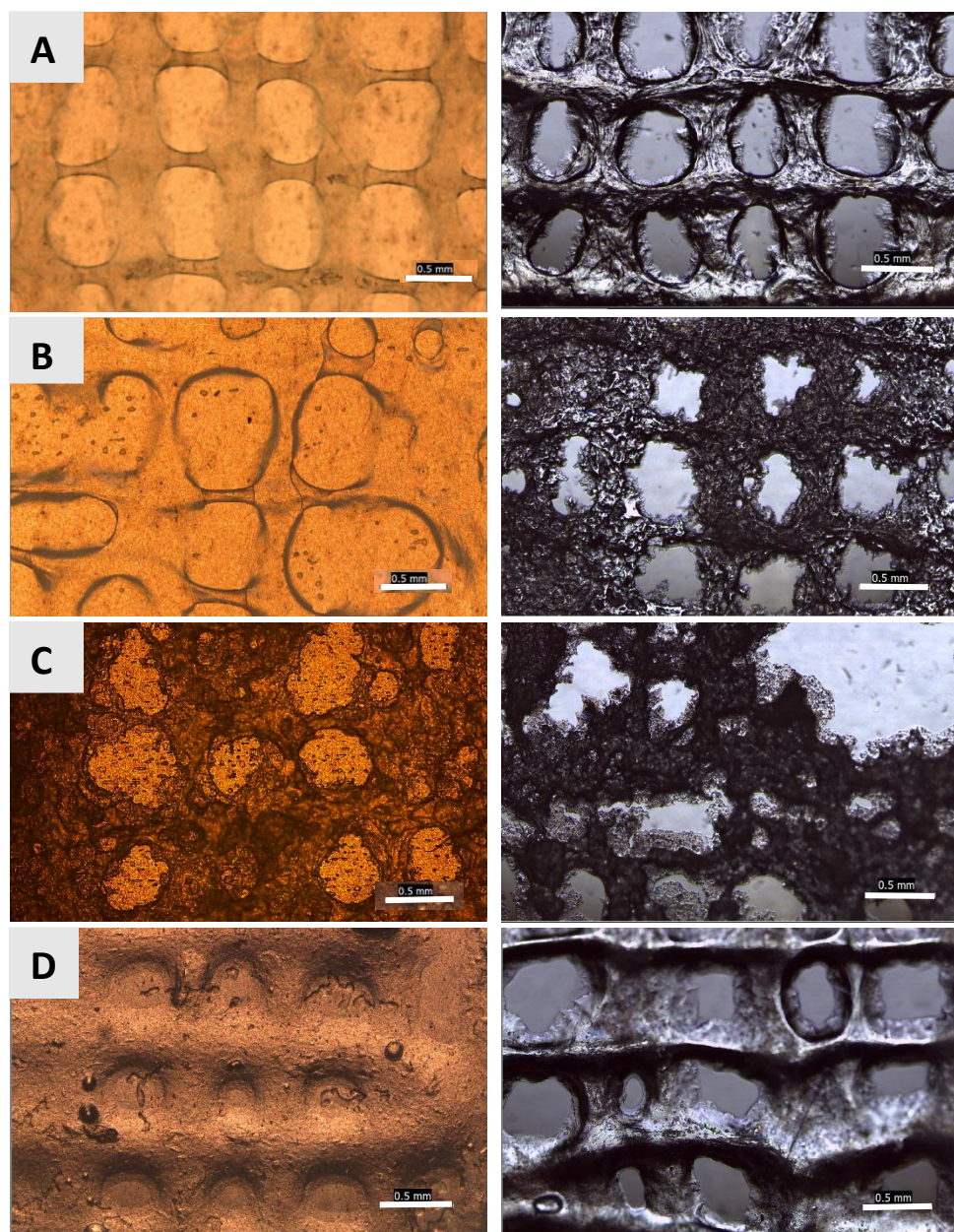


Figure 6.3. Microscopic images printed hydrogel meshes imaged immediately after printing (left) and microscopic image (4X) of vacuum dried hydrogel meshes after vacuum drying (right) of G (A), GH0.5 (B), GH1 (C) and GC1 (D); scale bar = 0.5 mm.

The incorporation of 0.5% HA in formulation GH0.5 led to inconsistency in the printed structure with variations in line diameters and pore sizes. This might be contributed to the effect of HA on the shear-thinning properties of the hybrid hydrogel that resulted in extrusion inconsistency while printing. Moreover, the incorporation of 1% HA in the GelMA hydrogel composition led to thicker lines with a visibly rough surface due to extrusion from a thicker needle (25 G). In the case of incorporation of collagen, the

printed lines were thicker and maintained their layer height and showed no sign of spreading compared to the printed structure of G hydrogels. This proves that the incorporation of collagen results in printed structures with high resolution and fidelity.

After vacuum drying, the meshes of G hydrogels looked the same as before drying as shown in Figure 5.7(A), however, those of GH0.5 showed shrinkage of the whole mesh, which resulted in smaller pore sizes. Both hydrogel formulations GH0.5 and GH1 containing HA showed rough and irregular lines after vacuum drying. On the other hand, the incorporation of 1% collagen within the 8% GelMA hydrogel meshes resulted in smooth straight lines after vacuum drying.

Furthermore, SEM was used to characterise the structure of freeze-dried G, GH0.5, GH1 and GC1 hydrogel meshes after swelling in PBS to determine the effect of hydration on the mesh structure as shown in Figure 5.9. There was no significant difference between the microscopic and SEM images of the vacuum-dried G and GC1 hydrogel meshes. However, the rough and irregular surface of the printed lines and the inconsistent pore sizes of GH0.5 and GH1 hydrogel meshes were more visible in the SEM images shown in Figure 5.9.

There were no obvious pores within the printed lines of the hydrated G and GC1 meshes, while porous lines were observed in GH0.5 and GH1 hydrated meshes where HA was incorporated. This might be related to the high volume of water absorbed by those hydrogels due to the hygroscopic nature of HA (Bansal, Kedige, & Anand, 2010). There was no significant difference in the shape or dimensions between G meshes before and after swelling. On the other hand, the swelling of GH0.5 and GH1 hydrogels resulted in the loss of the mesh structure due to the rapid degradation of the meshes in PBS during the swelling test. Interestingly, GC1 hydrogel meshes showed a uniform mesh structure and a very smooth surface after swelling as shown in Figure 5.9(D). The smooth surface of the mesh is very useful, especially when it is applied to the injured cornea.

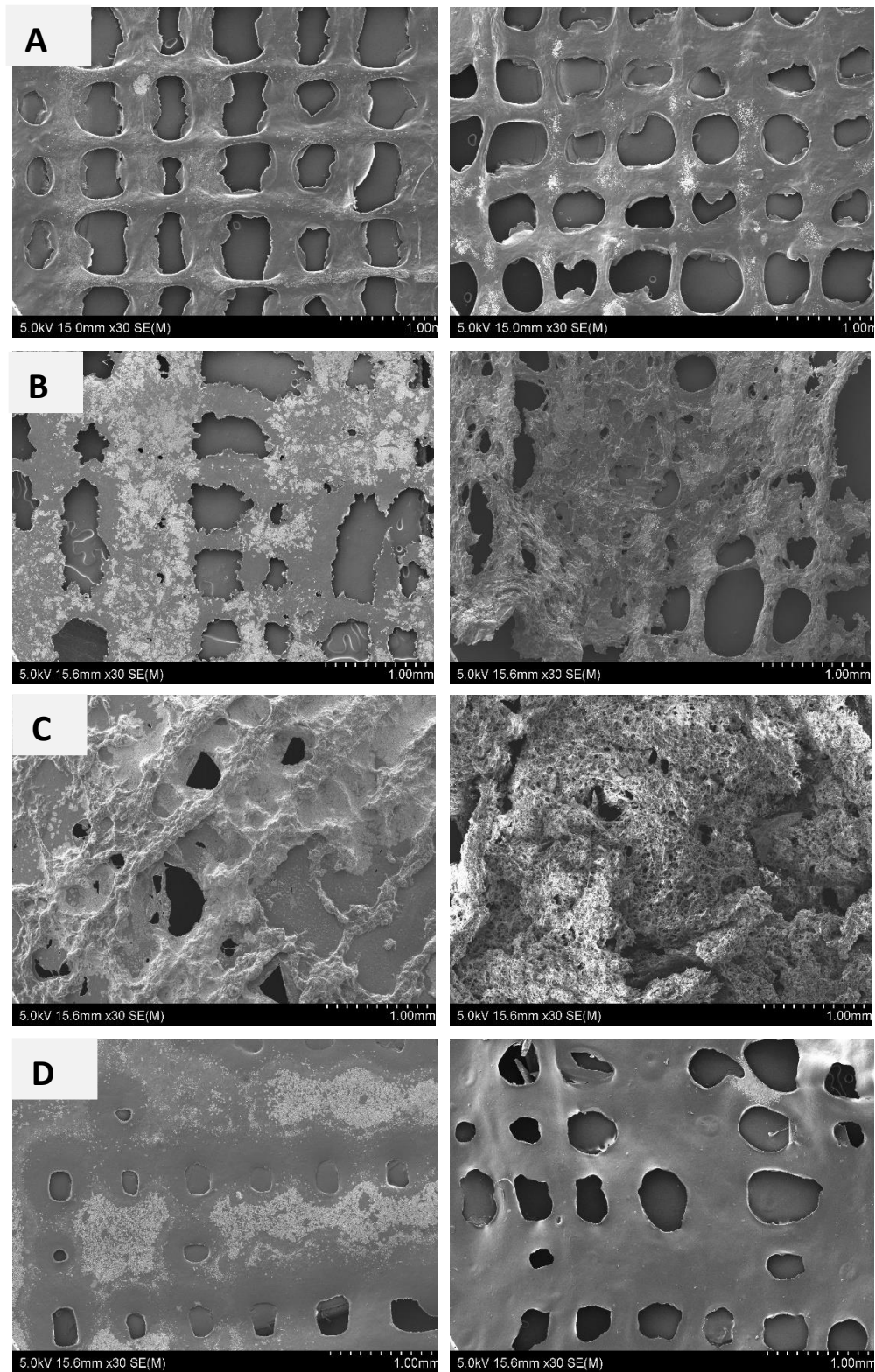


Figure 6.4. SEM images of 3D-printed 8% GelMA meshes after vacuum drying (left) and after swelling test (right) of 8% GelMA (A), 8% GelMA + 0.5% HA (B), 8% GelMA + 1% HA (C) and 8% GelMA + 1% collagen (D).

Degree of crosslinking

Although all the tested hydrogel meshes had the same concentration of GelMA (8%), same concentration of photoinitiator (0.5%) and same crosslinking parameters (13 mW/cm² intensity for 150 s), the incorporation of HA and collagen impacted the sol fraction dissolved from each hydrogel composition in PBS after 24 h. The incorporation of 0.5 and 1% HA to 8% GelMA hydrogel led to a significant rise in the sol fraction from 9.07 ± 0.85 to 21 ± 1.4 and $28 \pm 3.79\%$, respectively, as shown in Figure 6.5. This might be explained by the large volume of water absorbed by HA resulting in the quick degradation of the hydrogel matrix. The sol fraction of GC1 hydrogels increased slightly from 9.07 ± 0.85 to 12 ± 0.54 compared to G hydrogels, but this crosslinking value is within the acceptable range of 15%.

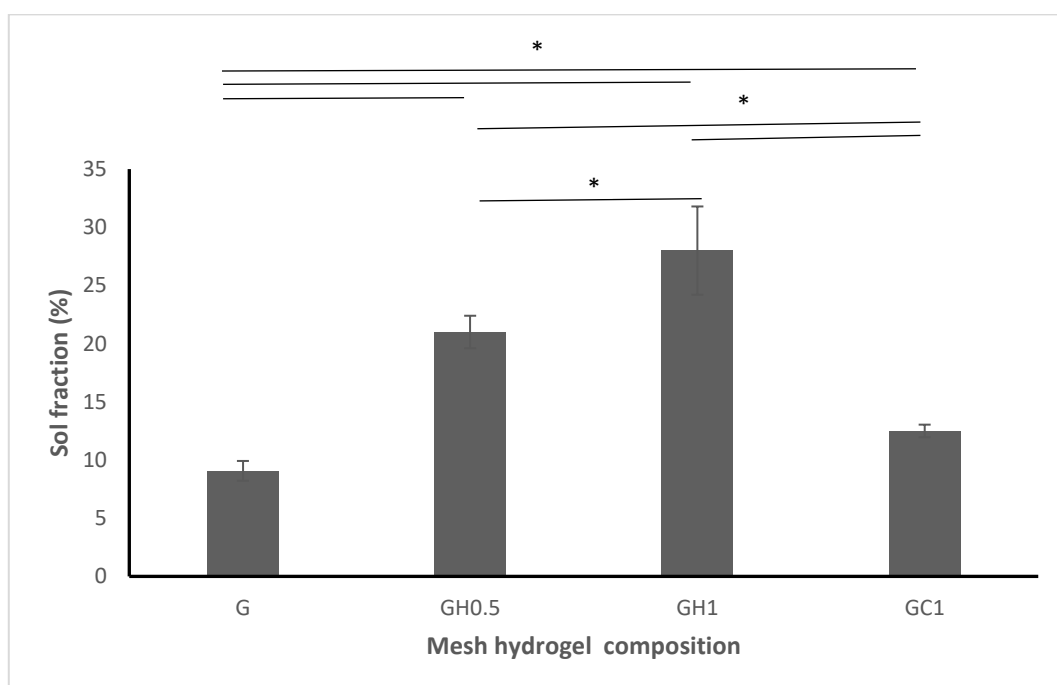


Figure 6.5. The effect of hydrogel composition on the crosslinking properties of 8% GelMA hydrogel meshes cured under 13 mW/cm² for 150 s. *Statistically significant at $p < 0.05$; $n = 3$; mean \pm SD.

Swelling studies

The swelling ratio is the ratio of water uptake of a hydrogel in relation to its dry weight. It is dependent on the mesh size of the polymer network, the degree of crosslinking and the polymer-solvent interaction (Hoch et al., 2012). The ESR is the maximum water uptake taken by the hydrogel.

In this study, the swelling ratios of G, GH0.5, GH1 and GC1 hydrogel meshes were 714.2 ± 36 , 618 ± 51 , 387 ± 56 and 593 ± 25 , respectively. The swelling ratio of the hydrogel decreased significantly with the increase in the amount of HA incorporated as shown in Figure 6.6. This is in compliance with the swelling test studies performed by Camci-Unal et al. (2013), which demonstrated that increasing the concentrations of HAMA within the GelMA/HAMA hybrid hydrogels decreased the ESR compared to hydrogels composed solely of GelMA. This was contributed to the increase in the crosslinking density following the addition of HAMA to the hydrogel network, which generates hydrogels with smaller pore sizes. The smaller pores cause less water penetration and thus results in less swelling (Camci-Unal, Cuttica, Annabi, Demarchi, & Khademhosseini, 2013). A similar effect on the swelling of the hydrogel meshes was observed with the incorporation of collagen with a reduction in the ESR compared to the GelMA meshes. However, the incorporation of 1% collagen did not reduce the ESR to the same extent as with the incorporation of 1% HA. This might be explained by the low molecular weight of collagen compared to the HA used, which in turn will not have the same effect on the crosslinking density of the hydrogels formed.

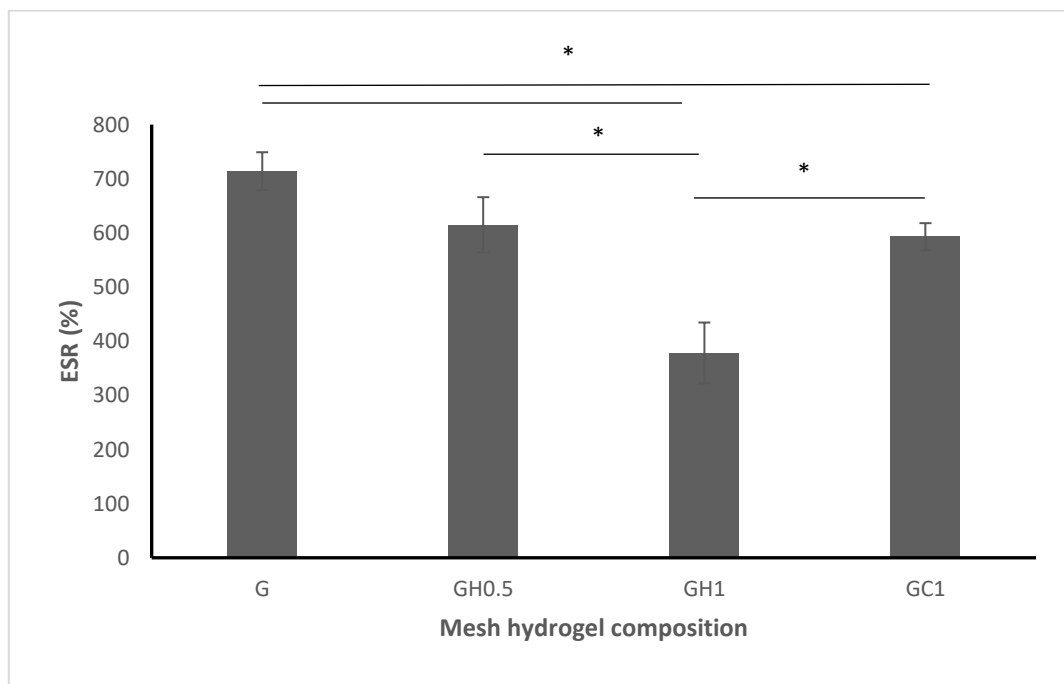


Figure 6.6. The effect of hydrogel composition on the ESR of 8% GelMA dry hydrogel meshes. *Statistically significant at $p < 0.05$; $n = 3$; mean \pm SD.

***In vitro* degradation**

The tested hydrogels should mimic the extracellular matrix and promote proliferation and differentiation of the carried cells. Moreover, they should have a certain degree of biodegradability to allow for cell remodelling. Therefore, it is crucial to develop hydrogels with tuneable mechanical and biological properties and test the effect of incorporation of various hydrogels within the hybrid hydrogel network structure (Hutson et al., 2011).

When HA and collagen were incorporated within the hydrogel network of GelMA, they influenced the degradation profiles of 8%GelMA hydrogel meshes as shown in Figure 6.7. Although all the tested meshes degraded after day 5, they had different degradation patterns. Both hydrogel formulations containing HA (GH0.5 and GH1) had a significantly higher degradation rate compared to G hydrogel meshes. GH0.5 and GH1 degraded to almost 50% of its original dry weight between days 2 and 3, compared to day 4 in case of G hydrogel meshes.

On the other hand, the incorporation of collagen did not affect the degradation rate between days 1 and 3 compared to G hydrogel meshes, with an abrupt increase in degradation rate at day 4. The gel fraction remaining at day 4 for GC1 was 23 ± 8.0 compared to 43 ± 6.7 in case of G hydrogel meshes as shown in Figure 6.7.

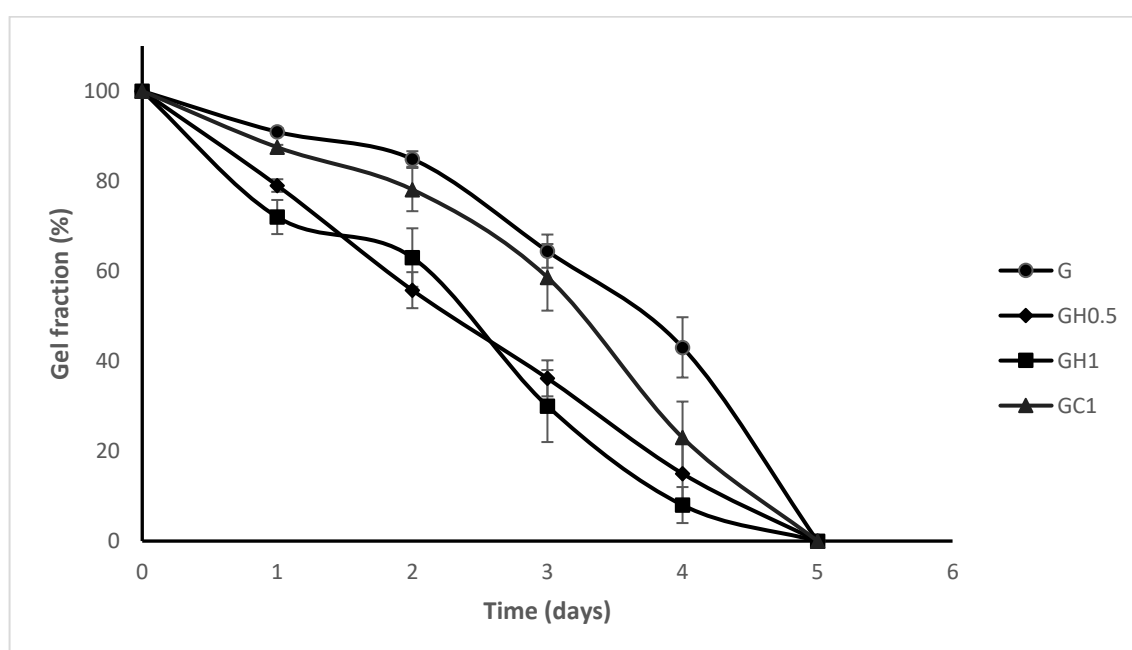


Figure 6.7. Degradation profiles of G, G0.5, GH1 and GC1 hydrogel meshes in PBS at 37 °C. n = 3; mean \pm SD.

Cell viability

The effect of the hydrogel mesh composition on the viability and growth of the seeded cells were examined to determine the feasibility of using these composite hydrogels as an epithelial cells carrier to promote corneal healing. The distribution of viable cells within the 3D-printed hydrogel meshes was also investigated (J. Park et al., 2017).

Live/dead cell staining assay was used to investigate the cell viability of the HCEpC cultured on the surface of G, GH0.5, GH1 and GC1 hydrogel meshes for 7 days and the z-stacked images of the confocal microscope are displayed in Figure 6.8. Most cells were alive, with homogenous distribution within the hydrogel matrix after 7 days culturing in all the tested meshes. This showed that the incorporation of HA and collagen with GelMA had no effect on cell viability and thus can be used in the composition of the scaffolds.

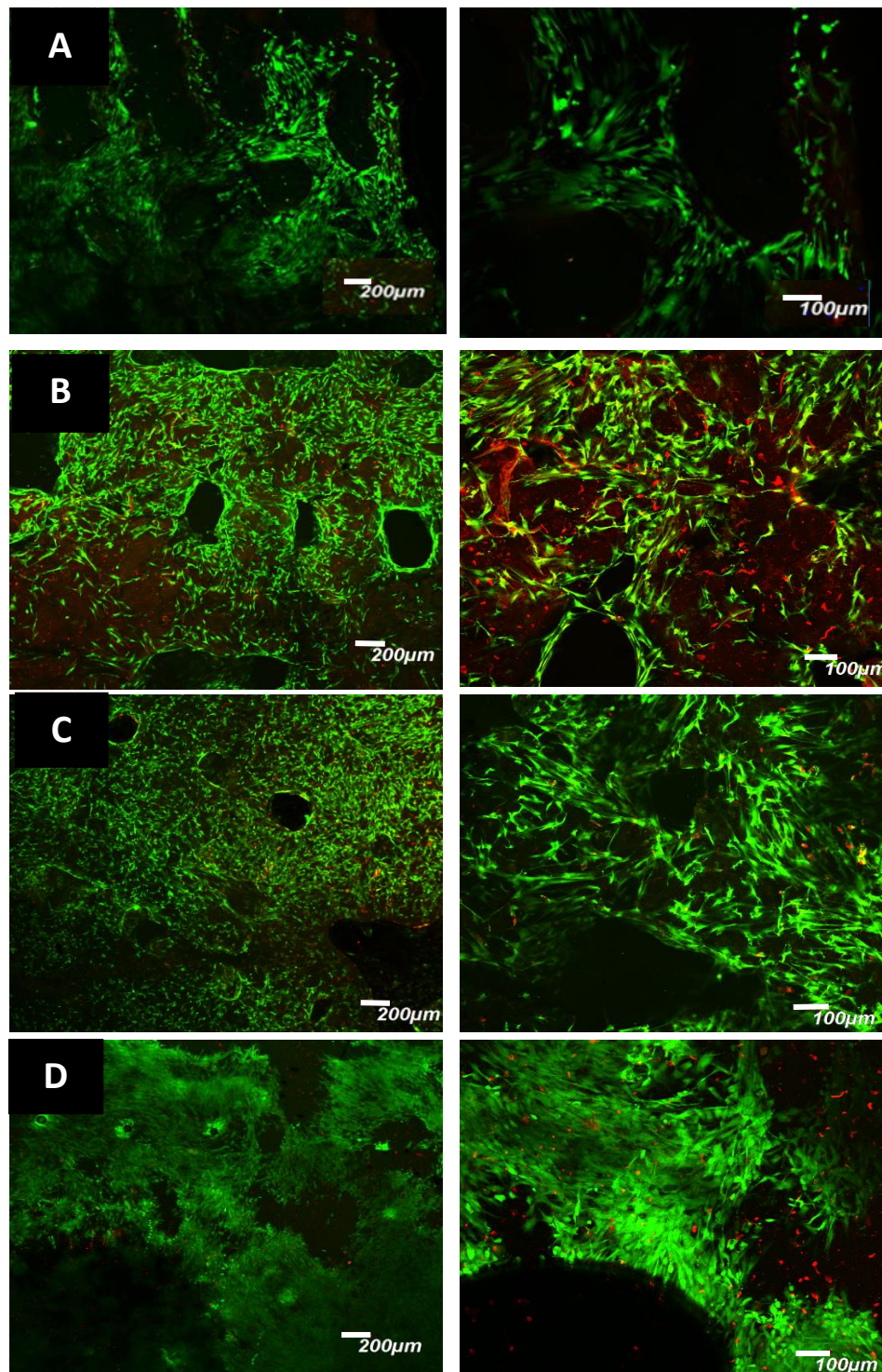


Figure 6.8. Z-stacked confocal microscopic image of 8% GelMA (A), 8% GelMA + 0.5% HA (B), 8% GelMA + 1% HA (C), and 8% GelMA + 1% collagen (D) hydrogel meshes stained with live/dead assay after 1-week incubation with HCEpC. The green colour indicates the live cells, while the red colour shows the dead ones.

The incorporation of 0.5 and 1% HA in GH0.5 and GH1 hydrogel meshes, respectively, resulted in a higher number of growing cells compared to G hydrogel meshes (0% HA) as shown in Figure 6.8. This showed that HA has a positive effect on cell growth, which

might be related to its role in stimulating the adhesion, migration and proliferation of corneal epithelium of rabbit and human corneal cells (Gomes et al., 2004; M. Inoue & Katakami, 1993; Nishida et al., 1991). With the increase in the number of live cells grown on GH0.5 hydrogel meshes, the number of dead cells increased compared to G hydrogel meshes due to the regular cell life cycle. Due to the viscosity and thickness of the hydrogel meshes, it is difficult for the dead cells to be flushed away within the culture media or with the washing of the meshes with PBS prior to imaging. On the other hand, a fewer number of dead cells were visible in GH1 meshes, which might be contributed to the highly porous structure that aids flushing away of dead cells within the culture media and while washing with PBS.

In the case of GC1 hydrogel mesh, there was a visible high density of cells growing within the mesh and forming a cell sheet after 7 days of incubation. This might be related to the cells' high affinity to collagen since this is the major hydrogel present in the cornea. Moreover, collagen is known to modulate cell proliferation, migration differentiation and gene expressions (Köse et al., 2005; C. Liu et al., 2008; L. Zhang et al., 2005).

6.4 Conclusion

In this work, the effect of various GelMA hydrogel compositions on the 3D-printed mesh scaffolds as a carrier of HCEpC for the treatment of corneal injuries were studied. Two concentrations of HA (0.5 and 1%) and one for collagen (1%) were evaluated to see their impact on the 3D-printing parameters, printed structure, swelling, crosslinking and degradation properties of the hydrogel mesh. Moreover, the effect of hydrogel composition on cell viability was studied.

The incorporation of 0.5% HA within the 8%GelMA in GH0.5 hydrogel composition resulted in a continuous flow filament with low extrusion pressure required during printing, which is beneficial in case of incorporation of cells within the hydrogel bioink in the printing process. However, the printed meshes showed a generally rough surface and rapid degradation profile compared to the 8% GelMA hydrogel meshes with no HA incorporated. This roughness and rapid degradation profile were enhanced with the increase in HA concentration in case of GH1 hydrogel meshes. However, the presence of HA in GH0.5 and GH1 hydrogel meshes enhanced the growth of HCEpC cultured within the hydrogel matrix. From the previous results, it can be concluded that the presence of

small concentrations of HA within the hydrogel is beneficial within the printing process and enhances cell growth, adhesion, migration and proliferation of the seeded HCEpC. Moreover, it is expected to promote healing of the injured cornea and provide the required moisture to the injured eye that might suffer from dryness due to the applied mesh on the eye surface. This evaluation could be the subject of future studies.

The best outcomes were obtained from meshes GC1, with a composition of 8% GelMA and 1% collagen. A continuous flow filament with low extrusion pressure required during printing was obtained. The printed meshes showed a very smooth surface after drying and moderate degradation profile. This makes them suitable to be applied on the eye surface for the proposed application as an ocular bandage. Moreover, the presence of collagen within the hydrogel meshes significantly enhanced the growth of HCEpC cultured within the hydrogel matrix forming a cell sheet.

We can conclude from the previous results that 8% GelMA is a good hydrogel base for the 3D-printed scaffold. The incorporation of a small concentration of HA within the hydrogel composition is beneficial to obtain a continuous flow filament, which in turn helps reduce the pressure and increase the speed during printing. The presence of collagen within the hydrogel composite obtained a smooth printed mesh, that can be applied on the eye as a corneal bandage, and had a significant role in enhancing HCEpC attachment, proliferation and migration within the hydrogel matrix forming a sheet of cells within the printed structure.

Chapter 7 General discussion

7.1 Thesis overview

Corneal injuries resulting from trauma, burns, infection or following complications after corneal surgery, are a leading cause of blindness worldwide. Minimising corneal inflammation and promoting controlled wound healing is a crucial step in the healing process of the cornea and is vital for preventing scarring that can permanently affect visual quality. Current therapy involves the use of anti-inflammatory eye drops that have poor bioavailability, with less than 5% of the drug penetrating the cornea. Improper patient adherence to the dosage regimen is a problem and can lead to serious complications and improper healing of the cornea. Furthermore, in severe cases of corneal injury, where the limbus is affected, the cornea loses its ability to regenerate and this leads to loss of sight. Currently, limbal injuries are treated by limbal graft surgeries which are invasive, expensive and involve long waiting periods. There is a **clinical need** for a drug-eluting/cell integrated corneal bandage, with current demand from ophthalmologists to have better therapeutic options for reducing complications arising from the limitations of current therapies.

The aim of this thesis was to develop two types of cost-effective BCLs that can be easily applied to the injured eye to reduce inflammation, promote faster healing and prevent scarring following corneal injuries. The first bandage was designed with the view of it being used for the treatment of mild to moderate corneal injury; this BCL can act as a physical barrier protecting the inflamed cornea from microorganisms and environmental conditions as well as a matrix for cell migration and proliferation while delivering essential anti-inflammatory medications in a controlled manner over a period of 1 week. The second bandage has been designed to be used for the treatment of moderate to severe corneal injury; the incorporation of HCEpC within the BCL is expected to promote corneal healing when the limbus is affected and the eye loses its ability to self-regenerate the cornea. This second cell-loaded BCL has the potential to reduce the need for corneal grafts.

7.2 Interpretation of main thesis findings

Current approaches for corneal wound healing which include the use of corneal bandages were reviewed in chapter 2, highlighting the opportunities and limitations for their use. Various types of bandages, including amniotic membranes, collagen shields and silicone hydrogel BCLs, were discussed. It was found that silicone hydrogel BCLs are commonly used with minimum complications as they are soft, comfortable and allow for high oxygen permeability thereby extending their application for up to 30 days. Although there are current approaches to use BCLs after corneal surgeries for covering the injured cornea and provide a matrix for epidermal cell adhesion and proliferation, there is currently no drug-eluting BCL available in the market. Several attempts have been made by researchers to formulate drug-loaded silicone hydrogel BCLs, however, none have been marketed yet. Commercial lens manufacturing companies have several weekly and monthly silicone hydrogel lenses that can be used as a base for medicated BCLs, however, there are usually few unrevealed components, which makes it harder for scientists to utilise and alter those successful formulations as a base for drug-eluting BCLs. Hence, drug-loaded silicone hydrogel BCLs were formulated in chapter 3 using some of the monomers used in marketed silicone hydrogel lenses. Moreover, the literature review revealed other materials that are used in the formulation of BCLs and include hydrophilic and hydrophobic monomers utilised in the production of silicone hydrogel lenses, collagen in collagen shields, HA and chitosan incorporated in some lenses to enhance their functional or material properties. This was very useful in setting a firm foundation for this thesis and trying to incorporate various polymers and evaluate their effect on the drug release and lens properties.

Drug-eluting silicone hydrogel BCLs were formulated using the solvent casting technique to deliver the loaded anti-inflammatory drug (DEX) over a period of 2 weeks. The BCL acts as an all-in-one therapeutic approach to deliver DEX as an anti-inflammatory medication over a period of 2 weeks while acting as a bandage that covers and protects the injured eye and provides a matrix to promote cell adhesion and proliferation. *p*(HEMA-*co*-TRIS-*co*-PDMS) lenses were prepared and the molar ratios of the comonomers were varied to evaluate their effect on the controlled release of DEX and the mechanical properties of the formulated BCLs. Extended release of DEX for up to 14 days

was achieved from these lenses whilst also providing mechanical properties comparable to commercial silicone hydrogel contact lenses.

In chapter 4, 3D-printed drug-loaded GelMA hydrogel lenses were designed and prepared to deliver DEX to the eye over a period of 1 week. Drug-loaded GelMA/PEGDA hydrogel lenses were prepared using the solvent casting and the 3D-printing techniques. Two concentrations of GelMA (5 and 8%) were tested with 4 concentrations of PEGDA (0, 5, 10, and 15%). It was found that the incorporation of PEGDA improved the lenses' resistance to handling and protected them during the degradation test, reduced the EWC values and prolonged the release of the incorporated drug. Moreover, the 3D-printing technique increased the EWC and thus resulted in a rapid drug release profile compared to the lenses prepared using solvent casting. Nevertheless, there was still a sustained release of DEX from the 3D-printed lenses for up to 7 days until they were fully degraded.

As a next step, GelMA/PEGDA composite 3D-printed hydrogel meshes with high printing fidelity, adequate mechanical properties and controllable degradation profiles were developed to be used as a cell carrier for tissue regeneration purposes. The incorporation of PEGDA enhanced the mechanical properties of GelMA hydrogels, increased their degree of crosslinking and significantly reduced their *in vitro* degradation rates. *In vitro* cell culture experiments using HCEpC showed high adhesion, proliferation and viability over a period of 1 week. This proved that PEGDA can be incorporated with GelMA or other hydrogel polymers as a polymeric crosslinker to enhance the mechanical properties and prolong the biodegradation of tissue-engineered hydrogels without a negative effect on the viability of the seeded cells.

In chapter 6, a novel non-invasive technique using a hydrogel mesh carrier acting as a therapeutic BCL was proposed for the delivery of HCEpC to an injured cornea. This proposed treatment involves placing the cell-loaded hydrogel mesh on the ocular surface to promote regeneration of the injured cornea without the need for surgical intervention. GelMA or its composites with either hyaluronic acid or collagen were used to prepare the hydrogel matrix. It was found that the incorporation of a small concentration of HA within the hydrogel composition is beneficial to obtain a continuous flow filament, which helps to reduce the pressure and increase the speed during

printing. The presence of collagen within the hydrogel composite produced a smooth printed mesh that could be applied on the eye as a corneal bandage, and significantly enhance HCEpC attachment, proliferation and migration within the hydrogel matrix forming a sheet of cells within the printed structure.

7.3 Thesis implications

Cataract is the leading cause of blindness worldwide, with 10 out of the 30 million blind population worldwide is due to cataract, and over 35 million of the world population being visually impaired due to cataract (Khairallah et al., 2015). Cataract surgery is the most common surgical procedure performed in those over the age of 65 in New Zealand and the world (Raczyńska, Glasner, Serkies-Minuth, Wujtewicz, & Mitrosz, 2016; Riley et al., 2001), which is expected to grow in number with the current world ageing population (Randers, 2012). Moreover, corneal healing is becoming a significant clinical problem due to the constantly increasing numbers of refractive surgeries worldwide (Ljubimov & Saghizadeh, 2015). After surgery, patients are required to remove the bandage covering their eye several times a day in order to apply therapeutic eye drops. There is poor adherence to this strategy, is inconvenient and can lead to post-operative complications such as **endophthalmitis** which result in poor sealing of the wound site (Song, Li, Zhang, Shi, & Li, 2018). Improper corneal healing after corneal trauma is the most common cause of corneal defects, with 6-7,000 patients presenting to the Auckland Eye Department alone each year. If the abrasion involves more than half of the corneal surface, healing can take up to 5 days, and 28% of these patients will have recurrent symptoms for up to 3 months after injury. Recurrent corneal erosions (RCE) are quoted as being common due to the wide variety of associated conditions including chemical and thermal injuries, previous viral or bacterial infections and systemic conditions such as diabetes (Miller, Hasan, Simmons, & Stewart, 2019). It is expected that the application of therapeutic BCLs will promote rapid corneal healing and the reduce complications associated with frequent patch removal for the application of medicated eye drops.

Patients other than those who suffer from corneal injuries can also benefit from the use of BCLs as a drug delivery device. It is reported that **patients who require frequent installation of therapeutic eye drops**, including glaucoma and cystinosis patients,

mostly fail to adhere to the dosage regimen, which can usually result in complications. Those chronic patients will potentially benefit from using therapeutic BCLs and can achieve a better quality of life and improved clinical outcomes (L. W. Jones et al., 2016). Thus, a well-designed drug-eluting BCL can offer a safe and therapeutically efficient alternative to eye drops that can be more appropriate for some patients depending on their lifestyle and medical condition (K.-H. Hsu et al., 2014). Furthermore, drugs with high systemic toxicity, including timolol, pilocarpine and atropine, can be delivered using BCLs without fear of drug drainage through the nasal cavity reaching the vascular nasal mucosa and thus causing systemic side effects (Farkouh, Frigo, & Czejka, 2016). Moreover, the high bioavailability of drugs administered via BCLs allows for fewer doses and therefore fewer side effects (K.-H. Hsu et al., 2014).

In terms of the monomers that can be utilised in the development of the drug-eluting silicone hydrogel BCLs, several attempts have been made by researchers to develop the lenses using various hydrophilic and hydrophobic monomer compositions. However, there are very few studies incorporating HEMA hydrophilic monomers with both TRIS and PDMS as the hydrophobic monomers. A study performed by Guidi et al. (2014) showed the effect of incorporating 9.7 mole% of PDMS, 9.7 mole% of TRIS with 77.6 mole% of either HEMA or DMA hydrophilic monomers and 3 mole% of EGDMA as a crosslinker to extend the release of DEX and test some of the lens properties including the swelling behaviour and contact angle measurements to determine the surface wettability. All the drug release profiles showed an extended release for more than 2 weeks, which is comparable to the results reported in chapter 3 of this thesis. It is worth noting that they performed the drug release tests on the prepared lenses without being washed, which will almost certainly affect the amount of drug released. Washing of the silicone hydrogel lenses is important to remove the unreacted monomers to prevent eye irritation. There was no research done on the effect of hydrophobic monomer composition on preventing the escape of the loaded drug during this essential washing phase, and therefore this was conducted in this thesis. Moreover, the EWC values obtained from lenses prepared by those researchers were only 11.3% compared to a value of 32.5% obtained from lenses containing 3 mole% PDMS and 10 mole% TRIS in this thesis. This might be due to the high concentration of the hydrophobic PDMS monomer used in their study. It is worth noting that the EWC of commercial silicone

hydrogel contact lenses is between 20 and 55% for patient's comfort and to prevent the eye from dryness (Musgrave & Fang, 2019). This was confirmed by their findings stating that the incorporation of PDMS resulted in reducing the EWC values of the lenses from 21 to 11% (Guidi et al., 2014).

To our knowledge, there was only one study that incorporated PDMS and TRIS with DMA, and not with HEMA, to extend the release of the loaded drug within the silicone hydrogel BCL. Various concentrations of the hydrophobic monomers were evaluated to determine their effect on the optical clarity, EWC and mechanical properties. EGDMA was only incorporated in one formulation and proved to extend the release of the loaded drug from 3 to 6 days (Kaczmarek et al., 2014). Although their hydrogel composition included high concentrations of 24 and 20 mole% of PDMS and TRIS, respectively, the release of the drug from the lenses were only extended for 6 days compared to more than 14 days in this thesis from the formulations containing 3 and 20 mole% PDMS and TRIS, respectively. This might be attributed to the small molecular weight of the PDMS they used (1000 g/mole) compared the PDMS used in this thesis which had a molecular weight of 5000 g/mole. This implies that the molecular weights of the incorporated monomers, as well as their concentration, can affect the release profile of the loaded drug.

The use of 3D-printing technology can help solve many of the problems associated with drug-eluting BCLs. For example, due to the nature of the drug or the polymers used, the BCL might not be transparent, and thus cannot be used during the day for chronic patients. Printing a BCL with a clear centre or even a hollow circle can solve this problem and increase patient compliance. Furthermore, patient-specific BCLs can be designed and printed according to the eye size and shape, which is beneficial in some cases such as in patients suffering from keratoconus. However, 3D-printing of hydrogels for the development of BCLs is limited by the properties of the materials used. GelMA is a widely used hydrogel material in extrusion-based 3D-printers due to its rheological properties and the ability to tailor its degree of methacrylation to achieve a crosslinked hydrogel with tuneable mechanical properties. To our knowledge, there were no studies done on the use of GelMA as the main component of a drug-eluting BCL. This was successfully achieved in chapter 4 of this thesis by incorporating PEGDA, which a safe biocompatible crosslinker, to prolong the release of DEX for 1 week.

Although altering the degree of methacrylation of GelMA affects the degree of crosslinking of the hydrogel and thus its mechanical properties, there is a limited window for changing the stiffness of the hydrogel. As less than 5% of the total amino acids of gelatine are actively available to react with MAA producing GelMA (Wei et al., 2015), it cannot be used alone to develop tissue engineering scaffolds that require high mechanical strength and long degradation time. The incorporation of PEGDA within the GelMA pre-polymer solution increases the chances of hydrogel crosslinking due to the presence of double active groups within the PEGDA polymer (Y. Wang et al., 2018). Wang et al. (2018) have tested the effect of incorporating 5% PEGDA (Mn=500) within 10, 20 and 30% GelMA hydrogels to develop hydrogel materials for bone regeneration. They proved that the presence of PEGDA as a crosslinker reduced the hydrogel swelling ratio, prolonged its degradation, and did not affect the cell viability within the hydrogel matrices during their 1 week incubation period which is in line with the results shown in chapter 5 of this thesis (Y. Wang et al., 2018). In this thesis, PEGDA (Mn=700) was used at concentrations of 1 and 10% within 8% GelMA hydrogel that was 3D-printed into square meshes with specific pore diameter that can be used in several tissue regeneration applications. In chapter 5, 3D-printing technology was used in the development of the hydrogel matrix and to study the effect of different concentrations of PEGDA on the printing parameters, properties of the printed structure and cell viability within the hydrogel matrix. To our knowledge, this has not been done before.

Due to the limitations associated with corneal transplants, restoration of the limbal stem cell population is currently the main treatment pathway to restore vision in cases of LSCD. This can be done through *in vitro* expansion of limbal epithelial stem cells (LESCs) on a natural or biosynthetic substrate that can be transplanted (de la Mata et al., 2013). Examples of natural substrata used as a carrier of corneal cells are AM (Sabater & Perez, 2017), fibrin (Meyer-Blazejewska et al., 2011), and 3T3 fibroblasts (Osei-Bempong, Ghareeb, Lako, Figueiredo, & Armitage, 2018), however, as these materials are natural products, they are associated with limitations including contamination risks, possibility of transmission of infections and variations between donor tissues, which renders them hard to be standardised (de la Mata et al., 2013; Ye et al., 2014). Hydrogel biosynthetic materials have therefore widely gained popularity as cell-sheet carriers in tissue regeneration applications and specifically corneal tissue regeneration (Lai & Li, 2010b).

Gelatine hydrogel disks have previously been used to carry human corneal endothelial cell (HCEC) sheets for the treatment of endothelial dysfunction. Upon surgical insertion of the disk into the anterior chamber of a rabbit's eye, they swelled within the anterior chamber, and the cell sheet adhered to the corneal posterior surface due to the bioadhesive properties of gelatine. Moreover, the gelatine disks biodegraded within after 6 weeks of the implantation period and the reconstruction of the corneal endothelium (Lai, Lu, Chen, Tabata, & Hsiue, 2006).

Chitosan-gelatine hydrogel polymer crosslinked using GA was evaluated as a carrier for limbal epithelial cell delivery (de la Mata et al., 2013). Moreover, gelatine-PLLA hydrogel nanofibrous scaffolds were developed as a corneal epithelial cell carrier (Yan et al., 2012) and Collagen-gelatine-HA biomimetic films were formulated using EDC and NHS crosslinkers as an HCEC carrier for corneal tissue engineering applications (Yang Liu, Ren, & Wang, 2013). However, 3D-printing technology has not yet been utilised in the development of porous GelMA hydrogel meshes solely or hybridised with HA or collagen as potential cell carriers of HCEpC for treating cases of moderate to severe corneal injuries. Therefore, this concept was explored in chapter 6 of this thesis.

The use of GelMA in 3D-printing applications within the field of tissue regeneration has been explored previously (Celikkin, Costantini, Rinoldi, Lin, & Świążzkowski, 2018; J. Liu et al., 2019; W. Zhu, George, Sorger, & Zhang, 2017). However, it hasn't been sufficiently investigated in the ocular field. Recently, primary endothelial cells were cultured on dehydrated gelatine discs and then implanted into the anterior chamber of a rabbit's eye to promote regeneration of the endothelium. However, the dense gelatine scaffold reduced the flow of the aqueous humour, which resulted in disturbing the flow of nutrients to the other tissues and thus increased the ocular pressure. Researchers have tried to make highly porous gelatine membranes using a stirring-freeze drying process followed by chemical crosslinking to enable rapid degradation of the scaffold (Rose et al., 2014). However, this can be potentially easier to achieve via 3D-printing technology, where a porous structure of GelMA can be printed and the degradation rate can be easily adjusted by tuning the degree of methacrylation in GelMA.

7.4 Study limitations and future recommendations

A hydrophobic drug (DEX) was chosen in chapters 3 and 4, to determine the effect of the hydrogel polymer composition on the release rates of the loaded drug. However, no other therapeutics such as hydrophilic drugs were tested. It is expected that hydrophilic drugs will have more rapid release profiles compared to DEX, and thus other methods of controlling the release such as drug encapsulation in nanoparticles (Behl, Iqbal, O'Reilly, McLoughlin, & Fitzhenry, 2016; Jung et al., 2013), and incorporation of diffusion barriers such as vitamin E or molecular imprinting techniques (Hui et al., 2012) might have to be used. Furthermore, only one concentration of EGDMA (3%) was used in chapter 3 in the prepared silicone hydrogel contact lenses, therefore it will be useful to test the effect of various concentrations of EGDMA on the drug release profiles and lens properties. It is worth noting that preliminary tests incorporating higher concentrations of EGDMA with HEMA hydrogel resulted in stiff films that are not suitable in BCL applications.

BCLs that are intended to be applied for more than one day and therefore should have high oxygen permeability, which is a parameter that measures the ability of the lens to allow the diffusion of oxygen to the eye so as to prevent corneal hypoxia and neovascularisation (Nasr, Khoee, Dehghan, Chaleshtori, & Shafiee, 2016). The high oxygen permeability of commercially available silicone hydrogel contact lenses is due to the presence of siloxane groups (Nicolson & Vogt, 2001). Moreover, other studies have confirmed that the incorporation of 0.75 M PDMS results in oxygen permeability of 75 Barrer, therefore all the silicone hydrogel lens formulations prepared in chapter 3 are expected to be within the acceptable oxygen permeability limits (J. J. Wang et al., 2012). It is expected that for the 3D-printed BCLS developed in chapters 4, 5 and 6 of this thesis, the printed pores within the lens enable the diffusion of oxygen into the cornea. However, testing the oxygen permeability of the BCLs is beneficial to confirm their suitability for prolonged use. This can be done using an oxygen permeation apparatus that consists of a donor chamber (holding oxygenated deionised water) and a receiver chamber (holding a larger volume of water that was deoxygenated by bubbling nitrogen gas) where the lens is placed in between. The oxygen concentration in the receiver chamber is measured over time and the data is fitted in a diffusion model to determine the oxygen permeability of the lens (Jung et al., 2013; Nasr et al., 2016).

Another important consideration in the development of BCLs is their surface wettability which is an important parameter that affects eye comfort, maintains a stable tear film, enhances the adhesion between the BCLs and the ocular surface and prevent the accumulation of proteins and lipid on the surface (Lasowski & Sheardown, 2016; C. Xu et al., 2016). Efforts to enhance the surface wettability of silicone hydrogel BCLs developed were not within the scope of this thesis. Surface treatment with hydrophilic monomers or incorporation of an internal wetting agent such as poly(ethylene oxide) (PEO) and polyvinyl pyrrolidone (PVP) (Kaczmarek et al., 2014) are usually performed in commercial silicone hydrogel contact lenses (Soluri et al., 2012). However, incorporating a hydrophilic wetting agent within the silicone hydrogel lenses might result in rapid drug release profiles, therefore surface treatment is recommended. **Plasma surface treatment can be used to oxidise the lens surface converting the surface organic silicone to a layer of inorganic silicates with high wettability** (Wagner, 2018) or to **deposit a thin layer of a hydrophilic polymer on the lens surface** (J.-S. Chen, Ting, Tsou, & Liu, 2018). Moreover, **surface treatment can be performed by means of surfactants** (Tran, Sung, Copley, & Radke, 2012) or **grafting a layer of a hydrophilic material such as HA** (Myrto Korogiannaki, Jones, & Sheardown, 2018). The surface wettability of the lens is determined by contact angle measurement between a droplet of water and the lens surface (L. Cheng et al., 2004). As for GelMA BCLs, prepared in chapters 4, 5 and 6, the hydrophilic nature of the hydrogel might be helpful in preventing protein and lipid adsorption. Furthermore, it was reported that the incorporation of immobilised HA resulted in a dramatic decrease in adsorption of tear proteins on contact lenses (Van Beek, Weeks, Jones, & Sheardown, 2008).

Transparency studies were not performed in this thesis since it is not a critical property for BCLs that are indicated in corneal injuries and post-surgery. The cornea at this stage is fragile and covering the eye for 1 week while the BCLs are in place is the best option. Moreover, the thickness of the prepared BCLs was 0.35 mm, which is thicker than the marketed BCLs of an average thickness of 0.07 mm. Therefore, results are hard to compare (Razmjoo et al., 2012).

Several hydrogel formulations have been successfully printed using an extrusion-based 3D-printer. According to the nature of the formulated hydrogel and its printing behaviour, the nozzle diameter, extrusion pressure and speed were chosen via manual

trial and error methods. It was evident that the concentration and type of the hybrid polymers inks affected the printing parameters and the printed structure due to the different rheological properties of each hybrid polymer mixture. Unfortunately, the rheological parameters of the formulated polymers in this thesis have not been assessed, however, it would be beneficial to determine the effect of the incorporated polymers on the viscosity and shear thinning properties of the formulated GelMA hydrogel polymer mixtures. The viscosity and shear stress of the hydrogel polymer solution at the printing temperature is determined via a rheometer that applies linearly increasing shear rate values on the hydrogel (Lim et al., 2016). It is also important to consider that printing fidelity increases with increasing the viscosity of the ink (Malda et al., 2013). Furthermore, the effect of the polymer composition on the shear-thinning properties of the ink can be determined via shear recovery experiments that determine the response of the material to the application and removal of shear strain in a 2 min interval. High-shear thinning properties of hydrogels is beneficial in extrusion-printing applications, where the material is viscous enough to be extruded in a continuous filament, viscosity drops within the printing needle and rapidly regains its viscosity after extrusion to resist deformation of the printed structure and allow layer-by-layer application for more complex constructs (Liliang Ouyang, Christopher B Highley, Christopher B Rodell, Wei Sun, & Jason A Burdick, 2016).

In chapters 5 and 6, HCEpC were successfully loaded into the GelMA hydrogel matrices to be used as therapeutic BCLs that could potentially be used for the treatment of moderate-severe corneal injuries. However, further studies are required to determine how the loaded cells will behave *in vivo*. This can be performed by inducing a burn on an animal ocular surface after applying an anaesthetic, fixing the cell-loaded BCL on the eye surface via suturing the upper and lower lids in the experimental group. Control groups should be included in the trial using non-medicated BCL or no lens at all. Eyes should be examined and photographed immediately after the treatment, after 3 days and 7 days. Images obtained at each time point should be compared to the original images of the burned eye before the start of the treatment protocols, which help assess their effectiveness (W. Xu et al., 2018). Another method of visualising and imaging the injured part of the cornea is by using a slit-lamp(Lai et al., 2010) or a fluorescent dye that sticks to the injured cornea and can be visualised under blue light (Ye et al., 2014).

In the proposed cell-loaded BCL, the cells should optimally detach from the BCL and reattach to the corneal surface of the injured eye, therefore testing how many days after culturing of the cells on the BCLs it should be applied on the injured eye must also be performed as part of the pre-clinical development process. It has been reported that autologous epithelial stem cells were successfully transplanted onto silicone hydrogel contact lenses and applied onto the injured cornea for 2 weeks to treat patients with LSCD (L. W. Jones et al., 2016). Furthermore, it would be also beneficial to determine whether or not the hydrophilic nature of HA will help maintain the moisture content of the BCL and the eye during the application time and prevent the eye from drying out. It is worth noting that some artificial tears eye drops contain HA for the treatment of dry eyes (Aragona et al., 2002; Fezza, 2018). Further studies incorporating both HA and collagen with GelMA hydrogel can obtain a better image of how those three hydrogels work together as a hydrogel hybrid material used to formulate BCLs for the treatment of corneal injuries.

7.5 Conclusion

In this thesis, solvent casting and 3D-printing techniques were employed to successfully develop corneal bandages for the treatment of corneal injuries. Depending on the type of loaded therapeutics, the BCL was designed to treat different stages of injuries. Mainly, DEX loaded BCL were developed to reduce inflammation and promote rapid corneal healing in mild-moderate corneal injuries, while the cell-loaded BCL was developed to promote corneal healing in moderate-severe corneal injuries where the cornea loses its ability to self-regenerate following the full or partial loss of the limbus. The use of drug-eluting BCLs will ensure the delivery of the loaded drug in a controlled manner with high patient compliance, and thus without fluctuation of the drug doses. This will result in improved clinical outcomes and fewer side effects due to the lower doses of drug delivered compared to the eye drops.

The importance of scar-free corneal healing increases with the increase in corneal surgeries such as cataract and refractive surgeries performed every day. Moreover, corneal scarring resulting from conditions and diseases affecting the cornea can lead to vision-impairing disabilities which severely impact on a patient's independence and quality of life (Bergwerk, 2011). The innovative, patient-friendly and cost-effective cell-

loaded BCL is a potential breakthrough in corneal wound healing therapy. The proposed corneal bandage will pave the way for a more customised approach to benefit people who require treatment for conditions resulting from blinding corneal eye pathology and everyday patients of corneal surgery to minimise current post-operative complications. The lenses can be customised to suit specific end-user needs since they can be tailor-designed and capable of carrying and slowly releasing various loaded therapeutics, thus improving patients' outcomes. This thesis is expected to have a significant impact on the development of corneal bandages and sets the scene for future opportunities towards optimising the treatment protocols for the treatment of corneal injuries.

References

- Abduo, J., Lyons, K., & Bennamoun, M. (2014). Trends in computer-aided manufacturing in prosthodontics: a review of the available streams. *International journal of dentistry*, 2014.
- Agban, Y., Lian, J., Prabakar, S., Seyfoddin, A., & Rupenthal, I. D. (2016). Nanoparticle cross-linked collagen shields for sustained delivery of pilocarpine hydrochloride. *International Journal of Pharmaceutics*, 501(1), 96-101.
- Agorogiannis, G. I., Alexaki, V.-I., Castana, O., & Kymionis, G. D. (2012). Topical application of autologous adipose-derived mesenchymal stem cells (MSCs) for persistent sterile corneal epithelial defect. *Graefe's Archive for Clinical and Experimental Ophthalmology*, 250(3), 455-457.
- Agrawal, V. B., & Tsai, R. J. F. (2003). Corneal epithelial wound healing [Review]. *Indian Journal of Ophthalmology*, 51(1), 5-15.
- Ali, S., Saik, J. E., Gould, D. J., Dickinson, M. E., & West, J. L. (2013). Immobilization of cell-adhesive laminin peptides in degradable PEGDA hydrogels influences endothelial cell tubulogenesis. *BioResearch open access*, 2(4), 241-249.
- Altay, Y., Tamer, S., Burcu, A., & Balta, Ö. (2016). Amniotic membrane transplantation in bacterial and herpetic stromal keratitis [Article]. *Turkish Journal of Medical Sciences*, 46(2), 457-462.
- Amescua, G., Atallah, M., Nikpoor, N., Galor, A., & Perez, V. L. (2014). Modified simple limbal epithelial transplantation using cryopreserved amniotic membrane for unilateral limbal stem cell deficiency [Article]. *American Journal of Ophthalmology*, 158(3), 469-475.
- Anderson, D. F., Prabhasawat, P., Alfonso, E., & Tseng, S. C. G. (2001). Amniotic membrane transplantation after the primary surgical management of band keratopathy [Article]. *Cornea*, 20(4), 354-361.
- Andrade-Vivero, P., Fernandez-Gabriel, E., Alvarez-Lorenzo, C., & Concheiro, A. (2007). Improving the loading and release of NSAIDs from pHEMA hydrogels by copolymerization with functionalized monomers. *Journal of Pharmaceutical Sciences*, 96(4), 802-813.
- Ang, J., & Efron, N. (1990). Corneal hypoxia and hypercapnia during contact lens wear. *Optometry and vision science: official publication of the American Academy of Optometry*, 67(7), 512-521.
- Aragona, P., Papa, V., Micali, A., Santocono, M., & Milazzo, G. (2002). Long term treatment with sodium hyaluronate-containing artificial tears reduces ocular surface damage in patients with dry eye. *British Journal of Ophthalmology*, 86(2), 181-184.

- Asari, A., Morita, M., Sekiguchi, T., Okamura, K., Horie, K., & Miyauchi, S. (1996). Hyaluronan, CD44 and fibronectin in rabbit corneal epithelial wound healing. *Japanese Journal of Ophthalmology*, 40(1), 18-25.
- Ashby, B., Garrett, Q., & Willcox, M. (2014). Corneal injuries and wound healing—review of processes and therapies. *Austin J Clin Ophthalmol*, 1, 1-25.
- Badawi, A. A., El-Laithy, H. M., El Qidra, R. K., El Mofty, H., & El Dally, M. (2008). Chitosan based nanocarriers for indomethacin ocular delivery [Article]. *Archives of Pharmacal Research*, 31(8), 1040-1049.
- Bansal, J., Kedige, S. D., & Anand, S. (2010). Hyaluronic acid: A promising mediator for periodontal regeneration. *Indian Journal of Dental Research*, 21(4), 575.
- Baradaran-Rafii, A., Aghayan, H. R., Arjmand, B., & Javadi, M. A. (2007). Amniotic membrane transplantation [Review]. *Journal of Ophthalmic and Vision Research*, 2(1), 58-75.
- Baradaran-Rafii, A., Biazar, E., & Heidari-Keshel, S. (2015). Cellular response of limbal stem cells on PHBV/gelatin nanofibrous scaffold for ocular epithelial regeneration. *International Journal of Polymeric Materials and Polymeric Biomaterials*, 64(17), 879-887.
- Barar, J., Asadi, M., Mortazavi-Tabatabaei, S. A., & Omid, Y. (2009). Ocular drug delivery; impact of in vitro cell culture models. *Journal of ophthalmic & vision research*, 4(4), 238.
- Becker, D. L., Phillips, A. R., Duft, B. J., Kim, Y., & Green, C. R. (2016). Translating connexin biology into therapeutics. *Seminars in Cell & Developmental Biology*, 50, 49-58.
- Behl, G., Iqbal, J., O'Reilly, N. J., McLoughlin, P., & Fitzhenry, L. (2016). Synthesis and Characterization of Poly(2-hydroxyethylmethacrylate) Contact Lenses Containing Chitosan Nanoparticles as an Ocular Delivery System for Dexamethasone Sodium Phosphate. *Pharmaceutical Research*, 33(7), 1638-1648.
- Bergwerk, K. (2011). Vision impairment. In *Neurodevelopmental disabilities* (pp. 277-296): Springer.
- Bernkop-Schnürch, A., & Dünnhaupt, S. (2012). Chitosan-based drug delivery systems. *European Journal of Pharmaceutics and Biopharmaceutics*, 81(3), 463-469.
- Bigi, A., Cojazzi, G., Panzavolta, S., Rubini, K., & Roveri, N. (2001). Mechanical and thermal properties of gelatin films at different degrees of glutaraldehyde crosslinking. *Biomaterials*, 22(8), 763-768.
- Browning, M. B., & Cosgriff-Hernandez, E. (2012). Development of a biostable replacement for PEGDA hydrogels. *Biomacromolecules*, 13(3), 779-786.
- Buanz, A. B., Saunders, M. H., Basit, A. W., & Gaisford, S. (2011). Preparation of personalized-dose salbutamol sulphate oral films with thermal ink-jet printing. *Pharmaceutical Research*, 28(10), 2386-2392.

- Bukhari, S. M. H., Khan, S., Rehanullah, M., & Ranjha, N. M. (2015). Synthesis and characterization of chemically cross-linked acrylic acid/gelatin hydrogels: effect of pH and composition on swelling and drug release. *International Journal of Polymer Science*, 2015.
- Camci-Unal, G., Cuttica, D., Annabi, N., Demarchi, D., & Khademhosseini, A. (2013). Synthesis and characterization of hybrid hyaluronic acid-gelatin hydrogels. *Biomacromolecules*, 14(4), 1085-1092.
- Canabrava, S., Diniz, A., Schor, P., Fagundes, D. F., Lopes, A., & Batista, W. D. (2015). Production of an intraocular device using 3D printing: An innovative technology for ophthalmology [Letter]. *Arquivos Brasileiros de Oftalmologia*, 78(6), 393-394.
- Carvalho, I. M., Marques, C. S., Oliveira, R. S., Coelho, P. B., Costa, P. C., & Ferreira, D. C. (2015). Sustained drug release by contact lenses for glaucoma treatment-A review. *Journal of Controlled Release*, 202, 76-82.
- Çaykara, T., & Turan, E. (2006). Effect of the amount and type of the crosslinker on the swelling behavior of temperature-sensitive poly (N-tert-butylacrylamide-co-acrylamide) hydrogels. *Colloid and Polymer Science*, 284(9), 1038-1048.
- Celikkin, N., Costantini, M., Rinoldi, C., Lin, F.-H., & Świążkowski, W. (2018). 3D bioprinted GelMA bioink with high structural fidelity for skeletal muscle regeneration: Division of Materials Design.
- Chandler, E. M., Berglund, C. M., Lee, J. S., Polacheck, W. J., Gleghorn, J. P., Kirby, B. J., & Fischbach, C. (2011). Stiffness of photocrosslinked RGD-alginate gels regulates adipose progenitor cell behavior. *Biotechnology and Bioengineering*, 108(7), 1683-1692.
- Cheah, C. M., Leong, K. F., Chua, C. K., Low, K. H., & Quek, H. S. (2002). Characterization of microfeatures in selective laser sintered drug delivery devices [Article]. *Proceedings of the Institution of Mechanical Engineers, Part H: Journal of Engineering in Medicine*, 216(6), 369-383.
- Chen, H. C., Tan, H. Y., Hsiao, C. H., Huang, S. C. M., Lin, K. K., & Ma, D. H. K. (2006). Amniotic membrane transplantation for persistent corneal ulcers and perforations in acute fungal keratitis [Article]. *Cornea*, 25(5), 564-572.
- Chen, J.-S., Ting, Y.-S., Tsou, H.-M., & Liu, T.-Y. (2018). Highly hydrophilic and antibiofouling surface of zwitterionic polymer immobilized on polydimethylsiloxane by initiator-free atmospheric plasma-induced polymerization. *Surface and Coatings Technology*, 344, 621-625.
- Cheng, L., Muller, S. J., & Radke, C. J. (2004). Wettability of silicone-hydrogel contact lenses in the presence of tear-film components. *Current Eye Research*, 28(2), 93-108.
- Cheng, Y.-H., Tsai, T.-H., Jhan, Y.-Y., Chiu, A. W.-h., Tsai, K.-L., Chien, C.-S., . . . Liu, C. J.-I. (2016). Thermosensitive chitosan-based hydrogel as a topical ocular drug delivery system of latanoprost for glaucoma treatment. *Carbohydr Polym*, 144, 390-399.

- Cherry, P. (1996). The treatment of pain following excimer laser photorefractive keratectomy: additive effect of local anesthetic drops, topical diclofenac, and bandage soft contact. *Ophthalmic Surgery and Lasers*, 27(5 Suppl), S477-480.
- Chiang, Z.-C., Yu, S.-H., Chao, A.-C., & Dong, G.-C. (2012). Preparation and characterization of dexamethasone-immobilized chitosan scaffold. *Journal of Bioscience and Bioengineering*, 113(5), 654-660.
- Childs, A., Li, H., Lewittes, D. M., Dong, B., Liu, W., Shu, X., . . . Zhang, H. F. (2016). Fabricating customized hydrogel contact lens. *Scientific Reports*, 6, 34905.
- Cho, K., Chung, T., Kim, B., Kim, M., Lee, J., Wee, W., & Cho, C. (2003). Release of ciprofloxacin from poloxamer-graft-hyaluronic acid hydrogels in vitro. *International Journal of Pharmaceutics*, 260(1), 83-91.
- Ciolino, J. B., Dohlman, C. H., & Kohane, D. S. (2009). Contact lenses for drug delivery. *Seminars in Ophthalmology*, 24(3), 156-160.
- Ciolino, J. B., Hoare, T. R., Iwata, N. G., Behlau, I., Dohlman, C. H., Langer, R., & Kohane, D. S. (2009). A drug-eluting contact lens. *Investigative Ophthalmology and Visual Science*, 50(7), 3346-3352.
- Ciolino, J. B., Hudson, S. P., Mobbs, A. N., Hoare, T. R., Iwata, N. G., Fink, G. R., & Kohane, D. S. (2011). A prototype antifungal contact lens. *Investigative Ophthalmology and Visual Science*, 52(9), 6286-6291.
- Colin, J., Malet, F., Chastel, C., & Richard, M. C. (1991). Use of collagen shields in the treatment of herpetic keratitis [Article]. *Current Eye Research*, 10(s1), 189-191.
- Colosi, C., Costantini, M., Barbetta, A., & Dentini, M. (2017). Microfluidic bioprinting of heterogeneous 3d tissue constructs. In *3D Cell Culture* (pp. 369-380): Springer.
- Costa, V. P., Harris, A., Stefansson, E., Flammer, J., Krieglstein, G. K., Orzalesi, N., Heijl, A., Renard, JP., & Serra, L. M. (2003). The effects of antiglaucoma and systemic medications on ocular blood flow. *Progress in Retinal and Eye Research*, 22(6), 769-805.
- Cotsarelis, G., Cheng, S.-Z., Dong, G., Sun, T.-T., & Lavker, R. M. (1989). Existence of slow-cycling limbal epithelial basal cells that can be preferentially stimulated to proliferate: implications on epithelial stem cells. *Cell*, 57(2), 201-209.
- Cousen, P., Cackett, P., Bennett, H., Swa, K., & Dhillon, B. (2007). Tear production and corneal sensitivity in diabetes. *Journal of Diabetes and Its Complications*, 21(6), 371-373.
- Cui, R., Lu, Q., Teng, Y., Li, K., & Li, N. (2017). Chitosan promoted the Corneal epithelial wound healing via activation of ERK pathway. *Current Eye Research*, 42(1), 21-27.
- Ćuruvija-Opačić, K. (2007). Soft Contact Lenses and Long Term Corneal Hypoxia: What is Changing with Silicone Hydrogel Lens? *Acta Clinica Croatica*, 46(1-Supplement 1), 17-20.

- Dai, T., Tanaka, M., Huang, Y. Y., & Hamblin, M. R. (2011). Chitosan preparations for wounds and burns: Antimicrobial and wound-healing effects [Review]. *Expert Review of Anti-Infective Therapy*, 9(7), 857-879.
- Dartt, D. A. (2010). *Encyclopedia of the Eye (Vol. 1)*: Academic Press.
- Das, S., & Seitz, B. (2008). Recurrent Corneal Erosion Syndrome. *Survey of Ophthalmology*, 53(1), 3-15.
- de la Mata, A., Nieto-Miguel, T., López-Paniagua, M., Galindo, S., Aguilar, M. R., García-Fernández, L., Gonzalo, S., Vázquez, B., San Román, J., & Corrales, R. M. (2013). Chitosan–gelatin biopolymers as carrier substrata for limbal epithelial stem cells. *Journal of Materials Science: Materials in Medicine*, 24(12), 2819-2829.
- Dexamethasone, CID=5743. Retrieved Nov. 11, 2019, from <https://pubchem.ncbi.nlm.nih.gov/compound/Dexamethasone>.
- Di Girolamo, N., Bosch, M., Zamora, K., Coroneo, M. T., Wakefield, D., & Watson, S. L. (2009). A contact lens-based technique for expansion and transplantation of autologous epithelial progenitors for ocular surface reconstruction. *Transplantation*, 87(10), 1571-1578.
- Dixon, P., Shafor, C., Gause, S., Hsu, K. H., Powell, K. C., & Chauhan, A. (2015). Therapeutic contact lenses: A patent review [Review]. *Expert Opinion on Therapeutic Patents*, 25(10), 1117-1129.
- dos Santos, J.-F. R., Alvarez-Lorenzo, C., Silva, M., Balsa, L., Couceiro, J., Torres-Labandeira, J.-J., & Concheiro, A. (2009). Soft contact lenses functionalized with pendant cyclodextrins for controlled drug delivery. *Biomaterials*, 30(7), 1348-1355.
- dos Santos, J.-F. R., Couceiro, R., Concheiro, A., Torres-Labandeira, J.-J., & Alvarez-Lorenzo, C. (2008). Poly (hydroxyethyl methacrylate-co-methacrylated- β -cyclodextrin) hydrogels: synthesis, cytocompatibility, mechanical properties and drug loading/release properties. *Acta Biomaterialia*, 4(3), 745-755.
- Drury, J. L., & Mooney, D. J. (2003). Hydrogels for tissue engineering: scaffold design variables and applications. *Biomaterials*, 24(24), 4337-4351.
- Dua, H., & Forrester, J. (1987). Clinical patterns of corneal epithelial wound healing. *American Journal of Ophthalmology*, 104(5), 481-489.
- Dua, H. S., Gomes, J. A. P., & Singh, A. (1994). Corneal epithelial wound healing [Review]. *British Journal of Ophthalmology*, 78(5), 401-408. doi:10.1136/bjo.78.5.401
- Dupps Jr, W. J., & Wilson, S. E. (2006). Biomechanics and wound healing in the cornea [Review]. *Experimental Eye Research*, 83(4), 709-720.
- Eke, T., Morrison, D. A., & Austin, D. J. (1999). Recurrent symptoms following traumatic corneal abrasion: prevalence, severity, and the effect of a simple regimen of prophylaxis. *Eye*, 13, 345-347.

- El-Feky, G. S., Zayed, G. M., Elshaier, Y. A., & Alsharif, F. M. (2018). Chitosan-gelatin hydrogel crosslinked with oxidized sucrose for the ocular delivery of timolol maleate. *Journal of Pharmaceutical Sciences*, 107(12), 3098-3104.
- El-Harazi, S. M., & Feldman, R. M. (2001). Control of intra-ocular inflammation associated with cataract surgery. *Current Opinion in Ophthalmology*, 12(1), 4-8.
- ElShaer, A., Mustafa, S., Kasar, M., Thapa, S., Ghatara, B., & Alany, R. G. (2016). Nanoparticle-laden contact lens for controlled ocular delivery of prednisolone: formulation optimization using statistical experimental design. *Pharmaceutics*, 8(2), 14.
- Eslani, M., Baradaran-Rafii, A., Movahedan, A., & Djalilian, A. R. (2014). The ocular surface chemical burns [Review]. *Journal of ophthalmology*, 2014.
- Fairbanks, B. D., Schwartz, M. P., Bowman, C. N., & Anseth, K. S. (2009). Photoinitiated polymerization of PEG-diacrylate with lithium phenyl-2, 4, 6-trimethylbenzoylphosphinate: polymerization rate and cytocompatibility. *Biomaterials*, 30(35), 6702-6707.
- Farkouh, A., Frigo, P., & Czejka, M. (2016). Systemic side effects of eye drops: a pharmacokinetic perspective. *Clinical Ophthalmology (Auckland, NZ)*, 10, 2433.
- Feng, Y., Borrelli, M., Reichl, S., Schrader, S., & Geerling, G. (2014). Review of alternative carrier materials for ocular surface reconstruction [Review]. *Current Eye Research*, 39(6), 541-552.
- Fernandes, M., Sridhar, M. S., Sangwan, V. S., & Rao, G. N. (2005). Amniotic membrane transplantation for ocular surface reconstruction. *Cornea*, 24(6), 643-653.
- Fezza, J. P. (2018). Cross-linked hyaluronic acid gel occlusive device for the treatment of dry eye syndrome. *Clinical Ophthalmology (Auckland, NZ)*, 12, 2277.
- Filipe, H. P., Henriques, J., Reis, P., Silva, P. C., Quadrado, M. J., & Serro, A. P. (2016). Contact lenses as drug controlled release systems: a narrative review. *Revista Brasileira de Oftalmologia*, 75(3), 241-247.
- Fitzgerald, S. (2015). FDA Approves First 3D-Printed Epilepsy Drug Experts Assess the Benefits and Caveats. *Neurology Today*, 15(18), 26-27.
- Florence, A. T. (2010). *An introduction to clinical pharmaceutics*: Pharmaceutical Press.
- Franklin, A. (2004). Stiffness and elasticity in contact lens materials. *OPTICIAN-SUTTON*, 27-35.
- Fu, Y., Xu, K., Zheng, X., Giacomini, A. J., Mix, A. W., & Kao, W. J. (2012). 3D cell entrapment in crosslinked thiolated gelatin-poly (ethylene glycol) diacrylate hydrogels. *Biomaterials*, 33(1), 48-58.
- Gao, Y., Hou, M., Yang, R., Zhang, L., Xu, Z., Kang, Y., & Xue, P. (2019). Therapeutics transdermal delivery through dissolvable gelatin/sucrose film coated on PEGDA

- microneedle array with improved skin permeability. *Journal of Materials Chemistry B*.
- Gaudio, P. (2004). A review of evidence guiding the use of corticosteroids in the treatment of intraocular inflammation. *Ocular Immunology and Inflammation*, 12(3), 169-192.
- Gerecht, S., Burdick, J. A., Ferreira, L. S., Townsend, S. A., Langer, R., & Vunjak-Novakovic, G. (2007). Hyaluronic acid hydrogel for controlled self-renewal and differentiation of human embryonic stem cells. *Proceedings of the National Academy of Sciences*, 104(27), 11298-11303.
- Gheorghe, A., Pop, M., Mrini, F., Barac, R., & Vargau, I. (2016). Ocular surface reconstruction in limbal stem cell deficiency [Review]. *Romanian journal of ophthalmology*, 60(1), 2-5.
- Gicquel, J. J., Bejjani, R. A., Ellies, P., Mercié, M., & Dighiero, P. (2007). Amniotic membrane transplantation in severe bacterial keratitis [Article]. *Cornea*, 26(1), 27-33.
- Gilhotra, R., & Mishra, D. (2008). Alginate-chitosan film for ocular drug delivery: effect of surface cross-linking on film properties and characterization. *Die Pharmazie-An International Journal of Pharmaceutical Sciences*, 63(8), 576-579.
- Gomes, J., Amankwah, R., Powell-Richards, A., & Dua, H. (2004). Sodium hyaluronate (hyaluronic acid) promotes migration of human corneal epithelial cells in vitro. *British Journal of Ophthalmology*, 88(6), 821-825.
- Gonzalez-Meijome, J. M., Gonzalez-Perez, J., Fernandes, P. R. B., Lopes-Ferreira, D. P., Molla, S., & Compan, V. (2014). Silicone Hydrogels Materials for Contact Lens Applications (WOS:000351707400020). Retrieved from <Go to ISI>://WOS:000351707400020
- Greenwald, Y., & Kleinmann, G. (2008). Use of collagen shields for ocular-surface drug delivery [Review]. *Expert review of ophthalmology*, 3(6), 627-633.
- Guidi, G., Hughes, T. C., Whinton, M., Brook, M. A., & Sheardown, H. (2014). The effect of silicone hydrogel contact lens composition on dexamethasone release. *Journal of Biomaterials Applications*, 29(2), 222-233.
- Guo, K., & Chu, C. (2005). Synthesis and characterization of novel biodegradable unsaturated poly (ester amide)/poly (ethylene glycol) diacrylate hydrogels. *Journal of Polymer Science Part A: Polymer Chemistry*, 43(17), 3932-3944.
- Hao, Y., Ma, D. H. K., Hwang, D. G., Kim, W. S., & Zhang, F. (2000). Identification of antiangiogenic and antiinflammatory proteins in human amniotic membrane [Article]. *Cornea*, 19(3), 348-352.
- Hathout, R. M., & Omran, M. K. (2016). Gelatin-based particulate systems in ocular drug delivery. *Pharmaceutical Development and Technology*, 21(3), 379-386.

- Hiraoka, M., Amano, S., Oshika, T., Kato, S., & Hori, S. (2001). Factors contributing to corneal complications after vitrectomy in diabetic patients. *Japanese Journal of Ophthalmology*, 45(5), 492-495.
- Hoare, T. R., & Kohane, D. S. (2008). Hydrogels in drug delivery: Progress and challenges. *Polymer*, 49(8), 1993-2007.
- Hoch, E., Schuh, C., Hirth, T., Tovar, G. E., & Borchers, K. (2012). Stiff gelatin hydrogels can be photo-chemically synthesized from low viscous gelatin solutions using molecularly functionalized gelatin with a high degree of methacrylation. *Journal of Materials Science: Materials in Medicine*, 23(11), 2607-2617.
- Hockaday, L. A., Kang, K. H., Colangelo, N. W., Cheung, P. Y. C., Duan, B., Malone, E., Wu, J., Girardi, L. N., Bonassar, L. J., Lipson, H., Chu, C. C., & Butcher, J. T. (2012). Rapid 3D printing of anatomically accurate and mechanically heterogeneous aortic valve hydrogel scaffolds [Article]. *Biofabrication*, 4(3).
- Hori, K., Sotozono, C., Hamuro, J., Yamasaki, K., Kimura, Y., Ozeki, M., . . . Kinoshita, S. (2007). Controlled-release of epidermal growth factor from cationized gelatin hydrogel enhances corneal epithelial wound healing. *Journal of Controlled Release*, 118(2), 169-176.
- Horst, C. R., Brodland, B., Jones, L. W., & Brodland, G. W. (2012). Measuring the modulus of silicone hydrogel contact lenses. *Optometry and Vision Science*, 89(10), 1468-1476.
- Hsu, C. C., Peng, C. H., Hung, K. H., Lee, Y. Y., Lin, T. C., Jang, S. F., . . . Chang, Y. L. (2015). Stem cell therapy for corneal regeneration medicine and contemporary nanomedicine for corneal disorders [Review]. *Cell Transplantation*, 24(10), 1915-1930.
- Hsu, K.-H., Fentzke, R. C., & Chauhan, A. (2013). Feasibility of corneal drug delivery of cysteamine using vitamin E modified silicone hydrogel contact lenses. *European Journal of Pharmaceutics and Biopharmaceutics*, 85(3), 531-540.
- Hsu, K.-H., Gause, S., & Chauhan, A. (2014). Review of ophthalmic drug delivery by contact lenses. *Journal of Drug Delivery Science and Technology*, 24(2), 123-135.
- Hsu, K. H., Gause, S., & Chauhan, A. (2014). Review of ophthalmic drug delivery by contact lenses [Review]. *Journal of Drug Delivery Science and Technology*, 24(2), 123-135.
- Hu, X., Hao, L., Wang, H., Yang, X., Zhang, G., Wang, G., & Zhang, X. (2011). Hydrogel contact lens for extended delivery of ophthalmic drugs. *International Journal of Polymer Science*, 2011.
- Huang, A., & Tseng, S. (1991). Corneal epithelial wound healing in the absence of limbal epithelium. *Investigative Ophthalmology and Visual Science*, 32(1), 96-105.
- Huang, W. B., & Zhang, X. L. (2014). 3D printing: Print the future of ophthalmology [Article]. *Investigative Ophthalmology and Visual Science*, 55(8), 5380-5381.

- Hui, A., Sheardown, H., & Jones, L. (2012). Acetic and Acrylic Acid Molecular Imprinted Model Silicone Hydrogel Materials for Ciprofloxacin-HCl Delivery. *Materials*, 5(1), 85-107.
- Hutson, C. B., Nichol, J. W., Aubin, H., Bae, H., Yamanlar, S., Al-Haque, S., Koshy, S. T., & Khademhosseini, A. (2011). Synthesis and characterization of tunable poly (ethylene glycol): gelatin methacrylate composite hydrogels. *Tissue Engineering Part A*, 17(13-14), 1713-1723.
- Im, S. K., Lee, K. H., & Yoon, K. C. (2010). Combined ethylenediaminetetraacetic acid chelation, phototherapeutic keratectomy and amniotic membrane transplantation for treatment of band keratopathy [Article]. *Korean journal of ophthalmology : KJO*, 24(2), 73-77.
- Inoue, K., Kato, S., Ohara, C., Numaga, J., Amano, S., & Oshika, T. (2001). Ocular and systemic factors relevant to diabetic keratoepitheliopathy. *Cornea*, 20(8), 798-801.
- Inoue, M., & Katakami, C. (1993). The effect of hyaluronic acid on corneal epithelial cell proliferation. *Investigative Ophthalmology and Visual Science*, 34(7), 2313-2315.
- Institute, N. E. (2019, August, 2019). Eye conditions and diseases. Retrieved November 11, 2019, from <https://www.nei.nih.gov/learn-about-eye-health/eye-conditions-and-diseases/corneal-conditions>
- Jabs, D. A., Mudun, A., Dunn, J., & Marsh, M. J. (2000). Episcleritis and scleritis: clinical features and treatment results. *American Journal of Ophthalmology*, 130(4), 469-476.
- Jain, D., Carvalho, E., Banthia, A. K., & Banerjee, R. (2011). Development of polyvinyl alcohol–gelatin membranes for antibiotic delivery in the eye. *Drug Development and Industrial Pharmacy*, 37(2), 167-177.
- Jayakumar, R., Prabakaran, M., Kumar, P. S., Nair, S., & Tamura, H. (2011). Biomaterials based on chitin and chitosan in wound dressing applications. *Biotechnology Advances*, 29(3), 322-337.
- Jhanji, V., Young, A. L., Mehta, J. S., Sharma, N., Agarwal, T., & Vajpayee, R. B. (2011). Management of Corneal Perforation [Review]. *Survey of Ophthalmology*, 56(6), 522-538.
- Jonathan, G., & Karim, A. (2016). 3D printing in pharmaceuticals: A new tool for designing customized drug delivery systems [Review]. *International Journal of Pharmaceutics*, 499(1-2), 376-394.
- Jones, L., & Powell, C. H. (2013). Uptake and release phenomena in contact lens care by silicone hydrogel lenses [Conference Paper]. *Eye and Contact Lens*, 39(1), 29-36.
- Jones, L. W., Chauhan, A., Di Girolamo, N., Sheedy, J., & Smith III, E. (2016). Expert views on innovative future uses for contact lenses. *Optometry and Vision Science*, 93(4), 328-335.

- Jones, R. T. (2004). Gelatin: Manufacture and physico-chemical properties. *Pharmaceutical capsules*, 23-60.
- Jung, H. J., Abou-Jaoude, M., Carbia, B. E., Plummer, C., & Chauhan, A. (2013). Glaucoma therapy by extended release of timolol from nanoparticle loaded silicone-hydrogel contact lenses. *Journal of Controlled Release*, 165(1), 82-89.
- Jung, H. J., & Chauhan, A. (2012). Temperature sensitive contact lenses for triggered ophthalmic drug delivery. *Biomaterials*, 33(7), 2289-2300.
- Kaczmarek, J. C., Tieppo, A., White, C. J., & Byrne, M. E. (2014). Adjusting biomaterial composition to achieve controlled multiple-day release of dexamethasone from an extended-wear silicone hydrogel contact lens. *Journal of Biomaterials Science, Polymer Edition*, 25(1), 88-100.
- Kadmiel, M., Janoshazi, A., Xu, X., & Cidlowski, J. A. (2016). Glucocorticoid action in human corneal epithelial cells establishes roles for corticosteroids in wound healing and barrier function of the eye. *Experimental Eye Research*, 152, 10-33.
- Kalkandelen, C., Ozbek, B., Ergul, N., Akyol, S., Moukbil, Y., Oktar, F., . . . Gunduz, O. (2017). Effect of temperature, viscosity and surface tension on gelatine structures produced by modified 3D printer. IOP Publishing. Symposium conducted at the meeting of the IOP Conference Series: Materials Science and Engineering.
- Kapoor, Y., & Chauhan, A. (2008). Drug and surfactant transport in Cyclosporine A and Brij 98 laden p-HEMA hydrogels. *Journal of Colloid and Interface Science*, 322(2), 624-633.
- Katagiri, Y., Brew, S. A., & Ingham, K. C. (2003). All six modules of the gelatin-binding domain of fibronectin are required for full affinity. *Journal of Biological Chemistry*, 278(14), 11897-11902.
- Kawaguchi, Y., & Oishi, T. (2004). Synthesis and properties of thermoplastic expandable microspheres: The relation between crosslinking density and expandable property. *Journal of Applied Polymer Science*, 93(2), 505-512.
- Khademhosseini, A., Langer, R., Borenstein, J., & Vacanti, J. P. (2006). Microscale technologies for tissue engineering and biology. *Proceedings of the National Academy of Sciences*, 103(8), 2480-2487.
- Khairallah, M., Kahloun, R., Bourne, R., Limburg, H., Flaxman, S. R., Jonas, J. B., Keeffe, J., Leasher, J., Naidoo, K., & Pesudovs, K. (2015). Number of people blind or visually impaired by cataract worldwide and in world regions, 1990 to 2010. *Investigative Ophthalmology and Visual Science*, 56(11), 6762-6769.
- Kim, J., Conway, A., & Chauhan, A. (2008). Extended delivery of ophthalmic drugs by silicone hydrogel contact lenses. *Biomaterials*, 29(14), 2259-2269.
- Kim, J. S., Kim, J. C., Hahn, T. W., & Park, W. C. (2001). Amniotic membrane transplantation in infectious corneal ulcer [Article]. *Cornea*, 20(7), 720-726.

- Klausner, E. A., Peer, D., Chapman, R. L., Multack, R. F., & Andurkar, S. V. (2007). Corneal gene therapy [Review]. *Journal of Controlled Release*, 124(3), 107-133.
- Kogan, G., Šoltés, L., Stern, R., & Gemeiner, P. (2007). Hyaluronic acid: a natural biopolymer with a broad range of biomedical and industrial applications. *Biotechnology Letters*, 29(1), 17-25.
- Korogiannaki, M., Guidi, G., Jones, L., & Sheardown, H. (2015). Timolol maleate release from hyaluronic acid-containing model silicone hydrogel contact lens materials. *Journal of Biomaterials Applications*, 30(3), 361-376.
- Korogiannaki, M., Jones, L., & Sheardown, H. (2018). Impact of a hyaluronic acid-grafted layer on the surface properties of model silicone hydrogel contact lenses. *Langmuir*, 35(4), 950-961.
- Köse, G. T., Korkusuz, F., Özkul, A., Soysal, Y., Özdemir, T., Yildiz, C., & Hasirci, V. (2005). Tissue engineered cartilage on collagen and PHBV matrices. *Biomaterials*, 26(25), 5187-5197.
- Krumova, M., Lopez, D., Benavente, R., Mijangos, C., & Perena, J. (2000). Effect of crosslinking on the mechanical and thermal properties of poly (vinyl alcohol). *Polymer*, 41(26), 9265-9272.
- Kuo, C. Y., Guo, T., Cabrera-Luque, J., Arumugasaamy, N., Bracaglia, L., Garcia-Vivas, A., . . . Kim, P. (2018). Placental basement membrane proteins are required for effective cytotrophoblast invasion in a three-dimensional bioprinted placenta model. *Journal of Biomedical Materials Research Part A*, 106(6), 1476-1487.
- Kurpakus-Wheater, M., Kernacki, K. A., & Hazlett, L. D. (2001). Maintaining corneal integrity how the "window" stays clear [Review]. *Progress in Histochemistry and Cytochemistry*, 36(3), 185-259.
- Kusuma, V. A., Gunawan, G., Smith, Z. P., & Freeman, B. D. (2010). Gas permeability of cross-linked poly (ethylene-oxide) based on poly (ethylene glycol) dimethacrylate and a miscible siloxane co-monomer. *Polymer*, 51(24), 5734-5743.
- Lai, J.-Y. (2013a). Corneal stromal cell growth on gelatin/chondroitin sulfate scaffolds modified at different NHS/EDC molar ratios. *International Journal of Molecular Sciences*, 14(1), 2036-2055.
- Lai, J.-Y. (2013b). Influence of solvent composition on the performance of carbodiimide cross-linked gelatin carriers for retinal sheet delivery. *Journal of Materials Science: Materials in Medicine*, 24(9), 2201-2210.
- Lai, J.-Y., & Li, Y.-T. (2010a). Evaluation of cross-linked gelatin membranes as delivery carriers for retinal sheets. *Materials Science and Engineering: C*, 30(5), 677-685.
- Lai, J.-Y., & Li, Y.-T. (2010b). Functional assessment of cross-linked porous gelatin hydrogels for bioengineered cell sheet carriers. *Biomacromolecules*, 11(5), 1387-1397.

- Lai, J.-Y., Li, Y.-T., Cho, C.-H., & Yu, T.-C. (2012). Nanoscale modification of porous gelatin scaffolds with chondroitin sulfate for corneal stromal tissue engineering. *International journal of nanomedicine*, 7, 1101.
- Lai, J.-Y., Lu, P.-L., Chen, K.-H., Tabata, Y., & Hsiue, G.-H. (2006). Effect of charge and molecular weight on the functionality of gelatin carriers for corneal endothelial cell therapy. *Biomacromolecules*, 7(6), 1836-1844.
- Lai, J.-Y., Ma, D. H.-K., Cheng, H.-Y., Sun, C.-C., Huang, S.-J., Li, Y.-T., & Hsiue, G.-H. (2010). Ocular biocompatibility of carbodiimide cross-linked hyaluronic acid hydrogels for cell sheet delivery carriers. *Journal of Biomaterials Science, Polymer Edition*, 21(3), 359-376.
- Lai, J.-Y., Ma, D. H.-K., Lai, M.-H., Li, Y.-T., Chang, R.-J., & Chen, L.-M. (2013). Characterization of cross-linked porous gelatin carriers and their interaction with corneal endothelium: biopolymer concentration effect. *PloS One*, 8(1), e54058.
- Lasowski, F., & Sheardown, H. (2016). Atropine and Roscovitine Release from Model Silicone Hydrogels. *Optometry and Vision Science*, 93(4), 404-411.
- Latinovic, O., Hough, L. A., & Ou-Yang, H. D. (2010). Structural and micromechanical characterization of type I collagen gels. *Journal of Biomechanics*, 43(3), 500-505.
- Lee, B., Lum, N., Seow, L., Lim, P., & Tan, L. (2016). Synthesis and characterization of types a and b gelatin methacryloyl for bioink applications. *Materials*, 9(10), 797.
- Lee, C. H., Singla, A., & Lee, Y. (2001). Biomedical applications of collagen. *International Journal of Pharmaceutics*, 221(1), 1-22.
- Li, C.-C., & Chauhan, A. (2006). Modeling ophthalmic drug delivery by soaked contact lenses. *Industrial & Engineering Chemistry Research*, 45(10), 3718-3734.
- Li, X., Chen, S., Li, J., Wang, X., Zhang, J., Kawazoe, N., & Chen, G. (2016). 3D culture of chondrocytes in gelatin hydrogels with different stiffness. *Polymers*, 8(8), 269.
- Lim, K. S., Schon, B. S., Mekhileri, N. V., Brown, G. C., Chia, C. M., Prabakar, S., Hooper, G. J., & Woodfield, T. B. (2016). New visible-light photoinitiating system for improved print fidelity in gelatin-based bioinks. *ACS biomaterials science & engineering*, 2(10), 1752-1762.
- Lindstrom, R. (2015). Thoughts on Cataract Surgery: 2015. Review of Ophthalmology. Web.(9 Mar 2015). http://www.reviewofophthalmology.com/content/t/surgical_education/c/53422.
- Liu, C., Xia, Z., Han, Z., Hulley, P., Triffitt, J., & Czernuszka, J. (2008). Novel 3D collagen scaffolds fabricated by indirect printing technique for tissue engineering. *Journal of Biomedical Materials Research Part B: Applied Biomaterials: An Official Journal of The Society for Biomaterials, The Japanese Society for Biomaterials, and The Australian Society for Biomaterials and the Korean Society for Biomaterials*, 85(2), 519-528.

- Liu, J., Li, L., Suo, H., Yan, M., Yin, J., & Fu, J. (2019). 3D printing of biomimetic multi-layered GelMA/nHA scaffold for osteochondral defect repair. *Materials & Design*, 171, 107708.
- Liu, X., Gu, Y.-s., & Xu, Y.-s. (2008). Changes of tear film and tear secretion after phacoemulsification in diabetic patients. *Journal of Zhejiang University-Science B*, 9(4), 324-328.
- Liu, Y., & Chan-Park, M. B. (2010). A biomimetic hydrogel based on methacrylated dextran-graft-lysine and gelatin for 3D smooth muscle cell culture. *Biomaterials*, 31(6), 1158-1170.
- Liu, Y., Ren, L., & Wang, Y. (2013). Crosslinked collagen–gelatin–hyaluronic acid biomimetic film for cornea tissue engineering applications. *Materials Science and Engineering: C*, 33(1), 196-201.
- Ljubimov, A. V., & Saghizadeh, M. (2015). Progress in corneal wound healing [Review]. *Progress in Retinal and Eye Research*, 49, 17-45.
- Loebel, C., Rodell, C. B., Chen, M. H., & Burdick, J. A. (2017). Shear-thinning and self-healing hydrogels as injectable therapeutics and for 3D-printing. *Nature Protocols*, 12(8), 1521.
- Long, J., Gholizadeh, H., Lu, J., Bunt, C., & Seyfoddin, A. (2016). Review: Application of fused deposition modelling (FDM) method of 3D printing in drug delivery. *Current Pharmaceutical Design*.
- Long, J., Nand, A. V., Bunt, C., & Seyfoddin, A. (2019). Controlled release of dexamethasone from poly (vinyl alcohol) hydrogel. *Pharmaceutical Development and Technology*, 1-10.
- Lu, P.-L., Lai, J.-Y., Ma, D. H.-K., & Hsiue, G.-H. (2008). Carbodiimide cross-linked hyaluronic acid hydrogels as cell sheet delivery vehicles: characterization and interaction with corneal endothelial cells. *Journal of Biomaterials Science, Polymer Edition*, 19(1), 1-18.
- Lupeanu, M.-E., Rennie, A. E., Rosu, M.-M., & Moagar-Poladian, G. (2014). Research strategy on developing additive manufactured bespoke ophthalmic instruments assisted by an online integrated platform. *UPB Scientific Bulletin, Series D: Mechanical Engineering*, 76(2), 143-162.
- Maharajan, V. S., Shanmuganathan, V., Currie, A., Hopkinson, A., Powell-Richards, A., & Dua, H. S. (2007). Amniotic membrane transplantation for ocular surface reconstruction: Indications and outcomes [Article]. *Clinical and Experimental Ophthalmology*, 35(2), 140-147.
- Mahor, A., Prajapati, S. K., Verma, A., Gupta, R., Iyer, A. K., & Kesharwani, P. (2016). Moxifloxacin loaded gelatin nanoparticles for ocular delivery: Formulation and in-vitro, in-vivo evaluation. *Journal of Colloid and Interface Science*, 483, 132-138.

- Malda, J., Visser, J., Melchels, F. P., Jüngst, T., Hennink, W. E., Dhert, W. J., Groll, J., & Hutmacher, D. W. (2013). 25th anniversary article: engineering hydrogels for biofabrication. *Advanced materials*, 25(36), 5011-5028.
- Malhotra, C., & Jain, A. K. (2014). Human amniotic membrane transplantation: different modalities of its use in ophthalmology. *World journal of transplantation*, 4(2), 111.
- Mau, R., Nazir, J., John, S., & Seitz, H. (2019). Preliminary Study on 3D printing of PEGDA Hydrogels for Frontal Sinus Implants using Digital Light Processing (DLP). *Current Directions in Biomedical Engineering*, 5(1), 249-252.
- Maulvi, F. A., Soni, T. G., & Shah, D. O. (2015). Extended release of hyaluronic acid from hydrogel contact lenses for dry eye syndrome. *Journal of Biomaterials Science, Polymer Edition*, 26(15), 1035-1050.
- Maulvi, F. A., Soni, T. G., & Shah, D. O. (2016). A review on therapeutic contact lenses for ocular drug delivery. *Drug Delivery*, 23(8), 3017-3026.
- McAvoy, K., Jones, D., & Thakur, R. R. S. (2018). Synthesis and characterisation of photocrosslinked poly (ethylene glycol) diacrylate implants for sustained ocular drug delivery. *Pharmaceutical Research*, 35(2), 36.
- McCulley, J. P., Horowitz, B., Hussein, Z. M., & Horowitz, M. (1993). Topical fibronectin therapy of persistent corneal epithelial defects. Fibronectin Study Group. *Transactions of the American Ophthalmological Society*, 91, 367.
- Meek, K. M. (2008). The cornea and sclera. In *Collagen: Structure and Mechanics* (pp. 359-396). Retrieved from <https://www.scopus.com/inward/record.uri?eid=2-s2.0-84886198695&partnerID=40&md5=ad64edffacefb6d832714d446420cfea>. doi:10.1007/978-0-387-73906-9_13. Retrieved from Scopus database.
- Meek, K. M., & Knupp, C. (2015). Corneal structure and transparency [Review]. *Progress in Retinal and Eye Research*, 49, 1-16.
- Melchels, F. P. W., Blokzijl, M. M., Levato, R., Peiffer, Q. C., Ruijter, M. D., Hennink, W. E., Vermonden, T., & Malda, J. (2016). Hydrogel-based reinforcement of 3D bioprinted constructs [Article]. *Biofabrication*, 8(3).
- Merrett, K., Fagerholm, P., McLaughlin, C. R., Dravida, S., Lagali, N., Shinozaki, N., Watsky, M. A., Munger, R. Kato, Y., & Li, F. (2008). Tissue-engineered recombinant human collagen-based corneal substitutes for implantation: performance of type I versus type III collagen. *Investigative Ophthalmology and Visual Science*, 49(9), 3887-3894.
- Meyer-Blazejewska, E. A., Call, M. K., Yamanaka, O., Liu, H., Schlötzer-Schrehardt, U., Kruse, F. E., & Kao, W. W. (2011). From hair to cornea: Toward the therapeutic use of hair follicle-derived stem cells in the treatment of limbal stem cell deficiency. *Stem Cells*, 29(1), 57-66.
- Miller, D. D., Hasan, S. A., Simmons, N. L., & Stewart, M. W. (2019). Recurrent corneal erosion: a comprehensive review. *Clinical Ophthalmology (Auckland, NZ)*, 13, 325.

- Miyauchil, S., Sugiyama, T., Machida, A., Sekiguchi, T., Miyazaki, K., Tokuyasu, K., & Nakazawa, K. (1990). The effect of sodium hyaluronate on the migration of rabbit corneal epithelium. I. An in vitro study. *Journal of Ocular Pharmacology and Therapeutics*, 6(2), 91-99.
- Mohammadpour, M., Shakoor, D., Hashemi, H., Meybodi, M. A., Rajabi, F., & Hosseini, P. (2017). Comparison of bandage contact lens removal on the fourth versus seventh post-operative day after photorefractive keratectomy: A randomized clinical trial. *Journal of Current Ophthalmology*, 29(2), 103-107.
- Monteiro, N., Thirivikraman, G., Athirasala, A., Tahayeri, A., França, C. M., Ferracane, J. L., & Bertassoni, L. E. (2018). Photopolymerization of cell-laden gelatin methacryloyl hydrogels using a dental curing light for regenerative dentistry. *Dental Materials*, 34(3), 389-399.
- Moreland, L. W. (2003). Intra-articular hyaluronan (hyaluronic acid) and hylans for the treatment of osteoarthritis: mechanisms of action. *Arthritis Research & Therapy*, 5(2), 54.
- Mostafalu, P., Kiaee, G., Giatsidis, G., Khalilpour, A., Nabavinia, M., Dokmeci, M. R., Sonkusale, S., Orgill, D. P., Tamayol, A., & Khademhosseini, A. (2017). A textile dressing for temporal and dosage controlled drug delivery. *Advanced Functional Materials*, 27(41), 1702399.
- Mu, C., Guo, J., Li, X., Lin, W., & Li, D. (2012). Preparation and properties of dialdehyde carboxymethyl cellulose crosslinked gelatin edible films. *Food Hydrocolloids*, 27(1), 22-29.
- Mu, C., Liu, F., Cheng, Q., Li, H., Wu, B., Zhang, G., & Lin, W. (2010). Collagen cryogel cross-linked by dialdehyde starch. *Macromolecular Materials and Engineering*, 295(2), 100-107.
- Murphy, S. V., & Atala, A. (2014). 3D bioprinting of tissues and organs. *Nature Biotechnology*, 32(8), 773-785.
- Musgrave, C. S. A., & Fang, F. (2019). Contact lens materials: A materials science perspective. *Materials*, 12(2), 261.
- Muzzarelli, R. A. (2009). Genipin-crosslinked chitosan hydrogels as biomedical and pharmaceutical aids. *Carbohydr Polym*, 77(1), 1-9.
- Nakamura, M., Mishima, H., Nishida, T., & Otori, T. (1994). Binding of hyaluronan to plasma fibronectin increases the attachment of corneal epithelial cells to a fibronectin matrix. *Journal of Cellular Physiology*, 159(3), 415-422.
- Nakamura, T., Inatomi, T., Sotozono, C., Koizumi, N., & Kinoshita, S. (2016). Ocular surface reconstruction using stem cell and tissue engineering. *Progress in Retinal and Eye Research*, 51, 187-207.

- Nasr, F. H., Khoee, S., Dehghan, M. M., Chaleshtori, S. S., & Shafiee, A. (2016). Preparation and evaluation of contact lenses embedded with polycaprolactone-based nanoparticles for ocular drug delivery. *Biomacromolecules*, 17(2), 485-495.
- Nejabat, M., Masoumpour, M. B., Eghtedari, M., Azarpira, N., Ashraf, M. J., & Astane, A. R. (2009). Amniotic membrane transplantation for the treatment of pseudomonas keratitis in experimental rabbits [Article]. *Iranian Red Crescent Medical Journal*, 11(2), 149-154.
- Nguyen, A. H., McKinney, J., Miller, T., Bongiorno, T., & McDevitt, T. C. (2015). Gelatin methacrylate microspheres for controlled growth factor release. *Acta Biomaterialia*, 13, 101-110.
- Nicolson, P. C., & Vogt, J. (2001). Soft contact lens polymers: an evolution. *Biomaterials*, 22(24), 3273-3283.
- Nishida, T., Nakamura, M., Mishima, H., & Otori, T. (1991). Hyaluronan stimulates corneal epithelial migration. *Experimental Eye Research*, 53(6), 753-758.
- Norman, J., Madurawe, R. D., Moore, C. M., Khan, M. A., & Khairuzzaman, A. (2016). A new chapter in pharmaceutical manufacturing: 3D-printed drug products. *Advanced Drug Delivery Reviews*. doi:10.1016/j.addr.2016.03.001
- Noshadi, I., Hong, S., Sullivan, K. E., Sani, E. S., Portillo-Lara, R., Tamayol, A., Shin, S. R., Gao, A. E., Stoppel, W. L., & Black III, L. D. (2017). In vitro and in vivo analysis of visible light crosslinkable gelatin methacryloyl (GelMA) hydrogels. *Biomaterials science*, 5(10), 2093-2105.
- OASIS. (n.d.). SOFT SHIELD Collagen Corneal Shield. Retrieved May, 25, 2017, from <http://oasismedical.com/soft-shield-collagen-corneal-shield.html>
- Ormonde, S., Chou, C.-Y., Goold, L., Petsoglou, C., Al-Taie, R., Sherwin, T., McGhee, C. N. J., & Green, C. R. (2012). Regulation of connexin43 gap junction protein triggers vascular recovery and healing in human ocular persistent epithelial defect wounds. *Journal of Membrane Biology*, 1-8.
- Osei-Bempong, C., Ghareeb, A. E., Lako, M., Figueiredo, F. C., & Armitage, W. J. (2018). Defining the optimal cryoprotectant and concentration for cryopreservation of limbal stem cells. *Cryobiology*, 84, 98-102.
- Ospina, P. D., Díaz, M. C., & Plaza, J. P. (2014). A review in innovation in ocular prostheses and visual implants: New biomaterials and neuro-implants is the challenge for the visual care. *Journal of Ocular Diseases and Therapeutics*, 2, 9-16.
- Ouasti, S., Donno, R., Cellesi, F., Sherratt, M. J., Terenghi, G., & Tirelli, N. (2011). Network connectivity, mechanical properties and cell adhesion for hyaluronic acid/PEG hydrogels. *Biomaterials*, 32(27), 6456-6470.
- Ouyang, L., Highley, C. B., Rodell, C. B., Sun, W., & Burdick, J. A. (2016). 3D Printing of Shear-Thinning Hyaluronic Acid Hydrogels with Secondary Cross-Linking [Article]. *ACS Biomaterials Science and Engineering*, 2(10), 1743-1751.

- Ouyang, L., Highley, C. B., Rodell, C. B., Sun, W., & Burdick, J. A. (2016). 3D printing of shear-thinning hyaluronic acid hydrogels with secondary cross-linking. *ACS biomaterials science & engineering*, 2(10), 1743-1751.
- Ozcelik, B., Brown, K. D., Blencowe, A., Daniell, M., Stevens, G. W., & Qiao, G. G. (2013). Ultrathin chitosan–poly (ethylene glycol) hydrogel films for corneal tissue engineering. *Acta Biomaterialia*, 9(5), 6594-6605.
- Pampaloni, F., Reynaud, E. G., & Stelzer, E. H. (2007). The third dimension bridges the gap between cell culture and live tissue. *Nature reviews Molecular cell biology*, 8(10), 839.
- Panduranga Rao, K. (1996). Recent developments of collagen-based materials for medical applications and drug delivery systems. *Journal of Biomaterials Science, Polymer Edition*, 7(7), 623-645.
- Park, H. C., Champakalakshmi, R., Panengad, P. P., Raghunath, M., & Mehta, J. S. (2011). Tissue adhesives in ocular surgery. *Expert review of ophthalmology*, 6(6), 631-655.
- Park, J., Lee, S. J., Chung, S., Lee, J. H., Kim, W. D., Lee, J. Y., & Park, S. A. (2017). Cell-laden 3D bioprinting hydrogel matrix depending on different compositions for soft tissue engineering: Characterization and evaluation [Article]. *Materials Science and Engineering C*, 71, 678-684.
- Pataky, K., Braschler, T., Negro, A., Renaud, P., Lutolf, M. P., & Brugger, J. (2012). Microdrop Printing of Hydrogel Bioinks into 3D Tissue-Like Geometries. *Advanced materials*, 24(3), 391-396.
- Paterson, S. M., Liu, L., Brook, M. A., & Sheardown, H. (2015). Poly (ethylene glycol)-or silicone-modified hyaluronan for contact lens wetting agent applications. *Journal of Biomedical Materials Research Part A*, 103(8), 2602-2610.
- Pati, F., Jang, J., Ha, D.-H., Kim, S. W., Rhie, J.-W., Shim, J.-H., Cho, D. Kim, Deok-Ho , K, & Dong-Woo, C. (2014). Printing three-dimensional tissue analogues with decellularized extracellular matrix bioink. *Nature communications*, 5, 3935.
- Peng, C.-C., Kim, J., & Chauhan, A. (2010). Extended delivery of hydrophilic drugs from silicone-hydrogel contact lenses containing vitamin E diffusion barriers. *Biomaterials*, 31(14), 4032-4047.
- Peppas, N., Bures, P., Leobandung, W., & Ichikawa, H. (2000). Hydrogels in pharmaceutical formulations. *European Journal of Pharmaceutics and Biopharmaceutics*, 50(1), 27-46.
- Poland, D. E., & Kaufman, H. E. (1988). Clinical uses of collagen shields [Article]. *Journal of Cataract and Refractive Surgery*, 14(5), 489-491.
- Prasad, L. K., & Smyth, H. (2016). 3D Printing technologies for drug delivery: A review. *Drug Development and Industrial Pharmacy*, 42(7), 1019-1031.

- Pratoomsoot, C., Tanioka, H., Hori, K., Kawasaki, S., Kinoshita, S., Tighe, P. J., & Rose, F. R. A. J. (2008). A thermoreversible hydrogel as a biosynthetic bandage for corneal wound repair [Article]. *Biomaterials*, 29(3), 272-281.
- Price, R. D., Berry, M., & Navsaria, H. A. (2007). Hyaluronic acid: the scientific and clinical evidence. *Journal of Plastic, Reconstructive & Aesthetic Surgery*, 60(10), 1110-1119.
- Raczyńska, D., Glasner, L., Serkies-Minuth, E., Wujtewicz, M. A., & Mitrosz, K. (2016). Eye surgery in the elderly. *Clinical Interventions in Aging*, 11, 407.
- Rafat, M., Li, F., Fagerholm, P., Lagali, N. S., Watsky, M. A., Munger, R., Matsuura, T. Griffith, M. (2008). PEG-stabilized carbodiimide crosslinked collagen–chitosan hydrogels for corneal tissue engineering. *Biomaterials*, 29(29), 3960-3972.
- Ramamurthi, S., Rahman, M., Dutton, G., & Ramaesh, K. (2006). Pathogenesis, clinical features and management of recurrent corneal erosions. *Eye*, 20(6), 635.
- Randers, J. (2012). 2052: A global forecast for the next forty years: Chelsea Green Publishing.
- Ranjha, N. M., & Qureshi, U. F. (2014). Preparation and characterization of crosslinked acrylic acid/hydroxypropyl methyl cellulose hydrogels for drug delivery. *Int J Pharm Pharm Sci*, 6(400), 410.
- Rathore, K. S., Nema, R., & Sisodia, S. (2010). Preparation and characterization of timolol maleate ocular films. *Int J PharmTech Res*, 2(3), 1995-2000.
- Rauz, S., & Saw, V. P. (2010). Serum eye drops, amniotic membrane and limbal epithelial stem cells-tools in the treatment of ocular surface disease [Article]. *Cell and Tissue Banking*, 11(1), 13-27.
- Rawas-Qalaji, M., & Williams, C. A. (2012). Advances in ocular drug delivery [Review]. *Current Eye Research*, 37(5), 345-356.
- Reinstein, D. Z., Archer, T. J., Gobbe, M., Coleman, D. J., & Silverman, R. H. (2008). Epithelial thickness in the normal cornea: three-dimensional display with Artemis very high-frequency digital ultrasound. *Journal of Refractive Surgery*, 24(6), 571-581.
- Ribeiro, A., Blokzijl, M. M., Levato, R., Visser, C. W., Castilho, M., Hennink, W. E., Vermonden, T., & Malda, J. (2017). Assessing bioink shape fidelity to aid material development in 3D bioprinting. *Biofabrication*, 10(1), 014102.
- Ribeiro, A. M., Figueiras, A., & Veiga, F. (2015). Improvements in topical ocular drug delivery systems: Hydrogels and contact lense [Article]. *Journal of Pharmacy and Pharmaceutical Sciences*, 18(5), 683-695.
- Riley, A. F., Grupcheva, C. N., Malik, T. Y., Craig, J. P., & McGhee, C. N. (2001). The Auckland Cataract Study: demographic, corneal topographic and ocular biometric parameters. *Clinical & Experimental Ophthalmology*, 29(6), 381-386.

- Rizwan, M., Peh, G. S., Ang, H.-P., Lwin, N. C., Adnan, K., Mehta, J. S., Tan, W. S., & Yim, E. K. (2017). Sequentially-crosslinked bioactive hydrogels as nano-patterned substrates with customizable stiffness and degradation for corneal tissue engineering applications. *Biomaterials*, 120, 139-154.
- Rose, J., Pacelli, S., Haj, A., Dua, H., Hopkinson, A., White, L., & Rose, F. (2014). Gelatin-based materials in ocular tissue engineering. *Materials*, 7(4), 3106-3135.
- Ruiters, S., Sun, Y., De Jong, S., Politis, C., & Mombaerts, I. (2016). Computer-aided design and three-dimensional printing in the manufacturing of an ocular prosthesis [Article]. *British Journal of Ophthalmology*, 100(7), 879-881.
- Sabater, A. L., & Perez, V. L. (2017). Amniotic membrane use for management of corneal limbal stem cell deficiency. *Current Opinion in Ophthalmology*, 28(4), 363-369.
- Sánchez-González, J.-M., López-Izquierdo, I., Gargallo-Martínez, B., De-Hita-Cantalejo, C., & Bautista-Llamas, M.-J. (2019). Bandage contact lens use after photorefractive keratectomy. *Journal of Cataract and Refractive Surgery*.
- Schacht, E. (2004). *Polymer chemistry and hydrogel systems* IOP Publishing. Symposium conducted at the meeting of the Journal of Physics: Conference Series
- Schermer, A., Galvin, S., & Sun, T.-T. (1986). Differentiation-related expression of a major 64K corneal keratin in vivo and in culture suggests limbal location of corneal epithelial stem cells. *The Journal of cell biology*, 103(1), 49-62.
- Seliktar, D. (2012). Designing cell-compatible hydrogels for biomedical applications. *Science*, 336(6085), 1124-1128.
- Sheth, R., Balesh, E. R., Zhang, Y. S., Hirsch, J. A., Khademhosseini, A., & Oklu, R. (2016). Three-dimensional printing: an enabling technology for IR. *Journal of Vascular and Interventional Radiology*, 27(6), 859-865.
- Siu, G. D. J. Y., Young, A. L., & Jhanji, V. (2014). Alternatives to corneal transplantation for the management of bullous keratopathy [Review]. *Current Opinion in Ophthalmology*, 25(4), 347-352.
- Slaughter, B. V., Khurshid, S. S., Fisher, O. Z., Khademhosseini, A., & Peppas, N. A. (2009). Hydrogels in regenerative medicine. *Advanced materials*, 21(32-33), 3307-3329.
- Smewing, J. (2015). *Texture Analysis in Action: the Film Support Rig*. Retrieved 25 January, 2020, from <https://textureanalysisprofessionals.blogspot.com/2015/02/texture-analysis-in-action-film-support.html>
- Solomon, A., Meller, D., Prabhasawat, P., John, T., Espana, E. M., Steuhl, K. P., & Tseng, S. C. G. (2002). Amniotic membrane grafts for nontraumatic corneal perforations, descemetocelles, and deep ulcers [Article]. *Ophthalmology*, 109(4), 694-703.
- Soluri, A., Hui, A., & Jones, L. (2012). Delivery of Ketotifen Fumarate by Commercial Contact Lens Materials. *Optometry and Vision Science*, 89(8), 1140-1149.

- Song, H., Li, Y., Zhang, Y., Shi, D., & Li, X. (2018). Bandage Lenses in the Postoperative Care for Cataract Surgery Patients: A Substitute for Eye Patch? *Journal of ophthalmology*, 2018.
- Song, Y., Nagai, N., Saijo, S., Kaji, H., Nishizawa, M., & Abe, T. (2018). In situ formation of injectable chitosan-gelatin hydrogels through double crosslinking for sustained intraocular drug delivery. *Materials Science and Engineering: C*, 88, 1-12.
- Sonmez, B., Kim, B. T., & Aldave, A. J. (2007). Amniotic membrane transplantation with anterior stromal micropuncture for treatment of painful bullous keratopathy in eyes with poor visual potential [Article]. *Cornea*, 26(2), 227-229.
- Sridhar, M. S. (2018). Anatomy of cornea and ocular surface. *Indian Journal of Ophthalmology*, 66(2), 190.
- Stratosteffen, H., Köpf, M., Kreimendahl, F., Blaeser, A., Jockenhoevel, S., & Fischer, H. (2017). GelMA-collagen blends enable drop-on-demand 3D printability and promote angiogenesis. *Biofabrication*, 9(4), 045002.
- Su, G., Zhou, T., Zhang, Y., Liu, X., & Zhang, A. (2016). Microdynamics mechanism of D₂O absorption of the poly (2-hydroxyethyl methacrylate)-based contact lens hydrogel studied by two-dimensional correlation ATR-FTIR spectroscopy. *Soft Matter*, 12(4), 1145-1157.
- Sullad, A. G., Manjeshwar, L. S., & Aminabhavi, T. M. (2010). Novel pH-sensitive hydrogels prepared from the blends of poly (vinyl alcohol) with acrylic acid-graft-guar gum matrixes for isoniazid delivery. *Industrial & Engineering Chemistry Research*, 49(16), 7323-7329.
- Suri, K., Kosker, M., Raber, I., Hammersmith, K., Nagra, P., Ayres, B., Halfpenny, C., & Rapuano, C. (2013). Sutureless Amniotic Membrane ProKera for Ocular Surface Disorders: Short-Term Results. *Eye Contact Lens*, 39(5), 341-347.
- Tabatabaei, S. A., Soleimani, M., Behrouz, M. J., Torkashvand, A., Anvari, P., & Yaseri, M. (2017). A randomized clinical trial to evaluate the usefulness of amniotic membrane transplantation in bacterial keratitis healing. *The Ocular Surface*.
- Tan, F., Xu, X., Deng, T., Yin, M., Zhang, X., & Wang, J. (2012). Fabrication of positively charged poly (ethylene glycol)-diacrylate hydrogel as a bone tissue engineering scaffold. *Biomedical materials*, 7(5), 055009.
- Taylor, K. R., Caldwell, M. C., Payne, A. M., Apey, D. A., Townley, J. R., Reilly, C. D., & Panday, V. A. (2014). Comparison of 3 silicone hydrogel bandage soft contact lenses for pain control after photorefractive keratectomy. *Journal of Cataract and Refractive Surgery*, 40(11), 1798-1804.
- Tiwari, G., Tiwari, R., Sriwastawa, B., Bhati, L., Pandey, S., Pandey, P., & Bannerjee, S. K. (2012). Drug delivery systems: An updated review. *International Journal of Pharmaceutical Investigation*, 2(1), 2-11.

- Tran, V. B., Sung, Y. S., Copley, K., & Radke, C. J. (2012). Effects of aqueous polymeric surfactants on silicone-hydrogel soft- contact-lens wettability and bacterial adhesion of *Pseudomonas aeruginosa* [Article]. *Contact Lens and Anterior Eye*, 35(4), 155-162.
- Troiano, P., & Monaco, G. (2008). Effect of hypotonic 0.4% hyaluronic acid drops in dry eye patients: a cross-over study. *Cornea*, 27(10), 1126-1130.
- Tsai, I. L., Hsu, C. C., Hung, K. H., Chang, C. W., & Cheng, Y. H. (2015). Applications of biomaterials in corneal wound healing. *Journal of the Chinese Medical Association*, 78(4), 212-217.
- Van Beek, M., Weeks, A., Jones, L., & Sheardown, H. (2008). Immobilized hyaluronic acid containing model silicone hydrogels reduce protein adsorption. *Journal of Biomaterials Science, Polymer Edition*, 19(11), 1425-1436.
- Van Den Bulcke, A. I., Bogdanov, B., De Rooze, N., Schacht, E. H., Cornelissen, M., & Berghmans, H. (2000). Structural and rheological properties of methacrylamide modified gelatin hydrogels. *Biomacromolecules*, 1(1), 31-38.
- Vandooren, J., Van den Steen, P. E., & Opdenakker, G. (2013). Biochemistry and molecular biology of gelatinase B or matrix metalloproteinase-9 (MMP-9): the next decade. *Critical Reviews in Biochemistry and Molecular Biology*, 48(3), 222-272.
- Völker-Dieben, H., Regensburg, H., & Kruit, P. (1994). A double-blind, randomized study of Healon GV compared with Healon in penetrating keratoplasty. *Cornea*, 13(5), 414-417.
- Vyas, S., & Rathi, V. (2009). Combined phototherapeutic keratectomy and amniotic membrane grafts for symptomatic bullous keratopathy [Article]. *Cornea*, 28(9), 1028-1031.
- Wagner, H. (2018). Polish Up Your Practice: Today's Contact Lens Surfaces. *Review of Optometry*, 155(8), 46-51.
- Wakuta, M., Morishige, N., Chikama, T.-i., Seki, K., Nagano, T., & Nishida, T. (2007). Delayed wound closure and phenotypic changes in corneal epithelium of the spontaneously diabetic Goto-Kakizaki rat. *Investigative Ophthalmology and Visual Science*, 48(2), 590-596.
- Wang, J. J., & Liu, F. (2012). UV-curing of simultaneous interpenetrating network silicone hydrogels with hydrophilic surface. *Polymer bulletin*, 69(6), 685-697.
- Wang, J. J., Liu, F., & Wei, J. (2012). Hydrophilic silicone hydrogels with interpenetrating network structure for extended delivery of ophthalmic drugs. *Polymers for Advanced Technologies*, 23(9), 1258-1263.
- Wang, S., Lee, J. M., & Yeong, W. Y. (2015). Smart hydrogels for 3D bioprinting. *International Journal of Bioprinting*, 1(1).
- Wang, X., Ao, Q., Tian, X., Fan, J., Tong, H., Hou, W., & Bai, S. (2017). Gelatin-based hydrogels for organ 3D bioprinting. *Polymers*, 9(9), 401.

- Wang, Y., Ma, M., Wang, J., Zhang, W., Lu, W., Gao, Y., Zhang, B., & Guo, Y. (2018). Development of a photo-crosslinking, biodegradable GelMA/PEGDA hydrogel for guided bone regeneration materials. *Materials*, 11(8), 1345.
- Waran, V., Narayanan, V., Karuppiyah, R., Pancharatnam, D., Chandran, H., Raman, R., Rahman, Z., Ariff, A., & Aziz, T. Z. (2014). Injecting realism in surgical training—initial simulation experience with custom 3D models. *Journal of Surgical Education*, 71(2), 193-197.
- Weadock, K., Olson, R. M., & Silver, F. H. (1983). Evaluation of collagen crosslinking techniques. *Biomaterials, medical devices, and artificial organs*, 11(4), 293-318.
- Weeks, A., Luensmann, D., Boone, A., Jones, L., & Sheardown, H. (2012). Hyaluronic acid as an internal wetting agent in model DMAA/TRIS contact lenses. *Journal of Biomaterials Applications*, 27(4), 423-432.
- Wei, D., Xiao, W., Sun, J., Zhong, M., Guo, L., Fan, H., & Zhang, X. (2015). A biocompatible hydrogel with improved stiffness and hydrophilicity for modular tissue engineering assembly. *Journal of Materials Chemistry B*, 3(14), 2753-2763.
- White, C. J., & Byrne, M. E. (2010). Molecularly imprinted therapeutic contact lenses [Review]. *Expert Opinion on Drug Delivery*, 7(6), 765-780.
- White, C. J., McBride, M. K., Pate, K. M., Tieppo, A., & Byrne, M. E. (2011). Extended release of high molecular weight hydroxypropyl methylcellulose from molecularly imprinted, extended wear silicone hydrogel contact lenses. *Biomaterials*, 32(24), 5698-5705.
- Wichterle, O., & Lim, D. (1960). Hydrophilic gels for biological use. *Nature*, 185(4706), 117-118.
- Williams, C. G., Malik, A. N., Kim, T. K., Manson, P. N., & Elisseeff, J. H. (2005). Variable cytocompatibility of six cell lines with photoinitiators used for polymerizing hydrogels and cell encapsulation. *Biomaterials*, 26(11), 1211-1218.
- Willoughby, C. E., Batterbury, M., & Kaye, S. B. (2002). Collagen corneal shields [Review]. *Survey of Ophthalmology*, 47(2), 174-182.
- WM, H., JY, L., & GH, H. (2013). Transplantation of human corneal endothelial cells using functional biomaterials. *Hsu WM, Chen KH, Lai JY(5)*.
- World Health Organization. (2005). *State of the world's sight: Vision 2020: the right to sight: 1999-2005*: WHO Press.
- Wright, B., Mi, S., & Connon, C. J. (2013). Towards the use of hydrogels in the treatment of limbal stem cell deficiency. *Drug Discovery Today*, 18(1), 79-86.
- Xin-Yuan, S., & Tian-Wei, T. (2004). New contact lens based on chitosan/gelatin composites. *Journal of Bioactive and Compatible Polymers*, 19(6), 467-479.

- Xinming, L., Yingde, C., Lloyd, A. W., Mikhalovsky, S. V., Sandeman, S. R., Howel, C. A., & Liewen, L. (2008). Polymeric hydrogels for novel contact lens-based ophthalmic drug delivery systems: A review. *Contact Lens and Anterior Eye*, 31(2), 57-64.
- Xu, C., He, R., Xie, B., Ismail, M., Yao, C., Luan, J., & Li, X. (2016). Silicone hydrogels grafted with natural amino acids for ophthalmological application. *Journal of Biomaterials Science, Polymer Edition*, 27(13), 1354-1368.
- Xu, J., Li, X., & Sun, F. (2011). In vitro and in vivo evaluation of ketotifen fumarate-loaded silicone hydrogel contact lenses for ocular drug delivery. *Drug Delivery*, 18(2), 150-158.
- Xu, J., Xue, Y., Hu, G., Lin, T., Gou, J., Yin, T., He, H., Zhang, Y., & Tang, X. (2018). A comprehensive review on contact lens for ophthalmic drug delivery. *Journal of Controlled Release*, 281, 97-118.
- Xu, W., Wang, Z., Liu, Y., Wang, L., Jiang, Z., Li, T., Zhang, W., & Liang, Y. (2018). Carboxymethyl chitosan/gelatin/hyaluronic acid blended-membranes as epithelia transplanting scaffold for corneal wound healing. *Carbohydr Polym*, 192, 240-250.
- Yamamoto, S., Hirata, A., Ishikawa, S., Ohta, K., Nakamura, K.-i., & Okinami, S. (2013). Feasibility of using gelatin-microbial transglutaminase complex to repair experimental retinal detachment in rabbit eyes. *Graefe's Archive for Clinical and Experimental Ophthalmology*, 251(4), 1109-1114.
- Yan, J., Qiang, L., Gao, Y., Cui, X., Zhou, H., Zhong, S., Wang, Q., & Wang, H. (2012). Effect of fiber alignment in electrospun scaffolds on keratocytes and corneal epithelial cells behavior. *Journal of Biomedical Materials Research Part A*, 100(2), 527-535.
- Yang, F., Williams, C. G., Wang, D.-a., Lee, H., Manson, P. N., & Elisseff, J. (2005). The effect of incorporating RGD adhesive peptide in polyethylene glycol diacrylate hydrogel on osteogenesis of bone marrow stromal cells. *Biomaterials*, 26(30), 5991-5998.
- Yang, M., Yang, Y. F., Lei, M., Ye, C. T., Zhao, C. S., Xu, J. G., Wu, K. L. & Yu, M. B. (2016). Experimental studies on soft contact lenses for controlled ocular delivery of pirfenidone: in vitro and in vivo. *Drug Delivery*, 23(9), 3538-3543.
- Ye, J., Shi, X., Chen, X., Xie, J., Wang, C., Yao, K., Gao, C., & Gou, Z. (2014). Chitosan-modified, collagen-based biomimetic nanofibrous membranes as selective cell adhering wound dressings in the treatment of chemically burned corneas [Article]. *Journal of Materials Chemistry B*, 2(27), 4226-4236.
- Yin, J., Yan, M., Wang, Y., Fu, J., & Suo, H. (2018). 3D bioprinting of low-concentration cell-laden gelatin methacrylate (GelMA) bioinks with a two-step cross-linking strategy. *ACS applied materials & interfaces*, 10(8), 6849-6857.
- Yue, K., Trujillo-de Santiago, G., Alvarez, M. M., Tamayol, A., Annabi, N., & Khademhosseini, A. (2015). Synthesis, properties, and biomedical applications of gelatin methacryloyl (GelMA) hydrogels. *Biomaterials*, 73, 254-271.

- Yurchenco, P. D. (2011). Basement membranes: cell scaffoldings and signaling platforms. *Cold Spring Harbor Perspectives in Biology*, 3(2), a004911.
- Zellander, A., Wardlow, M., Djalilian, A., Zhao, C., Abiade, J., & Cho, M. (2014). Engineering copolymeric artificial cornea with salt porogen. *Journal of Biomedical Materials Research Part A*, 102(6), 1799-1808.
- Zhang, L., Hum, M., Wang, M., Li, Y., Chen, H., Chu, C., & Jiang, H. (2005). Evaluation of modifying collagen matrix with RGD peptide through periodate oxidation. *Journal of Biomedical Materials Research Part A: An Official Journal of The Society for Biomaterials, The Japanese Society for Biomaterials, and The Australian Society for Biomaterials and the Korean Society for Biomaterials*, 73(4), 468-475.
- Zhang, X., Do, M. D., Casey, P., Sulistio, A., Qiao, G. G., Lundin, L., Lillford, P., & Kosaraju, S. (2010). Chemical cross-linking gelatin with natural phenolic compounds as studied by high-resolution NMR spectroscopy. *Biomacromolecules*, 11(4), 1125-1132.
- Zhang, Y. S., Yue, K., Aleman, J., Mollazadeh-Moghaddam, K., Bakht, S. M., Yang, J., Jia, W., Dell'Erba, V., Assawes, P., & Shin, S. R. (2017). 3D bioprinting for tissue and organ fabrication. *Annals of Biomedical Engineering*, 45(1), 148-163.
- Zhang, Z., Ortiz, O., Goyal, R., & Kohn, J. (2014). Chapter 23 - Biodegradable Polymers. In R. Lanza, R. Langer, & J. Vacanti (Eds.), *Principles of Tissue Engineering (Fourth Edition)* (pp. 441-473). Boston: Academic Press. Retrieved from <http://www.sciencedirect.com/science/article/pii/B9780123983589000239>.
- Zhao, D., Jiao, X., Zhang, Y., An, D., Shi, X., Lu, X., Qiu, G., & Shea, K. J. (2015). Polymerization mechanism of poly (ethylene glycol dimethacrylate) fragrance nanocapsules. *RSC Advances*, 5(116), 96067-96073.
- Zhao, Y., & Ma, L. (2015). Systematic review and meta-analysis on transplantation of ex vivo cultivated limbal epithelial stem cell on amniotic membrane in limbal stem cell deficiency. *Cornea*, 34(5), 592-600.
- Zhu, M., Wang, Y., Ferracci, G., Zheng, J., Cho, N.-J., & Lee, B. H. (2019). Gelatin methacryloyl and its hydrogels with an exceptional degree of controllability and batch-to-batch consistency. *Scientific Reports*, 9.
- Zhu, W., George, J. K., Sorger, V. J., & Zhang, L. G. (2017). 3D printing scaffold coupled with low level light therapy for neural tissue regeneration. *Biofabrication*, 9(2), 025002.
- Ziaei, M., Greene, C., & Green, C. R. (2018). Wound healing in the eye: Therapeutic prospects. *Advanced Drug Delivery Reviews*, 126, 162-176.